Journal of Engineering

ISSN 1726-4073

A Scientific Refereed Journal Published by College of Engineering University of Baghdad

February
2015

Number 2

Volume 21

مجلة الهندسة

ISSN 1726-4073

مجلة علمية محكمة تصدرها
كلية الهندسة ـ جامعة بغداد

شباط
2015

العدد 2

المجلد 21

ENGINEERING

College of Engineering Baghdad University Baghdad

List of Contents

English Section: Page

قائمة المحتويات

القسم العربي:

Impact Analysis of Reinforced Concrete Columns with Side Openings Subjected to Eccentric Axial Loads

Dr. Nazar Kamil Ali
Professor
Civil Engineering Department
College of Engineering
University of Baghdad
E-Mail:
dr_nazar12000@yahoo.com

Dr. Ali Ihsan Salahaldin
Instructor
Civil Engineering Department
College of Engineering
University of Kirkuk
E-Mail:
ali_salahaldin@yahoo.com

Ahmed Jabbar Hamza
Researcher
Civil Engineering Department
College of Engineering
University of Baghdad
E-Mail:
ahmed_87jabbar@yahoo.com

ABSTRACT

In this research the behavior of reinforced concrete columns with large side openings under impact loads was studied. The overall cross sectional dimensions of the column specimens used in this research were (500*1400) mm with total height of (14000) mm. The dimensions of side openings were (600*2000) mm. The column was reinforced with (20) mm diameter in longitudinal direction, while (12) mm ties were used in the transverse direction. The effect of eccentric impact loads on the horizontal and vertical displacement for this column was studied.

Nonlinear finite element analysis has been carried out using ready computer finite element package (ANSYS) to simulate the behavior of the reinforced concrete column with large side openings. Two load cases were considered in this investigation (C1, C2) with three different load values for each case. In the first case (C1) the loads was applied to one side of the column and in the second case (C2) the loads was applied to both sides. An Equilateral triangular load-time function was used for simulation the impact load results from gantry cranes supported by the column with total time duration (0.1 sec).

In order to verify the analysis method, as no experimental data exist for comparing the obtained results, another analysis is made for tested conventional column under impact load at mid-height and good agreement has been obtained.

For the above mentioned column, the maximum displacements were (33.3, 22.2) mm in the horizontal and longitudinal direction respectively, location of the maximum horizontal displacement was at the crown of the column. By comparing the results of the first loading case with the second one it is shown that in the horizontal direction, maximum displacement increases by (139%), (208%), and (147%) respectively, also the maximum vertical displacement increases by (150%), (172%), and (172%) respectively.

Key words: impact analysis, concrete columns, columns with side openings, eccentric loads.

التحليل الصدمي لأعمدة خرسانيه مسلحة حاوية على فتحات جانبيه ومعرضة لأحمال محورية لا مركزية

أ.د. نزار كامل علي
جامعة بغداد / كلية الهندسة

م. د. علي احسان صلاح الدين
جامعة كركوك / كلية الهندسة

أحمد جبار حمزة
جامعة بغداد / كلية الهندسة

الخلاصة

في هذا البحث تم دراسة سلوك عمود خرساني يحتوي على فتحات جانبية كبيرة (عمود ذو جزئين) تحت تأثير احمال صدمية لامركزية, حيث تم اعتماد عمود ذو مقطع (500*1400) ملم وبأرتفاع (14000) ملم ويحتوي على فتحات جانبية كبيرة بأبعاد (2000*600) ملم وتم تسليح العمود بأستخدام حديد بقطر 20 ملم في الاتجاة الشاقولي وقطر 12 ملم في الاتجاه العرضي .وتم دراسة تأثير تغير مقدار التحميل على الازاحه لهذا العمود.

تم اعتماد التحليل اللاخطي بأستخدام طريقة العناصر المحدده وبالاستعانه ببرنامج (ANSYS) ليُحاكي تصرف العمود المحتوي على فتحات جانبيه وتم تسليط الاحمال بحالتين وكل حالة تحتوي على ثلاث قيم مختلفة للحمل ,حيث في الحالة الاولى تم التحميل من جانب واحد وفي الحالة الثانيه تم التحميل من جانبين, , وتم استخدام دالة حمل مثلثة الشكل متساوية الساقين لتمثيل الحمل الصدمي المسلط خلال فترة تحميل تبلغ (0.1) ثانيه.

اكبر ازاحه تم الحصول عليها كانت (33.3) ملم مع المحور (X) و (22.2) ملم مع المحور (Y), وأن موقع اكبر ازاحه افقيه كان عند قمة العمود. وعند مقارنة النتائج لحالتي التحميل (التحميل من جانب واحد والتحميل من الجانبين) تبين ان نسبه الزياده في الازاحه الافقيه هي (139%, 208% , 147%)على التوالي, في حين ان نسبه الزياده في الازاحه العموديه هي (150%, 172%, 172%) على التوالي .

1. INTODUCTION

1.1 General

Openings and holes are used in reinforced concrete columns for providing access for services like plumbing, water network, electric and communication system etc. In some cases it is required to use very long column to carry light load like the columns of ware house. In this case using column with small cross sectional area leads to stability problem due to large slenderness ratio and using column with large cross sectional area may become uneconomical, therefore, the designer heads towards using two-legs column with large horizontal opening between two sides of the column, which provides both stability and economy.

A lot of research work were studied the behavior of longitudinal hollow column like **Cheng et al., 2005, Lignola et al., 2007,** and **Ali Al- Ahmed,2010**. Also, few researches were studied the behavior of column with side openings as Son et al. in 2006.

1.2 Objectives of Present Study

The objective of the present work is to investigate the deformation characteristics of the two-leg concrete column with large side openings subjected to eccentric impact load. The research covers the behavior of column under different load cases and different load values applied to an individual selected column.

2. FINITE ELEMENT MODELING

2.1 ANSYS Model

The ready package finite element computer program designated ANSYS version 11.0 has been used for modeling the reinforced concrete column. The dimensions of the modeled column was (14m) in height and with different cross sections along its length, **Fig.1** shows overall dimensions of the column with location of some sections, these cross sections are shown in **Fig.2**.

2.1 Element Types

Solid65 element type was used for modeling the concrete, while Solid45 element type was used for modeling steel base plates at the corbel of the column. Link8 element type was used for modeling steel reinforcement in all directions.

2.2 Real Constants

In the finite element simulation, the second step after choosing the elements type, is giving the value of real constants. For Soid65 all input data equal to zero and that physically means no smeared reinforcement was chosen for this simulation, where the analysis forward in the direction of discrete reinforcement approach, therefore, the cross sectional areas for link8 elements were (314 and 113mm^2) for longitudinal and transverse reinforcement respectively.

2.3 Material Properties

In this research, material nonlinearity was considered for steel and concrete. Five points stress – strain curve was selected for concrete with compressive strength of (25) MPa and Poisson's ratio of (0.17).

Bilinear stress – strain hardening curve was used for steel reinforcement with yielding stress of (420) MPa and Poisson's ratio of (0.3).

2.4 Modeling

The concrete column were modeled using ten distinguish volumes; these volumes are shown in **Fig.3**.

2.5 Meshing

In order to obtain accurate simulation of this column with exact location of openings, concrete covers and location of steel bars in both longitudinal and transverse direction, small element length of (40) mm was chosen for this analysis and that leads to huge numbers of nodes and elements. In the other hand, these numbers allow the model to capture the real behavior of the column. Total (116928) nodes and (108441) different elements were exist along the column.

2.6 Supports

The supports were modeled in such a way that fix reaction was created by restraining the translation in X, Y, and Z directions at the base of column.

2.7 Loading

Two main impact load cases was considered in this research, in the first load case, the impact load was applied to one side of the column (in both vertical and horizontal directions) and it's called (C1), and in the second load case the load was applied to both sides of column at the same time (in both

vertical and horizontal direction) and it's called (C2). Load cases are shown in **Fig.4** and **Fig. 5.** Furthermore each case has three stages of impact loading, where the first loading stage is (30 kN and 15 kN) for vertical and horizontal directions respectively, second loading stage is (50 kN and 25 kN) for vertical and horizontal directions respectively, and third loading stage is (100 kN 50 kN) for vertical and horizontal forces respectively. The impact load was simulated as equilateral triangular function with load time duration of (0.1) sec and maximum load occur at (0.05) sec. **Fig.6** shows variation of load with time and the value of loading was chosen theoretically on the bases usual range of gantry-crane load carrying capacity for factories and warehouses.

3.VERIFICATION EXAMPLE

To prove that the proposed method for modeling reinforced concrete columns with side openings under the influence of impact loads match of the correct method, and because of the absence of the required information from experimental test results or other theoretical analysis procedure. For this reason an ordinary reinforced concrete column has been modeled using finite element method under the same types of loads (impact loads) and the numerical values of displacement obtained from analysis was compared with experimental test carried by Remennikov and Kaewuaruen (2006). **Fig.7** presents load-deflection curve for the reinforced concrete column under transverse impact load. Investigation of this curve shows acceptable agreement between experimental test results and the proposed finite element model.

4. NUMERICAL RESULTS

The behavior of the analyzed column under impact load will be studied by investigating the displacements at different nodes along the column. Locations of these nodes are shown in **Fig.8**.

4.1 Displacement Along the Column

The horizontal displacement due to maximum loading at time (0.05) sec is shown in **Fig. 9** and **Fig.10** for load-cases C1 and C2 respectively. The horizontal displacement means the displacement along the x- axis and is called (Ux). From these figures it's obvious that column behavior goes in three parts for all cases. First part starting from the base of column (N1) to the level of (N9) where there is increase in horizontal displacement with height. The second part covers the region between (N9) to (N11) where there is small increase in lateral displacement as this solid part of column displaces approximately as one unit. The third part of the curve covers the region between (N11) which represents the points of applying load to (N13) which represents top of column, where large horizontal displacements are noticed due to rotational effect of solid part of column under the neck.

By comparing the results in **Fig.9** for node (N11) it is seen that the increase in the impact force from (15) kN to (25) kN (from C1L1 to C1L2) will cause increasing in horizontal displacement by (66.7%) and when the impact load increases from (15) kN to (50) kN (from C1L1 to C1L3) this will lead to increasing in horizontal displacement by (391%).

When the load is applied at both sides of the column (C2) as shown in **Fig.10** for node (N11) it is seen that the increase in the impact load from (15) kN to (25) kN (from C2L1 to C2L2) will cause increasing in horizontal displacement by (120%) and when the impact load increases from (15) kN to (50) kN (from C2L1 to C2L3) this will lead to increasing in horizontal displacement by (409%).

By comparing the results in **Fig.9** and **Fig.10** it appears that the maximum horizontal displacement increases by (139%), (208%), and (147%) respectively as compared with C1 and C2.

The vertical displacements due to loading cases at time equals to (0.05) sec are shown in **Fig.11** and **Fig.12** for columns C1 and C2 respectively. The vertical displacement means the displacement is along y-axis and is called (Uy). From these figures it's obvious that column behavior goes in five parts for all load cases. The first part starts from the base of column (N1) to the level of (N7) where there is gradual increase in displacement with height. The second part represents the zone from (N7) to (N9) where there is a sharp change in vertical displacement with increasing the height. The third part of the curve starts from (N9) to (N11) where this nodes represents the cross beam over two parts of column at level (from 9240 to 10050) mm, where the upper and lower faces of the cross beam move in the same pattern due to high flexural rigidity of cross-beam. The fourth part covers the region from N11 to N12 where there is a decrease in vertical displacement value with the distance towards the upper end, and this is due node N11 undergoes flexural and axial loads at the same time while node N12 is free from load and that leads to combined effect which controls this behavior. The fifth part starts from N12 to N13 where there is no change in the displacement value as no load applied to this part of the column.

By comparing the results at **Fig.11** for node (N11) it is seen that by increasing the impact force from (15) kN to (25) kN (from C1L1 to C1L2) will cause an increase in vertical displacement by (64.7%) and when the impact load increases from (15) kN to (50) kN (from C1L1 to C1L3) this will lead to an increase in the vertical displacement by (264.7%).

When the load is applied to both sides of column (C2) as shown in **Fig.12** for node (N11), it is seen that by increasing the impact load from (15) kN to (25) kN (from C2L1 to C2L2) will cause increasing in vertical displacement by (76%) and when the impact load increases from (15) kN to (50) kN (from C2L1 to C2L3) this will lead to an increases in the vertical displacement by (281%).

From comparing the results in **Fig.11** and **Fig.12** it appears the maximum vertical displacement increases by (150%), (172%), and (172%) respectively as compared with C1 and C2.

Fig.13 and **Fig.14** show the values of residual horizontal displacement of columns C1 and C2 respectively. it appears that no residual displacements (horizontal and vertical) exist for load cases C1L1, C1L2, C2L1, and C2L2 which means full elastic behavior is achieved for these columns, while only some residual horizontal displacement is noticed along column (although it is very small) for C1L3 and C2L3, which means some cracks occurs at the column.

Two-leg concrete columns have large stiffness compared to regular normal concrete column, where the link member that connects the two branches reduces the unbraced length of each part of column. **Fig.15** and **Fig.16** show variation of horizontal displacement along column at the link between two branches of column for C1 and C2 respectively at time equals to (0.05) sec., and as comparing these figures it appears that the horizontal displacement of these link members shows approximately linear variation with the height and also with the amount of impact load. This is due to large rigidity of these members. In addition, the applied load is relatively small compared with the capacity of the structure.

Fig.18 and **Fig19** show variation of vertical displacement along column at link between two branches of column C1 and C2 respectively at maximum load at time equals to (0.05) sec. and by comparing these results, it appears that the vertical displacement of link member shows approximately linear variation with the height and shows the displacement decreases with increasing the height, from studying data, it is shows that no vertical displacement is recorded for columns C1L1, C1L2, C2L1, and C2L2. The reason of this behavior is due to position of link member in the

center of the column where one branch resists the compression forces and the other resist the tension forces if exist. **Fig.19** shows the value of residual horizontal displacement of link between two branches column for C2. It appears that no residual displacement exists for load cases of columns C1L1, C1L2, C1L3, C2L1, and C2L2 which means full elastic behavior is achieved for these columns, while some residual displacement is noticed along column C2L3 (although it is very little), which means some cracks occur in column.

4.1 Maximum Displacement

From **Figs**.**9, 10, 15**, and**Fig.16** it appears that the maximum horizontal displacement occurs at the crown of column (N13) and this part of the structure is the most critical in this type of column because the section returns to normal shape (square or rectangular shape stand alone as cantilever). Furthermore, this part of column usually carries the weight of the roof which consists of vertical load due to dead load in addition to horizontal force due to wind load. And from **Figs. 11, 12, 17,** and **Fig.18** it appears that the maximum vertical displacement occurs at (N8) at level (8240 mm). **Fig.20** and **Fig.21** show maximum horizontal displacement for the columns C1 and C2 respectively. While **Fig.22** and **Fig.23** show maximum vertical displacement for the column at C1 and C2 respectively. The horizontal displacement at the crown of the column is more than the horizontal displacement at location of applied load. This is because rotation of cross beam that connects two branches of column at level (9240 mm) which leads to additional movement at upper part of the column although no load was applied on it.

4.2 Variation of Displacement with Time

Maximum horizontal displacement of the columns C1 and C2 occurs at node (N13) while maximum vertical displacement occurs at node (N8).

Fig.24 and **Fig**.**25** show variation of the horizontal displacement with time at (N13) for columns C1 and C2 respectively, while **Fig.26** and **Fig.27** show variation of vertical displacement with time at (N8) for columns C1 and C2 respectively.

Examination of **Figs. 24, 25, 26** and **27** show similar behavior in general, the horizontal displacement is equal to zero at time zero as no load exists. Since a triangle load function is used to applied impact force with peak point in (0.05 sec), the horizontal displacement increases but this increment is smooth in columns C1L1 and C1L2 while it takes sharp shape in column C1L3 until reaching maximum value at (0.05 sec). After that as the load decreases until it reaches zero at (0.1 sec) the horizontal displacement is reduced in sharp manner till it reaches zero in (0.06-0.08) sec this is due to large stiffness of this type of column which absorbs all impact energy.

Studying the data obtained from finite element analysis for this type of columns it is observed that no displacement is recorded in Z-direction; therefore, these values will be ignored.

5 .CON LUSIONS

The following conclusions are drawn from the evaluation of analysis of the concrete columns with side openings model under the effect of the impact of regular gantry cranes loads:

1. Horizontal displacement increases with the height of the column in approximately linear pattern up to the position of major cross beam for all loading values.
2. Under large impact load (C1L3 and C2L3), the upper part of the column shows excessive horizontal movement, so these parts require special consideration in design in order to carry additional moment resulting from load eccentricity.

3. Investigation of the load-horizontal displacement curves shows proportional relationship between applied loading and resulting displacements.
4. After removing the loading, no effect appears for horizontal displacement for all loading values except (C1L3 and C2L3) which indicate concrete cracking at some regions along column height.
5. The link members which connect the branches of the column reduce the unbraced length of each part and prevent buckling failure of columns.
6. After removing the loads no effect appears for the vertical displacement along Y-axis.
7. Horizontal displacement in Z-axis equal zero for all cases of loading, as no load applied in that direction and volumetric changes are negligible in that direction.
8. By comparing the results for columns C1 with C2 it appears that the maximum horizontal displacement increases by (139%), (208%), and (147%) respectively.

REFFERNCES

- Detroit, 2008.ACI 318M-08,*Building Code Requirements for Reinforced Concrete and Commentary*, American concrete institute.

- Ali Al-Ahmed, 2010, *Nonlinear Behavior of Reinforced Concrete Rectangular Columns with (PVC) Embedded Pipes*, PH.D. Thesis Baghdad university .

- AL-Janabi A. H., 2001, *Nonlinear Finite Element Analysis of Reinforced Concrete Eccentrically Loaded Short Columns*, M.Sc. Thesis University of Technology, Baghdad, PP.111.

- A.M. Remennikov and S. Kaewunruen , 2006, *Impact resistance of Reinforced Concrete Columns Experimental Studies and Design Considerations A.M*. 19th Australasian Conference on the Mechanics of Structures and Materials, Nov 29-Dec 1, Christchurch, New Zealand, 817-824. Copyright 2007 Tailor & Francis.

- Ando T, Kishi N, Mikami H, Matsuoka KG. 2001, *Applicability of FE Analysis on RC Columns under Lateral Impact Loading*, In: Proceedings of the Third International Conference on Concrete under Severe Conditions, p. 581-588.

- ANSYS help release 11.0.

- Cheng, C. T., Mo, Y. L. and Yeh, Y. K, 2005, *Evaluation of As- built Retrofitted and Repaired Shear- Critical Hollow Bridge Columns under Earthquake-Type Loading*, journal of bridge engineering, ASCE, Vol.10, No. 5, September, PP.520-529.

- Chung W. Y. M. and Lam E. S. S. *Confinement of Columns with Non- seismic Detailing*, internet, 2004, PP.1-9

- Kwan, K. H. and Liauw, T. C.1985, *Computer Aided Design of Reinforced Concrete Member Subjected to Axial Compression and Biaxial Bending*, The Structure Engineer, Vol.63B, No.2, June 1985, PP.34-40.

- Lignola, G. P.; Porta, A.; Manfredi, G. and Cosenza, E., 2007, *Experimental Performance of RC Hollow Columns Confined with CFRP*, Journal of Composites for Construction, ASCE, Vol. 11, No.1, January-February 2007, pp. 42-49.

- Son , K. S., Pilakoutas, K. and Neocleous, K., *Behavior of Concrete Columns with Drilled Holes* Magazine of Concrete Research Vol. 58, No.7, September 2006, PP.41-419.

- Winter, G. and Nilson,A. H., 2012,*Design of Concrete Structure*, 14th edition, McGraw-Hill, New York.

- Willam, K. J. and Warnke, E. P.,1974, *Constitutive Model for Triaxial Behavior of Concrete*,, Seminar on Concrete Structures Subjected to Triaxial Stresses, International Association of Bridge and Structural Engineering Conference, Bergamo, Italy, 197, pp. 174.

- Yang I-Y. 2004. E*ffect of Transverse Impact On Buckling Behavior Of A Column Under Static Axial Compressive* ,International Journal of Impact Engineering. V.30: 465-475.

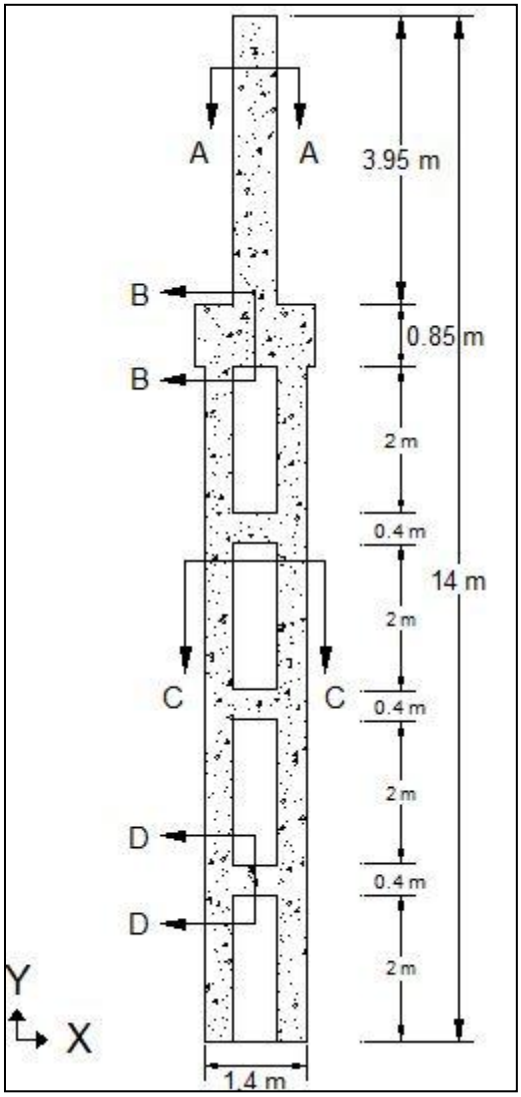

Figure 1. Location of sections along column.

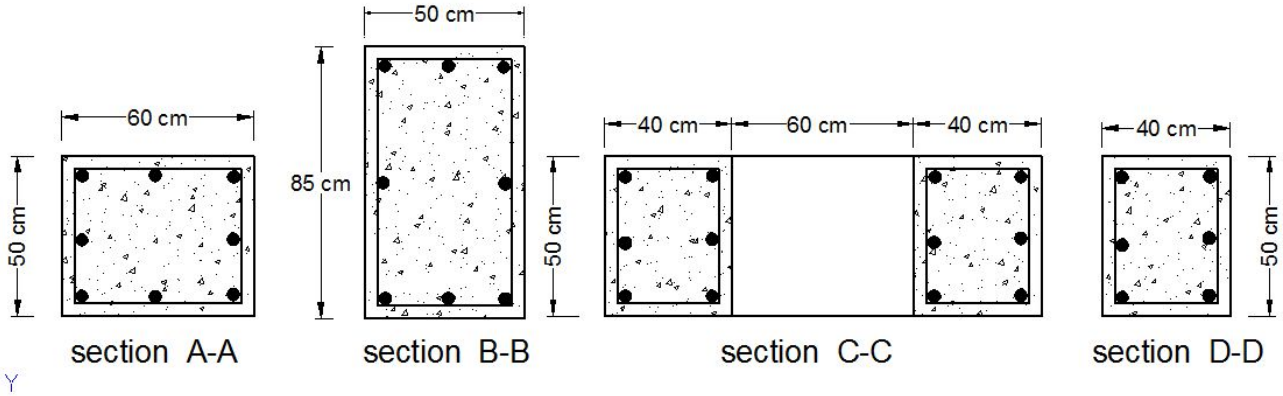

Figure 2. Different sections of the selected column.

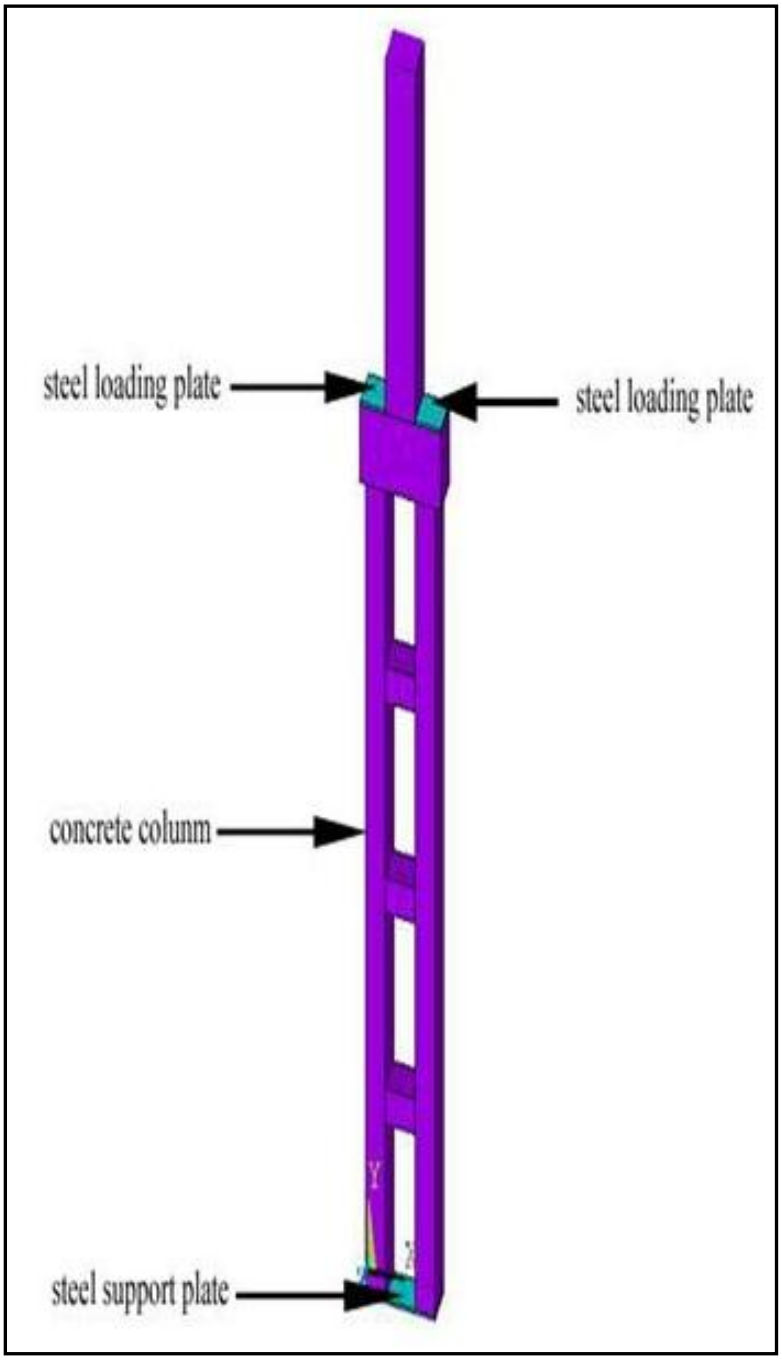

Figure 3. Volumes created in ANSYS**.**

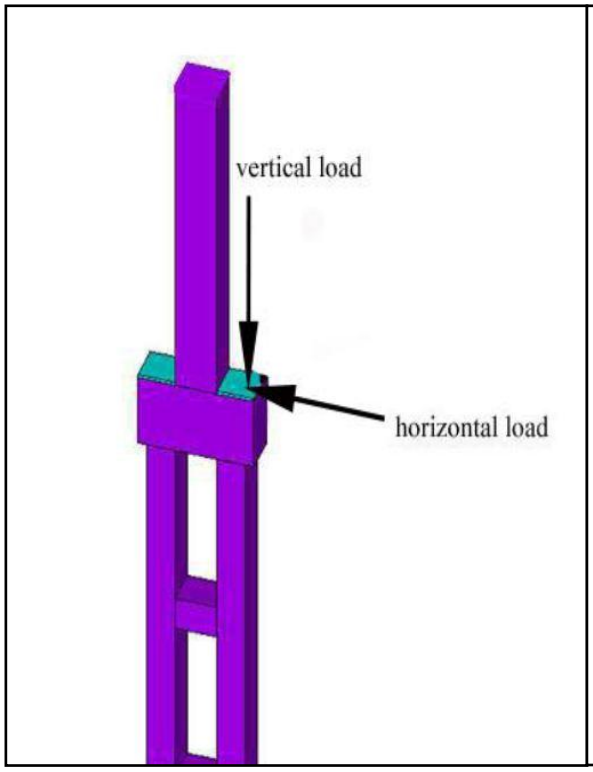

Figure 4. First load case (C1).

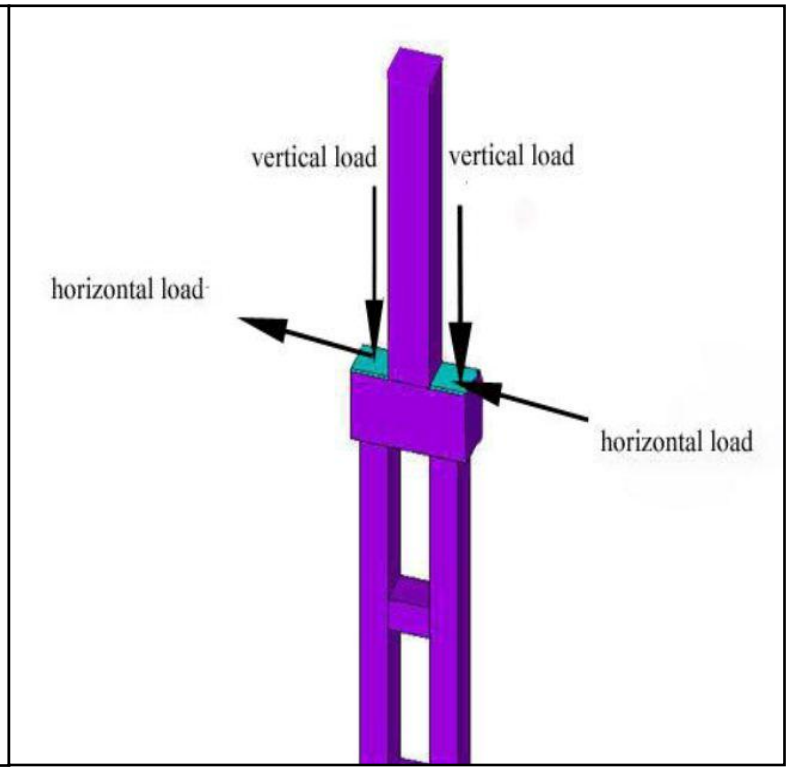

Figure 5. Second load case (C2).

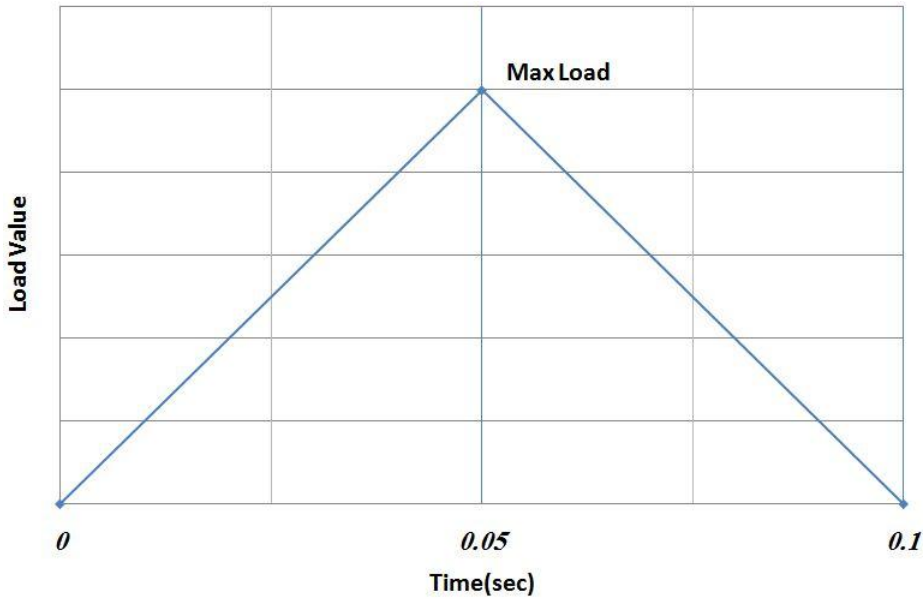

Figure 6. Variation of load with time**.**

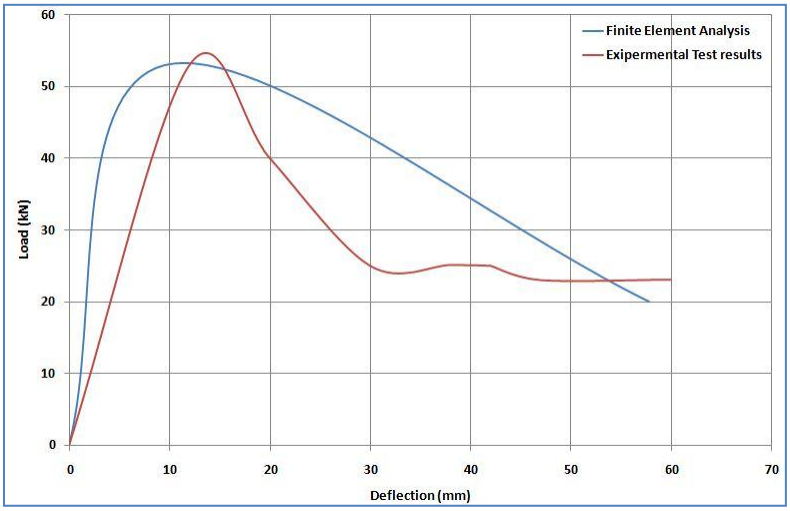

Figure 7. Load-deflection curves for verification example.

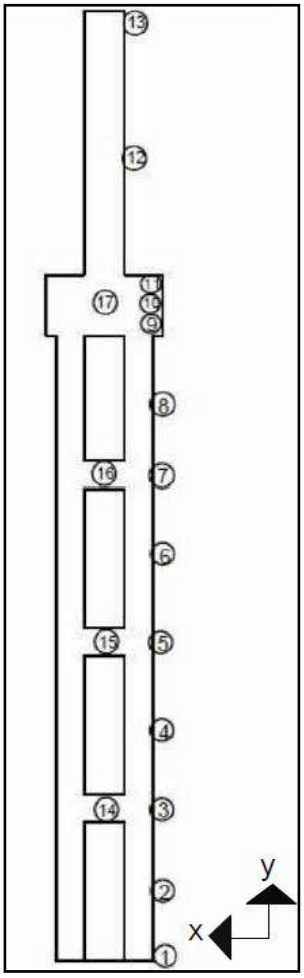

Figure 8. Locations of nodes where the results are recorded.

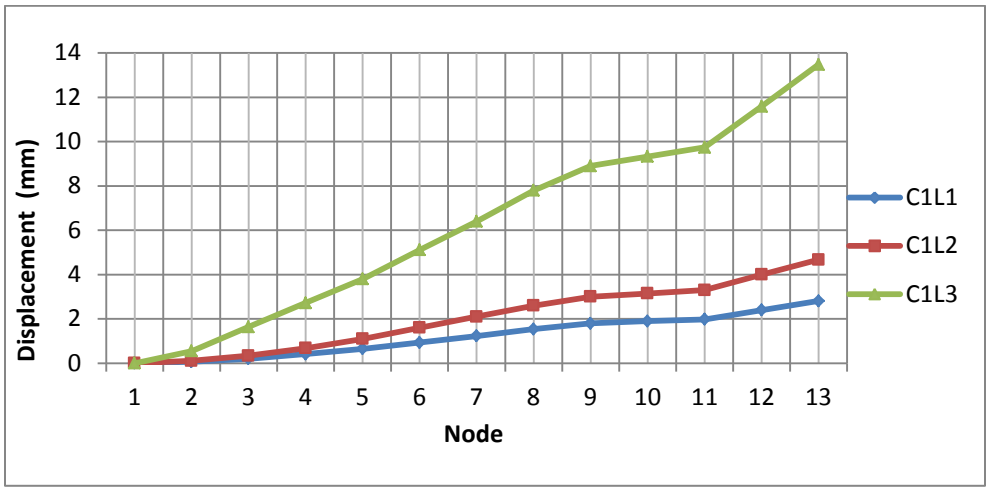

Figure 9. Horizontal displacements along column C1.

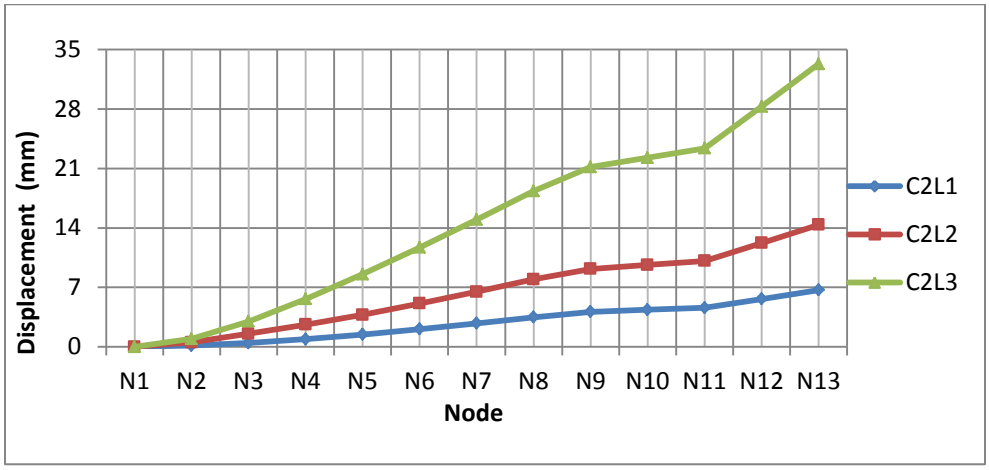

Figure 10. Horizontal displacements along column C2.

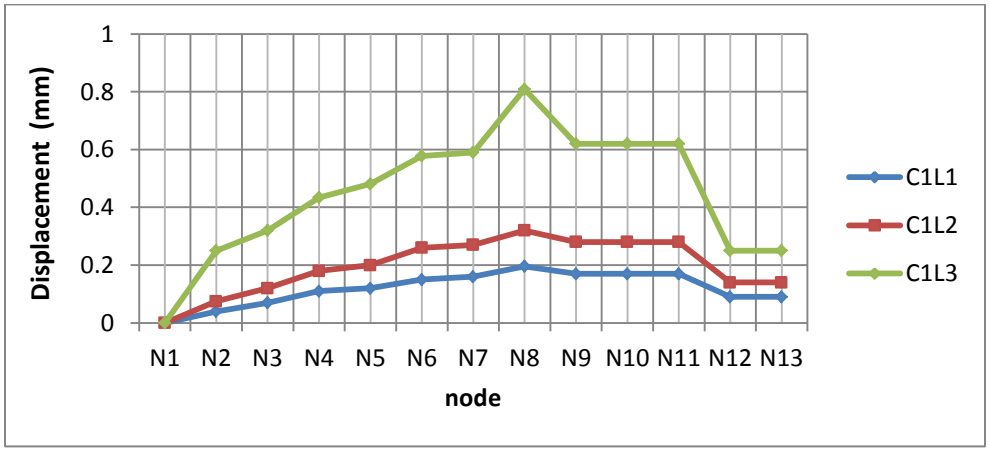

Figure 11. Vertical displacements along column C1.

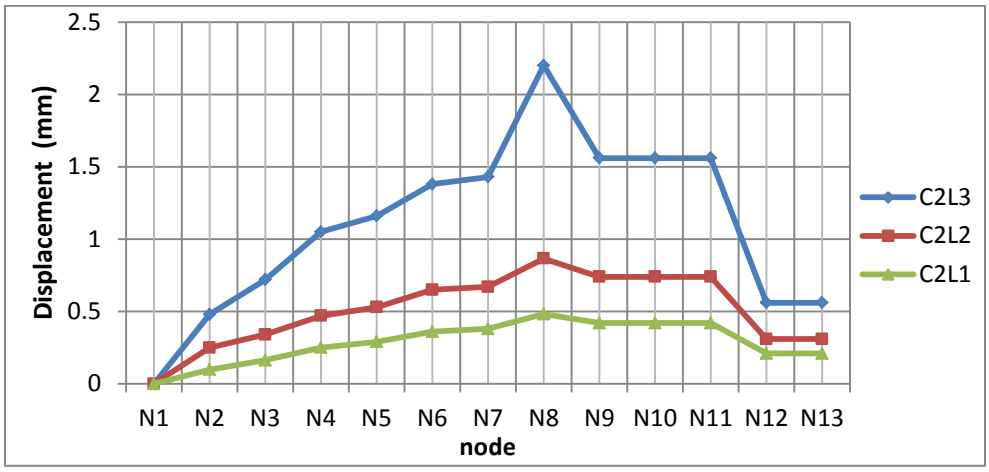

Figure 12. Vertical displacements along column C2.

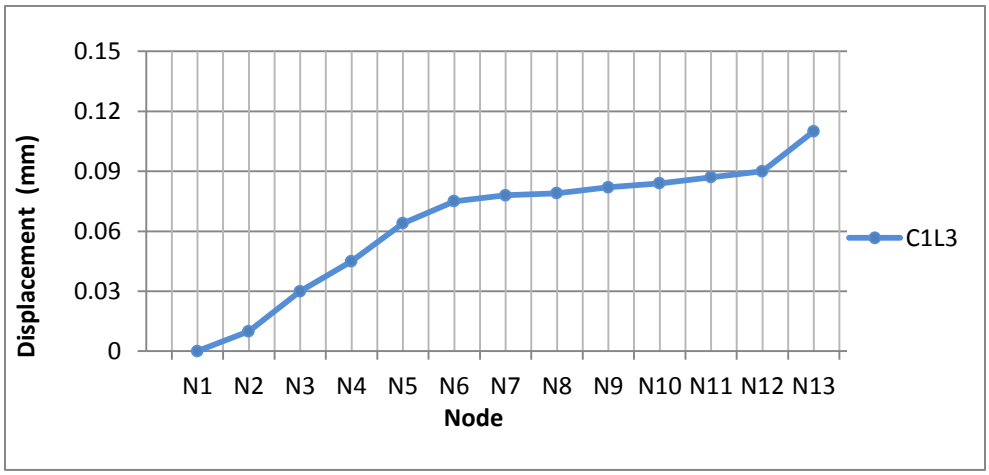

Figure 13. Residual horizontal displacements along column C1

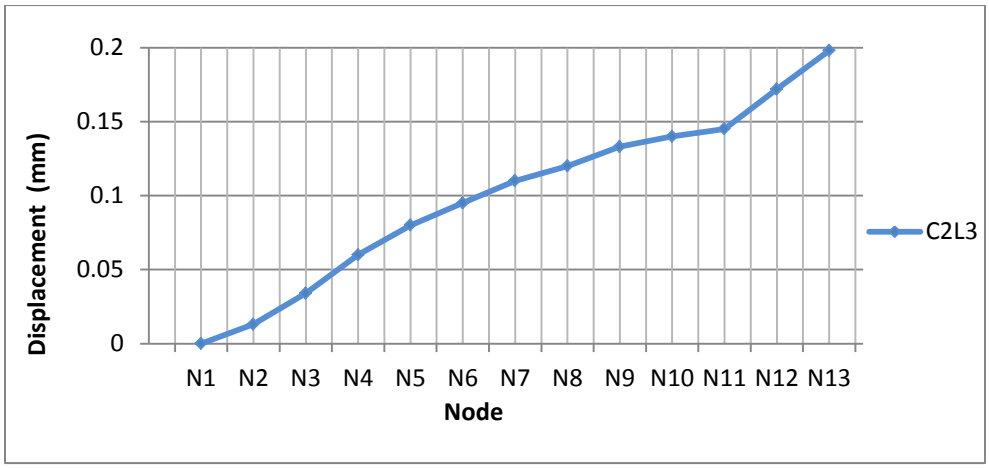

Figure 14. Residual horizontal displacements along column C2.

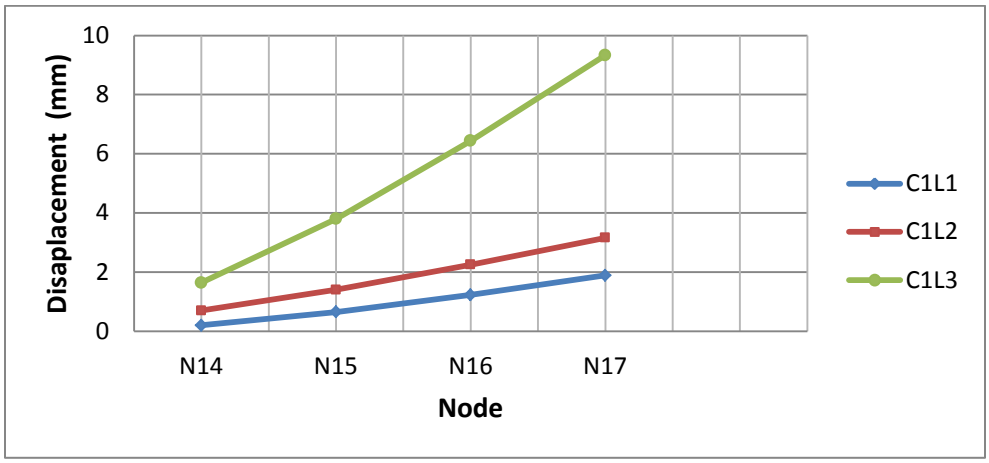

Figure 15. Horizontal displacements at the link between two branches of column C1.

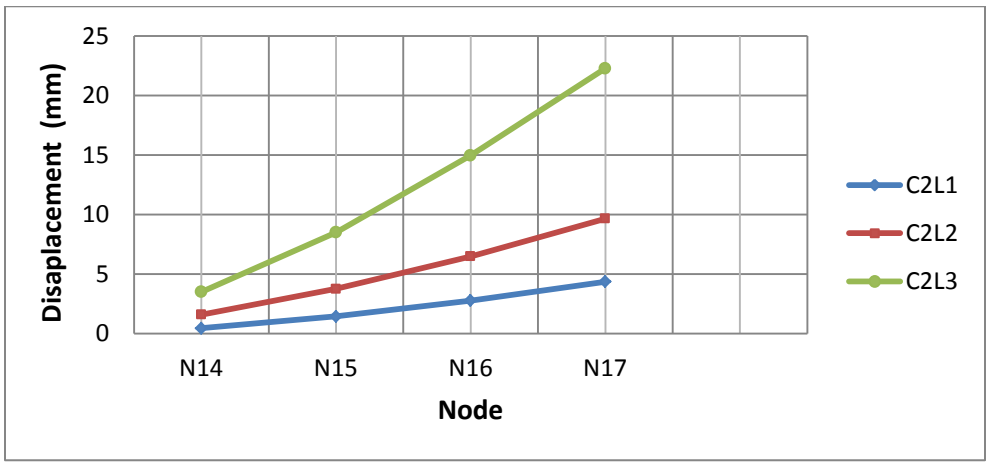

Figure 16. Horizontal displacements at the link between two branches of column C2.

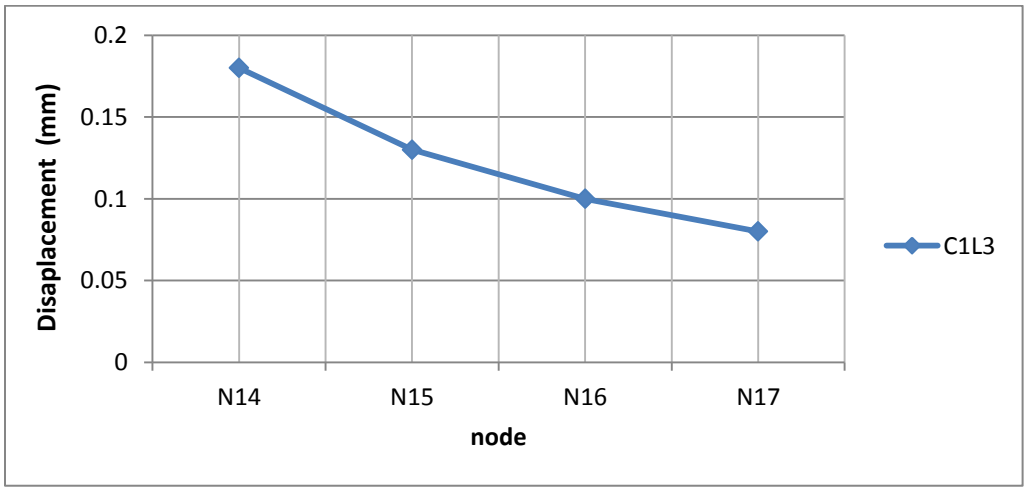

Figure 17. Vertical displacements at the link between two branches of column C1.

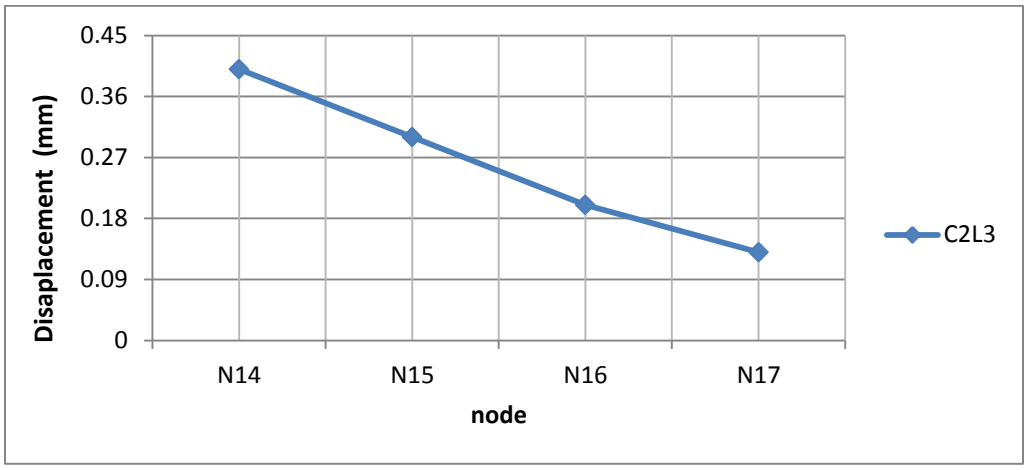

Figure 18 .Vertical displacements at the link between two branches of column for C2.

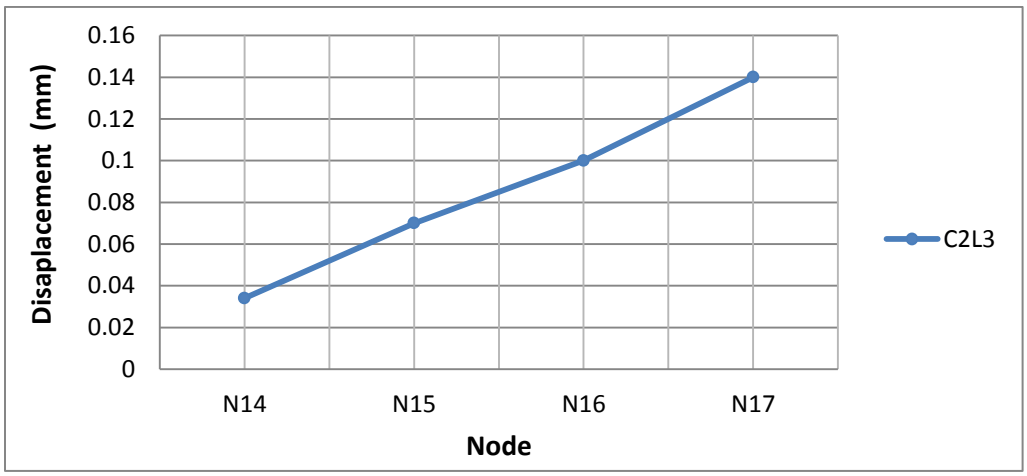

Figure 19. Residual horizontal displacements at the link between two branches of column for C2.

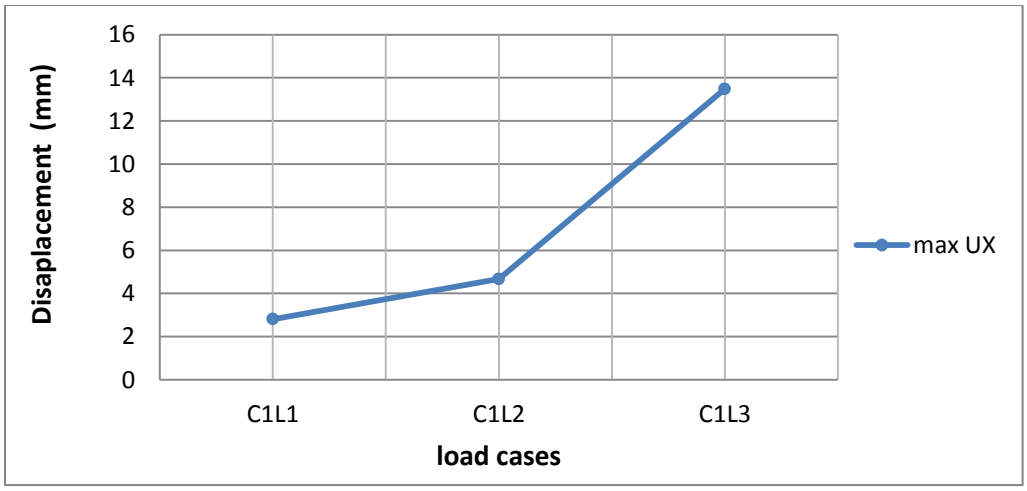

Figure 20. Maximum horizontal displacements at N13 for column C1.

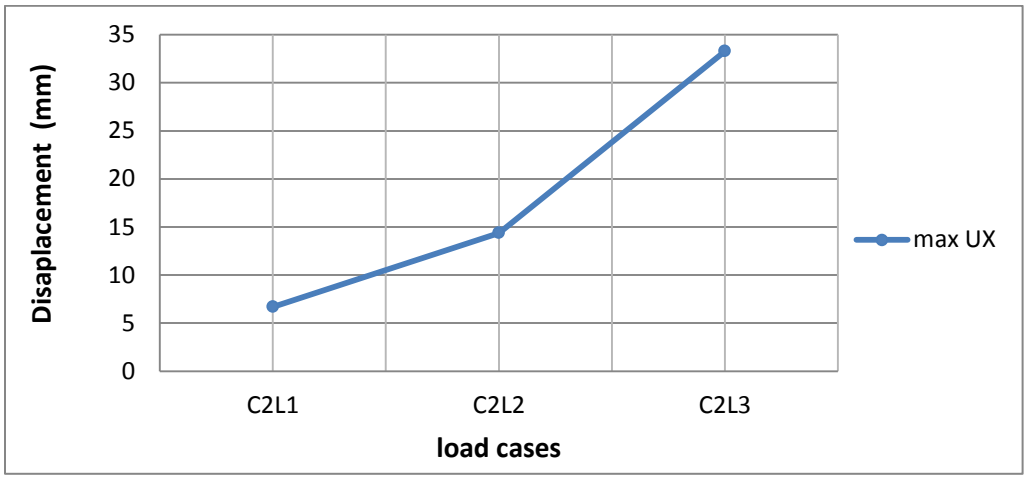

Figure 21. Maximum horizontal displacements at N13 for column C2.

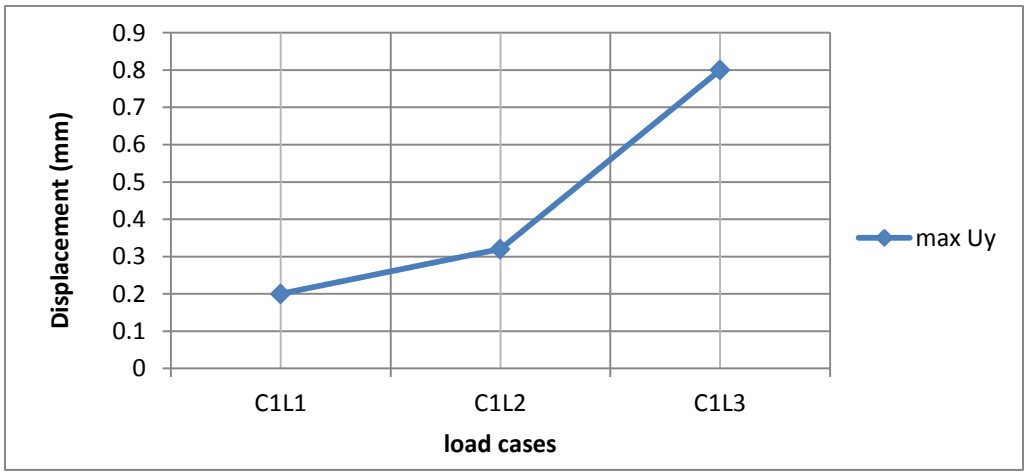

Figure 22. Maximum vertical displacements at N8 for column C1.

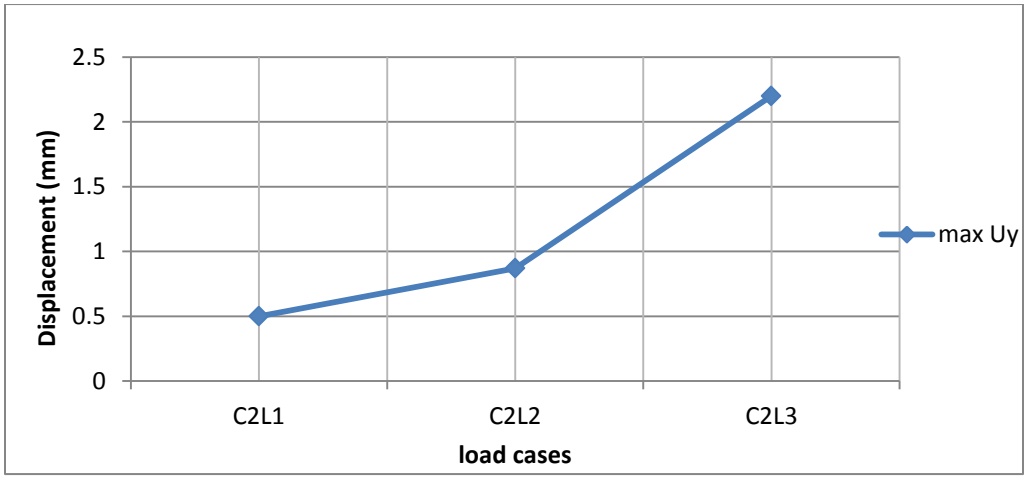

Figure 23. Maximum vertical displacements at N8 for column C2.

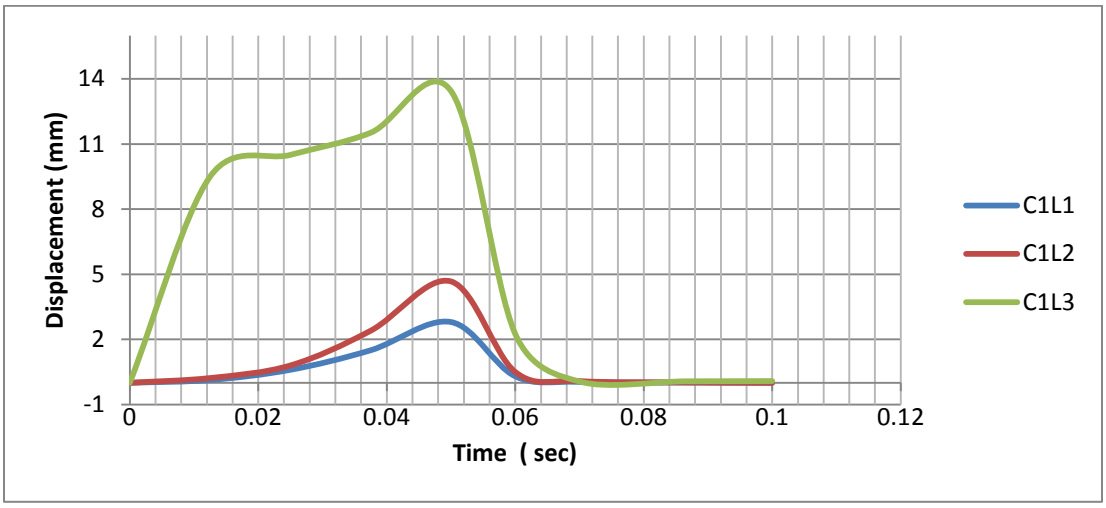

Figure 24. Variation of Ux with time at N13 for column C1.

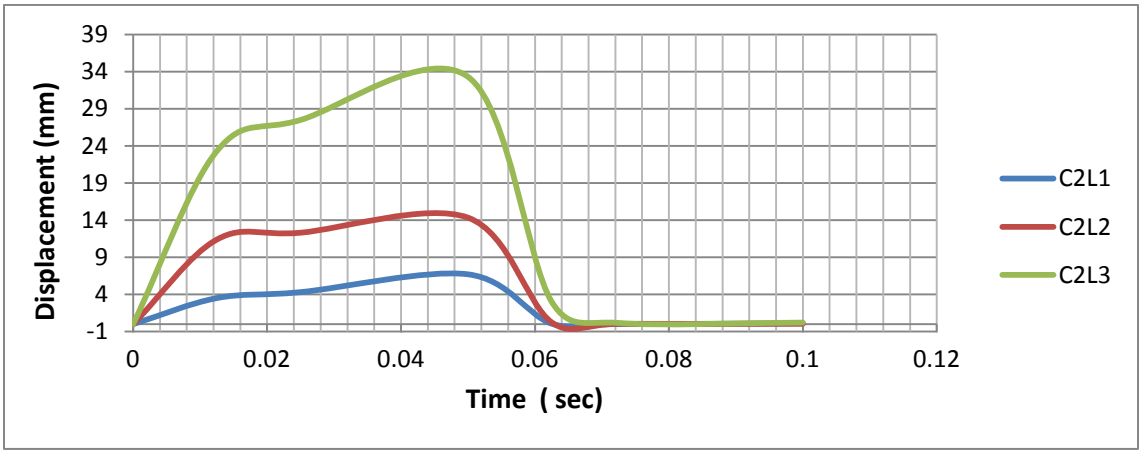

Figure 25. Variation of Ux with time at N13 for column C2.

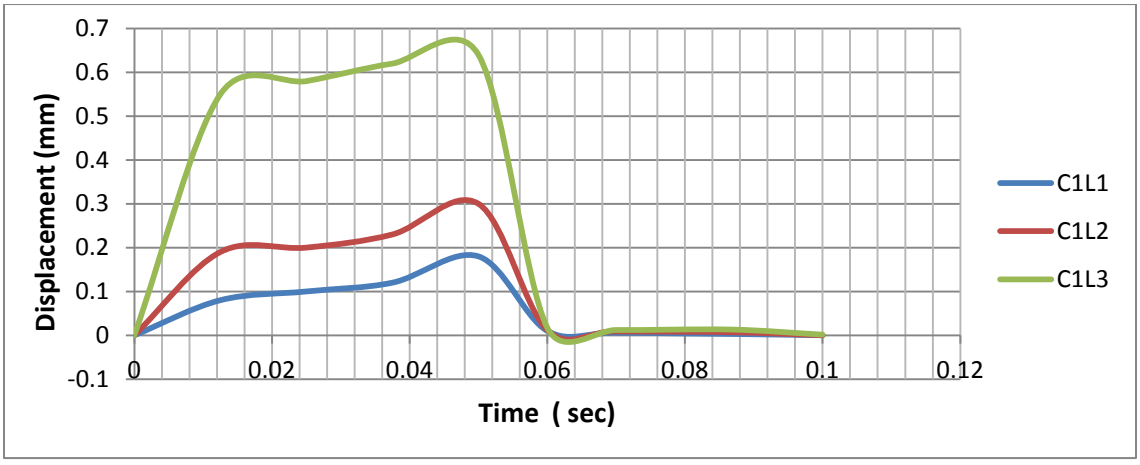

Figure 26. Variation of Uy with time at N8 for column C1.

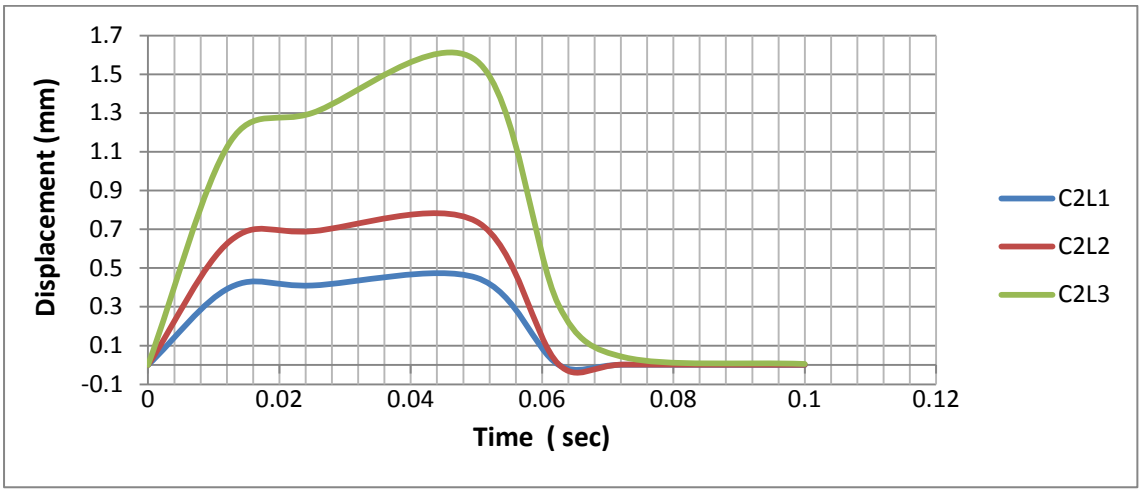

Figure 27 Variation of Uy with time at N8 for column C2.

Effect of Saturation of Sandy Soil on the Displacement Amplitude of Soil Foundation System under Vibration

Prof. Dr. Mosa Jawad Al-Mosawi
Department of Civil Engineering
College of Engineering
University of Baghdad
e-mail: prof_mosa_2006@yahoo.com@yahoo.com

Prof. Dr. Mohammed Yousif Fattah
Building and Construction Department
University of Technology
e-mail:myf_1968@yahoo.com

Lect. Dr. Abbas Fadhil Ibrahim Al-Ameri
Department of Civil Engineering
College of Engineering
University of Baghdad
e-mail: alameri.abbas@gmail.com

ABSTRACT

In this study, the response and behavior of machine foundations resting on dry and saturated sand was investigated experimentally. A physical model was manufactured to simulate steady state harmonic load at different operating frequencies. The effect of relative density, depth of embedment, foundation area as well as the imposed harmonic load was investigated. It was found that the amplitude of displacement of the foundation increases with increasing the amplitude of dynamic force and operating frequency meanwhile it decreases with increasing the relative density of sand, degree of saturation, depth of embedment and contact area of footing. The maximum displacement was noticed at 33.34 to 41.67 Hz. The maximum displacement amplitude response of the foundation resting on dry sand models is more than that on the saturated sand by about 5.0 to 10 %.

Keywords: displacement amplitude, settlement, steady state dynamic, absorbed boundary.

تأثير اشباع التربة الرملية بالماء على الاستجابة الديناميكية للازاحة تحت تأثير احمال الاهتزاز

أ. د. موسى جواد الموسوي
اقسم الهندسة المدنية
كلية الهندسة-جامعة بغداد

أ.د. محمد يوسف فتاح
هندسة البناء والانشاءات
الجامعة التكنولوجية

م.د. عباس فاضل ابراهيم العامري
اقسم الهندسة المدنية
كلية الهندسة-جامعة بغداد

الخلاصة

في هذا البحث، تم عمل دراسة عملية لاستجابة أسس المكائن المعرضة للاهتزازات والمستندة على تربة رملية جافة ومشبعة تماماً بالماء. حيث تم تصنيع أنموذج مختبري لغرض إجراء الدراسة العملية لتسليط الأحمال الحركية ذات النمطِ العمودي المتناسقِ الإهتزاز، وبعدد دورات مختلفة والمسلطة على تربة رملية. وتم دراسة تأثير تغير الكثافة النسبية، عمق الطمر، مساحة الاساس. وُجد ان الازاحات العمودية الحركية تزداد بزيادة ذروة الحمل الحركي وعدد دورات المحرك ووجد أن تلك الإزاحات تقل بزيادة الكثافة النسبية للتربة الرملية، وزيادة عمق طمر الأسس، وزيادة مساحة التلامس بين الاساس والتربة فضلاً عن زيادة درجة التشبع. ووُجد ان اقصى قيمة للإزاحة الشاقولية تكون عند اهتزاز المحرك بتردد يتراوح بين 33.34 الى 41.67 هيرتز. ووُجد أن مقدار الإزاحة الشاقولية للتربة الجافة اكبر من الإزاحة الشاقولية للتربة المشبعة بنسبة 5.0 الى 10.0 %.

الكلمات الرئيسية: سعة الازاحة، الهبوط، الحالة الديناميكية المنتظمة، الحدود الماصة.

1. INTRODUCTION

Machine foundations is regarded as the most important elements of industrial structures like power plants, steel plants, petrochemical complexes, fertilizer plants etc., which consist of a number of reciprocating and centrifugal machines, these play an important part to ensure efficient operation of the process, and that the output of the product is of the required quality, **Chowdhury** and **Dasgupta, 2010**.

The response of soil subjected to dynamic loading depends on many factors such as permeability, relative density, the nature of the dynamic loading, the magnitude and rate of strain, **Daghigh, 1993**.

Kassir et al., 1989, studied the dynamic response of a circular footing experiencing oscillatory vertical motion on the surface of a liquid-filled, porous, elastic half-space. From their theoretical study, it was found that the presence of ground water in the elastic medium affects the magnitude and character of the influence functions over the frequency range of practical interest and should be included in determining the response of surface structures to dynamic loadings.

Al-Homoud and **Al-Maaitah, 1996,** found that there is an increase in natural frequency and a reduction in amplitude with the increase in degree of saturation of sandy soil subjected to vertical forced vibration loading. On the other hand, for free vibration test, the results showed that for different footing models resting on sandy soil, there is an increase in damping ratio with increasing in the degree of saturation. As well as the damping ratio of footing on saturated sand is higher than that on dry sand.

Kim et al., 2001, performed an intensive study for the dynamic analysis for foundations of vibrating equipment. The analysis took into consideration the soil structure interaction. As shown in **Fig. 1**, it was concluded that the dynamic response of foundation with ground water (dash line) is higher than this without the groundwater (solid line) in the lower frequency domain. The amplitude of horizontal vibration is 13.3 μm calculated with groundwater and 4.5 μm calculated without the groundwater at the operating speed of 8.45 Hz.

Livaoglu and Dogangun, 2007, investigated the effect of saturation ratio on shear modulus and damping parameters of sand. It was concluded that the dynamic stiffness and damping characteristic were substantially independent of saturation ratio in the range of 25 to 75%. However, by approaching the full saturation state, the values of modulus fall sharply and damping of loose samples increases dramatically from corresponding values of unsaturated levels.

Al-Shammary, 2013, performed numerical study to investigate the dynamic response of strip footing resting on saturated sandy soil. The numerical study was executed by finite element software, PLAXIS 2D. A parametric study was carried out to evaluate the dependency of machine foundation on various parameters including the amplitude of the dynamic load, the frequency of the dynamic load, the damping of soil mass, the thickness of the foundation, and the embedment of foundation. It was found that the embedment generally leads to a beneficial reduction in dynamic displacement response for all soil types but with different degrees depending on the other parameters such as soil density and damping ratio.

2. RESEARCH OBJECTIVES

The main objectives of this research are to study the effect of steady state harmonic loading on the response of foundation-soil system resting on sandy soil with different saturation conditions. The influence of footing size and depth of embedment would be elaborated in the present research.

3. RESEARCH METHODOLOGY

The present work is aimed to study the behavior of machine foundation resting on dry and saturated sandy soil subjected to vibration dynamic loadings. This research is carried by considering two sizes of rectangular footings. The sizes was (100×200×12.5 mm) and (200×400×5.0 mm) for intermediate to rigid rectangular footings. The footings were placed on sandy soil. The boundary of the problems was achieved experimentally by using nonreflecting boundary materials (styropor cork). The setups of the experimental components are illustrated in **Fig. 2**. The variables that were taken into considerations are:

a) Size of footing,
b) The depth of embedment was studied by placing the footing at the surface and at a depth of 50 mm below the soil surface.
c) The operating frequency was studied at different values starting from 500 to 3500 rpm. The unbalanced weight was not changed throughout the study.
d) The soil was studied for two conditions of saturation, dry and saturated sand.
e) The effect of relative density of the sand was studied. Foundations are rested on sand at loose state (Dr=30 %) and very dense state (Dr=80%).

For all the above-mentioned parameters, the response of the soil-foundation system was evaluated by conducting the following measurements:

- The force-time history of the force applied by the machine on the center of foundation surface.
- The vertical displacement-time history of the footing at one point.
- The vertical total settlement of the footing at the end of machine oscillation was measured at one point.

4. MATERIALS USED IN THE EXPERIMENTS

The physical properties of sand used include specific gravity, grain size distribution and the maximum and minimum dry unit weights of the sand. A summary of the test results with standard specification followed for each test is presented in **Table 1**.

According to the Unified Soil Classification System (USCS), the sand is classified as (SP) and described as poorly graded sand. The material of footing was steel. The initial Young's modulus of the steel used is 140. GPa and the secant modulus is 37.26 GPa. In addition, the unit weight of the steel used is about 77.6 kN/m^3.

5. TESTING PROGRAM AND EXPERIMENTAL WORKS

In general, the testing program consists of two major parts. The first part is devoted to dry sand models with total number of tests of 56. The tests were performed in loose and dense soil state. Two footing sizes and the models were tested at the surface of the footing and at a depth of 5.0 cm. The second part is concerned with saturated sand models with total number of 28 models. The same parameters were taken into consideration except that the models were prepared from dense sand only. The details of abbreviation for the tested samples as well as example of models naming are explained below.

DL1020S: **D**ry **L**oose state sand, footing **10×20** cm, footing placed at the **S**urface.
SD2040E: **S**aturated **D**ense state sand, footing **20×40** cm, footing **E**mbedded

5.1 Testing Program and Experimental Works

A series of model loading tests were conducted inside a rigid steel box of dimensions (1200×1000×600 mm), made of steel plate of 5.0 mm thickness. These dimensions were chosen to satisfy the boundary effects of physical models subjected to dynamic loading. The overall

description of test components and measuring devices is shown in **Fig. 2**. To create a physical model, a small container was manufactured from steel plate. The container, which has the dimensions of (length 1200 mm, width 1000 mm and height 600 mm), was used to prepare the bed of soil. The tested soil is clean sand passing through ASTM standard sieve No. 10 (2.0 mm) and retained on the ASTM standard sieve No. 100 (0.150 mm) to obtain uniform sand.
Two alloy steel model footings of size (200 × 100 × 12.5) mm and (400 × 200 × 5.0) mm were placed centrally over the prepared soil layer, and then a mechanical oscillator was fixed to the footing to act as a single unit. The size of the footing was chosen to obtain intermediate to rigid footing.

In the present model, special boundary conditions were adopted by using cork (styropor) sheets of 30.0 mm thickness. The styropor cork sheets can reduce the slight friction that might be developed between the box faces and soil as well as it works as absorbing boundaries to prevent reflected waves.
Preliminary tests were performed to check the efficiency of such materials as boundary absorbing purposes. This approach was achieved by measuring the dynamic response at the boundaries with and without absorbing layers.

5.2 Sample Preparation

Tamping and pouring procedures were used to prepare the sandy soil inside the steel box. This method was followed to ensure the desired relative density as well as to ensure the same method of sample preparation in loose and dense state. In addition to that, hygroscopic water content (≈ 0.5-3.0%) was added to the sand prior to compaction and pouring to ensure small cementation of soil before testing. This water content is regarded as uncontrolled water content that is always present within the sample without oven drying.
For the loose state sand models, the sample was prepared by pouring the soil inside the box from a certain height. The hygroscopic water content for loose state was about 0.5-1.0%. The suitable height was decided by making a relation between the height of falling and the resulting dry density. It was found that a 30 cm falling height gave the desired value of dry density. For the sake of accuracy and reducing the sources of sample disturbance, the box was divided into sub layers of 50.0 mm. Filling operation throughout the test was performed using galvanized metal hopper with height of 30 cm having a valve to control sand raining by hand. On the other hand, for dense state soil models, hygroscopic water content of (2.0-3.0 %) was added to the sample to ensure compactness and cementation of soil within the model. The box was divided into sub layers of about 50 mm thickness; each layer was compacted using standard hammer.
After sample preparation commenced, the density was checked using sand balloon for field density test according to (ASTM D2167 08) specification. The variation of the resulting density was ±5 %. This variation is considered acceptable.
For preparation of saturated models, the soil was saturated by pouring a known minimum quantity of water that is required for saturation. This quantity of water was calculated from the basic relations in soil mechanics. For achieving permanent saturation of sand, additional water was added to the sample prior to test. Care was taken to ensure that no water could be draining out from the steel box.

5.3 Description of the Vibratory Machine

The model machine of the mechanical oscillator used in this study is shown in **Fig. 3.a**. The mechanical oscillator consists of a rotating disc manufactured from steel with diameter (54.0) mm and thickness (5.1) mm. A single mass (m_e) is placed on the rotating disc at an eccentricity

of (22.0) mm from the axis of rotation. This arrangement rotates in one direction when it is driven through a shaft by an AC motor having a maximum rated speed of up to 3500 rpm. Such an arrangement induces a vibratory force at the base of the oscillator. This vibratory force can be estimated from Eq. (1).
The basic principle of this device can be found in different textbooks such as **Bhatia, 2009**. Depending on the orientation of the counter-rotating shaft, a vertical dynamic force can be applied. The amplitude of vertical force produced (F_o) is:

$$F_o = m_e\, e\, \omega_r^2 \qquad \textbf{(1)}$$

where:
ω_r is the circular operating frequency of the machine,
e is the eccentric distance from the shaft to the unbalanced mass m_e, and
m_e is the unbalanced mass.
For this type of oscillator, the function of the harmonic vertical mode of vibration is sinusoidal. Therefore, the applied dynamic force F (t), at any time (t) is given by:

$$F\,(t) = F_o \sin \omega_r t = m_e\, e\, \omega_r^2 \sin \omega_r t \qquad \textbf{(2)}$$

In this research, a special AC Drive was used to control the speed of rotation. Calibration of this device with Tachometer was done to check the accuracy of the AC Drive. By varying the voltage supplied to the motor with the aid of the speed AC Drive, the speed of the motor and hence the oscillator can be varied which, in turn, causes a change in frequency of vibration induced by the oscillator.

5.4 Dynamic Load Measurement (F-t History)

For measuring the vibration force, a dynamic load cell was used specially for this purpose. The dynamic load cell was MLC215C-3T supported with MEP105A weighing indicator shown in **Fig. 3.b**, **Manyyear Technology Company Limited, 2011**. For obtaining high sensitivity of readings, the output lead wires of the dynamic load cell were connected to the Vishay Digital Strain Indicator that was provided with an analog output. The output signal from the strain indicator was captured by using a digital storage oscilloscope **TWINTEX (TSO 1202, 200MHz)** and then connected to data acquisition system by laptop computer device as shown in **Fig. 2**. The operation of storage type oscilloscope was enhanced with computer interface system that makes it more familiar to the computer uses, **Oscilloscope User Manual, 2011**.

5.5 Measurement of the Amplitude of Footing Displacement

The vertical amplitude of footing (Az) was measured at the surface of the footing. Vibration meter (**HG 6360**) of one channel was used in the test. This vibration meter has a working capacity of 0.001 to 4.0 mm, it is capable of measuring the displacement, velocity, and acceleration of motion depending on the function set prior to the test, **Operation Manual, 2011**. In addition, all the collected data can be transferred to the computer easily through built in software. During the tests, one vibration meter was used on the surface of the footing. The components of the HG 6360 vibration meter are shown in **Fig. 4**. The vibration meter within the testing models is shown in **Fig. 2**.

6. EXPERIMENTAL TEST RESULTS AND DISCUSSION

The displacement amplitude of footing (Az) was measured for all the tested models. The displacement was measured by using vibration meter. This device is used with computer interface software. The data can be directly taken from the software or it can be taken as displacement amplitude-time history (Az-t).

The test results of the displacement amplitude with time are obtained during tests, it was found that the trend of the test results is not unique for all the tests. This may be attributed to the test conditions and the dynamic response of soil. In addition, this trend is clear for the loose state models, while for dense state, the trend seems to be unique for all the tested models.

In most engineering practice, it is always desirable to get the maximum displacement amplitude of motion. Hence, the maximum values are picked up and presented in **Fig. 5 and Fig. 6**, and summarized in **Table 2.**

It can be seen that the displacement amplitude (Az) for dry dense sand models is less than that of dry loose sand models. For footing placed at the surface, the ratio of dense sand models amplitude to loose sand models is ranging from (0.27 to 1.00) and (0.03 to 0.94) for footing size (100×200 mm) and (200×400 mm), respectively. Meanwhile, for embedded footings this ratio becomes (0.24 to 0.99) and (0.10 to 0.97) for footing size (100×200 mm) and (200×400 mm), respectively. These results are attributed to the increase in the stiffness and the modulus of elasticity of dense sandy soil that makes the soil stiffer and resist vibrations as well as to it could be attributed to the trench and sidewall effects.

The displacement amplitude (Az) of the footing size (200×400 mm) is less than that of footing of size (100×200 mm). This is true for all dry models except model for dry loose sand and some of the saturated sand models. As can be seen, for dry loose sand models, the ratio between footing size (100×200 mm) to footing size (200×400 mm) is ranging from (1.29 to 1.75) and (1.12 to 4.79) for footing placed at the surface and embedded, respectively. On the other hand, for dry dense sand the ratio becomes (1.00 to 10.83) and (1.50 to 10.91) for footing placed on the surface and embedded, respectively. Meanwhile, for saturated dense sand, the rate of reduction reduces and goes from (1.10 to 3.61) for footing placed on the surface, while the behavior of embedded footing in saturated dense sand seems to have opposite behavior to the aforementioned trend. The reduction in response for large contact area is attributed to the reduction in the stresses due to large contact area.

On the other hand, the displacement amplitude (Az) of saturated soil samples exhibits the same resonance frequency, except for sample of footing size (200×400 mm) and embedded at 5.0 cm. This is due to the presence of water within the soil particles that may require high frequency to produce resonance phenomenon.

7. SUMMARY AND CONCLUSIONS

From the discussions carried out in the previous sections and other observations made during the experimental approach, the following conclusions are made.

- For dry and saturated conditions, the maximum amplitude of displacement decreases with increasing the relative density of sand and contact area of footing and increase with increasing the amplitude of loading. The maximum displacement amplitude response of the foundation resting on dry sand models is more than that on the saturated sand by about 5.0 to 10 %. The maximum displacement amplitude of footing is reduced to half when the size of footing increases to double for dry and saturated sand. The percentage of reduction in dry sand is more than that of saturated sand.

- The general response of the force-time history relationship possesses erratic distribution (fluctuated) at low operating speed, meanwhile for high operating speed (> 3000 rpm), the relationship exhibits sine wave trend.
- The embedment of footing in sandy soils leads to beneficial reduction in dynamic displacement response for all soil types in different percentages accompanied by an increase in soil strength.
- The maximum displacement amplitude exhibits its maximum value at the resonance frequency, which is found to be about 33.34 to 41.67 Hz.
- The maximum amplitude of displacement of saturated medium dense sand is less than that of loose sand. This means that the maximum displacement increases with decrease in the modulus of elasticity as well as the smaller the modulus is, the quicker the development of liquefaction zone.
- The displacement amplitude of saturated loose sand is greater than that of the dry sand especially when the frequency is greater than the resonance frequency.
- The amplitude of displacement of saturated sand models is slightly greater than that of the dry models. This is mainly attributed to the effect of water that may restrict the movement of soil particles during vibrations.

REFERENCES

- Al-Homoud, A. S. and Al-Maaitah, O. N., 1996, *An Experimental Investigation of Vertical Vibration of Model Footings on Sand*, Soil Dynamics and Earthquake Engineering, 15, No. 7, pp. 431-445.

- Al-Shammary, W. T. S., 2013, *Numerical Analysis of Machine Foundation on Saturated Sandy Soil*, M.Sc. Thesis, Building and Construction Engineering Department, University of Technology, Iraq.

- American Society of Testing and Materials (ASTM), 2006, *Standard test method for specific gravity of soil solids by water pycnometer*, ASTM D854, West Conshohocken, Pennsylvania, USA

- American Society of Testing and Materials (ASTM), 2006, *Standard Test Method for Particle Size-Analysis of Soils*, ASTM D422-63 (2002), West Conshohocken, Pennsylvania, USA

- American Society of Testing and Materials (ASTM), 2006, *Standard Test Method for Maximum Index Density and Unit Weight of Soils Using a Vibratory Table*, ASTM D4253-00 (2006), West Conshohocken, Pennsylvania, USA

- American Society of Testing and Materials (ASTM), 2006, *Standard Test Method for Minimum Index Density and Unit Weight of Soils and Calculation of Relative Density*, ASTM D4254-00 (2006), West Conshohocken, Pennsylvania, USA

- American Society of Testing and Materials (ASTM), 2006, *Standard Test Method for Direct Shear Test of Soils Under Consolidated Drained Conditions*, ASTM D3040-04, West Conshohocken, Pennsylvania, USA

- American Society of Testing and Materials (ASTM), 2006, *Standard Test Method for Density and Unit Weight of Soil in Place by the Rubber Balloon Method*, ASTM D2167-01 (2004), West Conshohocken, Pennsylvania, USA

- American Society of Testing and Materials (ASTM), 2006, *Standard Test Method for Unconsolidated-Undrained Triaxial Compression Test on Cohesive Soils*, ASTM D2850-03a, West Conshohocken, Pennsylvania, USA

- American Society of Testing and Materials (ASTM), 2006, *Standard Test Method for Permeability of Granular Soils (Constant Head)*, ASTM D2434-68, West Conshohocken, Pennsylvania, USA

- American Society of Testing and Materials (ASTM), 2006, *Standard Test Method for Classification of Soils for Engineering Purposes (Unified Soil Classification System)*, ASTM D2487-06, West Conshohocken, Pennsylvania, USA

- Bhatia, K., 2009, *Foundations for Industrial Machines: Handbook for Practicing Engineers*, CRC.

- Chowdhury, I. and Dasgupta, S. P., 2010, *Dynamics of Structure and Foundations-A Unified Approach: 2. Applications*, CRC Press.

- Daghigh, Y., 1993, *Numerical Simulation of Dynamic Behavior of an Earth Dam during Seismic Loading*, Ph.D. Thesis, Delft University of Technology, Netherlands.

- Kassir, M., Bandyopadhyay, K. and Xu, J., 1989, *Vertical Vibration of A Circular Footing on A Saturated Half-Space*, International Journal of Engineering Science, 27, No. (4), pp. 353-361.

- Kim, Y.-S., Miura, K., Miura, S. and Nishimura, M., 2001, *Vibration Characteristics of Rigid Body Placed on Sand Ground*, Soil Dynamics and Earthquake Engineering, 21, No. (1), pp. 19-37.

- Livaoglu, R. and Dogangun, A., 2007, *Effect of Foundation Embedment on Seismic Behavior of Elevated Tanks Considering Fluid–Structure-Soil*

Interaction, Soil Dynamics and Earthquake Engineering, 27, No. (9), pp. 855-863.

- Manyyear Technology Company Ltd., 2010, *www.manyyear.com*.

- Operation Manual, 2011, *Digital Vibration Meter Model HG 6360*, HUATEC Co., Ltd , www.huatecgroup.com

- User Manual, 2011, *Digital Storage Oscilloscope TSO-1202 Series Version No.: V1.6*, Twintex Electronics Co., Ltd , www.twintex.com.tw

NOMENCLATURE

Symbol	Meaning
ADS	data acquisition system
ASTM	american Society for Testing and Materials
Az	vertical displacement amplitude (mm)
Az-t	displacement Amplitude-Time History
Cc	coefficient of curvature
cps	cycle per second (Hz)
Cu	uniformity coefficient
D_{10}	diameter corresponding to percent passing of 10 % (mm)
D_{30}	diameter corresponding to percent passing of 30 % (mm)
D_{60}	diameter corresponding to percent passing of 60 % (mm)
DD1020E	dry dense soil supporting rectangular footing of 10×20 cm and embedded 5 cm in soil
DD1020S	dry dense soil supporting rectangular footing of 10×20 cm placed at the surface
DD2040E	dry dense soil supporting rectangular footing of 20×40 cm and embedded 5 cm in soil
DD2040S	dry dense soil supporting rectangular footing of 20×40 cm placed at the surface
DL1020E	dry loose soil supporting rectangular footing of 10×20 cm and embedded 5 cm in soil
DL1020S	dry dense soil supporting rectangular footing of 20×40 cm placed at the surface
DL2040E	dry loose soil supporting rectangular footing of 20×40 cm and embedded 5 cm in soil
DL2040S	dry loose soil supporting rectangular footing of 10×20 cm placed at the surface
Dr	relative density
e	eccentric distance from the shaft to the unbalanced mass m_e
e_{max}	maximum void ratio
e_{min}	minimum void ratio
F_o	amplitude of dynamic force (N)
F_t	transition surface (N)
F-t	force-time history
Gs	specific gravity

Symbol	Meaning
k	coefficient of Permeability (m/min)
LVDT	linear Variable Differential Transformer
m_e	eccentric mass in the manufactured machine (kg)
rpm	radian per minute
SD1020E	saturated dense soil supporting rectangular footing of 10×20 cm and embedded 5 cm within soil
SD1020S	saturated dense soil supporting rectangular footing of 10×20 cm placed at the surface
SD2040E	saturated dense soil supporting rectangular footing of 20×40 cm and embedded 5 cm within soil
SD2040S	saturated dense soil supporting rectangular footing of 20×40 cm placed at the surface
S_t	total settlement (mm)
STO	storage Types Oscilloscope
USCS	unified Soil Classification System
ϕ	angle of internal friction
γ_{dmax}	maximum dry unit weight (kN/m^3)
γ_{dmin}	minimum dry unit weight (kN/m^3)
ω_r	circular frequency of the system (rpm)

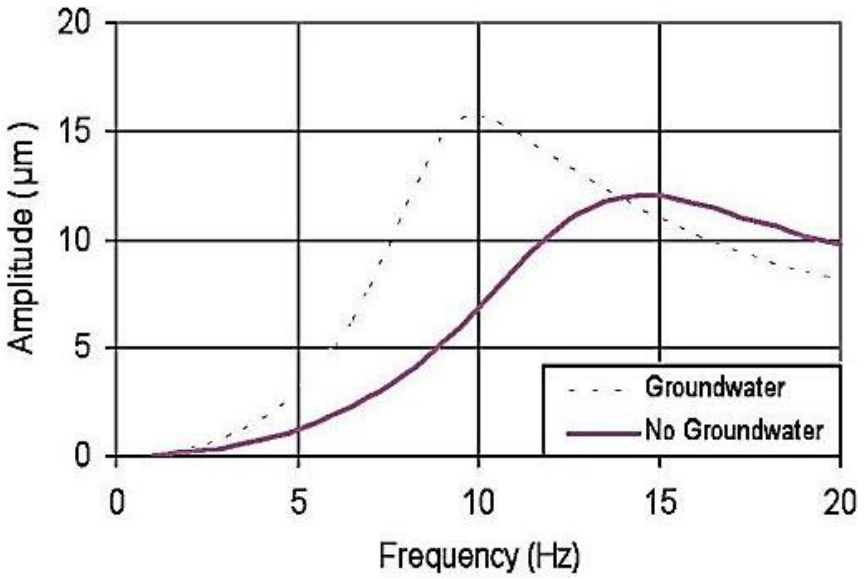

Figure 1. Effect of groundwater on dynamic response of pump foundation ,**after Kim et al., 2001**.

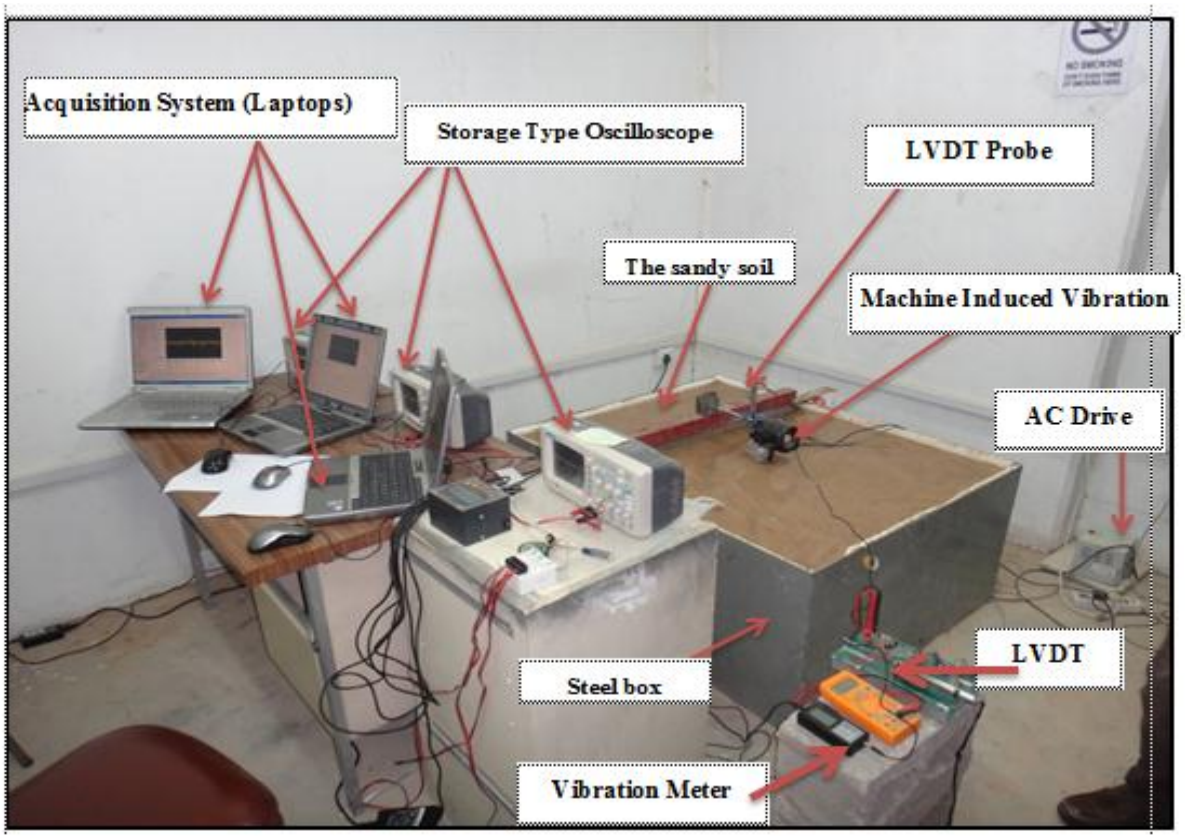

Figure 2. General view of the testing models and instruments.

Table 1. Physical and mechanical properties of the used sand.

Property			Value	Standard of the test
Specific gravity, Gs			2.65	ASTM D 854
Gravel (> 4.75 mm) %			0	ASTM D 422 and ASTM D 2487
Sand (0.075-4.75 mm)%			96	
Silt and clay (< 0.075 mm)%			4	
Coefficient of curvature, Cc			1.55	
Coefficient of uniformity, Cu			1.73	
D_{10}, D_{30}, D_{60} (mm)			0.11, 0.18, 0.19	
USCS-soil type			SP	
Dense state relative density, Dr, %			80.0	
Loose state relative density, Dr, %			30.0	
Maximum dry unit weight, γ_{dmax}, kN/m^3			18.2	ASTM D 4253-00
Minimum dry unit weight, γ_{dmin}, kN/m^3			14.3	ASTM D 4254-00
Dry unit weight in loose state (Used), kN/m^3			15.4	------
Dry unit weight in dense state (Used), kN/m^3			17.3	------
Angle of internal friction , ϕ	Loose state (30%)	Dry	28.0	ASTM D 3080
		Soaked	26.0	
	Dense state (80%)	Dry	40.0	
		Soaked	36.0	
Coefficient of permeability, k, m/sec		Loose state (30%)	0.0360	ASTM D2434-68
		Dense state (80%)	0.0065	

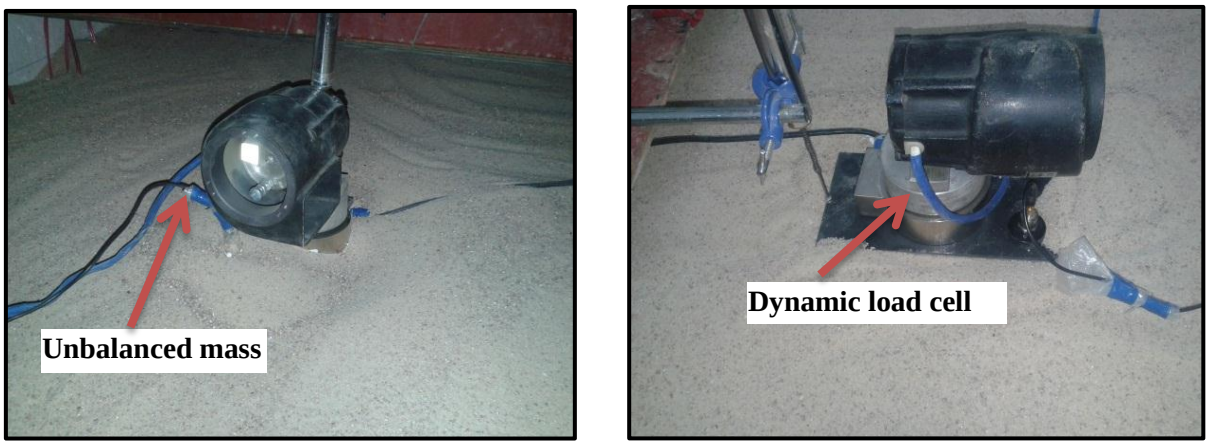

a) Machine for inducing vibration b) Location of the dynamic load cell

Figure 3. Equipment for inducing vibratory dynamic load.

Figure 4. HG 6360 vibration meter and its components.

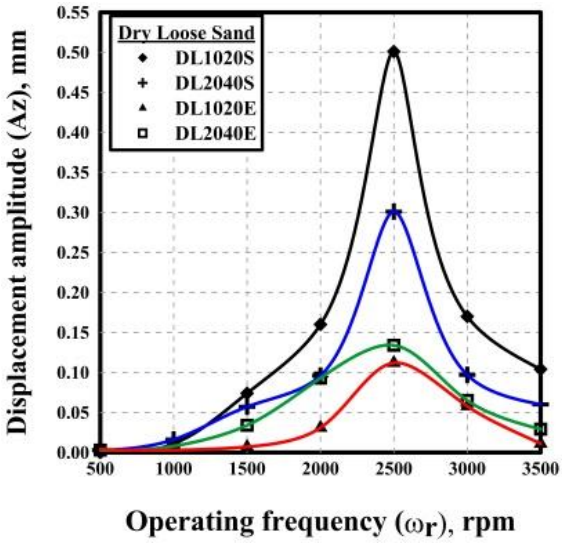

Figure 5. The maximum displacement amplitude versus operating frequency for dry loose sand models.

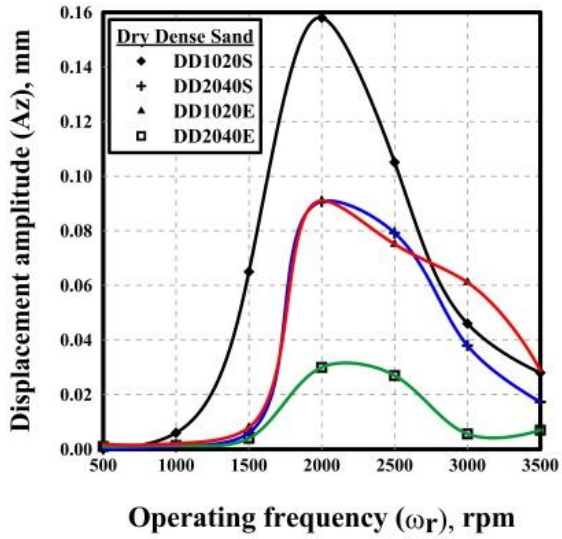

Figure 6. The maximum displacement amplitude versus operating frequency for dry dense sand models.

Table 2. Displacement amplitude for different test conditions from experimental tests.

Test No.	Test Condition	Operating Frequency, ω_r rpm	Az, mm	S_t, mm
1	**DL1020S**	500	0.0001	0.01
2		1000	0.0111	3.00
3		1500	0.0740	7.00
4		2000	0.1600	8.35
5		2500	0.5010	13.00
6		3000	0.1700	21.00
7		3500	0.1040	25.00
8	**DL2040S**	500	0.0030	0.00
9		1000	0.0162	0.30
10		1500	0.0572	0.80
11		2000	0.0961	1.55
12		2500	0.3010	2.15
13		3000	0.0970	3.60
14		3500	0.0601	7.00
15	**DL1020E**	500	0.0030	0.00

Test No.	Test Condition	Operating Frequency, ω_r rpm	Az, mm	S_t, mm
16		1000	0.0081	0.20
17		1500	0.0340	0.75
18		2000	0.0930	4.20
19		2500	0.1340	5.95
20		3000	0.0651	8.50
21		3500	0.0292	12.00
22	**DL2040E**	500	0.0040	0.05
23		1000	0.0030	0.10
24		1500	0.0071	0.10
25		2000	0.0310	1.10
26		2500	0.1120	1.70
27		3000	0.0580	2.55
28		3500	0.0110	5.45
29	**DD1020S**	500	0.0001	0.00
30		1000	0.0060	0.06
31		1500	0.0650	0.70
32		2000	0.1580	0.90
33		2500	0.1510	1.00
34		3000	0.0460	2.00
35		3500	0.0280	4.00
36	**DD2040S**	500	0.0001	0.00
37		1000	0.0010	0.05
38		1500	0.0060	0.10
39		2000	0.0907	0.60
40		2500	0.0792	0.70
41		3000	0.0380	0.75
42		3500	0.0173	0.90
43	**DD1020E**	500	0.0020	0.00
44		1000	0.0021	0.05
45		1500	0.0080	0.08
46		2000	0.0910	0.50
47		2500	0.0751	0.30
48		3000	0.0611	0.40

Test No.	Test Condition	Operating Frequency, ω_r rpm	Az, mm	S_t, mm
49		3500	0.0288	1.10
50	**DD2040E**	500	0.0010	0.00
51		1000	0.0014	0.00
52		1500	0.0040	0.00
53		2000	0.0300	0.05
54		2500	0.0270	0.10
55		3000	0.0056	0.15
56		3500	0.0070	0.25
57	**SD1020S**	500	0.0011	0.05
58		1000	0.0020	0.60
59		1500	0.0650	3.25
60		2000	0.3820	5.50
61		2500	0.1482	10.10
62		3000	0.0910	13.00
63		3500	0.0783	20.95
64	**SD2040S**	500	0.0010	0.05
65		1000	0.0033	-0.05
66		1500	0.0180	0.45
67		2000	0.2120	1.35
68		2500	0.0980	2.35
69		3000	0.0800	3.15
70		3500	0.0230	4.95
71	**SD1020E**	500	0.0250	0.10
72		1000	0.0411	0.50
73		1500	0.0940	0.85
74		2000	0.2780	0.90
75		2500	0.1802	2.25
76		3000	0.0480	4.75
77		3500	0.0250	7.00
78	**SD2040E**	500	0.0082	0.05
79		1000	0.0090	0.00
80		1500	0.0044	0.05
81		2000	0.2008	0.10

Test No.	Test Condition	Operating Frequency, ω_r rpm	Az, mm	S_t, mm
82		2500	0.2880	0.50
83		3000	0.0890	0.55
84		3500	0.0640	0.85

Unit Price and Cost Estimation Equations through Items Percentage of Construction Works in a Desert Area

Dr. Kadhim Raheem
Instructor
Department of Civil Engineering
University of Baghdad
Kadhim1969@yahoo.com

ABSTRACT

This research will cover different aspects of estimating process of construction work in a desert area. The inherent difficulties which accompany the cost estimating of the construction works in desert environment in a developing country, will stem from the limited information available, resources scarcity, low level of skilled workers, the prevailing severe weather conditions and many others, which definitely don't provide a fair, reliable and accurate estimation. This study tries to present unit price to estimate the cost in preliminary phase of a project. Estimations are supported by developing mathematical equations based on the historical data of maintenance, new construction of managerial and school projects. Meanwhile, the research has determined the percentage of project items, in such a remote environment. Estimation equations suitable for remote areas have been formulated. Moreover, a procedure for unite price calculation is concluded.

Key words : unit price, cost estimating, desert, items percentage

تخمين كلف الفقرات الانشائية ونسبها ومعادلاتها في المناطق الصحراوية

م. د. كاظم رحيم
قسم الهندسة المدنية-جامعة بغداد

الخلاصة

يغطي هذه البحث أوجه تقدير المختلفة لأعمال الانشاء في المناطق الصحراوية. يرافق تقدير كلفة الاعمال الانشائية في البيئة الصحراوية للبلدان النامية العديد من الصعوبات التي تنبع من محدودية المعلومات المتاحة وندرة الموارد، وانخفاض مستوى العمال الماهرين وسوء الاحوال الجوية وغيرها التي لا توفر بصورة جيدة تخمين عادل وموثوق ودقيق. حاول البحث تحديد أسعار الوحدات لتقدير التكاليف في المرحلة الأولية للمشروع . عملية التخمين دعمت بواسطة معادلات رياضية مطورة تستند على البيانات التاريخية للصيانة وإنشاءات جديدة لمشاريع ادارية ومدارس ولأربعة انواع من المشاريع. وفي الوقت نفسه، حدد البحث النسبة المئوية لفقرات فقرات المشروع، في مثل هذه البيئة النائية. حيث تم اشتقاق المعادلات الملائمة لعملية التخمين ، فضلا عن تحديد الاسعار لأغراض التخمين عى اساس الوحدة.

الكلمات الرئيسية: سعر الوحدة، تخمين الكلفه، المناطق الصحراويه، نسب الفقرات.

1. INTRODUCTION

Today's construction projects management faces many challenges due to the increased complexity and diversity of projects executive techniques, the need for huge verification of construction materials requires, updating of equipment and automation, computerization technique and management information systems. The need for continuous control on project costs to satisfy client's targets, gives rise to search for new concepts in estimating costs of construction items accompanying the completion of the design stage. The cost estimating before the design completion is called "Approximate cost" or "rough cost" which is less accurate than cost estimating after the detailed design. **Dutta, 2005**.

The successful estimating process essentially depends upon estimator's experience, and acquaintance with achieving an accurate cost estimate; which surly is not so much different from actual cost later, **Buchan, et al., 2006**. There is no denying the historical cost of previous projects or records will be used throughout the decision making phase that is related to feasibility to proceed adopting the execution of construction project or not. It becomes urgent to make the right decision because it gives the client an idea or indicators of cost level to make him capable of studying and examine carefully the financial situation. Meanwhile such an estimate will help in achieving the balance sheet especially for governmental projects, where some decisions are essential and urgent after completing the design; therefore the estimation of a project cost must be calculated effectively and efficiently, **Callahan, et al., 2007**. However, although the successful estimating process depends substantially upon estimator's experience, and familiarity with market, also the use of more real predication of material prices and production rates to get rather an accurate cost estimate, will make the estimation of cost not much different from actual cost later. Therefore the historical data of costs of previous project is represented as backbone of successful estimation of cost in addition to normal estimating techniques. **Mubarak S., 2010.**

2. RESEARCH OBJECTIVES

This research aims to prepare a practical approach to estimating the cost of projects in the desert area by submitting a price indexes and estimating equations supported by percentage of items to make the executive priority.

3. RESEARCH HYPOTHESIS

Research hypothesis focuses on the problems that are encountered in the construction projects of desert area in cost limitation especially in the first stages of the construction project work. This problem becomes clear when the execution begins, most of the problems appear when planning and execution interfere with each other. The resulting weakness in the project cost limitation is the result of price iteration, the emergency conditions and the materials ensuring. By ensuring the optimal limitation of cost of the project, the planner can optimally control the project activities costs.

3. RESEARCH METHODOLOGY

The research mythology will consist of the following steps:

1- Literature survey to review the familiar cost estimation types. The ratio of construction items and the suitable mathematical tool are used to represent the project cost behavior in construction units.

2- Data collection aims to collect historical data on activity costs of two types of buildings (construction of managerial building and school building), and periodic reports, invoice of payments, BOQ and tables of quantity surveying for maintenance activities.
3- Finding the optimum relationships by using mathematical regression model in (Excel package) between cost and construction units and finding the percentage of construction items and developing equations of cost estimating.
4- Displaying and discussing the results and drawing the final conclusions and recommendations.

4. COST ESTIMATION TYPES

The cost estimating for construction project starts in the preliminary phase or in feasibility study, to define the required financial requirements. The result of the estimation may differ according to the estimating techniques and to relevant information available, in construction field where there are different types of cost estimation as shown in **Table 1**.

The first type of estimation gives rough estimate, depending on unit basis used in preliminary study and is prepared by using various methods for different structures and works, as shown in **Table 2**. The plinth area or superficial area method is deduced from the cost of the similar building having similar specification, characteristics and construction techniques but at same height of each floor. In a locality the plinth area rate is computed by using historical data on several buildings. In the same context the cube rate can be estimated after checking the cubic volume of building to consider, where the height of building is a crucial factor, it's more flexible than plinth area and it will be used for different sizes of building with different design.

The approximate quantity method depends on expected length of walls by using running meter rate multiplying the total length of walls, while the detailed estimate needs a completed and detailed design with specification accompanying a completed quantity account.

Dagostino, et, al., 2011, referred to three others types of estimating approaches for approximate estimating which are as follows:

1- Assembly Estimating: in this estimation the projects are treated as a group of assemblies like residential, electrical , gypsum-board partitions wall, etc. These groups can be estimated either manually or by computer software which will make the estimate more quickly by such a breakdown of project.

2- Parametric Estimates: the equations that are concluded from the statistical process will be used by depending on one of the parameters in estimating the anticipated cost.

3- Model Estimating: the computer models will be used here when the estimator is asked questions and has to answer them such as length, width, height, floor thickness, depth of footing, fire sprinklers, etc.

5. DATA COLLECTION AND ANALYSIS

In this research the approximate estimate considers (unit basis, plinth area, cube rate). The case studies data came from new construction and maintenance

projects. The data on two types of projects (construction of managerial building and school),were obtained from projects office in Ghadame's Province in the great Arab desert 625 km south west of the capital Tripoli. A similar technique was used to study the maintenance **Table 3**. The second part of this study "the percentage of construction items" depends on final payment certificate of the project considered to define the ratio of cost of each items to total cost of project.

In this study, equations are derived by using Regression method (Excel package) to find out relations related to units and to explain cost behavior and finally, these equations were tested through correlation as shown in **Table 4** .

The raw data of this project is too large to be included in this research; therefore the researcher put the final information.

The units used for construction of managerial buildings in this study are area (square meter) and volume (cubic meter), these two units were used in maintenance also. For these types of building of school construction, the units used in maintenance were area (square meter), volume (cubic meter), number of students in each school and number of classes also.

6. THE RESULT AND DISCUSSION

The result of estimating of new construction works, are reasonable with low standard deviation **Tables 3** shows also the equations which have high correlation, and are more realistic than unit cost as shown in **Table 4**, where the following equations are related to new construction of managerial building :

$$y_{cms}=500.818x_s-1343.92 \quad (1)$$

$$y_{cmc}=73.51x_c+22049.53 \quad (2)$$

Even the equations that are related to new construction of schools are:

$$y_{css}=908.96x_s+13402.27 \quad (3)$$

$$y_{csc}=197.6x_c+13409.77 \quad (4)$$

$$y_{cst}=2423.9x_{st}+204519.2 \quad (5)$$

$$y_{csl}=43630.26x_{cl}+204519.2 \quad (6)$$

But the results of maintenance work have proved to be less realistic because of the inaccurate input raw data with clear variation in value of same work among the different projects which have the same basis .The maintenance work gives disappointing results, **Table 3** and **Table 4**,. It seems this result can never be used, therefore the maintenance data or cost does not reflect realistic cost. It is believed that, the main reason for great difference in maintenance cost lies in the manner of preparing bill of quantity which is usually done in office rather than on site, and the estimators were junior engineers having little experiences. For example, some items which don't cost very much are priced highly; items need a lower cost than fixed in the estimating sheets or in (BOQ).

For items cost percentage, the concrete work and finishing represent the higher percentage in construction work of the two types studied –managerial building and schools ,while for maintenance work, the electric work is greatest with ratio (%44)

for schools, while in office building, the greatest ratio was in finishing work, **Table 5** and the **Figs.1, 2, 3,** and **4** represent the illustration of item percentage of school and managerial building in case of either new construction or maintenance.

6. CONCLUSIONS AND RECOMMENDATIONS

6.1 Conclusions

1.The price of work for area, volume and units can be used as a basis for estimating and decision making stage, for managerial buildings and schools, while the students units and classes do also give accurate results.

2. The historical data of maintenance work is non-systematic indeterminate and reveals there are unsuitable relations with the factors or bases of approximate estimate.

3. Most of new construction equations that are concluded by regression are suitable for use to estimate the cost.

3. The final payment certificate of construction work is more realistic than that of maintenance work as a consequence of nature of work and the maintenance equation that is concluded is less suitable to use.

4. In this research, several projects are neglected because of lack of information and they are not documented which lead to inaccurate estimating.

6.2 Recommendations

1. The researcher suggests the price of approximate estimate in this research be used for estimating new project and update for each period be made.

2. The consulting offices should play a part in predicting costs using their estimating methods, pre-estimate procedure and experience methods.

3. Information about accounts and data cost of project must be documented and filed.

4. The annual maintenance must be estimated carefully by specialist committee based on database or by suggesting model for analysis of such fuzzy information.

REFERENCES

- 1-AL-Juruf, R.S., Shach, A.A., AL,1995, *Muyassir Dictionary of Const. Eng. and Management Terms,* S.A; Obekan.

- 2- Buchan, R. D., et al., 2006, *Estimating for Builders and Surveyors* , Butterworth Heinemann Oxford, UK.

- 3- Callahan, et al., 2007, *Construction Project Scheduling*, McGraw –Hill, Singapore,.

- Dagostino F. R., Peterson S. J., 2011, *Estimating in Building Construction*, Prentice Hall, New jersey US.

- Dutta, P.N., 2005, *Estimate and Costing*, India: Lucknow, 2005.

- 6-FIDIC, *Condition of Contract For works of Civil Engineering Construction*, 4th Edition.

- 7-Mendenvall, W., Behaver, R., 1994, *Introduction to Probability and Statistics*, California: Duxbury press.

- Mubarak S., 2010, *Construction Project Scheduling and Control*, John Wiley and Sons, Inc. New Jersey.
- Peurifoy, Robert L., 2011, *Construction Planning And Equipment Method*, McGraw-Hill, Singapore.

NOMENCLATURE:

x_s = estimated area m^2

x_c = estimated volume m^3

x_{st} = estimated number of students

x_{cl} = estimated number of classes

y_{cm} = estimated cost of managerial building based square meter

y_{cmc} = estimated cost of managerial building based cubic meter

y_{css} = estimated cost of school building based square meter

y_{csc} = estimated cost of school building based cubic meter

y_{cst} = estimated cost of school building based student number

y_{csl} = estimated cost of school building based classes number

Table 1. Types of cost estimating. [Researcher]

1- Approximate estimate	Estimate per unit basis
	Plinth area estimate for building.
	Cube rate estimate for building.
	Approximate quantity method
	Item rate estimate.
	Revised estimate.
	Supplementary estimate.
	Maintenance estimate.
2- Detailed estimate	*When the drawings , planning & specification & bill of quantities are ready*

Table 2. Units basis used to cost estimating, **Dutta, 2005.**

No.	Type of project		Unit of estimating
1	Buildings	School	Student or class room
		Hostel	Student
		Hospital	Bed
		Theater, cinema & halls	Seat
		Residential building	Tenement
		Dormitory	Barrack
2	Road and highways		Kilometer ,area
3	Irrigation channels		Kilometer depending on capacity of channel
4	Bridges and culverts		Running meter
5	Sewerage project and waters supply project		Population served or area covered
6	Overhead water tank		Capacity per cubic meter

Table 3. The unit prices per each unit basis.

Type of work	Type of structure	Cost estimated $ Per			
		Square meter	Cubic meter	Student	Class
construction	Managerial building	554.1 ±104.62	134.95 ±40		
	School	932.6 ±12.2	202.74 ±2.6	3962.5 ± (210.7)	71325.57 ± (3793.2)
maintenance	Managerial building	196.87 ±189.5	39.66 ±25.5		
	School	46.98 ±16.4	11.39 ±4.73	139.08 (101.04) ±	2347.78 ± (1136)

* By multiplying the above values by the related unit basis to get the estimating cost.

Table 4. The equation of cost estimating per unit.

Type of work	Type of structure	Equation concluded per unit (x)			
		Square meter	Cubic meter	Students	Classes
Construction	Managerial building	Y=500.818X-1343.92 R=0.987	Y=73.51X+22049.53 R=0.975		
	Schools	Y=908.96X+13402.27 R=0.983	Y=197.6X+13409.77 R=0.983	Y=2423.9X+204519.2 R=0.983	Y=43630.26X+204519.2 R=0.983
Maintenance	Managerial building	Y=126.535X+25037.03 R=0.469	Y=12.05X+54861.29 R=0.199		
	Schools	Y=31.93X+8440.676 R=0.193	Y=12.11X-1673 R=0.193	Y=20.41X+21218.6 R=0.193	Y=583.04X+19251.7 R=0.193

* The above equations are extracted by using regression tool after analysis of the raw data.

Table 5. The items ratio per total value of project (%).

Type of work	Maintenance		Construction	
Type of structures	Schools	Managerial building	Schools	Managerial building
Leveling and utilities		0.105	0.87	0.19
Clearing demolition	o.171	0.513		0.26
Excavation		5.07	1.66	1.26
Filling		0.243	2.0	1.37
Concrete		6.54	36.3	25.31
Masonry	0.231	2.88	7.045	13.34
Finishing	15.695	21.28	16.465	20.77
Roofing and flooring	5.171	9.109	7.485	6.13
Metal	8.252	14.649	4.125	5.86
Damp proof		1.51	4.585	3.77
Wood	5.66	7.51	4.287	6.75
Sanitary	20.107	12.85	6.015	5.44
Electric	44.09	11.87	5.737	4.67
Water tank		4.57		3.75
Final cleaning	0.612	1.21		0.48
others			2.365	1.01

* Some items were unavailable and are not considered in the original BoQ

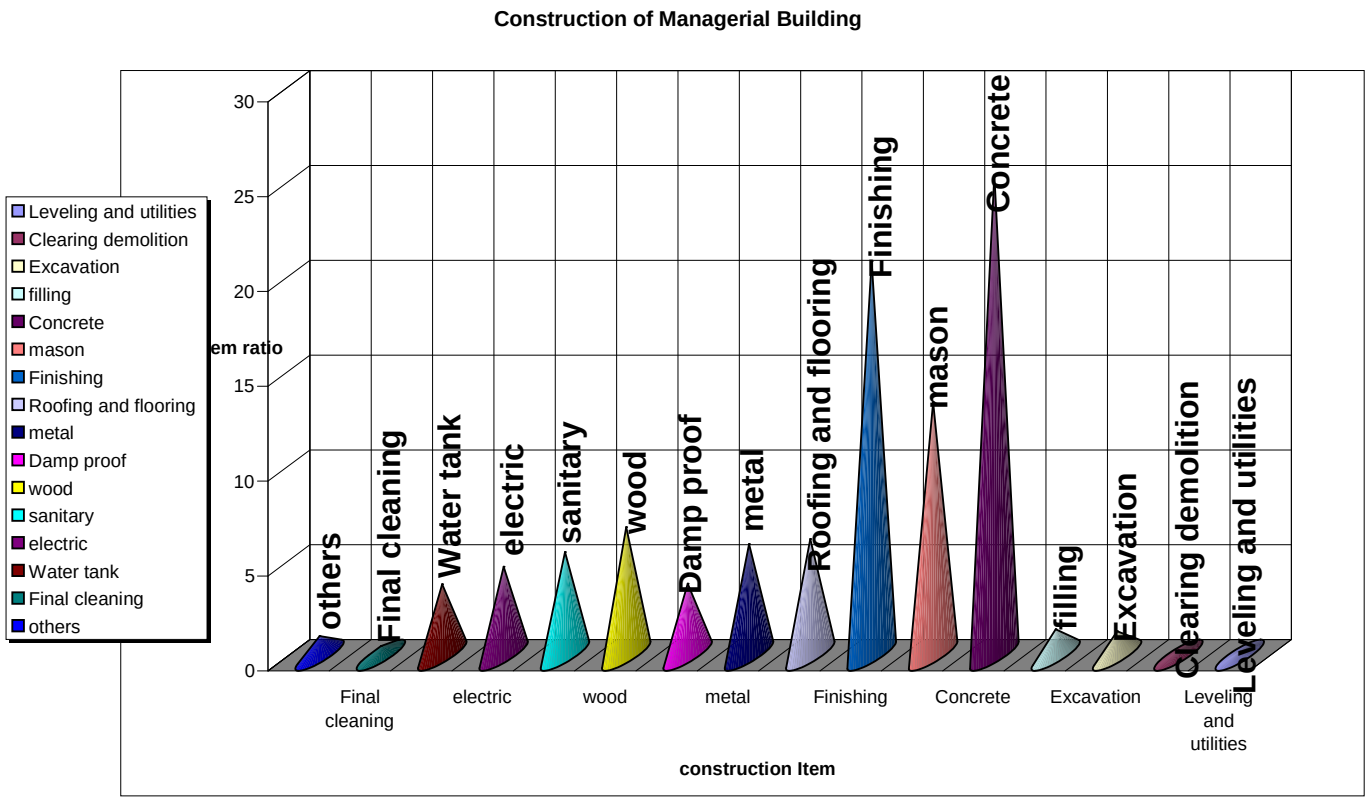

Figure1. Item Percentage of construction managerial building.

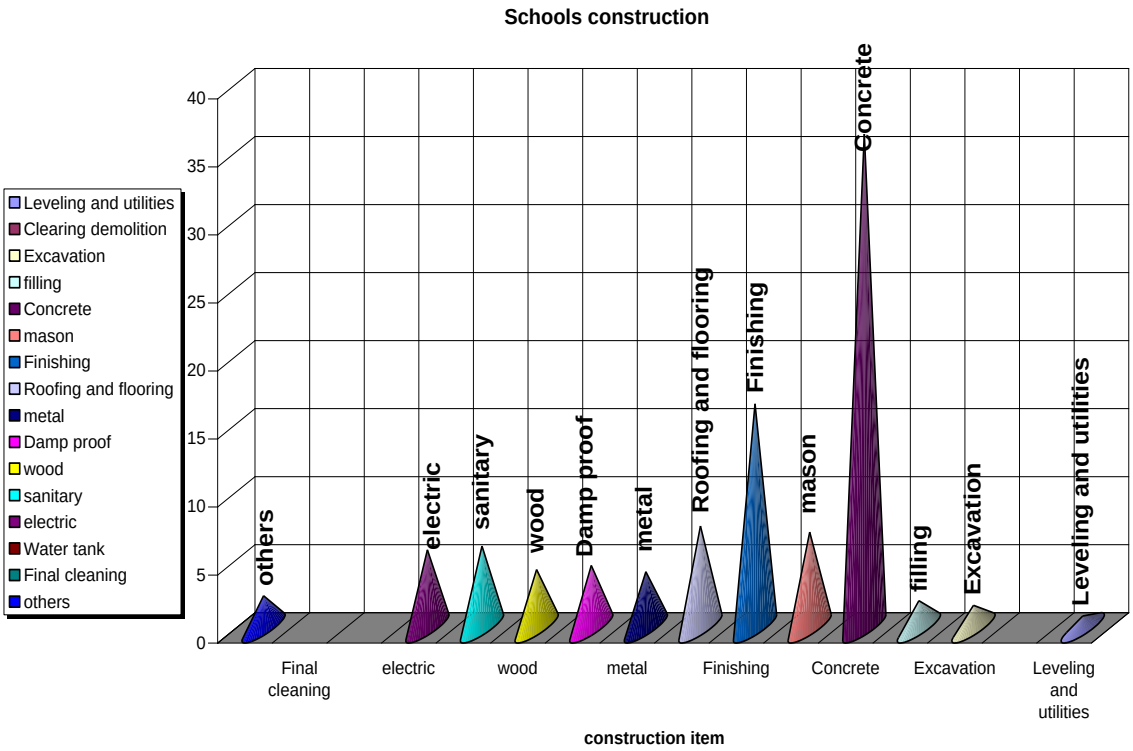

Figure 2. Item percentage of school construction.

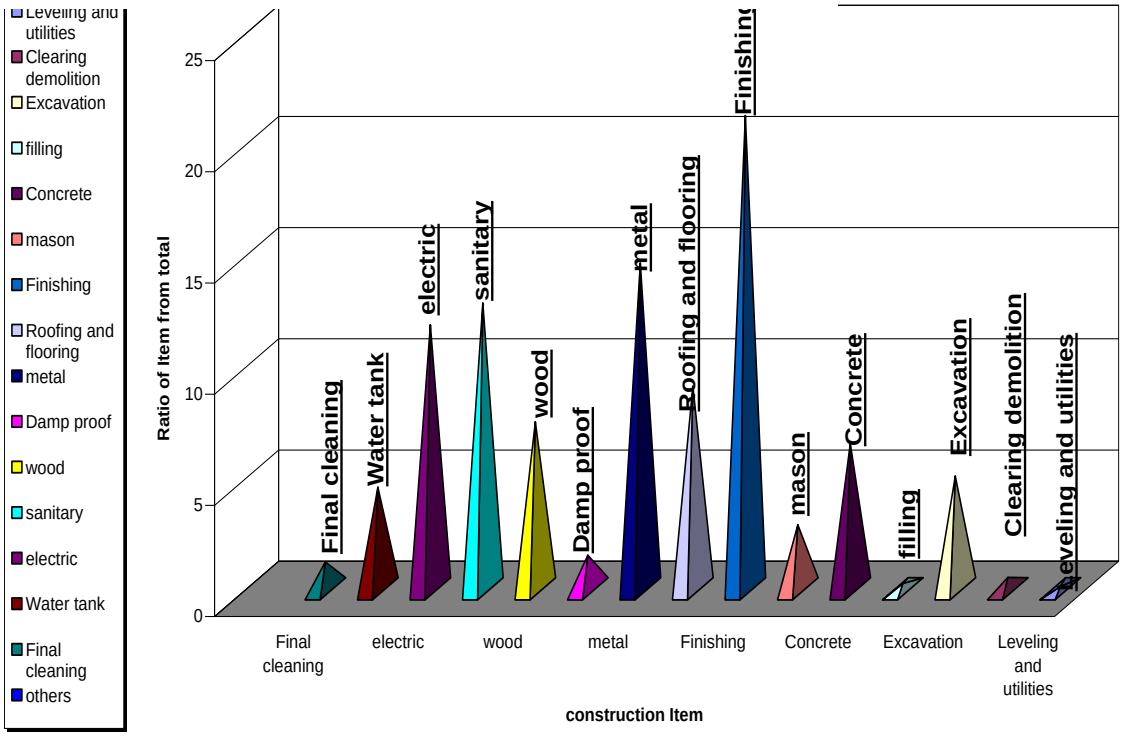

Figure 3. Item percentage of maintenance of managerial building.

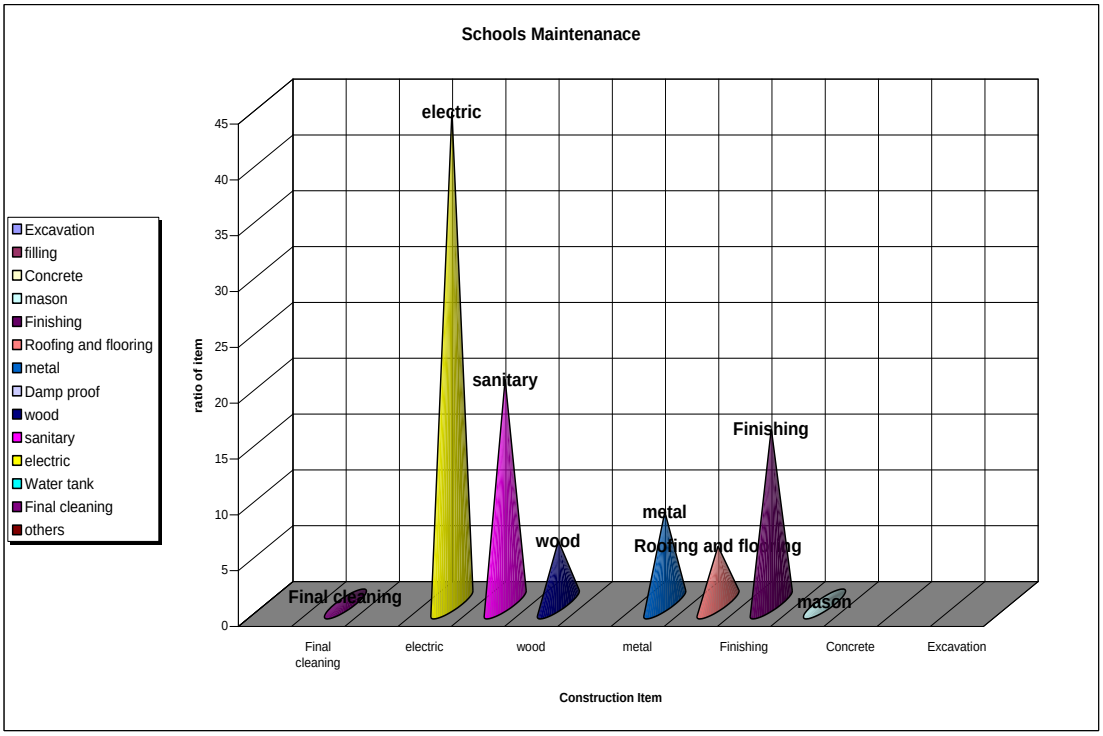

Figure 4. Item percentage schools maintenance.

Punching Shear Strength of Self Compacted Ferrocement Slabs

Abdulkhaliq Abdulyimah Jaafer
Lecturer
College of Engineering- Misan University
E mail: aljabery@uomisan.edu.iq
aljabery_1981@yahoo.com

Sa'ad Fahad Resan
Lecturer
College of Engineering- Misan University
E mail: sadresan@uomisan.edu.iq

ABSTRACT

This study aims to investigate the behavior and strength of self-compacted ferrocement slabs under punching shear load. Experimental results of thirteen square ferrocement slabs of 500×500 mm simply supported on all edges are presented. The main parameters investigated include the volume fraction of reinforcement, slab thickness and size of load-bearing plate. The load deflection and cracking characteristics of the tested slabs are studied and compared. The test results showed that the volume fraction of wire mesh has significant effect on both ultimate load and displacement. The increase of slab thickness leads to decrease in deflection values and increase in stiffness of slabs. Both ductility and stiffness increase as the loaded area size is increased.

Key words: self compacting mortar, ferrocement, punching shear, slabs, volume fraction

مقاومة القص الثاقب للبلاطات الفيروسمنتيه ذاتية الرص

د.عبدالخالق عبداليمه جعفر
مدرس
كلية الهندسة - جامعة ميسان

د. سعد فهد رسن
مدرس
كلية الهندسة - جامعة ميسان

الخلاصة

تهدف هذه الدراسة الى تحري سلوك ومقاومة البلاطات الفيروسمنتيه ذاتية الرص تحت تاثير حمل القص الثاقب. استعرضت الدراسة نتائج عمليه لثلاثة عشر بلاطة فيروسمنتيه مربعة الشكل بابعاد (500×500 ملم) وبسيطة الاسناد من جميع الجهات. تضمنت دراسة المتغيرات الرئيسية وهي النسبة الحجميه للتسليح, سمك البلاطة وحجم لوحة التحميل. وكذلك تم دراسة خصائص منحنى الحمل-التشوه وخصائص التشقق للبلاطات المفحوصة. بينت الدراسة ان النسبة الحجميه للتسليح لها تاثير كبير على كل من الحمل الاقصى والتشوه الاقصى. كما ان الزيادة في السمك تؤدي الى زيادة في جساءة البلاطة ونقصان في الهطول. و ان كلا من المطيلية والجساءة يزدادان بزيادة ابعاد لوحة التحميل.

الكلمات الرئيسيه: ملاط ذاتي الرص, فيروسمنت, القص الثاقب , بلاطات, الكسور الحجميه.

1. INTRODUCTION

Ferrocement is a type of thin wall reinforced concrete commonly constructed of hydraulic cement mortar reinforced with closely spaced layers of continuous and relatively small size wire mesh. The mesh may be made of metallic or other suitable materials **ACI Committee 549, 1999**. Ferrocement has a very high tensile strength-to-weight ratio and superior cracking behavior in comparison to conventional reinforced concrete. This means that thin ferrocement structures can be made relatively light and watertight. Hence, ferrocement is an attractive material for the construction of prefabricated housing units, boats, barges, and other portable structures **ACI, Committee 549, 1999**.

Also, ferrocement can be utilised in a number of practical application such as repair, rehabilitation and strengthening of different concrete structural members **Lub and Van, 1989, Fahmy and Shaheen, 1994, Romualdi et al., 1998, Fahmy et al., 1999, Razali et al., 2005, Dongyen et al., 2006, Jeyasehar and Vidivelli, 2006,** and **Shannag 2009**.

Recent and interesting applications are related to the adoption of self compacting mortar in the field of retrofitting and strengthening of reinforced concrete structures **Kazim, 2012**. It is preferred due to the easiness of application and mechanical advantages. The applied mortar to the structural members is usually hard to consolidate and vibration is not possible in most cases **Rathish and Srikanth, 2008**. In addition to these, the self-compactability of mortars may provide considerable advantages such as reducing the construction time and labor cost, enhancing the filling capacity of highly congested structural members **Kazim, 2012**.

Therefore, an experimental study is performed on self compacted cementitious slabs and reinforced with welded steel wire mesh to investigate its strength and behavior under patch loading. There are limited investigations that have been carried out to study the behavior of ferrocement members under punching shear. These include **Paramasivam and Tan, 1993, Al-Kubaisy and Jumaat, 1999, Mansur et al., 2000** and **2001, Ibrahim, 2011**.

Due to the limited studies, this paper is aimed to investigate the behavior and strength of self-compacted ferrocement slabs under punching shear load. The main parameters considered in this study include the volume fraction of reinforcement, overall thickness, and the size of the load bearing plate. Thirteen ferrocement slabs are tested. The results of these tests are presented and the influences of various parameters on the punching shear strength are discussed. The load-deflection of these slabs is also discussed in this paper.

2. EXPERIMENTAL PROGRAMS

2.1. Specimen Details and Test Parameters

A total of thirteen ferrocement slabs of identical length and width but different depths have been tested in the Construction Materials Laboratory of the College of Engineering at University of Misan. The casted slabs were 500 mm long × 500 mm wide with two different depths of 30 and 45 mm. The specimens comprised of two control ferrocement slabs cast with ordinary mortar and the other eleven made with self compacting mortar. Specimen details and main study parameters are summarized in **Table 1**. The slab specimens were simply supported along the four edges with corners free to lift and free to rotate about the support axes as shown in test setup in **Fig. 1**. The support-to-support span (l) for all the slabs was 400mm in each direction. The load has been applied by means of a hydraulic jack as shown in **Fig. 1**. A square rigid steel plate with side (w) of (40 and 80 mm) was placed between the jack and slab to apply the load in the center of the slab. A mechanical dial gauge was placed at the center of the slab to measure the vertical displacement while a calibrated load cell was used to record the load as shown in **Fig. 1**.

2.2. Materials and Mixing Proportions

Welded square wire mesh with a wire diameter of 1.0 mm and 12.5 mm spacing was provided as an internal reinforcement for ferrocement slabs. The mesh was tested according to the design guide on construction and repair of ferrocement reported by the **ACI committee 549, 1999**. The yield strength of the wire mesh was determined to be 405 MPa. The average ultimate strength of the wire mesh and modulus of elasticity was found to be 600 MPa and 95 GPa, respectively as shown in **Table 2**. Mortar matrix consisted of ordinary Portland cement locally available and natural sand with specific gravity of 2.60. In the mix, 10% by weight of cement was replaced by silka fume. The water and sand to binder ratios by weight were chosen to be 0.3 and 1.0 respectively. Supperplastcizer type **Sika Viscocrete ,2010,** was used as high range water reducer. The dose of superplasticizer used to obtain self compacted mortar was 3% by total binder weight. Potable water was used in the experimental work for both mixing and curing.

2.3. Mortar Mixing and Fresh Properties Tests

The batch of mortar was produced using rotating drum type of half bag capacity. The Portland cement and silica fume were initially dry mixed at low mixing speeds prior to the addition of other constituent materials. Further mixing sequences and durations were performed in accordance to standard procedures prescribed in **ASTM Standard C305**, **1999.**

After the mixing was completed, tests were conducted on fresh self compacting mortar to determine mini slump flow diameter and mini V-funnel flow time as shown in **Fig. 2.** The mini slump flow diameter and mini V-funnel flow time of self compacted mortar were presented in **Table 3**. Segregation and bleeding were visually checked during the slump flow test and was not observed.

2.4. Fabrication of Test Specimens

The wooden moulds dimensions were (500x500x30 or 45mm). The desired mesh layers were tied by fine steel wires and then placed inside the moulds. Fresh mortar mix was then poured into the wooden mould as shown in **Fig. 3**. Along with the slabs, a total of six (50x50x50 mm) mortar cubes and three (40x40x160 mm) mortar prisms were moulded. The mortar specimens were used for compressive and flexure strength tests. The matrix characterised by an average compressive and flexural strength of 70 and 7.7 MPa, respectively. Moulded specimens were cured in mould for 24 hour and then removed from their moulds, and immersed in the curing tank for 28 days.

Before the testing day, the slab was cleaned and painted with white paint on both surfaces, to achieve clear visibility of cracks during testing. The slab was carefully placed on the simple supports. The point load was applied at the centre of the top surface of the slab and the dial gauge was positioned under the centre of the bottom surface of the slab, so that a precise set-up of the testing equipment was achieved.

3. TEST RESULTS AND DISCUSSION

3.1. General Behavior

The general behavior of self compacting ferrocement slabs and normal ferrocement slabs are all nearly identical as shown in **Figs. 4** and **5**. When the load is applied to the slab specimen, the first visible crack (bending cracks) was observed at the tension face of the tested slab and the relationship between load and displacement is linear till flexural cracks occur. In all slabs, cracking on the tensile face began near the center and radiated towards the edges (semi-random phenomena). As the load is increased the cracking propagated to the opposite face. At higher

loads, the already formed cracks got widened while new cracks started to form. The new formed cracks are roughly semi-circular or elliptical in shape and occurred in the tension surface of the slab. Failure of the slab occurred when the cone of failure radial outward from the point of load application pushed up through the slab body (brittle failure with limited warning). At failure, the slab was no longer capable of taking additional load.

3.2. Cracking and Failure Patterns

Fig. 6 presents general patterns cracking and failure on the top and bottom faces of the self compacted and normal specimens after failure. No cracks are observed in the compression face of any slab, except those which are observed around the loaded area at failure, which are almost the same as that of the loading plate dimensions. The cracks on the bottom face of specimens are radial, propagating from the centre of slab. These patterns are occurred at the center of slabs and propagated across the slab to the sides in the redial direction. Different cracking patterns may be noticed in **Figs. 7** to **9** such as spacing, extent of cracks and perimeter of failure cone. These variations depending on the volume fraction of wire mesh, the thickness of specimens and size of loading plate. It can be noticed that combined flexural-punching failure mode is found in slabs with small amount of reinforcement ratio and pure punching shear failure is found in specimens that have moderate and high volume fraction. The crack patterns at failure became more closely spaced with increasing the reinforcement content.

3.3. Load-Deflection Response

The load-displacement relationships for self compacted ferrocement slabs and corresponding control (normal ferrocement) slabs are presented in **Figs. 4** and **5**. It can be noticed from these figures, that relationships are approximately identical at all loading stages. **Fig. 10** shows load-displacement relationship of the control slab (0-45-S) that it tested under patch load to determine the ultimate load carrying capacity of plain mortar specimen. When adding wire mesh of volume fraction (0.77, 1.154, 2.31 and 3.464 %) for slabs (2-45-S, 3-45-S, 4-45-S, 6-45-S and 9-45-S) respectively, the ultimate load increases (155, 188,366, 533 and 658%) respectively, as shown in **Fig. 11** and **Table 4**. It may be seen from **Fig. 11** that the specimen (9-45-S) with the high volume fraction has highest ultimate shear load and stiffness but less ductility when it is compared with the specimen with lower reinforcement ratio (2-45-S). This proves that the volume fraction of wire mesh has significant effect on both ultimate load and displacement at ultimate load.

Figs. 12 and **13** illustrate the load-deflection relationships of slabs with different size of loading plate. As it is clear from these figures, the increase of the loading plate size leads to increase of ultimate loads. The effect of the loading plate size on the ultimate shear load with various volume fractions is shown in **Fig. 14**. As shown in this figure, the increase of size causes an increasing in the ultimate strength of slabs. For slabs having volume fraction (1.154 and 2.31 %), the ultimate capacity is increased by (24 and 29%) respectively, when loading plate changed from 40 to 80 mm, respectively. The behavior of slabs of different thicknesses and reinforced with same volume fraction is denoted in **Figs. 15** to **17**.

The increase of slab thickness leads to decrease in deflection values at each stage of loading. **Fig. 18** shows the effect of the volume fraction on ultimate load of self compacted ferrocement slab. It is obvious from this figure that the ultimate capacity of the slabs increases with the increase of the thickness of slab at the same amount of reinforcement ratio.

4. PREDICTION OF PUNCHING SHEAR STRENGTH

Many codes and researchers have presented different formulas for predicting the punching shear strength of concrete slabs but no any code provision for punching shear in ferrocement. For concrete slabs, most codes present formulas, where the design punching load is a product of design nominal shear strength by the critical punching shear perimeter and the effective depth of the slab. The critical perimeter of punching shear depends on the shape of critical perimeter and its distance from loaded face. The characteristics of critical punching shear perimeter that considered in different codes such as **ACI 318-11Code**, **Eurocode 2-2004**, and **BS8110-1997** are shown in **Fig 19**.

In the **ACI 318M-11 Code,** the punching shear strength should be taken not greater than any of the following three equations:

$$P_u = 0.17\left(1+\frac{2}{\beta}\right)\sqrt{f_c'}\ u_o\ d \tag{1}$$

$$P_u = 0.083\left(\frac{\alpha_s\, d}{u_o}+2\right)\sqrt{f_c'}\ u_o\ d \tag{2}$$

$$P_u = 0.332\sqrt{f_c'}\ u_o\ d \tag{3}$$

where, u_o = 4(c + d), as shown in **Fig.19**; α_s= 40 for symmetric punching; β = the ratio of the long side to the short side of the concentrated load or reaction area,

The equation presented in **BS8110-97**, is as follows:

$$P_u = 0.79(100\,\rho)^{\frac{1}{3}}\left(\frac{400}{d}\right)^{\frac{1}{4}}\left(\frac{f_c'}{25}\right)^{\frac{1}{3}} u_o\ d \tag{4}$$

where; u_o = 4(c + 3 d) as shown in **Fig.19**; $(\frac{400}{d})$ ≥1.0; $25 \le f_c' \le 40$; $\rho \le 3\%$

The **Eurocode 2-2004,** recommends the following expression to estimate punching shear strength of concrete slabs:

$$P_u = 0.18\,k\,(100\,\rho\, f_c')^{\frac{1}{3}}\, u_o\, d \tag{5}$$

where: u_o = 4(c + π d) as shown in **Fig.19**; $k = 1+\sqrt{\frac{200}{d}} \le 2.0$; $f_c' \le 50$ MPa; $\rho \le 2\%$

In the case of ferrocement slab **Mansur and Ong, 1987**, suggested that the effective depth of slab (d) is replaced by thickness of slab (h) for the simplicity.

The above code provisions are used to calculate the ultimate punching load of normal and self compacted ferrocement slabs and the test and calculated values are summarized in **Table 5.** From this table, it can be observed that the experimental values are smaller than these calculated by ACI, Euro and BS codes. The ratio of experimental result to that calculated by **ACI**, **BS8110**, and **Eurocode 2** codes range from (0.28-0.98), (0.27-0.57) and (0.45-0.79), respectively.

Based on the test results and the above discussion, it can be concluded that these codes are unsafe and this is leaded to define specific procedure of punching shear of self compacted ferrocement slabs. For this purpose, the proposed model for punching load is given as:

$$P_u = V_u \; u_o \, h \tag{6}$$

An empirical relation was proposed by **Mansur et al., 2001**, is used to predict the punching shear strength of ferrocement slabs (V_u). The following exponential form of equation has been selected.

$$V_u = 0.39(f_c' V_f \frac{h}{l})^{0.5} \tag{7}$$

The critical punching shear perimeter (u_o) of ferrocement slabs as defined by ACI code is considered as.

$$u_o = 4(c + h) \tag{8}$$

Substituting Eqs. (7) and (8) in Eq. (6), gives a model for predicting shear load as:

$$P_u = 1.56 \, (f_c' V_f \frac{h}{l})^{0.5} \; (c + h) \, h \tag{9}$$

A comparison of the ultimate punching shear loads predicted by Eq. (9) with experimental values is given in **Fig. 20** and **Table 5**. From **Table 5** it can be noted that the ratio of test to predicted ultimate loads $(P_u)_{test}/(P_u)_{pred.}$ ranges from 0.84 to 1.34, with an average 1.12 and a standard deviation of 0.16. Thus the proposed equation is able to predict the ultimate punching shear load of self-compacted ferrocement slabs.

5. CONCLUSION

In this paper the experimental test is made on ferrocement slabs with normal and self-compacted mortar, subjected to patch loads. Based on the results obtained from the experiments, the following conclusions may be drawn:

The load-displacement relationships for self-compacted ferrocement slabs and corresponding normal ferrocement are approximately identical at all loading stages.

The specimen with high volume fraction specimen has highest ultimate shear load and stiffness but less ductility.

Failure mode of self-compacted ferrocement slabs mainly depends on volume fraction of reinforcement and combined flexural-punching failure mode may be changed into pure punching shear with increasing the reinforcement ratio.

The ultimate shear capacity of self compacted slabs is increased by (24% and 29%) respectively, when loading plate is changed from 40 to 80 mm, respectively.

The increase of slab thickness leads to decrease in deflection values at each stage of loading and increasing in stiffness of self-compacted ferrocement slab.

The code provisions for punching shear of structural concrete are not suitable for predicting the punching shear strength of self-compacted ferocement slabs.

REFERENCES

- ACI Committee 549, 1999, *Guide for the Design, Construction, and Repair of Ferrocement*, ACI Structural Journal 85 (3), pp. 325-351.

- ACI Committee 318, 2011, *Building Code Requirements for Structural Concrete (ACI 318M-11) and Commentary*, American Concrete Institute, Farmington Hills, MI 48331, USA.

- Al-Kubaisy, M., and Jumaat, M., 1999, *Punching Shear Strength of Ferrocement Slabs*, Journal of Ferrocement, 29(2): 99-114.

- ASTM C 305, 1999, *Standard Practice for Mechanical Mixing of Hydraulic Cement Pastes and Mortars of Plastic Consistency*, Vol. 4, pp. 1-3.

- British Standards Institution (B.S.8110), 1997, *Code of Practice for Design and Construction*, British Standards Institution, Part 1, London.

- Dongyen, A., Sayamipuk, S., Piyarakskul, S. and Nimityongskul, P., 2006, *Strengthening of Reinforced Concrete Beam and Slab System using Ferrocement Jacketing*, Proceedings of the Eighth International Symposium and Workshop on Ferrocement and Thin Reinforced Cement Composites, 6-8 February, Bangkok, Thailand.

- EFNARC, 2002, *Specification and Guidelines for Self Compacting Concrete*, February, pp. 1-32, www.efnarc.org.

- Eurocode 2, 2004, *Design of Concrete Structures-Part 1-1: General Rules and Rules for Buildings*, CEN, EN 1992-1-1, Brussels, Belgium.

- Fahmy, E. H., Shaheen, Y.B. I., and Korany, Y.S., 1999, *Repairing Reinforced Concrete Columns Using Ferrocement Laminates*, Journal of Ferrocement, 29, No.2, pp. 115-124.

- Fahmy, E. H., and Shaheen, Y.B. I, 1994, *Laminated Ferrocement for Strengthening and Repairing of Reinforced Concrete Beams*, Proceedings of the Annual Conference of the Canadian Society for Civil Engineering, 475-483.

- Ibrahim H. M., 2011, *Experimental Investigation of Ultimate Capacity of Wired Mesh-reinforced Cementitious Slabs*, Construction and Building Materials, 25, pp. 251-259.

- Jeyasehar, C.A., and Vidivelli, B., 2006, *Behavior of RC Beams Rehabilitated with Ferrocement Laminates*, Proceedings of the Eighth International Symposium and Workshop on Ferrocement and Thin Reinforced Cement Composites, 6-8 February, Bangkok, Thailand.

- Kazim, T., 2012, *Viscosity and Hardened Properties of Self-Compacting Mortars with Binary and Ternary Cementitious Blends of Fly Ash and Silica Fume*, Construction and Building Materials, 37, pp. 326–334.

- Lub and Van, W., 1989, *Test on Strengthening of RC Beam by Using Shotcrete Ferrocement* , Journal of Ferrocement, Vol. 19, No. 4, October, pp. 363-370.

- Mansur, M. A., and, Ong, K. C. G., 1987, *Shear Strength of Ferrocement Beams*. ACI Structural Journal, 84(1), 10–17.
- Mansur, M., Ahmad, I., and Paramasivam, P., 2000 *Punching Shear Behavior of Restrained Ferrocement Slabs*, ACI Structural Journal; 97(5), pp. 765-773.

- Mansur, M., Ahmad, I., and Paramasivam P., 2001, *Punching Shear Strength of Simply Supported Ferrocement Slabs*, Journal of Materials in Civil Engineering; 13(6), pp. 418-426.

- Paramasivam, P., and Tan, K., 1993, *Punching Shear Strength of Ferrocement Slabs*, ACI Structural Journal, 7(3), pp. 294-301.

- Kumar, R. P., and Srikanth, K., 2008, *Mechanical Characteristics of Fiber Reinforced self Compacting Mortars*, Asian Journal of Civil Engineering, Building and Housing, Vol. 9, No. 6, 647-657.

- Razali, M., Kadir, A., and Noorzaci J., 2005, *Repair and Structural Performance of Initially Cracked Reinforced Concrete Slabs*, Construction and Building Material Journal; 19(8), pp. 595-603.

- Romualdi, J. P., Lim, C. T. E., and Ong, K. C. G., 1998, *Strengthening of RC Beams with Ferrocement Laminates*, Cement Concr. Comp., vol.20, pp. 53-65.

- Shannag, M.J., 2009, *High Strength Ferrocement Laminates for Structural Repair*, Concrete Solutions, Edited by Michael Grantham, Valentina Salomoni, and Carmelo Majorana, CRC Press, Taylor & Francis Group, London, U.K.

- Sika ViscoCrete 5930, 2010, *Product Data Sheet*, Turkey, Version no. 01.10.

NOMENCLATURE

c = side length of column, mm
d = effective depth, mm
$f_c{}'$ = the compressive strength of the mortar, MPa
h = thickness of slab, mm
k = factor accounting for size effect, dimensionless
l = length of slab, mm
P_u = the ultimate punching shear load, kN
u_o = the perimeter of the critical section, mm
V_u = ultimate shear stress, MPa
V_f = volume fraction of reinforcement
w = side length of loaded plate, mm
α_s= a factor for slab column connections based on the location of the column (40 for interior, 30 for exterior, 20 for corner columns), dimensionless.

β = the ratio of the long side to the short side of the concentrated load or reaction area, dimensionless.
ρ = bending reinforcement ratio.

Table 1. Details of specimens.

Slab no.	Thickness (h) (mm)	Volume fraction Vf %	No. of wire mesh layers	Width of loading plate (w) (mm)	Compressive strength (f'c) (MPa)	Mortar type
0-45-S	45	0	0	40	70	Self compacting mortar
2-45-S		0.77	2			
3-45-S		1.154	3			
4-45-S		1.54	4			
6-45-S		2.31	6			
9-45-S		3.464	9			
2-30-S	30	1.154	2	40	71	
4-30-S		2.31	4			
6-30-S		3.464	6			
2-30-L	30	1.154	2	80	70	
4-30-L		2.31	4			
2-30-S-con	30	1.154	2	40	68	Normal mortar
4-30-S-con		2.31	4			

Table 2. Properties of wire mesh.

Specimens	Wire diameter (mm)	Yield strength (MPa)	Ultimate strength (MPa)	Modulus of elasticity (GPa)
S1	1.0	409	598	95.1
S2	1.0	392	586	94.3
S3	1.0	414	616	95.6
Average	1.0	405	600	95.0

Table 3. Fresh properties of self compacting mortar.

	Tested value of fresh mortar	**EFNARC Specification (2002)**
Mini Slump (mm)	259	Between (240 – 260) mm
Mini V-funnel (sec)	8.6	Less than 11 seconds

Table 4. Test results of slabs.

Slab no.	Mortar compressive strength (MPa)	Thickness (mm)	Load (kN)	Deflection (mm)
0-45-S	67	42	6.0	1.25
2-45-S	69	44	15.3	8.1
3-45-S	69	43	17.3	7.5
4-45-S	72	47	27.9	7
6-45-S	72	48	38	6.6
9-45-S	71	48	45.5	6.1
2-30-S	67	27	7.43	13.75
4-30-S	72	30	13.5	11
6-30-S	74	33	23.2	10
2-30-L	66	28	9.2	14.5
4-30-L	74	32	17.4	12
2-30-S-con	67	28	7.6	12.75
4-30-S-con	69	32	13.6	10.5

Table 5. Comparison of test results with codes of practice and proposed model.

Slab no.	Ultimate load (kN)					Ratio (1)/ (2)	Ratio (1)/(3)	Ratio (1)/(4)	Ratio (1)/ (5)
	Exp. (1)	ACI (2)	B.S 8110 (3)	EC-2 (4)	Pred. (5)				
2-45-S	15.3	40.53	43.5	29.91	13.9	0.38	0.35	0.51	1.10
3-45-S	17.3	39.13	48.5	32.84	16.3	0.44	0.36	0.53	1.06
4-45-S	27.9	42.54	57.54	39.12	23.0	0.66	0.48	0.71	1.21
6-45-S	38.0	47.31	73.1	50.23	29.4	0.80	0.52	0.76	1.29
9-45-S	45.5	46.32	79.31	57.34	35.8	0.98	0.57	0.79	1.27
2-30-S	7.43	19.55	24.6	14.7	6.4	0.38	0.30	0.51	1.16
4-30-S	13.5	23.52	36.27	22.1	11.6	0.57	0.37	0.61	1.16
6-30-S	23.2	27.35	45.07	29.7	17.3	0.85	0.51	0.78	1.34
2-30-L	9.2	32.43	34.22	20.51	10.9	0.28	0.27	0.45	0.84
4-30-L	17.4	40.70	51.55	31.7	20.7	0.43	0.34	0.55	0.84
2-30-S-con	7.6	20.57	25.88	15.63	6.9	0.37	0.29	0.49	1.10
4-30-S-con	13.6	25.26	33.32	24.66	12.8	0.54	0.41	0.55	1.06
Average						0.56	0.40	0.60	1.12
Standard deviation						0.22	0.10	0.12	0.16
Min. value						0.28	0.27	0.45	0.84
Max. value						0.98	0.57	0.79	1.34

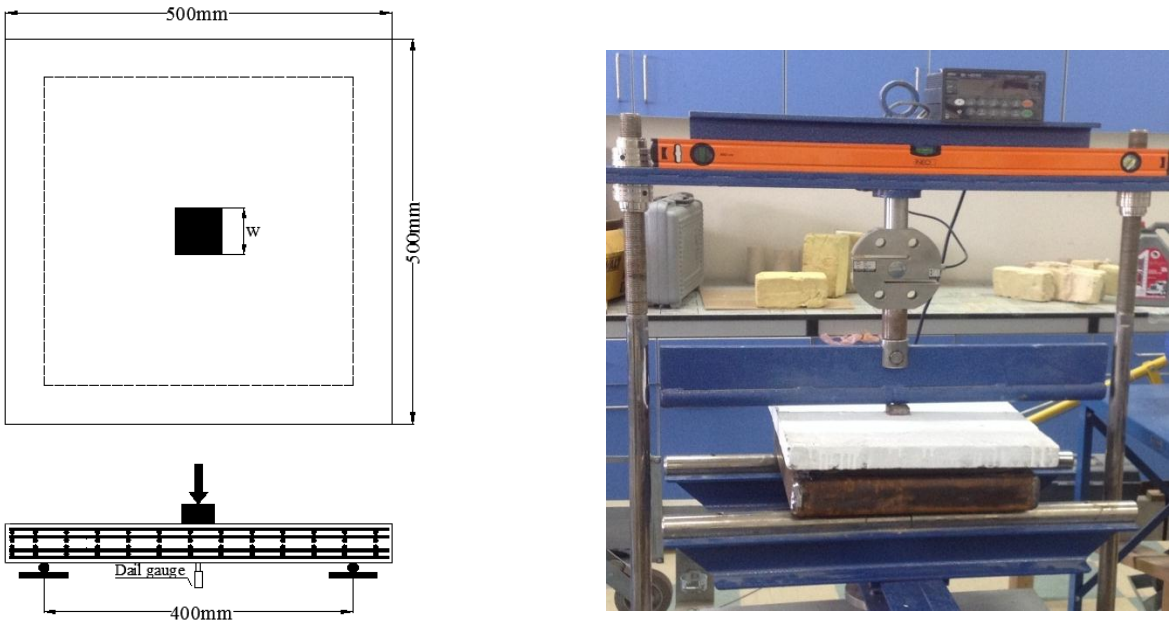

(a) Specimen detail. (b) Test setup.

Figure 1. Specimen detail and test setup.

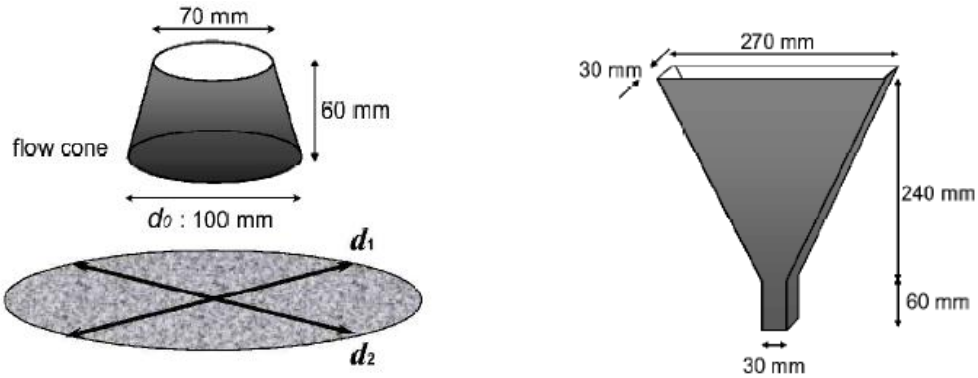

(a) Mini slump cone. (b) V-funnel apparatus.

Figure 2. Mortar flow and funnel tests.

Figure 3. Fabrication and cast of self compacting specimens.

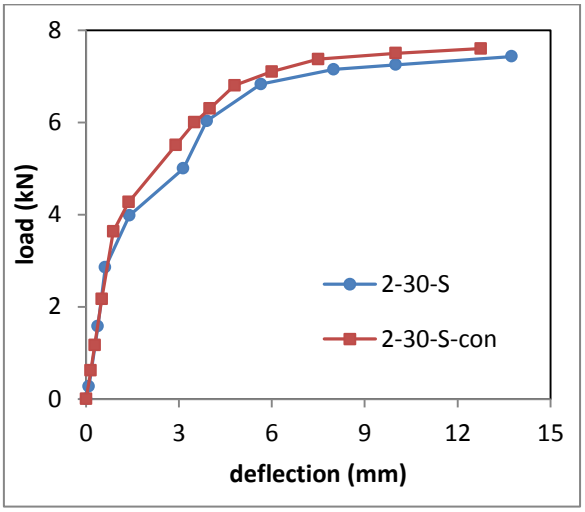

Figure 4. Comparison of load-central deflection response of self-compacted and normal slabs reinforced with Vf = 1.154%.

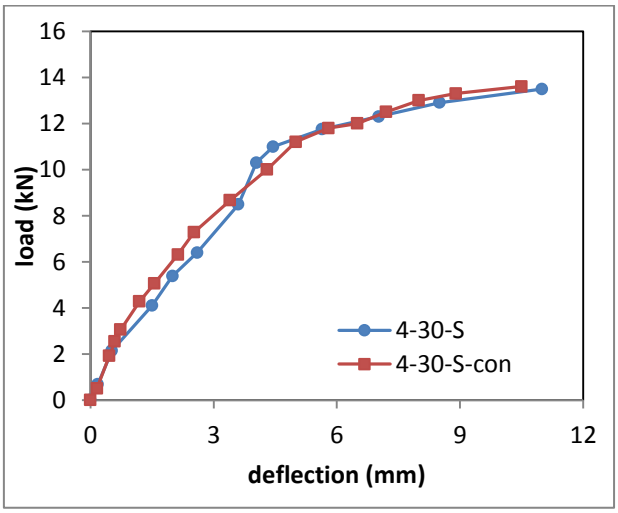

Figure 5. Comparison of load-central deflection response of self-compacted and normal slabs reinforced with Vf = 2.31%.

(a) 4-30-S-top face (b) 4-30-S-bottom face. (c) 4-30-S-con-top face. (d) 4-30-S-con- bottom face.

Figure 6. Punching failure mode of self-compacted and normal slabs.

(a) 2-30-S-bottom face. (b) 2-30-L-bottom face.

Figure 7. Failure mode of self compacted slabs with same volume fraction and different loading plate size.

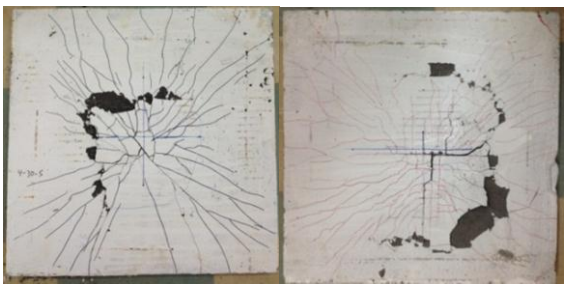

(a) 4-30-S-bottom face. (b) 6-45-S-bottom face.

Figure 8. Failure mode of self compacted slabs with same volume fraction and different thickness.

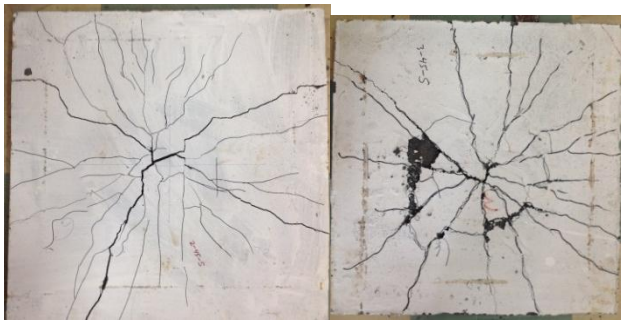

(a) 0-45-S-bottom face.	(b) 2-45-S-bottom face.	(c) 3-45-S-bottom face.

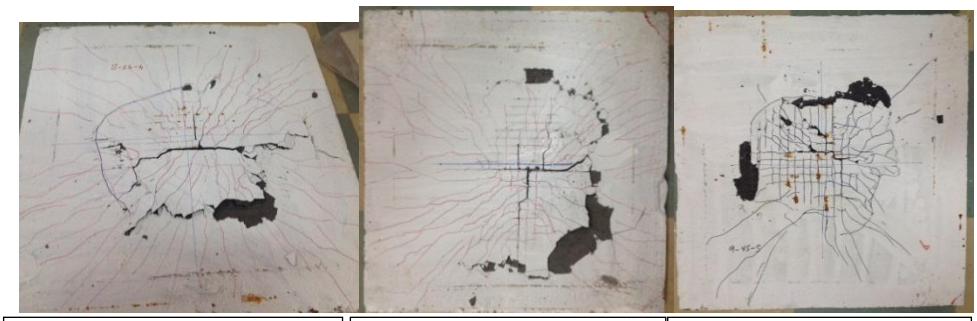

(d) 4-45-S-bottom face	(e) 6-45-S-bottom face	(f) 9-45-S-bottom face

Figure 9. Failure mode of self-compacted slabs with same thickness and different volume fraction.

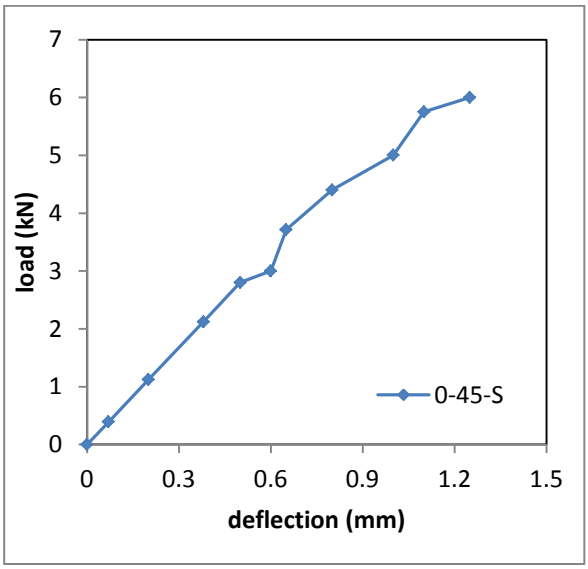

Figure 10. Load-central deflection response of plain self-compacted mortar.

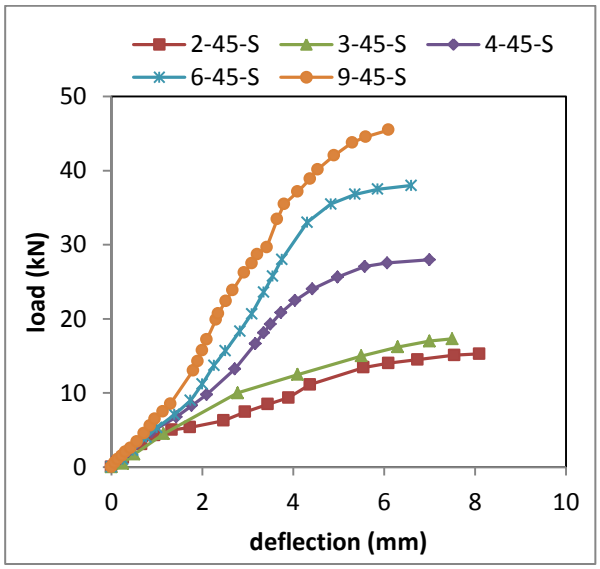

Figure 11. Comparison of load-central deflection response of self-compacted slabs reinforced with different volume fraction.

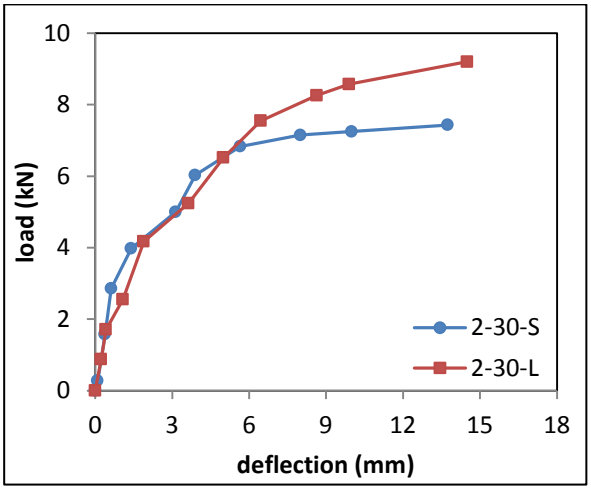

Figure 12. Comparison of load-central deflection response of self-compacted slabs reinforced with Vf = 1.154% and different loading plate size.

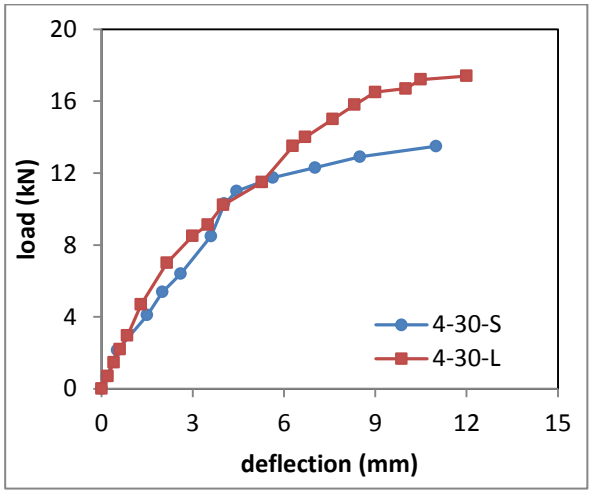

Figure 13. Comparison of load-central deflection response of self-compacted slabs reinforced with Vf = 2.31% and different loading plate size.

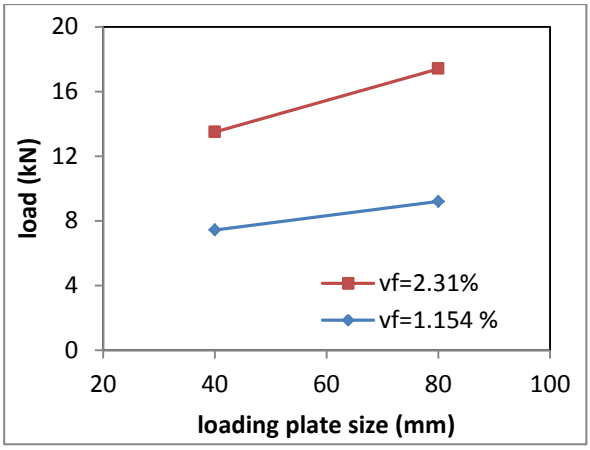

Figure 14. Effect of loading plate size on ultimate shear capacity of self-compacted slabs.

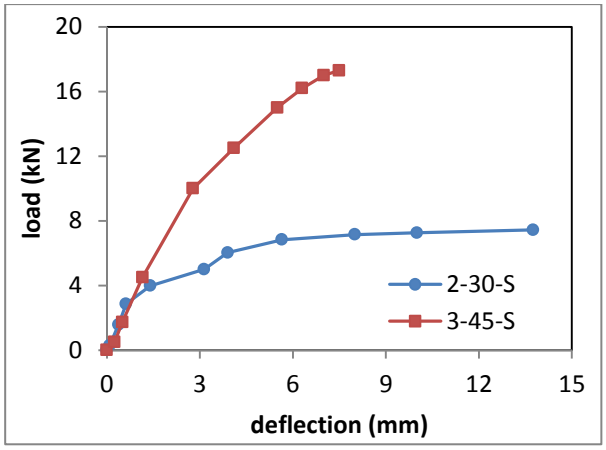

Figure 15. Comparison of load-central deflection response of self-compacted slabs reinforced with Vf = 1.154% and different slab thickness.

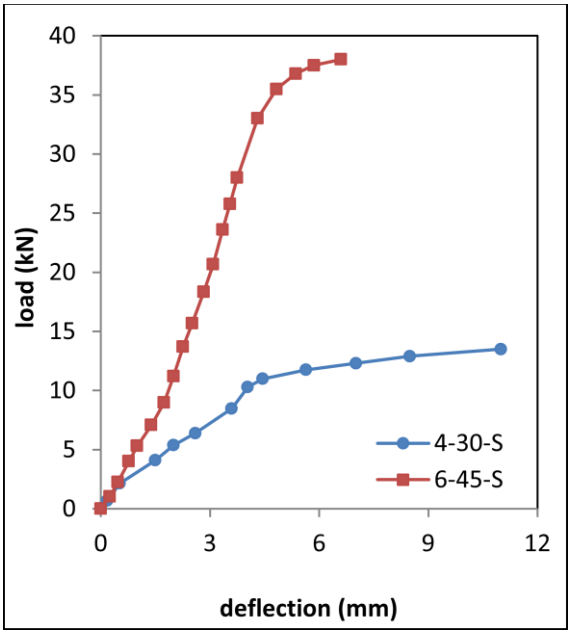

Figure 16. Comparison of load-central deflection response of self-compacted slabs reinforced with Vf = 2.31% and different slab thickness.

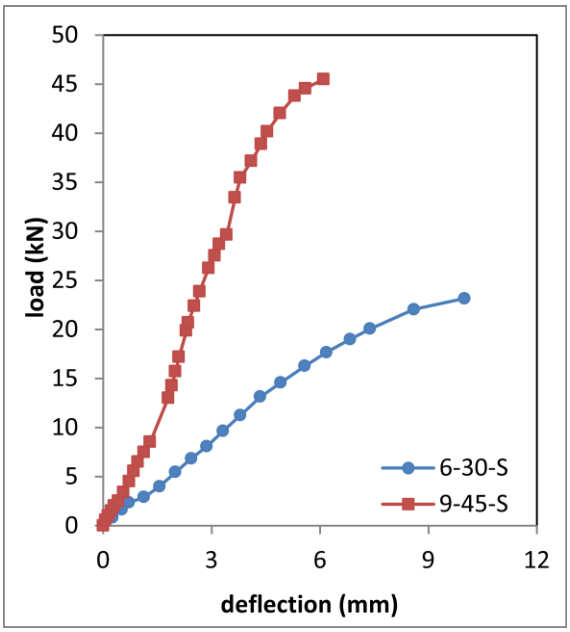

Figure 17. Comparison of load-central deflection response of self-compacted slabs reinforced with Vf = 3.464% and different slab thickness.

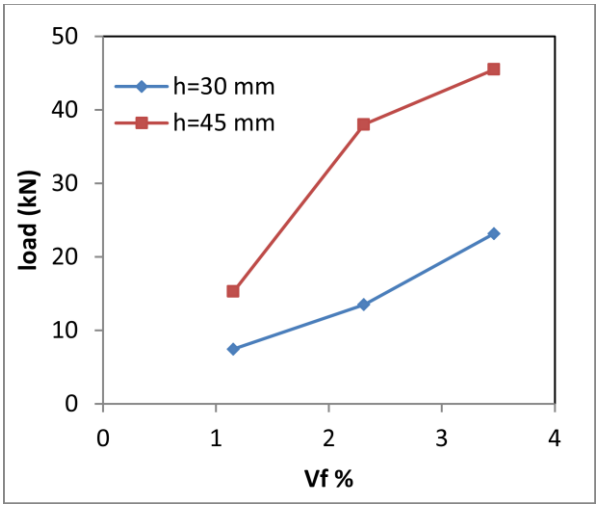

Figure 18. Effect of volume fraction on ultimate capacity of slabs.

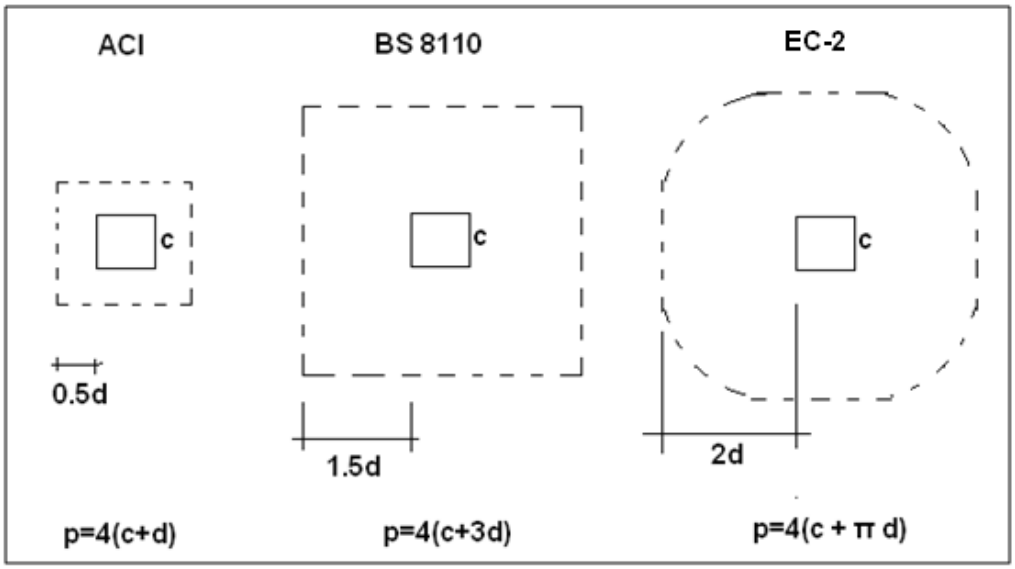

Figure 19. Critical section and perimeter of punching failure in different codes for square column.

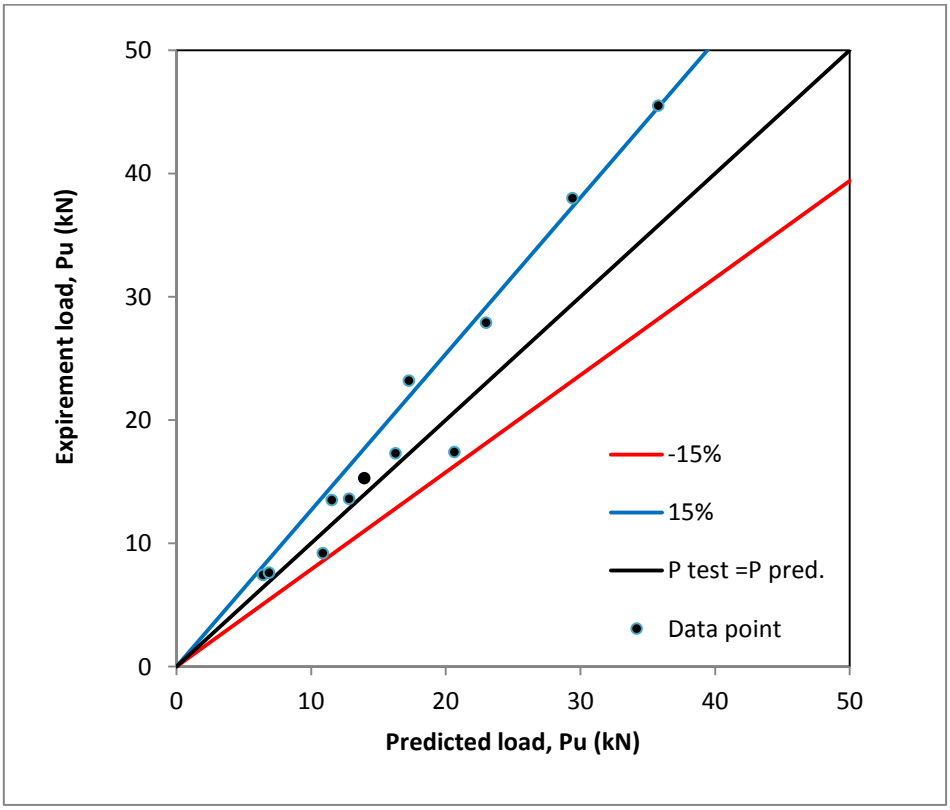

Figure 20. Comparison of experimental punching loads with prediction.

Planning of Distribution Networks in Baghdad City

Dr. Thamir M. Abdul-Wahhab
Lecturer
Department of Electrical Engineering
University of Technology
E-mail: thamir62@yahoo.com

Adeeb Nasser Hussein
M. Sc. Student
Department of Electrical Engineering
University of Technology
E-mail: adeeb.nasser@yahoo.com

ABSTRACT

Planning of electrical distribution networks is considered of highest priority at the present time in Iraq, due to the huge increase in electrical demand and expansions imposed on distribution networks as a result of the great and rapid urban development.
Distribution system planning simulates and studies the behavior of electrical distribution networks under different operating conditions. The study provide understanding of the existing system and to prepare a short term development plan or a long term plan used to guide system expansion and future investments needed for improved network performance.
The objective of this research is the planning of Al_Bayaa 11 kV distribution network in Baghdad city based on the powerful and efficient CYMDist software as a tool for the simulation and analysis of the network.
The planning method proposed in this thesis is to reach the optimum operating conditions of the network by combining the network reconfiguration in sequence with the insertion of capacitors with optimal sizing and locations. The optimum performance of the network is achieved by reducing losses, improving voltage profile and alleviating overload for transformers and cables.
Key words: Distribution network planning, CYMDist software, network reconfiguration, capacitor placement, loss minimization.

تخطيط شبكات التوزيع في مدينة بغداد

د. ثامر محمد عبد الوهاب
مدرس
قسم الهندسة الكهربائية
الجامعة التكنلوجية

أديب ناصر حسين
طالب ماجستير
قسم الهندسة الكهربائية
الجامعة التكنلوجية

الخلاصة

يعد تخطيط شبكات التوزيع الكهربائية من الأولويات في الوقت الحاضر في العراق نظراً للزيادة الهائلة في الأحمال الكهربائية و التوسعات المفروضة على الشبكات نتيجة التطور العمراني الكبير والسريع.
تخطيط منظومة التوزيع يحاكي ويدرس سلوك شبكات التوزيع الكهربائية في ظل ظروف تشغيل مختلفة. الدراسة توفر فهم المنظومة القائمة وإعداد خطة تنموية قصيرة الأجل أو خطة طويلة المدى تستخدم لتوجيه التوسع في المنظومة والاستثمارات المستقبلية اللازمة لتحسين أداء الشبكة.
الهدف من البحث هو تخطيط شبكة توزيع كهرباء البياع 11 kV في مدينة بغداد استناداً الى برمجيات CYMDist ذات القدرة والكفاءة العالية كأداة لتمثيلها حاسوبياً و اجراء التحليلات عليها.
ان طريقة التخطيط المقترحة في هذه الأطروحة للوصول الى حالة الأداء الأمثل للشبكة هي بأجراء عملية تغيير طوبوغرافية الشبكة بالتعاقب مع ادخال متسعات بسعات محسوبة وفي اماكن مثالية في منظومة التوزيع. ويتحقق الأداء الأمثل للشبكة بتقليل المفاقيد, وتحسين الجهد (voltage profile) ومعالجة مشكلة الحمل الزائد للمحولات والمغذيات.
الكلمات الرئيسية: تخطيط شبكات التوزيع, برنامج CYMDist, تغيير طوبوغرافية الشبكة, ادخال متسعات, تقليل المفاقيد.

1. INTRODUCTION

The objective of distribution network planning is to satisfy the annual load growth for the planning period, reduce line losses, improve voltage profile and increase reliability of the network. The power loss is significantly high in distribution networks because of lower voltage levels and higher currents, these losses cannot be eliminated but can be reduced, **,Satish, 2012.** Power loss minimization by reconfiguring the network and installing shunt capacitors are two main means for loss reduction. Network reconfiguration is defined as altering the topological structure of distribution networks by changing the open/closed status of the normally closed (sectionalizing) and normally open (tie) switches. If shunt capacitors are installed in the correct position and size it can significantly improve the performance of distribution circuits. **Literature Review: ,Baran, and Wu, 1989.** proposed a new solution method for network reconfiguration based on a branch-exchange for both loss reduction and load balancing between feeders. Two approximate load flow methods for radial systems have been developed, these are the simple Dist flow and Backward/Forward methods.

,Thiruvenkadam, et al., 2008. presented a feeder reconfiguration algorithm for loss reduction and load balancing at the same time. The proposed algorithm efficiently utilizes a heuristic based fuzzy strategy and constrained fuzzy operation along with back propagation neural network.

,Dong Zhang, et al., 2008. proposed a joint optimization algorithm of combining network reconfiguration and capacitor control for loss reduction in distribution systems. An improved adaptive genetic algorithm (IAGA) is developed to optimize capacitor switching, and a simplified branch exchange algorithm is developed to find the optimal network structure.**,Gupta et al., 2011.** presented a fast and efficient heuristic algorithm to explore the optimal number, locations and sizing of shunt capacitors in radial distribution systems under varying load conditions. A new constraint objective cost function (COCF) has been formulated to maximize the net annual saving by minimizing the real power losses and optimizing the annual investment on shunt capacitors while improving the system node voltage profile.

,Prasanna et al., 2012. proposed a new method of Second order PSO for a more effective capacitor sizing in radial distribution feeders to reduce the real power loss and to improve the voltage profile. The location of the nodes where the capacitors should be placed is decided by a set of rules given by the fuzzy expert system and the sizing of the capacitors is modeled by the objective function to obtain maximum savings using Particle Swarm Optimization (PSO).

2. THE PROPOSED METHOD

The proposed planning approach consists of:

1. Load allocation.
2. Reconfiguration of the network by changing switch status.
3. In case of operational constraints are violated in the reconfigured network, reactive power compensation is applied for candidate buses.

a. Load Allocation: In this work the connected kVA load allocation technique provided by CYMDist software is used which distributes the substation load demand (entered by the user in amps for each phase) along the feeder according to the connected kVA of the distribution transformers.

b. Network Reconfiguration: In the problem of system reconfiguration, the control variables are switching statuses. To get different choices of topologies, the switching statuses are randomly altered in between two values such as 1 for close or 0 for open. The objective function of the network reconfiguration problem is the minimization of power loss which can be expressed mathematically as follows **,Manju, et al., 2012.**

$$min.f = \sum_{i=1}^{n} k_i r_i \frac{P_i^2 + Q_i^2}{V_i^2} \quad (1)$$

Where: f the objective function, n total number of branches, r_i resistance of branch i, Q_i reactive power of branch i, P_i active power of branch i, V_i voltage on head node of branch i, k_i switch status on branch i (k_i =1 equal to closed, k_i= 0 equal to open).

2.1 Subject to the following constraints

Voltage Constraint: Voltage magnitude at each node must lie within its permissible range:

$$V_{min.} \leq V_{load} \leq V_{max.} \quad (2)$$

Where: $V_{min.}$ and $V_{max.}$ are the lower and upper voltage limits, respectively.

Radiality Constraints: each load node should be fed by only one substation (no loops are allowed in the network).

Power Source Limit Constraint: The total loads of a certain partial network cannot exceed the capacity limit of the corresponding power source:

$$P_t \leq P_s^{max.} \quad (3)$$
$$Q_t \leq Q_s^{max.} \quad (4)$$

Power factor constraint, harmonics constraint, and voltage angle constraint has not been taken into consideration to avoid the complexity of the problem.

2.2 The reconfiguration method

starts with a meshed distribution network obtained by considering all switches closed. Then, the switches are opened successively to eliminate the loops. The opening criterion is based on minimum total power loss increase, and this is determined using the power-flow program in CYMDist. The two procedures of this method are illustrated in **,Flávio, et al., 2005.**

2.3 Optimal capacitor placement and sizing

The problem is formulated to determine the optimal shunt capacitor size and location in a radial distribution network by minimizing the ohmic losses, taking into account cost of the capacitor. At the same time, the choice is restricted by electric network constraints. The sizes of capacitor banks are given by standard size, which makes the set of solutions to be discrete, **,Héctor, 2013.** For simplicity, the operation and maintenance cost of the capacitor placed in the distribution system is not taken into consideration.

Capacitor placement routine exists in CYMDist module, the routine performs single objective optimization (either P_{loss} or ΔV).

Subject to The Following Constraints:

Bus Voltage Limits: The bus voltage magnitudes are to be kept within acceptable operating limits throughout the optimization process:

$$V_{min.} \leq |V_i| \leq V_{max.} \quad (5)$$

Where: $V_{min.}$ Lower bus voltage limit; $V_{max.}$ Upper bus voltage limit; $|V_i|$ rms value of the i_{th} bus voltage.

The Line Current (I), should be less than the line rated current (I_{rated}).

$$I \leq I_{rated} \tag{6}$$

Power-Conservation Limit: The algebraic sum of all incoming and outgoing power including line losses over the whole distribution network should be equal to zero:

$$P_G - \sum_{i=1}^{n} P_D - P_{lt} = 0 \tag{7}$$

Where: P_G power generation, P_D power demand; P_{lt} total power losses

The Number and Sizes of Permissible Capacitor Banks Constraint:

The number of capacitor banks can be expressed to satisfy the following expression:

$$\sum_{i=1}^{m} Q_c \leq Q_t \tag{8}$$

Where: Q_c kVAr obtained from the capacitor bank; Q_t total reactive power flow required; *m* total number of capacitor banks.

The capacitor placement method determines the optimal sizes and placements of the capacitors that minimize the objective function and satisfy constraints.

3. FORWARD/BACKWARD SWEEP LOAD FLOW OF DISTRIBUTION SYSTEMS (Ladder Iterative Technique)

The backward-forward sweep method is an iterative means to solve the load flow equations of radial distribution networks which has two steps. The backward sweep, which updates currents using Kirchoff's Current Law (KCL), and the forward sweep, which updates voltage using voltage drop calculations, **,William, 2002.** The voltage magnitude and phase angle of the source should to be specified. Also the complex values of load demands at each node along the feeder should be known, **,Manas, 2014.**

4. COST OF ENERGY LOSSES

To calculate the annual cost of system losses, the built-in loss factor formula in CYMDist is used (eq. 9). The loss factor (L_{fls}) is an expression of the real power loss over a given period of time at a given loading condition.

$$Loss\ Factor = A \times LDF + (1 - A) \times LDF^2 \tag{9}$$

Where, A is a constant for distribution network and taken occasionally as 0.15 for distribution system **,Meghana, 2011.**, LDF is the load factor.

The following empirical formula is used to estimate the annual cost of active power losses after a load flow simulation, **,Sarwar, et al., 2012.**

$$Annual\ cost = P_{loss\ max.} \times L_{fls} \times T \times C \tag{10}$$

Where:

$P_{loss\ max}$: power loss at the peak load power (kW); L_{fls}: loss factor

T: time interval (h); C: tariff cost ($)

For reactive power compensation, the cost includes the cost of power loss and the investment cost of capacitor placement. The maximum capacitor size Q_{max} should not exceed the total reactive loads. The annual cost equation will be, **,Divya,** and **Siva, 2013.**

$$annual\ cost = P_{\substack{loss \\ max.}} \times L_{fls} \times T \times C + \sum_{j=1}^{k} K_j Q_j \quad (11)$$

Where: Q: Capacitor size (kVAr); K: Cost of capacitor size ($/kVAr)
j=1, 2… k represents the selected buses.

5. CYMDist SOFTWARE

CYMDist is a windows-based primary distribution analysis software available from CYME Inc, Canada. It is an advanced engineering tool that used for planning studies and simulating the behavior of electrical distribution networks in its present or future state under different operating conditions and scenarios. Analytical capabilities of the CYME software fully support any type of simulation, the graphical representation of network components can represented schematically or geographically, **,CYME Reference, Manual.**

a. Types of Loads Identified by CYMDist

Distributed loads are the "normal" loads in the system, while Spot loads are often representing predictable and substantially large loads, such as industrial customers.

In Iraq, loads are usually represented by spot load type, which often placed at the center of sections [MOE].

b. Network Modeling

The modeling process begins with acquiring all the input data required for the modeling, and the combined processed data are entered or imported from GIS software into CYMDist to create the distribution system model, with the single line diagram automatically generated.

c. Types of Analysis Features in CYMDist

The voltage drop calculation technique in CYMDist is an iterative technique that is specifically designed and optimized for radial or weakly meshed networks.

In this thesis, the studied networks are analyzed based on voltage drop analysis.

i. Load Allocation Methods

CYMDist provides four load allocation methods among these methods the connected kVA load allocation method is the one used in this work.

ii. Load Flow Analysis in CYME:

The backward-forward sweep method, also known as the ladder methodology, is used by the iterative software in CYMDist to compute the branch currents.

iii. CYMDist_SOM (Switching Optimization)

The module can determine the optimal location of the tie points by suggesting new locations or recommending new switching schemes for existing devices to achieve optimal network topologies.

6. THE PROPOSED PLANNING METHOD

The proposed planning method in this work is illustrated by the flow chart in **Fig.1**.

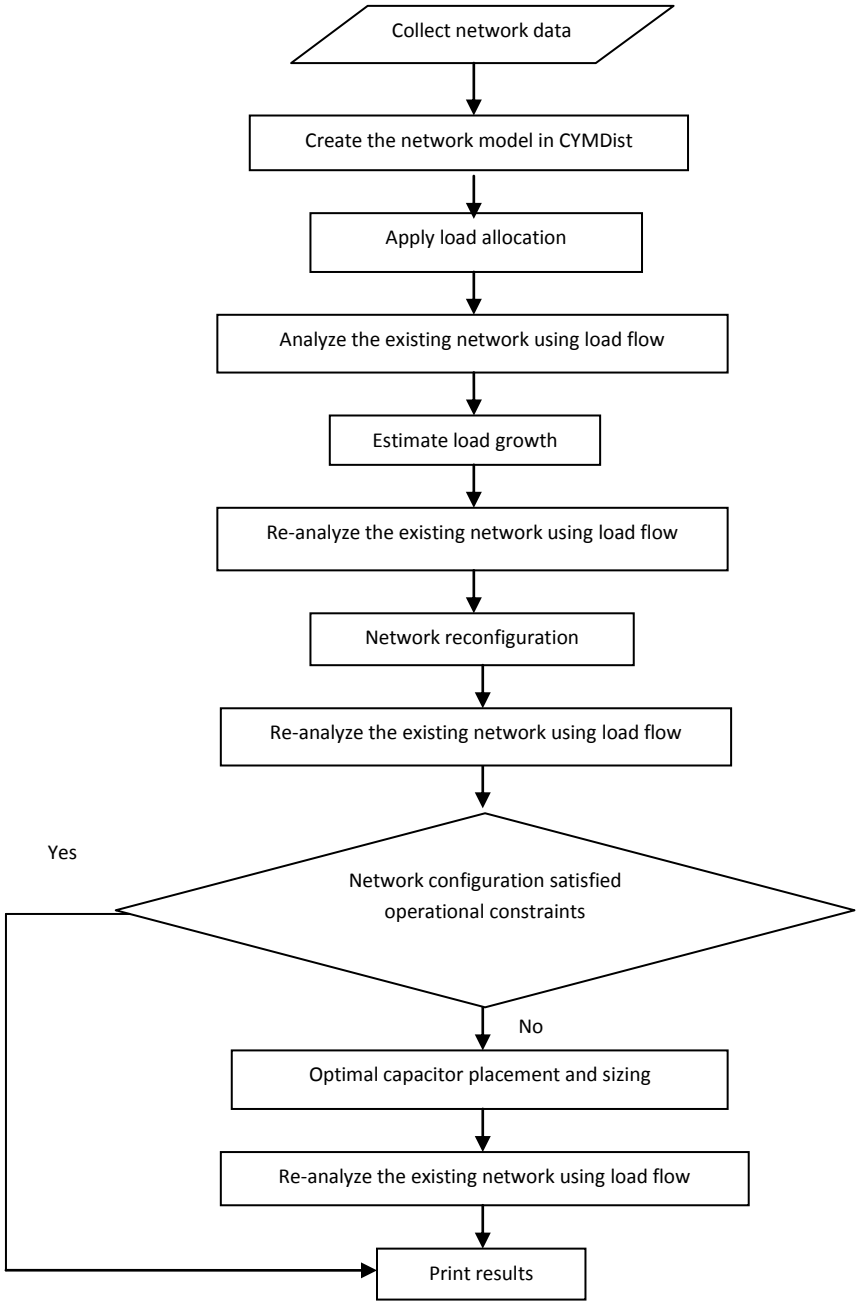

Figure 1. Flow chart representing the proposed planning method using CYMDist software.

7. CASE STUDY and RESULTS

The proposed analysis is implemented, using the CYMDist 4.5 (Rev.6) software, on Al_Bayaa distribution network in Baghdad city. The capacity of Al_Bayaa (33/11 kV) substation is (2*31.5 MVA), which is fed by two 33kV feeders from Al-Jazayr and Al-Dora expansion substations (132/33/11 kV). There are Fourteen (11 kV) feeders outgoing from Al_Bayaa substation serving a large area of mixed residential, commercial, and industrial loads. Only four feeders are considered in this work.

a. Al_Bayaa Distribution Network

Al_Bayaa network is rated at 11 kV, base MVA =100, and frequency of 50 Hz with (151) line sections, (145) buses, and six tie switches. The schematic diagram of Al_Bayaa system by CYMDist is shown in **Fig.2**. The load for Al_Bayaa feeders is mixed, approximately 94% residential and 6% commercial.

The load duration curve for the years of planning horizon is divided to three load levels (high, medium and low) as shown in **Table 1.**

Table 1. Load duration curve of Al_Bayaa substation [MOE].

Load (%)	100	70	40
Time of loading (%)	33	52	15
Duration (h)	2891	4555	1314

The modeling of Al_Bayaa network is based on the actual coordination's of the secondary distribution transformers. This coordination's are taken from Iraqi ministry of electricity depending on the global positioning system (GPS). The coordinates are entered to the CYMDist module as x and y coordinates for the nodes (buses) to build the model and specify the actual length of the network sections.

Before starting, some assumptions are made in this work:

- Balance voltage drop iterative method is used, the maximum number of iterations are 40 for load flow and the convergence error (dv) to be 0.01%.
- Tariff cost (cost of electrical energy) is 0.1 $/kWh according to Iraqi ministry of electricity.
- Voltage limitation is set to 5% over the voltage rating, or 5% under voltage rating.
- The objective functions of the switching optimization and capacitor placement are to minimize kW losses, for the average peak demand for the last year of planning horizon.
- The entire feeders load factor for the selected networks in this thesis is equal to 65%.
- The effect of harmonics is ignored.
- All the loads have the same power factor.
- The Stability is ignored.
- The basic distribution infrastructure and characteristics will remain as they are today.

By using the connected kVA method with (dv= 0.01%) tolerance for accuracy, loads are distributed in all sections for each phase depending on the current values at the head of each feeder and the secondary (11/0.4 kV) (Delta- Grounded wye) transformer capacities are as shown in **Table 2a. and Table 2b.**

Table 2a. The current at the top head of each feeder of Al_Bayaa network.

Top head feeder	Current / phase (A)	P.F (%)
Bayaa_7	240	80
Bayaa_8	200	80
Bayaa_11	220	80
Bayaa_12	170	80

Table 2b. Secondary transformer capacities of Al_Bayaa network.

Spot load number	Transformer capacity (kVA)
2, 3, 6, 11, 26, 27, 30, 31, 32, 34, 36, 37, 40, 41, 43, 46, 48, 49, 50, 56, 59, 63, 64, 68, 69, 71, 78, 82, 85, 88, 89, 91, 94, 95, 96, 97, 107, 111, 112, 113, 115, 117, 118, 120, 121, 125, 128, 130, 132, 134, 149.	250
4, 7, 8, 9, 12, 13, 14, 18, 19, 20, 21, 22, 23, 25, 29, 35, 38, 54, 58, 60, 67, 73, 84, 87, 90, 92, 98, 101, 102, 105, 109, 110, 123, 126, 138, 142, 144, 150.	400

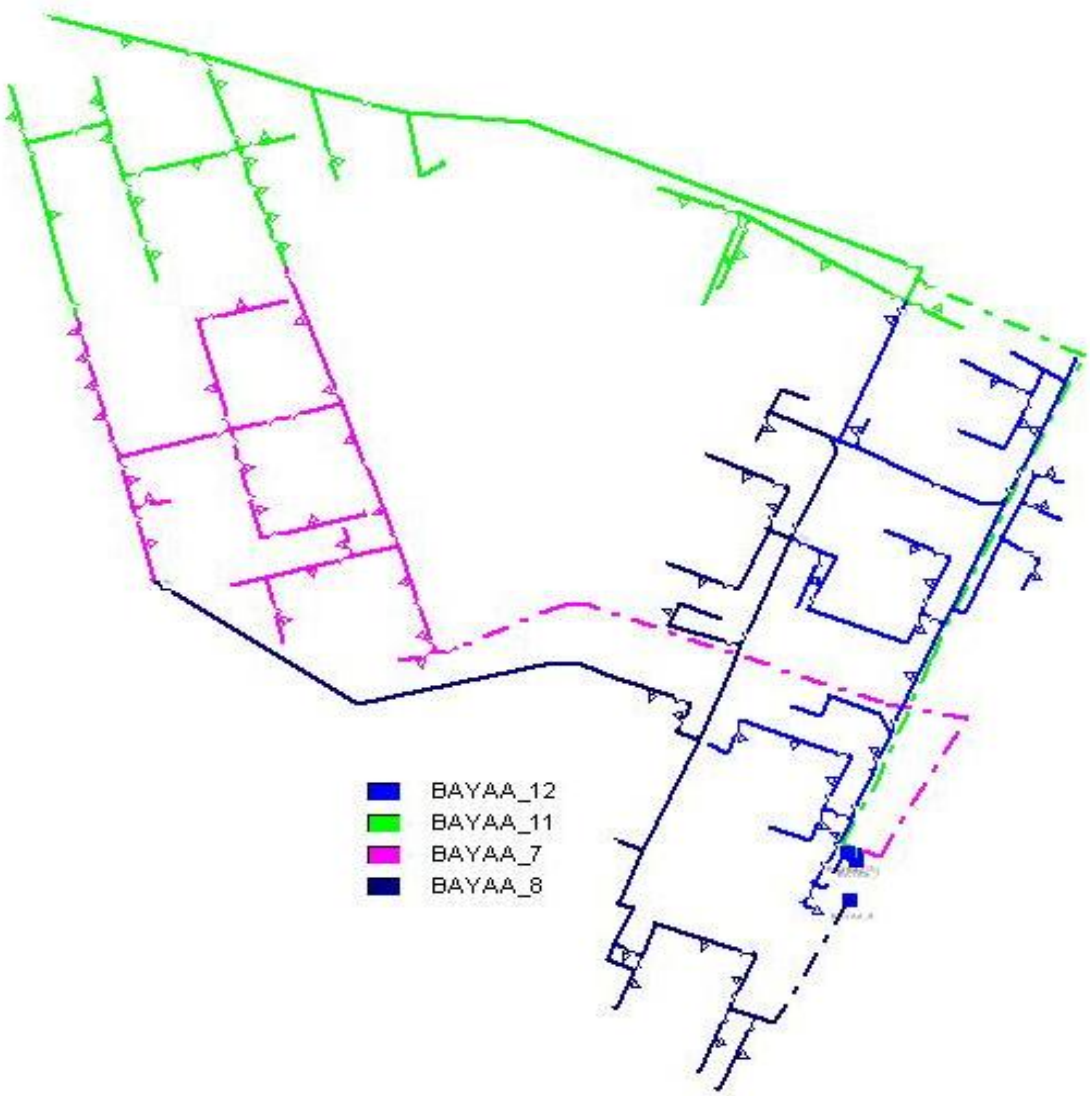

Figure 2. Initial configuration of Al_Bayaa network.

Before applying the short term planning to the existing network, it must be analyzed using load flow. Load growth analysis should be applied to the network in order to examine its consolidation and efficiency to yearly load growth. The network is assessed with the percentage annual load growth rate for the next 5 years (2013-2017) as shown in **Fig. 3**.

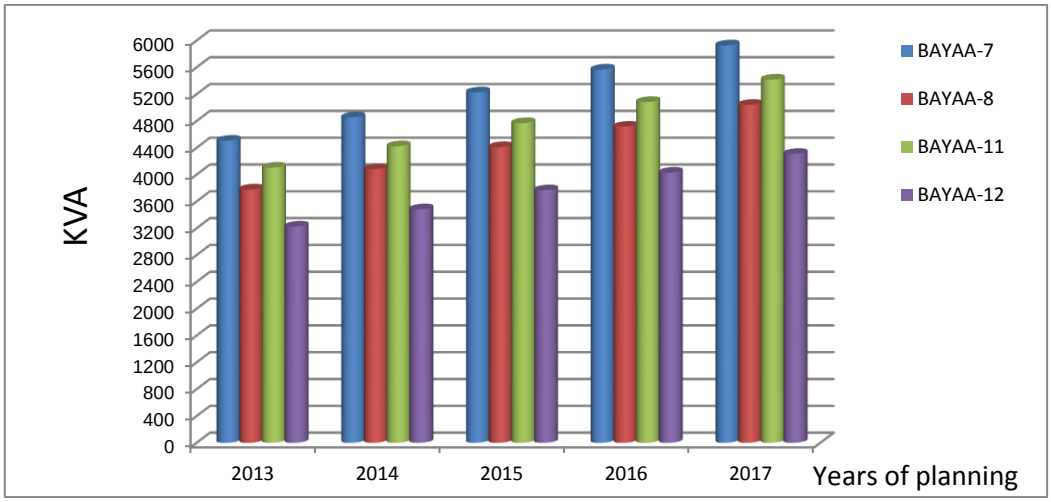

Figure 3. Load growth of the feeders of Al_Bayaa network.

There are 5 sections that operate in overloaded condition as shown in **Fig.4**. (All calculations are done for the last year of the planning horizon and for peak load only).

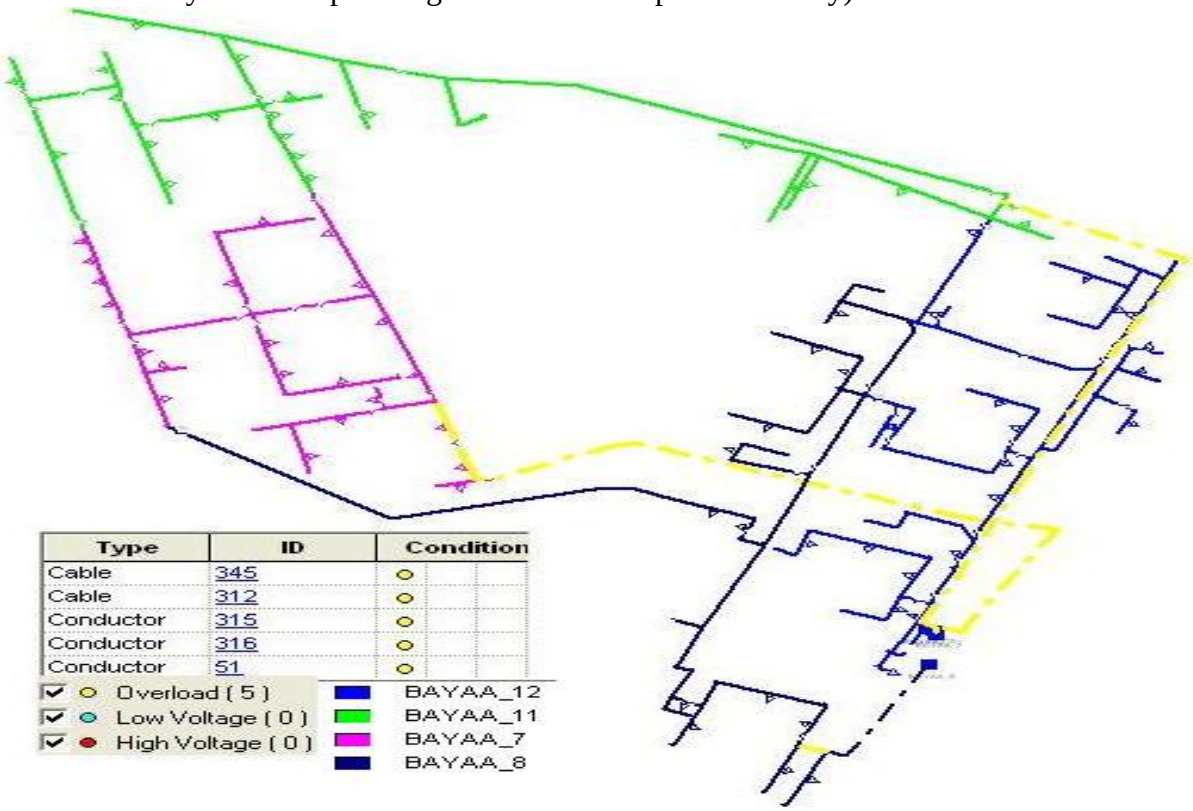

Figure 4. Abnormal conditions after load growth for Al_Bayaa network.

The simulation results listed in **Table 3.** shows that the initial system real power losses after load growth for all feeders were 269.36 kW. Applying the switching optimization technique to minimize losses and to distribute loads on a regular basis among feeders, the final power loss after reconfiguration became 229.29 kW, so the total reduction in power losses after reconfiguration became 40.07 kW (14.87 % of its initial value). The optimal configuration is shown in **Fig.5**. **Table 4.** shows the switching operation modes during system reconfiguration.

After applying the load flow, it is obvious that the network is still operating under abnormal conditions (5 sections are operating under overloaded conditions as shown in **Fig. 6**. Therefore, reactive power compensation can be the solution to this problem by increasing the capacity of these feeders. Optimal locations of capacitors are shown in **Fig.7** and **Table 5.** gives the optimal of capacitor placement and sizing. **Table 3.** gives the voltage drop before and after load growth, switching optimization and kVAr compensation. **Table 6.** gives the voltage drop summary for all feeders, the total system kW losses for all feeders are shown in **Fig.8**.

Table 3. Voltage drop before and after load growth, after switching optimization and kVAr compensation of Al_Bayaa network at peak load.

Bayaa_7		Total load used	Total adjusted shunt capacitor + total conductor capacitances	Total losses	Total source power
Before load growth	kW	3605.97	---	51.84	3657.81
	kVAr	2702.52	0+5.69	46.49	2743.32
	kVA	4506.29	---	69.64	4572.24
	P.F.	0.8	---	0.74	0.8
After load growth	kW	4744.08	---	90.68	4834.76
	kVAr	3555.49	0+5.67	81.32	3631.14
	kVA	5928.56	---	121.8	6046.49
	P.F.	0.8	---	0.74	0.8
After switching optimization	kW	4291.55	---	69.89	4361.44
	kVAr	3215.07	0+5.47	61.91	3271.51
	kVA	5362.28	---	93.36	5452.05
	P.F.	0.8	---	0.74	0.8
After kVAr compensation	kW	4291.55	---	44.9	4336.45
	kVAr	3215.07	3086.01+5.49	39.9	163.47
	kVA	5362.28	---	60.07	4339.53
	P.F.	0.8	---	0.74	0.99
Bayaa_8		Total load used	Total adjusted shunt capacitor + total conductor capacitances	Total losses	Total source power
Before load growth	kW	3025.22	---	23.16	3048.38
	kVAr	2265.19	0 + 2.69	23.78	2286.27
	kVA	3779.29	---	33.19	3810.47
	P.F.	0.8	---	0.69	0.8
After load growth	kW	4035.19	---	42.07	4077.26
	kVAr	3021.43	0 + 2.68	43.23	3061.98
	kVA	5041.01	---	60.32	5099
	P.F.	0.8	---	0.69	0.8
After switching optimization	kW	4117.04	---	52.52	4169.57
	kVAr	3083.26	0 + 2.63	54.56	3135.19
	kVA	5143.59	---	75.73	5216.77
	P.F.	0.8	---	0.69	0.8
After kVAr compensation	kW	4117.04	---	34.25	4151.29
	kVAr	3083.26	2204.31 + 2.65	35.54	911.84
	kVA	5143.59	---	49.36	4250.26
	P.F.	0.8	---	0.69	0.97

Table 3 continued

Bayaa_11		Total load used	Total adjusted shunt capacitor + total conductor capacitances	Total losses	Total source power
Before load growth	kW	3286.84	---	66.43	3353.27
	kVAr	2457.61	0 + 6.46	63.81	2514.96
	kVA	4104.04	---	92.11	4191.59
	P.F.	0.8	---	0.72	0.8
After load growth	kW	4339.6	---	117.22	4456.82
	kVAr	3244.77	0 + 6.43	112.55	3350.9
	kVA	5418.55	---	162.5	5576
	P.F.	0.8	---	0.72	0.8
After switching optimization	kW	4122.84	---	76.11	4198.95
	kVAr	3083.83	0 + 6.63	69.29	3146.5
	kVA	5148.58	---	102.93	5247.06
	P.F.	0.8	---	0.73	0.8
After kVAr compensation	kW	4125.43	---	50.02	4175.45
	kVAr	3085.77	2635.49 + 6.66	45.76	489.38
	kVA	5151.81	---	67.8	4204.03
	P.F.	0.8	---	0.73	0.99
Bayaa_12		Total load used	Total adjusted shunt capacitor + total conductor capacitances	Total losses	Total source power
Before load growth	kW	2580.34	---	10.8	2591.14
	kVAr	1934.26	0 + 2.32	11.41	1943.35
	kVA	3224.83	---	15.71	3238.92
	P.F.	0.8	---	0.68	0.8
After load growth	kW	3447.68	---	19.39	3467.07
	kVAr	2584.43	0 + 2.32	20.5	2602.61
	kVA	4308.8	---	28.21	4335.22
	P.F.	0.8	---	0.68	0.8
After switching optimization	kW	4038.62	---	30.77	4069.4
	kVAr	3026.58	0 + 2.4	32.7	3056.87
	kVA	5046.84	---	44.9	5089.64
	P.F.	0.8	---	0.68	0.8
After kVAr compensation	kW	4043.62	---	20.8	4064.42
	kVAr	3030.32	2224.38 + 2.41	22.12	825.64
	kVA	5053.08	---	30.36	4147.43
	P.F.	0.8	---	0.68	0.98

Table 4. Switching operations of Al_Bayaa network.

Section Id	142	14	103	124	140	51	55	136	61	24	88	102
Action	Close	Close	Close	Close	Close	Close	Open	Open	Open	Open	Open	Open
Switch Id	S142	S14	S103	S124	S140	S51	S55	S136	S61	S24	S88	S102

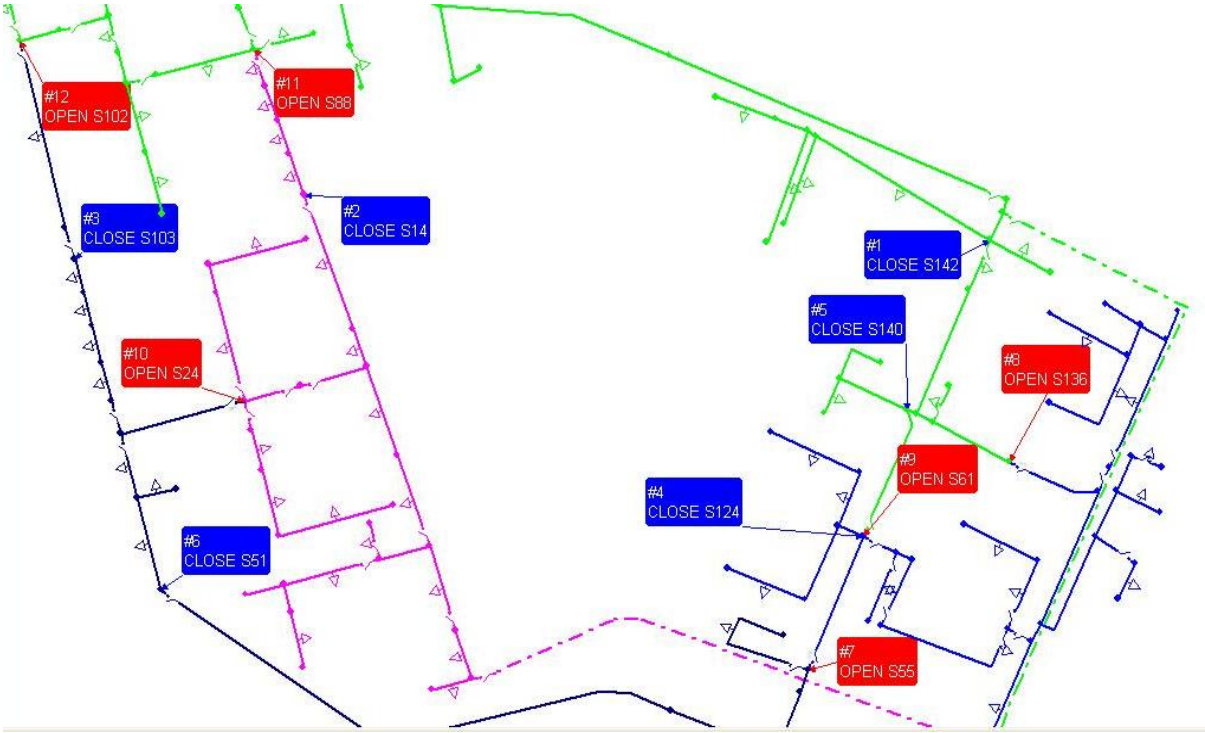

Figure 5. Optimal configuration of Al_Bayaa network.

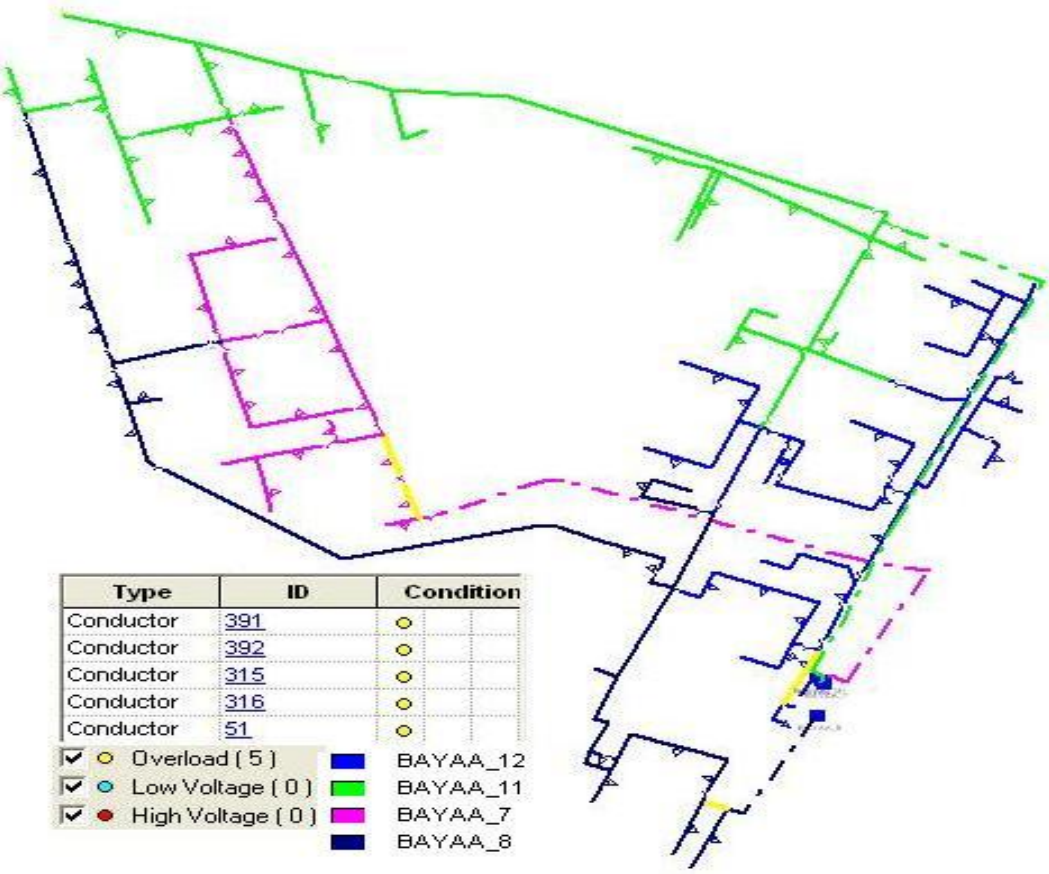

Figure 6. Abnormal conditions after applying switching optimization technique of Al_Bayaa network.

Table 5. Optimal location and size of capacitors for Al_Bayaa network at peak load conditions (100% loading).

Bayaa_7 : P.F corrected to 0.99			
Node Id	Cap. kV (L-L)	Total capacitors (kVAr)	Loss reduction (kW)
16	11	900	11.3
14	11	900	7.7
4	11	1350	0.58
Total		3150	23.9
Bayaa_8 : P.F corrected to 0.97			
29	11	900	10.9
49	11	450	4
39	11	900	3.1
Total		2250	18
Bayaa_11 : P.F corrected to 0.99			
96	11	450	9.5
85	11	900	10.3
66	11	1350	5.7
Total		2700	25.5
Bayaa_12 : P.F corrected to 0.98			
56	11	900	5.5
119	11	450	2.4
115	11	900	1.8
Total		2250	9.7

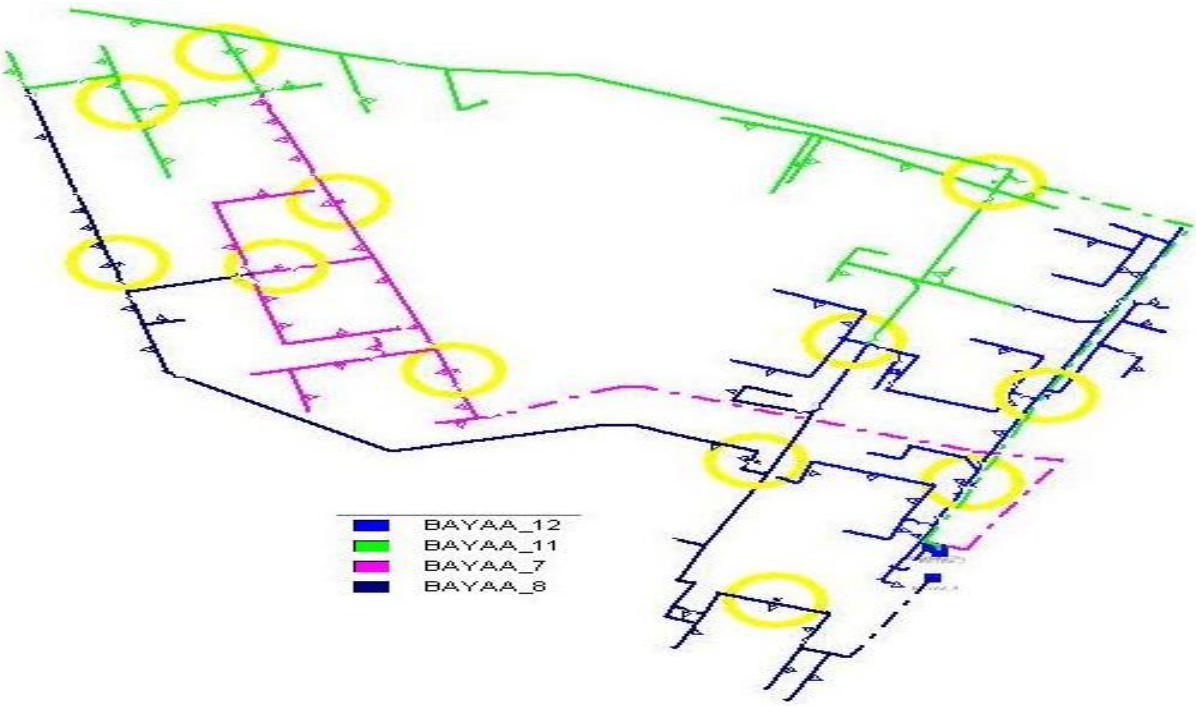

Figure 7. Optimal capacitor allocations for Al_Bayaa network.

Table 6. Summary of results of Al_Bayaa network using CYMDist

Bayaa_7	Before load growth	After load growth	After switching optimization	After kVAr compensation
Maximum voltage (p.u.)	1	1	1	1
Minimum voltage (p.u.)	0.982	0.976	0.98	0.987
Total Active power loss (kW)/phase	17.28	30.23	23.3	14.97
Total Reactive power loss (kVAr)/ phase	15.5	27.11	20.64	13.3
Total kW load/phase	1202	1581.4	1430.5	1430.5
Total kVAr load/phase	901	1185	1072	1072
Total actual kVA load/phase	1502	1976	1787	1787
Bayaa_8	Before load growth	After load growth	After switching optimization	After kVAr compensation
Maximum voltage (p.u.)	1	1	1	1
Minimum voltage (p.u.)	0.987	0.983	0.975	0.985
Total active power loss (kW)/phase	7.72	14.02	17.51	11.42
Total reactive power loss (kVAr)/ phase	7.93	14.41	18.19	11.85
Total kW load/phase	1011.5	1350.8	1372.3	1372.3
Total kVAr load/phase	757	1011	1028	1028
Total actual kVA load/phase	1264	1688	1715	1715
Bayaa_11	Before load growth	After load growth	After switching optimization	After kVAr compensation
Maximum voltage (p.u.)	1	1	1	1
Minimum voltage (p.u)	0.972	0.963	0.972	0.981
Total active power loss (kW/phase)	22.14	39.07	25.37	16.67
Total reactive power loss (kVAr/ phase)	21.27	37.52	23.1	15.25
Total kW load/phase	1096.1	1447.5	1377.2	1377.2
Total kVAr load/phase	820	1082	1030	1030
Total actual kVA load/phase	1369	1807	1720	1720

Table 6. continued

Bayaa_12	Before load growth	After load growth	After switching optimization	After kVAr compensation
Maximum voltage (p.u.)	1	1	1	1
Minimum voltage (p.u.)	0.993	0.991	0.987	0.992
Total active power loss (kW)/ phase	3.6	6.46	10.26	6.93
Total reactive power loss (kVAr)/ phase	3.8	6.83	10.9	7.37
Total kW load/phase	861.2	1151.3	1350.9	1350.9
Total kVAr load/phase	646	863	1012	1012
Total actual kVA load/phase	1076	1439	1688	1688

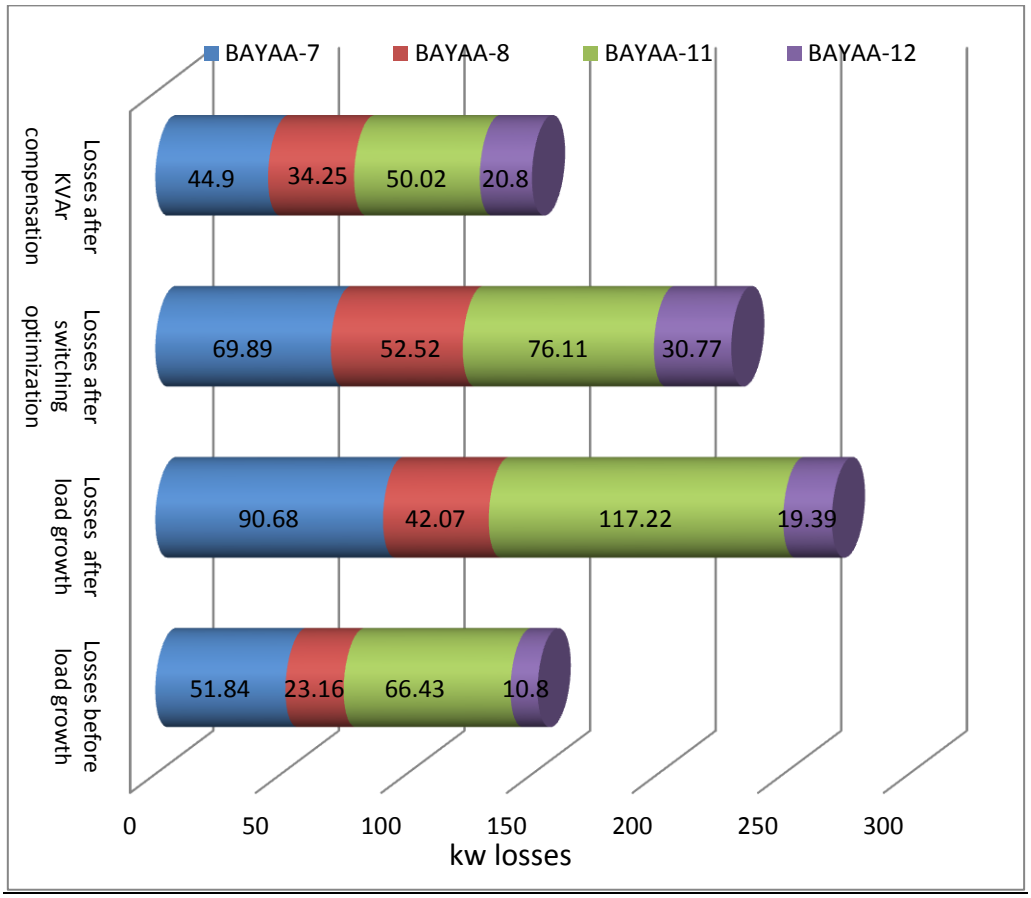

Figure 8. Al_Bayaa system kW losses.

From **Table 3.** the total system power losses before, after load growth, after switching optimization, and after kVAr compensation are 152.23, 269.36, 229.29 and 149.97 kW respectively. So the kW saving between the case after load growth and after kVAr compensation is 119.39 kW.

By using equation (10) and (11), the annual costs of the system losses are shown in **Table 7.** and the total net saving cost of the peak load is 13.7 k$/year.

Table 7. Annual cost of Al_Bayaa system losses (k$/year).

Feeder name	Feeder load factor (%)	Before load growth	After load growth	After switching optimization	After kVAr compensation
Bayaa_7	65	6.84	11.97	9.23	6.54
Bayaa_8	65	3.06	5.55	6.93	4.96
Bayaa_11	65	8.77	15.47	10.05	7.16
Bayaa_12	65	1.43	2.56	4.06	3.19
Total loss cost (k$)		20.1	35.55	30.27	21.85

Discussion of the results:

Fig. (9a, b, c, and d) show the bus voltage profile for Al_Bayaa selected feeders before and after load growth, after switching optimization and after capacitor placement. It is shown that after applying load growth, the overall voltage magnitudes will drop significantly within the specified limits. These values are improved after applying switching optimization technique and improved more after allocation of capacitors in these feeders so they became closer to 1 p.u.

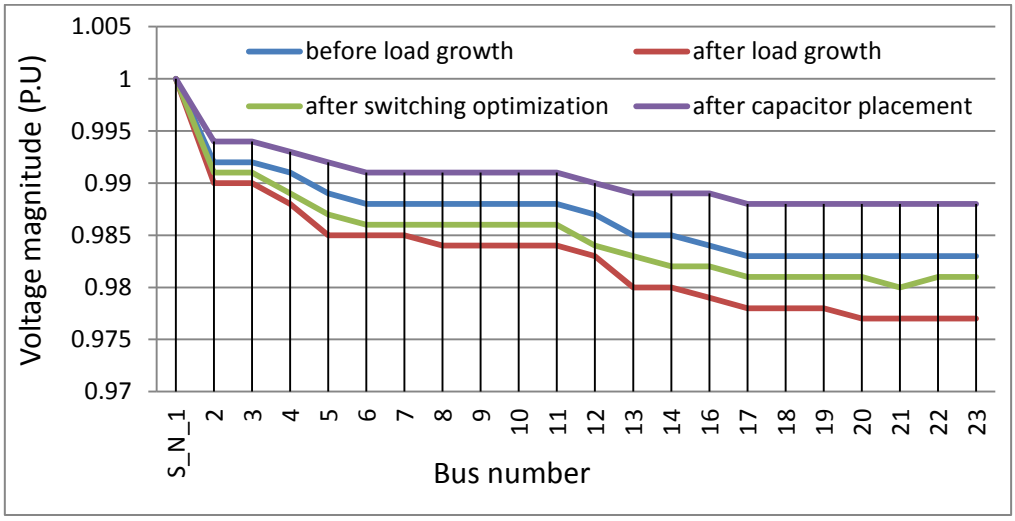

Figure 9a. Voltage profile of feeder Al_Bayaa_7.

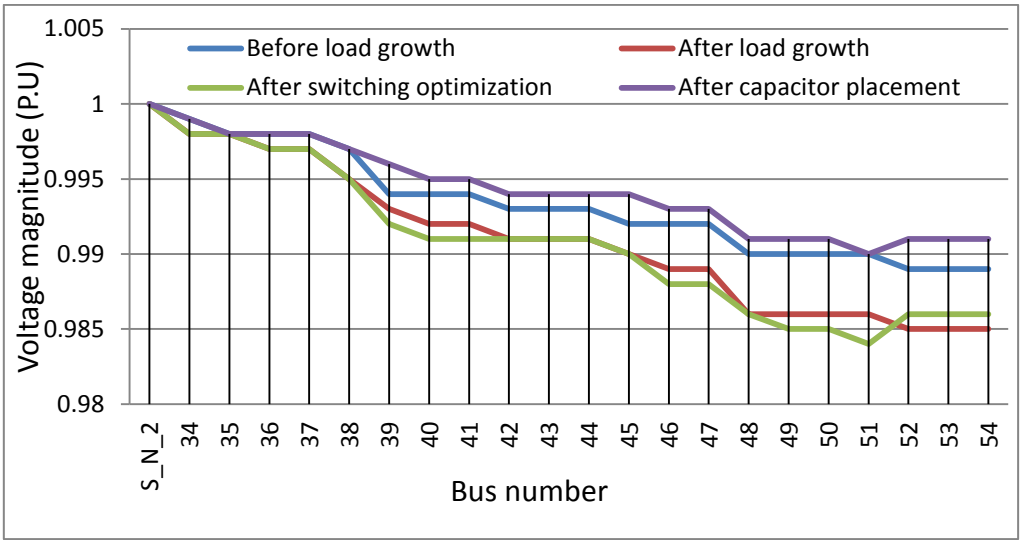

Figure 9b. Voltage profile of feeder Al_Bayaa_8.

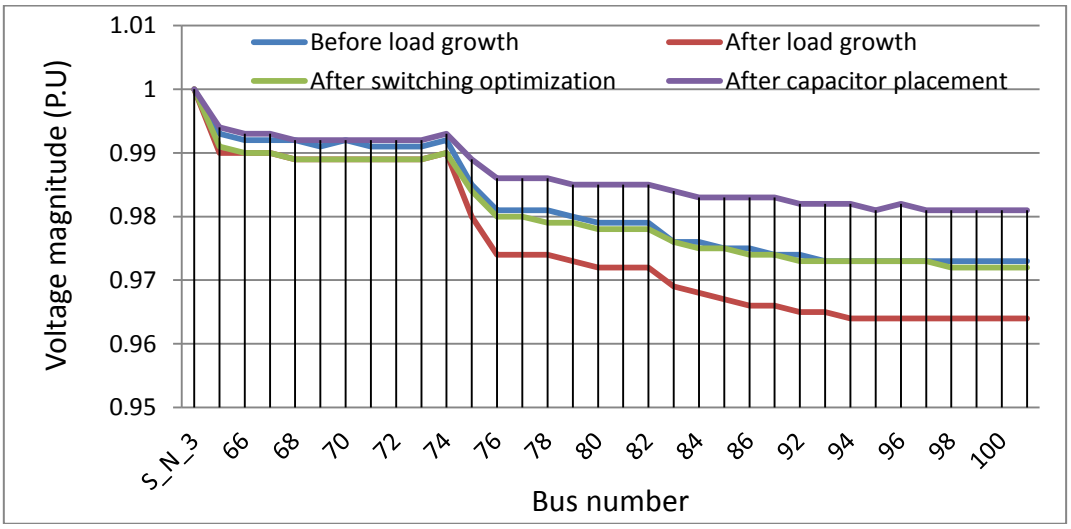

Figure 9c. Voltage profile of feeder Al_Bayaa_11.

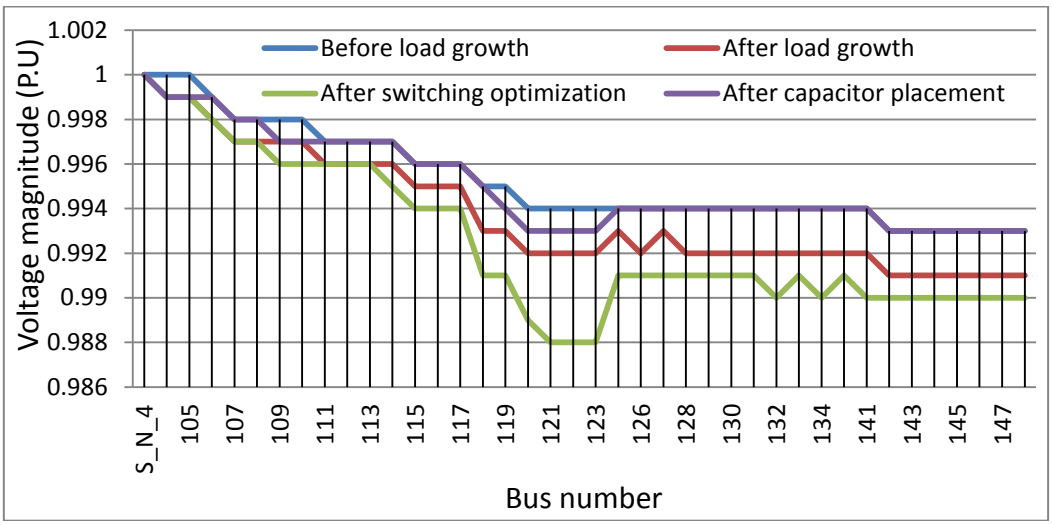

Figure 9d. Voltage profile of feeder Al_Bayaa_12.

Fig.10 shows the behavior of the total downstream reactive power profile with respect to distances for Al_Bayaa_7 feeder of each section for the longest path from the substation that feed this network to node 21. **Fig.10a** considers the behavior before load growth, **Fig.10b** considers the behavior after load growth, **Fig.10c** considers the behavior after switching optimization, and **Fig.10d** considers the behavior after kVAr compensation.

Section 1 (1321 m length) has 914.4 downstream kVAr/phase before compensation; this value is increased to 1210 kVAr/phase after load growth (above the maximum value). Then the kVAr/phase is reduced to 1091 after applying switching optimization. At the final step of the planning after placement of capacitors the kVAr/phase became 54.5 and so on for the other sections. The sections that have capacitors become a source of reactive power, the overall active and reactive power losses will be reduced. The overall P.F. of each feeder is improved as shown in **Table 3**.

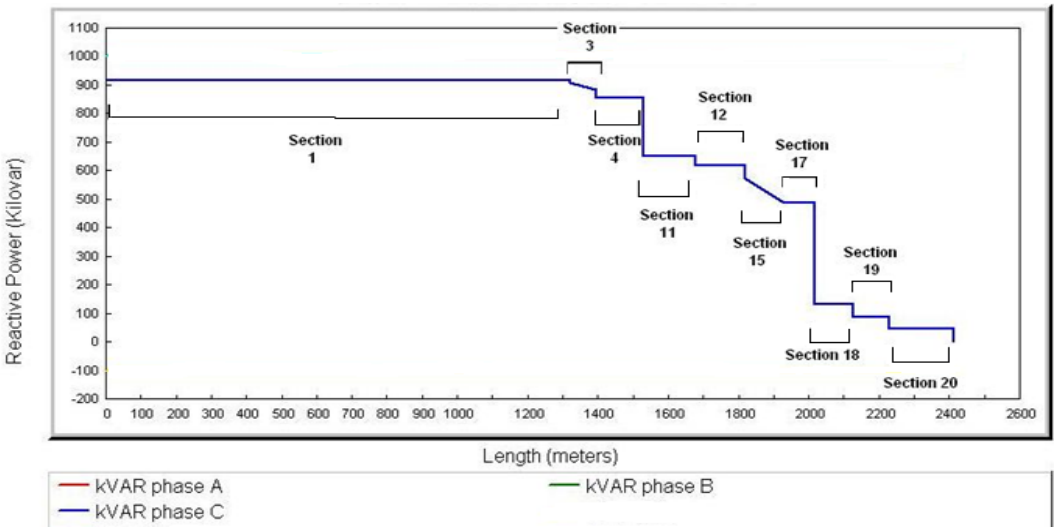

Figure 10a. kVAr profile of Al_Bayaa_7 before load growth.

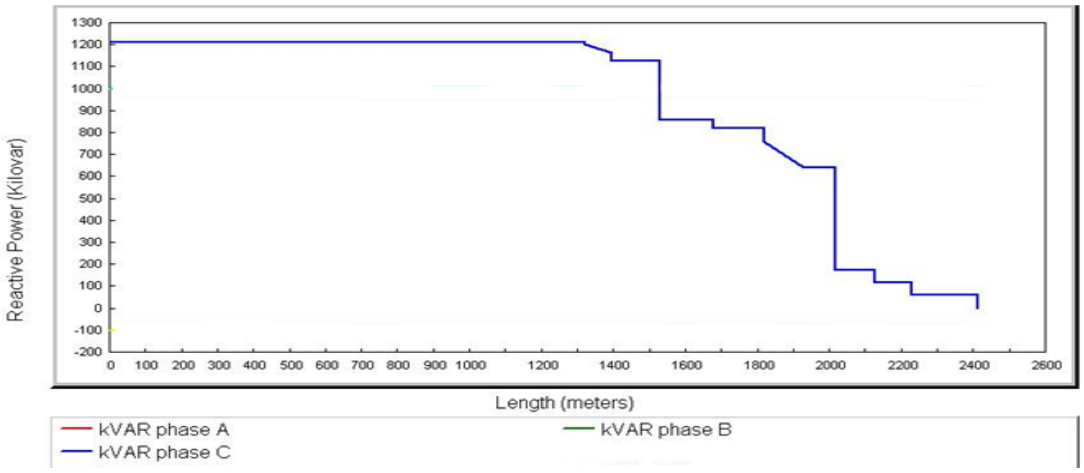

Figure 10b. kVAr profile of Al_Bayaa_7 after load growth.

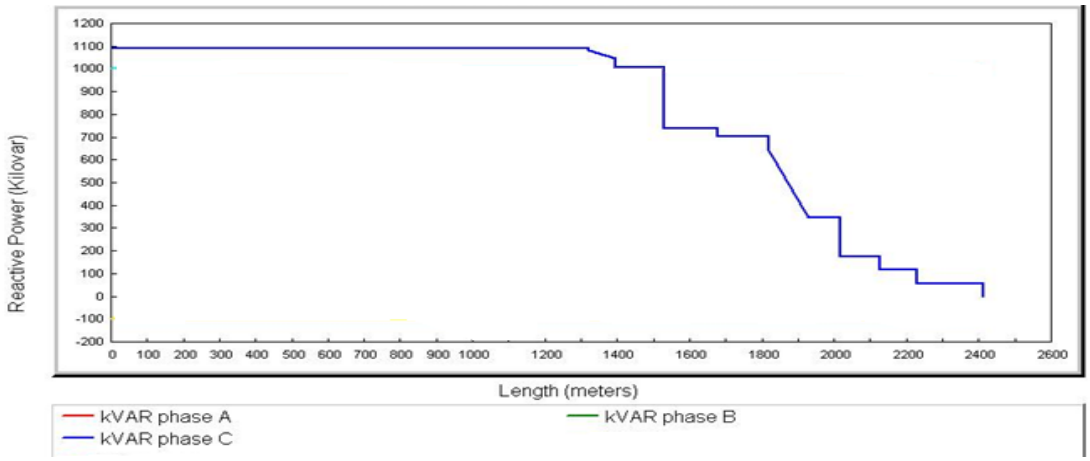

Figure 10c. kVAr profile of Al_Bayaa_7 after switching optimization.

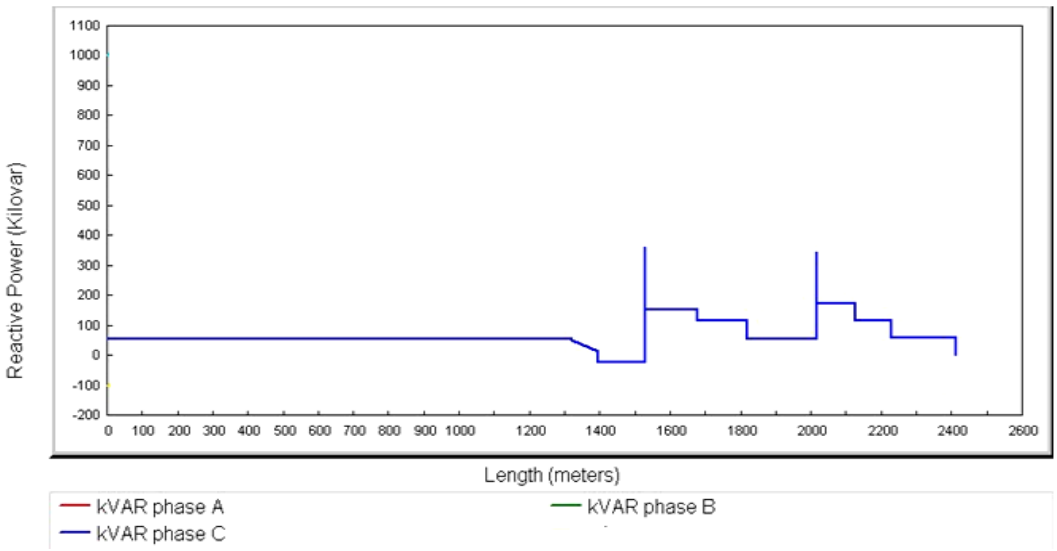

Figure 10d. kVAr profile of Al_Bayaa_7 after capacitor placement.

8. CONCLUSIONS

The results of planning Al_Bayaa distribution network by using CYMDist software show clearly the power loss reduction after applying the proposed method by using network reconfiguration in sequence with optimal capacitor placement.

The network model only needs to be created once; this may satisfy various types of simulation analysis required for the distribution network planning. Three simulation functions are achieved; load flow, switching optimization and capacitance optimal allocation.

Although, computational time increases with increasing system size, CYMDist module gives a very fast execution time even for large scale networks as compared to other methods documented in the literature, so it can be used in online distribution automation. Also, it gives accurate results depending on the accuracy of the input data.

REFERENCES

- Sarwar, M., Jaffery, Z. A., Siddiqui, A. S., and Quadri, I. A., 2012, *Techno-Economic Feasibility of HVDS Concept for Distribution Feeder Power Loss Minimisation*, IEEE 5th India International Conference on Power Electronics (IICPE).

- *CYME Reference Manual*, www.scribd.com/doc/136501684/CYME-502-Ref-EN-V1-2

- Divya, P., and Siva, K. R., 2013, *Proposed Strategy for Capacitor Allocation in Radial Distribution Feeders*, International Journal of Research in Engineering & Technology, Vol. 1, Issue 3, P.P. 85-92.

- Flávio, V. G., Sandoval, C. J., Jose, L. R., Marcio, P. V., Paulo, A. N., and Leandro, R. A., 2005, *A New Heuristic Reconfiguration Algorithm for Large Distribution Systems*, IEEE Transactions on Power Systems, Vol. 20, No. 3, P.P. 1373-1378.

- Héctor, M. L., 2013, *Optimization of Capacitor Banks in the Skagerak Networks Transmission Grid*, M. Sc. Thesis, University of Agder.

- William, H. K., 2002, *Distribution System Modeling and Analysis*, CRC Press LLC Book, New York Washington.

- Manas, R. N., 2014, *Optimal Feeder Reconfiguration of Distribution System with Distributed Generation Units using HC-ACO*, International Journal on Electrical Engineering and Informatics - Volume 6, Number 1.

- Manju, M., Sandeep S., Leena G., and Saxena, N. S., 2013, *Minimizing Distribution Losses by System Reconfiguration*, International Journal of Electrical, Electronics and Data Communication, Vol.1, Issue 10.

- Meghana, M., 2011, *Optimal Sitting and Sizing of Solar Photovoltaic Distributed Generation to Minimize Loss, Present Value of Future Asset Upgrades and Peak Demand Costs on a Real Distribution Feeder*, M. Sc. Thesis, University of Waterloo, Ontario, Canada.

- Satish, K. I., and Navuri, P. K., 2012, *Planning and Operation of Active Radial Distribution Networks for Improved Voltage Stability and Loss*

Reduction, World Journal of Modeling and Simulation, England, UK, Vol. 8, No. 3, P.P. 211-222.

- Baran, M. E. and Wu, F. F., *Network Reconfiguration in Distribution Systems for Loss Reduction and Load Balancing*, IEEE Transactions on Power Delivery, Vol. 4, No. 2, April, 1989.

- Thiruvenkadam, S., Nirmalkumar, A. Sakthivel, A., *MVC Architecture Based Neuro-Fuzzy Approach for Distribution Feeder Reconfiguration for Loss Reduction and Load Balancing*, IEEE Student's Conference on Electrical, Electronics and Computer Science, 2008.

- Dong Zhang, Zhengcai Fu, and Liuchun Zhang, *Joint Optimization for Power Loss Reduction in Distribution Systems*, IEEE Transactions on Power Systems, Vol. 23, No. 1, P.P. 161-169, February, 2008.

- Gupta, N., Swarnkar, A., and Niazi, K. R., *An Efficient Greedy Approach for Reactive Compensation on Large-Scale Distribution Systems*, IEEE Power and Energy Society General Meeting, 2011.

- Prasanna, M. Y. B., Balaji, T. R. N., and Kannan, S. M., *Maximization of Annual Savings by using Fuzzy-Second Order PSO based Optimal Capacitor Placement in RDF for Constant Load*, IEEE Student's Conference on Electrical, Electronics and Computer Science, 2012.

NOMENCLATURE

r_i= resistance of branch i, ohm.
P_i= active power of branch i, kW.
Q_i= reactive power of branch i, kVAr.
k_i= switch status of branch i, dimensionless.
$V_{min.}$= lower bus voltage limit, kV.
$V_{max.}$= upper bus voltage limit, kV.
$|V_i|$ = rms value of the i_{th} bus voltage, kV.
P_t = total active power load, kW.
$P_s^{max.}$= maximum active power source, kW.
Q_t = total reactive power load, kVAr.
$Q_s^{max.}$ = maximum reactive power source, kVAr.
$I_{rated} = line\ rated\ current, amp.$
P_G = power generation, kW.
P_D = power demand, kW.
P_{lt} = total power losses, kW.
Q_c = reactive power obtained from the capacitor bank, kVAr.
m = total number of capacitor banks, dimensionless.
LDF= load factor, dimensionless.
$P_{loss\ max}$ = power loss at the peak load power, kW.
L_{fls} = loss factor, dimensionless.
T= time interval, hours.
C= tariff cost, $.
K= cost of capacitor size, $/kVAr.

Desulfurization of Diesel Fuel by Oxidation and Solvent Extraction

Dr. Wadood Taher Mohammed
Assistant Professor
Department of Chemical Engineering
College of Engineering – University of Baghdad
Email: dr.wadood@yahoo.com

Dr.Raghad Fareed Kassim Almilly
Lecturer
Department of Chemical Engineering
College of Engineering – University of Baghdad
Email: rfkalm@yahoo.com

Sheam Bahjat Abdulkareem Al-Ali
Department of Chemical Engineering
College of Engineering – University of Baghdad
Email: Sheam1982@yahoo.com

ABSTRACT

This research presents a study in ultra-desulfurization of diesel fuel produced from conventional hydro desulfurization process, using oxidation and solvent extraction techniques. Dibenzothiophene (DBT) was the organosulfur compound that had been detected in sulfur removal. The oxidation process used hydrogen peroxide as an oxidant and acetic acid as homogeneous catalyst . The solvent extraction process used acetonitrile (ACN) and N-methyl – 2 - pyrrolidone (NMP) as extractants . Also the effect of five parameters (stirring speed :150 , 250 , 350 , and 450) rpm, temperature (30 , 40 , 45 , and 50) ^{o}C, oxidant/simulated diesel fuel ratio (0.5 , 0.75 , 1 , and 1.5) , catalyst/oxidant ratio(0.125,0.25,0.5,and0.75) , and solvent/simulated diesel fuel ratio(0.5,0.6,0.75,and1) were examined as well as solvent type. The results exhibit that the highest removal of sulfur is 98.5% using NMP solvent while it is 95.8% for ACN solvent. The set of conditions that show the highest sulfur removal is: stirring speed of 350 rpm , temperature 50°C , oxidant/simulated diesel fuel ratio 1 , catalyst/oxidant ratio 0.5 , solvent/simulated diesel fuel ratio 1. These best conditions were applied upon real diesel fuel (produced from Al-Dora refinery)with 1000 ppm sulfur content . It was found that sulfur removal was 64.4% using ACN solvent and 75% using NMP solvent.

Key words*:* ultra-desulfurization ,oxidation and extraction, simulated diesel fuel ,real diesel fuel.

ازالة الكبريت لوقود الديزل بواسطة الاكسدة و الاستخلاص بالمذيب

د. ودود طاهر محمد
أستاذ مساعد
قسم الهندسة الكيمياوية
كلية الهندسة – جامعة بغداد

د رغد فريد قاسم الملي
مدرس
قسم الهندسة الكيمياوية
كلية الهندسة – جامعة بغداد

شيم بهجت عبد الكريم العلي
قسم الهندسة الكيمياوية
كلية الهندسة – جامعة بغداد

الخلاصة

يقدم هذا البحث دراسة في الازالة فوق العادية للكبريت لوقود الديزل الناتج من عملية الازالة الهيدروجينية التقليدية للكبريت باستخدام تقنيات الاكسدة والاستخلاص بالمذيب .تم تتبع المركب العضوي الكبريتي البنزوثايوفين الثنائي في أزالة الكبريت . أجريت عملية الاكسدة باستخدام بيروكسيد الهيدروجين كعامل مؤكسد وحامض الخليك كعامل مساعد متجانس. تمت عملية الاستخلاص بالمذيب باستخدام الاسيتونايترايل و ن-مثيل-2-بايروليدون كعامل مستخلص . أيضا تم بحث تأثير خمسة عوامل

وهي :- سرعة الخلط (350,250,150, و 450) دورة\دقيقة ؛ درجة الحرارة (50,45,40,30و)^{o}م ؛نسبة العامل المؤكسد/مشبه وقود الديزل (1،5,1, 0،75 , 0،5) ؛نسبة العامل المساعد/ العامل المؤكسد (0،75,0،5,0،25, 0،125) ونسبة المذيب/مشبه وقود الديزل(1و,0،75,0،6,0،5) كما تم بحث نوع المذيب. أظهرت النتائج ان أعلى نسبة ازالة للكبريت هي 98،5% باستخدام مذيب ن- مثيل-2-بايروليدون بينما كانت 95،8% باستخدام مذيب الاسيتونابترايل . ان مجموعة الظروف التي أظهرت أعلى أزالة للكبريت هي: سرعة الخلط 350 دورة / دقيقة, درجة الحرارة 50 ^{o}م ,نسبة العامل المؤكسد/مشبه وقود الديزل 1,نسبة العامل المساعد/العامل المؤكسد 0,5 ,نسبة المذيب/مشبه وقود الديزل 1. طبقت افضل الظروف على وقود الديزل الحقيقي(المنتج في مصفى الدورة) والحاوي على محتوى كبريتي 1000 جزء بالمليون . وجد ان نسبة ازالة الكبريت كانت 64،4% باستخدام مذيب الاسيتونايترايل و 75% باستخدام مذيب ن-مثيل-2-بايروليدون .

الكلمات الرئيسية: الازالة فوق العادية للكبريت, الاكسدة والاستخلاص , مشبه وقود الديزل, وقود الديزل الحقيقي .

1. INTRODUCTION

The problem of fuel desulfurization has been attracted the researchers' interesting since the early time of oil refinery . This was because sulfur compounds have the most damaging effects on the equipment using fuel containing such compounds. The phenomenon of acid rain was first studied by Likens etal.,**Likens,et al.,1972**. Over the last decade many limitations were cited to reduce sulfur emissions from transportation means,**European Directive,2002**. Since then the main task of the refineries was to produce large yields of valuable products of the least sulfur content. This was achieved by hydro desulfurization (HDS) process , **Mochida,and Choi,2004** . Because sulfur–containing compounds have different reactivities and chemistries , HDS was of limited results in reducing sulfur content . Under this context , many researchers have developed alternative methods to meet the challenging requirements . This was done through many techniques such as: Desulfurization by adsorption , **Xiaoliang Ma, et al., 2003 ,** and **Al Zubaidy, et al. , 2013** ; Desulfurization by precipitation **, Milenkovic, et al., 1999** , and **Shiraishi, et al. , 2002**; Desulfurization via extraction **, Ali, et al., 2009** , and **Fa-tang , et al. , 2012** ; Desulfurization by alkylation , **Song, et al., 2002** , and **Arias, et al. , 2008** ; Desulfurization by selective oxidation (ODS) , **Campos-Martin, et al., 2010** , and **Ismagilov, et al., 2011** .

This research presents a study of deep desulfurization of diesel fuel by oxidation and solvent extraction technique. A detailed parametric study was performed with simulated diesel fuel doped with DBT to select the best set of conditions and then on real one. Hydrogen peroxide was selected as an oxidant, acetic acid as a homogeneous catalyst .Acetonitrile (ACN) and N-methyl -2 -pyrrolidone (NMP) were chosen as solvents. The oxidation and extraction steps were conducted once consecutively and other simultaneously.

2. EXPERIMENTAL WORK

2.1 Materials

N-heptane 99.5% purity (Gainland Chemical Company GCC) ; toluene 99% purity (Sigma US); hydrogen peroxide 50% (Sigma-Aldrich) ; acetic acid 95% purity (Tetenal UK) ; dibenzothiophene 99% (Himedia) ; acetonitrile 98% (Ptromchem.) ; N-methyl – 2 – pyrrolidone 99% (Himedia). Simulated diesel 200B n-heptane 80%wt , toluene 20%wt, doped with 1.7242 g of DBT for each liter to get a sulfur content of 355 ppm. Real diesel fuel with sulfur content of 1000 ppm was supplied by Al-Dora refinery .

2.2 Equipment

The experimental apparatus used in this study consisted of a 500-ml glass beaker immersed in a water bath (GFL) ; a thermometer (Eintauchtiefe 45 mm) which is inserted into the beaker to measure the temperature of the mixture ; mixer (Hiedolph RZR 2021) for stirring the mixture . The apparatus is shown in **Fig. 1**.The following parameters were studied .

2.3 Procedure

I-Simultaneous Technique: the oxidation and extraction were performed in one single step where the oxidation reaction occurred in the presence of a solvent (ACN once and NMP other time) . The model fuel , catalyst (acetic acid) and solvent were added at the required ratios. After the mixture had reached the desired temperature, hydrogen peroxide was added . The mixer stirring speed was set at the desired value . After 2 h it was stopped .The mixture was left 24 h in a 250-ml separating funnel to ensure settling and phase separation . The upper layer (simulated fuel) was then withdrawn and analyzed .

II-Consecutive Technique : In this technique , the oxidation was performed first and then immediately followed by extraction as follows:

1-The prepared amount of simulated diesel fuel was transferred to the reactor together with the desired amount of acetic acid (catalyst).

2-Waiting until the mixture reached the desired temperature .

3-Hydrogen peroxide (oxidant) added to the mixture .

4-The mixer stirring speed was set on the required value . After 2 h , it was stopped .

5-The mixture was transferred to a 250-ml separating funnel to allow the separation of phases .

6-The upper layer (oxidized simulated diesel fuel) was separated and mixed with certain amount of solvent (ACN or NMP) for another 2 h under proper stirring speed .

7- After the stirring was stopped , the phases were allowed to settle and separate in 24 h. The upper layer was withdrawn and analyzed .

The experiments were conducted according to 2^k factorial design. There are four factors that can be varied during a single experiment, keeping the others constant according to preliminary studying (temperature 50^oC , stirring speed 350 rpm). These are:

Solvent type (ACN , NMP)

Solvent/model fuel ratio (0.5,0.6,0.75, and 1)

Oxidant/model fuel ratio (0.5,0.75,1, and 1.5)

Catalyst/oxidant ratio (0.125,0.25,0.5, and 0.75)

2.4 Test Methods

1-Pyro-Fluorescence:This analysis was done in Al-Dora refinery using ANTEK 9000 N/S analyzer to give sulfur content in the simulated diesel fuel .

2-X-ray Fluorescence: This analysis was done in the oil training institute using Horiba sulfur – in-oil analyzer (SLFA-2100) to give sulfur content in real diesel fuel.

3. RESULTS and DISCUSSION

The experimental runs were carried out in two – stage testing, preliminary and main study. The first one includes selection of best technique, simultaneous or consecutive and effect of stirring speed. The other included detailed study for the best operational conditions to remove dibenzothiophene (DBT) from simulated diesel fuel and the real one. This study included effect of the temperature, solvent/simulated diesel fuel ratio, H_2O_2/simulated diesel fuel ratio and acetic acid/H_2O_2 ratio.

3.1 Preliminary Study

- Technique selection

This study included three experiments with different conditions elected from literature and preliminary experiments . The results are illustrated in **Fig. 2**, showing that the outcomes of consecutive versus simultaneous oxidation and extraction procedures are almost the same. However; simultaneous technique was more attractive to applied.

- Effect of stirring speed

The results obtained showing that using stirring speed of 350 rpm gave the highest sulfur removal keeping other variables constant (temperature 50 ˚C, solvent/simulated diesel fuel ratio (either acetonitrile or N-methyl-2-pyrrolidone) 1:1, Oxidant / simulated diesel fuel ratio 1:1 and catalyst/oxidant ratio 0.5:1). **Fig. 3** indicates that the percentage removal of DBT is increased by increasing the stirring speed up to 350 rpm. At this stirring speed, it reached to 95.8% sulfur removal using ACN and 98.5% using NMP .Then the percentage removal became quickly impressive and mass transfer limitations were found to be insignificant at higher speeds. Therefore; the stirring speed was kept at that value for all next experiments.

The contact and mixing conditions between the two phases have a great influence on the interface transfer and emulsion droplet. At lower mixing speed, there are fewer droplets in the emulsion; hence, the reaction rate is low with less contact surface area. Increasing the mixing speed leads to the formation of more droplets, more uniform shape resulted in larger surface area. Therefore; high mass transfer will be gained and the reaction will be accelerated. However, if the mixing speed is too high, whirlpools will be formed in the system, and, in this situation mass transfer will be decreased and the reaction will be slowed. These results were in agreement with that of Hang et al.**, Hang, et al., 2006** .

3.2 Main Study

- Effect of temperature

The effect of temperature studied at a range from 30 to 50 ˚C keeping other variables constant at two different conditions according to the experimental design proposed. The first one done at (0.5:1 solvent/simulated diesel fuel, 0.5:1 H_2O_2/simulated diesel ratio and 0.125:1 acetic acid/H_2O_2 ratio) and the other at (1:1 solvent/simulated diesel fuel ratio, 1:1 H_2O_2/simulated diesel fuel ratio and 0.5:1 acetic acid/H_2O_2 ratio) for 2 h of reaction time.The results of this set are illustrated in **Figs. 4 and 5**.

When the temperature is increased from 30 ˚C to 50 ˚C in the first set of conditions mentioned above, sulfur removal is increased from 25.6% to 32.5% for ACN and from 41% to 46.8% for NMP. While for the second set of conditions, increasing temperature from 30˚C to 50 ˚C led to increase sulfur removal from 87.9% to 95.8 % for ACN and from 94.1% to 98.5% for NMP.

The factors that influence the removal of DBT were also related to the solubility of $DBTO_2$ in the solvent. Sulfur compounds are oxidized to sulfoxides or sulfones. These are highly polar compounds, which have high solubility in polar extractants. The results suggested that the solubility of $DBTO_2$ in the polar solvent increased with increasing temperature. Beside that

increasing temperature decreased the solvent viscosity which played a positive role in sulfur removal due to the great effect on their extraction ability. Namely it facilitated mass transfer of S-compounds from the oil to the solvents.

It had been noticed that at higher temperatures (above 50 °C), a solvent miscibility in the model fuel phases occurred. This caused losing of solvent. It also caused thermal decomposition of H_2O_2. Therefore, increasing temperature above 50 °C was avoided.

These results were in agreement with that of Hang et al., **Hang, et al., 2006** , **Ali et al., Ali, et al., 2009** , and Fa-tang Li et al., **Fa-tang , et al., 2012** .

- Effect of oxidant (H_2O_2)/simulated diesel fuel ratio

The effect of the ratio of hydrogen peroxide/simulated diesel feul on the sulfur removal was found to be a very important parameter due to its effect on the conversion of DBT to $DBTO_2$. The results are illustrated in **Figs. 6-9** .These results indicate that increasing the ratio of (H_2O_2)/simulated diesel fuel leads to increase sulfur removal.

The experiments showed that increase the H_2O_2/simulated diesel fuel ratio from 0.5:1 to 1:1 leads to increase the sulfur removal from 32.5% to 43.7% for ACN and from 46.8% to 71.3% for NMP at operational conditions of 50 °C, solvent/ simulated diesel fuel 0.5:1 and acetic acid/H_2O_2 0.125:1. While reducing temperature to 30 °C and keeping the other parameters constant, the sulfur removal was increased from 25.6% to 33.5% for ACN and from 41% to 48.1% for NMP.

This effect was investigated at other conditions: 50 °C, solvent/ simulated diesel fuel 1:1 and acetic acid/H_2O_2 0.5:1, while H_2O_2/simulated diesel fuel 1:1, sulfur removal was increased from 87.8% to 95.8% for ACN and from 91.5% to 98.5% for NMP. While reducing temperature to 30 °C with the same other conditions, sulfur removal was increased from 75.2% to 87.9% for ACN and from 90% to 96.3% for NMP.

It had been noticed that the sulfur removal reached the highest value at H_2O_2/simulated diesel fuel ratio of 1:1. After that it almost stayed constant, which indicates that this ratio is the best one to achieve almost complete DBT conversion into $DBTO_2$ within a reasonable period of time (2h).

In fact, the oxidation efficiency of H_2O_2 can be affected by several factors, including temperature, degree of hindrance of sulfur-containing compounds and catalyst (acetic acid)/H_2O_2 ratio.

Temperature is the most significant factor which suggested an important interaction between temperature and H_2O_2/simulated diesel fuel ratio. At high temperatures (above 50 °C), more excess oxidant would be necessary because of the loss of H_2O_2 due to thermal decomposition. In contrast, the water hindrance of H_2O_2 aqueous solution in desulfurization progress would be more significant at temperatures about 50 °C.

- Effect of acetic acid/H_2O_2 ratio

The effect of catalyst (acetic acid) to the oxidizing agent (hydrogen peroxide) was found to be one of the important parameters due to its multiple effects on both the conversion of DBT to $DBTO_2$ and removal of sulfur content from diesel fuel.

The results are plotted in **Figs. 10-13**. These results indicate that increasing the ratio of acetic acid/H_2O_2 from 0.125:1 to 0.5:1 leads to increase sulfur removal from 32.5% to 86.6% for ACN and from 46% to 94.9% for NMP at operating conditions of 50 °C, solvent/ simulated diesel fuel 0.5:1, and H_2O_2/simulated diesel fuel 0.5:1. Further increase of acetic acid/ H_2O_2 ratio to 0.75:1 leads to decrease in sulfur removal to 79.3% and 85% for ACN and NMP, respectively. Decreasing the temperature to the value above 30◦C and keeping other conditions constant lead to increase in sulfur removal from 25.6% to 52.2% for ACN and from 41% to 60.8% for NMP. Then at acetic acid/ H_2O_2 ratio of 0.75:1, sulfur removal decrease to 47.2% for ACN and to 55.2% for NMP.

The subject has been investigated in other conditions, 50 °C, solvent/ simulated diesel fuel ratio 1:1, and H_2O_2/simulated diesel fuel ratio 1:1. The results showed that the sulfur removal increases from 35% to 95.8% for ACN and from 65.8% to 98.5% for NMP as acetic acid/H_2O_2 ratio increases from 0.125: to 0.5:1. Then sulfur removal decreased to 85.6% for ACN and 89% for NMP when the ratio of acetic acid/H_2O_2 increased further to 0.75:1.

Again sulfur removal investigated at temperature 30°C, solvent/simulated diesel fuel ratio 1:1, H_2O_2/simulated diesel fuel ratio 1:1. The results of NMP solvent showed that the sulfur removal increases from 74.2% to 94.1% then decreases to 86.8% at acetic acid/ H_2O_2 ratio of 0.75:1, while for ACN, it increases from 31.3% to 87.9% then decreases to 80.1%.

It was concluded from the set of experiments that the optimal ratio of acetic acid/H_2O_2 is 0.5:1; it is not efficient to increase this ratio further more because a decline in DBT conversion would be noticed due to a decline in acetic acid dissociation, which is necessary as a catalyst for the sulfur oxidation reaction.

The decline in organic acid dissociation is a result of acid self – dimerization and / or association with water. Another factor contributing to this observation is the decline in the availability of the proton necessary for peroxide dissociation to yield oxygen which is necessary for sulfur oxidation. This decline in proton availability is due to the decreasing in water concentration upon adding more organic acid.

According to our experimental results, the reversible reaction of acetic acid with hydrogen peroxide produces peroxyacetic acid as a high active oxidant which can efficiently oxidize DBT to respective sulfoxide (DBTO) and then to respective sulfone ($DBTO_2$). That illustrates the effect of acetic acid as a catalyst on the oxidation process by increasing the efficiency of hydrogen peroxide. With the increase of H_2O_2 and CH_3COOH (to a certain limit), the oxidant have more opportunities to react with DBT, and as a result, the sulfur removal increases.

These results were in agreement with that of Ali et al., **Ali, et al., 2009** , and **Fa-tang Li et al., Fa-tang , etal., 2012**.

*Effect of solvent/simulated diesel fuel ratio

Although DBT had been converted to DBTDO by oxidation process, the sulfur would not completely be removed from the simulated diesel fuel. The basis of using acetonitrile or N-methyl-2-pyrrolidone as an extraction solvent is that the solubility of $DBTO_2$ in such solvent is one order of magnitude higher than that in the simulated diesel fuel. This supports the need of adding acetonitrile, N-methyl-2-pyrrolidone or any other suitable solvent.

The results are illustrated in **Figs. 14-17** .These results indicate that increasing the ratio of solvent (either ACN or NMP)/simulated diesel fuel leads to increase in sulfur removal. The experiments showed that increase the solvent/simulated diesel fuel ratio from 0.5:1 to 1:1 leads to increase the sulfur removal from 32.5% to 71.2% for ACN and from 46.8% to 91% for NMP at operational conditions of 50 °C, H_2O_2/simulated diesel fuel ratio of 0.5:1 and acetic acid/ H_2O_2 ratio of 0.125:1. While reducing the temperature to 30 °C and keeping the other factors constant lead to increase in sulfur removal from 25.6% to 67% for ACN and from 41% to 72% for NMP.

This effect was investigated at other conditions: 50 °C, H_2O_2/simulated diesel fuel ratio of 1:1 and acetic acid/ H_2O_2 ratio of 0.5:1. Results showed that increasing the ratio of solvent/simulated diesel fuel ratio from 0.5:1 to 1:1 leads to increase in sulfur removal from 89.3% to 95.8% for ACN and from 95% to 98.5% for NMP. While reducing the temperature to 30 °C showed that the percent removal changed from 84.5% 87.9% for ACN and from 88.1% to 94.1% for NMP.

From all above, when DBT was converted to its corresponding polar compound ($DBTO_2$) by means of oxidation, the capabilities of the tested solvents for sulfur removal enhanced significantly.

NMP exhibits a notable sulfur removal of 98.5% for DBT because of the similarity – intermisicibility theory based on the fact that NMP and DBT contain five-membered ring.

ACN was appropriate solvent because it is able to extract and dissolve the reaction products and exhibits a low surface tension, which facilitate the transfer of products and reagents at the polar-polar interphase, increasing notably the mass transfer along the interphase. However, ACN is partially dissolved in the (polar) fuel phase, then ACN molecules are present in the fuel phase, in consequence the final nitrogen concentration in the fuel will increase. To avoid this, a later separation unit is mandatory to remove the fraction of ACN transferred to the fuel phase.
During oxidation/extraction process, DBT was oxidized to its corresponding sulfone (DBTDO) by per acetic acid (CH_3COOOH) obtained from H_2O_2 and CH_3COOH and then extracted from the oil phase into the solvent phase. The decrease in DBT concentration in the solvent promoted the extraction process, and the sulfur content in oil phase decreased continuously. Increasing of sulfone (polar compound) leads to increase extraction ability of the solvents (due to similar polarity). This illustrates the effect of oxidation process on the efficiency of extraction process. It was clear that the solvent efficiency was affected by the ratios of oxidant and catalyst. If no oxidant was added, sulfur removal would significantly decrease by extraction step only. With increasing in oxidant and catalyst, the oxidant had more opportunities to react with DBT, and thus the sulfur removal increased.
The results were in agreement with those of Ali et al**., Ali, et al., 2009 ,** Capel-Sanchez et al., **Capel-Sanchez, et al., 2010** , **and Fa-tang Li et al**., **Fa-tang , et al., 2012** .

3.3 Desulfurization of Real Diesel Fuel

The removal of sulfur content from the real diesel fuel was more difficult than that from the simulated diesel fuel because many nitrogen, oxygen, and aromatic compounds exist in actual oil.
Two experiments with best conditions that had been concluded from the set of experiments applied on simulated diesel fuel [temperature of 50 $^{\circ}$C, solvent/real diesel fuel ratio of 1:1, H_2O_2/real diesel fuel of 1:1, acetic acid/ H_2O_2 of 0.5:1 and stirring speed of 350 rpm] were applied. Results are plotted in **Fig. 18** showing that sulfur removal reached to 62.5% and 75% for acetonitrile and N-methyl-2-pyrrolidone respectively.
Another experiments with more severe conditions were conducted to study the behavior of the real diesel fuel (i.e. temperature of 70 $^{\circ}$C, stirring speed of 500 rpm, solvent/real diesel fuel of 2:1, H_2O_2/real diesel fuel of 2:1 and acetic acid/ H_2O_2 of 0.5:1). Sulfur removal was almost the same for ACN and NMP as shown previously. It is suggested that the reason of remaining sulfur removal constant despite of varying the conditions, is due to the presence of nitrogen compounds in real diesel fuel beside other types of sulfur compounds that do not react in our process technique.
These results were in agreement with that of Rao et al. , **Rao, et al., 2007** , and **Fa-tang Li et al.** , **Fa-tang Li, et al., 2011**.

4. CONCLUSIONS

- The techniques of consecutive versus simultaneous (oxidation , extraction) processes are almost the same .
- Simultaneous oxidation / extraction process had the ability to remove almost all the DBT from the simulated diesel fuel.
- The time 2 h was sufficient for converting DBT to DBTDO by oxidation step .
- The solvent NMP was found to be better for the removal of sulfur than ACN .

- The optimum conditions to operate the simultaneous oxidation / extraction are [stirring speed 350 rpm , temperature 50 ^{o} C , solvent / simulated diesel fuel 1:1 , H_2O_2/ simulated diesel fuel 1:1 , acetic acid / oxidant 0.5:1] for both NMP and ACN .

- It is impossible to obtain ultra- desulfurization using extraction process only , nevertheless ; using NMP or ACN .

REFERENCES

- Ali, S. H., Hamad, D. M., Albusairi, B. H., and Fahim, M. A., 2009, *Removal of Benzothiophenes From Fuels by Oxy-Desulfurization*, Energy and Fuels, Vol. 23, PP. 5986-5994.
- Al Zubaidy, I.A.H., Taresh, F.B., Darwish, N.N., Sweidan, B., Abdul Majeed, S., Al Sharafi, A., and Abu Chacra,L., 2013, *Adsorption Process of Sulfur Removal From Diesel Oil Using Sorbent Materials*.
- Arias, M., Laurenti, D., Geantet, C., Vriant, M., Hideyyuki, I., and Yoshimura, Y., 2008, *Gasoline Desulfurization by Catalytic Alkylation Over Silica – Supported Heteroployacids: From Model Reaction to Real Feed Conversion*, Catal Today, Vol. 130, PP. 190-194.
- Campos – Martin, JM., Capel – Sanchez, MC., Perez – Presas, P., and Fierro, JLG., 2010, *Oxidative Processes of Desulfurization of Liquid Fuels*, J Chem Technol Biotechnol, Vol. 85, PP. 879 -890.
- Capel-Sanchez, M.C., Perez-Presas, P., Campos-Martin, J.M., and Fierro, J. I. G., 2010, *Highly Efficient Deep Desulfurization of Fuels by Chemical Oxidation*, E-mail: j.m.campos@icp.csis.es
- European Directive for Emissions of Light Duty Vehicles(70/220/CE amended by 99/69/EC as Euro 3 and 2002/80/EC as Euro 4) , European Directive for Emissions of Heavy Duty Vehicles (88/77/CE amended by 1999/96/EC as Euro 4 and Euro 5).
- -Fa-Tang, L., Cheng-Guang, K., Zhi-Min, S., Ying-Juan, H., Rui-Hong, L., and Di-Shun, Z., 2012, *Deep Extractive and Oxidative Desulfurization of Dibenzothiophene with $C_5H_9NO.SnCl_2$ Coordinated ionic Liquid*, Journal of Hazardous Materials , No. 205-206, PP. 164-170.
- Huang, D., Wang, Y. J., Yang, L. M., and Luo, G. S., 2006, *Chemical oxidation of dibenzothiophene with a directly combined amphiphilic catalysts for deep desulfurization*, Ind. Eng. Chem. Res., Vol. 45.
- Ismagilov, Z., Yashnik, S., Kerzhentsev, M., Parmon, V., Bourane, A., Al- Shahrani, FM., Hajji, AA., and Koseoglu, OR., 2011, *Oxidative Desulfurization of Hydrocarbon Fuels*, Catal. Rev. Sci. Eng., Vol. 53, PP. 199-255.
- Likens, G. E., Bormann, F. H., and Johnson, N. N., 1972, *Acid Rain*, Environment, Vol. 14,No. 2, PP. 33.
- Milenkovic, A., Shulz, E., Meille, V., Lofferdo, D., Forissier, M., Vriant, M., Saultet, P., and Lemair, M., 1999, Energy Fuels, Vol. 13, PP. 881.
- Mochida, I., and Choi, K. H., 2004, J. Jpn. Petol. Inst.,Vol. 47 , PP. 145.

- -Rao, T. V., Sudha Kafola, B. S., Nautiyal, B. R., Sharma, Y. K., Nanoti, S. M., and Grag, M. O., 2007, *Oxidative Desulfurization of HDS Diesel Using the Aldehyde / Molecular Oxygen Oxidation System*, Energy & Fuels, Vol. 21, PP. 3420-3424.
- -Shiraishi, Y., Taehibana, K., Hirai, T., and Komasawa, I., 2002, *Desulfurization and Denitrogenation Process for Light Oils Based on Chemical Oxidation Followed by Liquid-Liquid Extraction*, Industrial & Engineering Chemistry Research, Vol. 41, No. 17, PP. 4362-4375.
- Song, C., 2002, *New Approaches to Deep Desulfurization for Ultra- Clean Gasoline and Diesel Fuels: An Overview*, Prepr Pap Am Chem Soc Div Fuel Chem, Vol. 47, No. 2, PP. 438-444.
- Song , C., and Ma, X., 2003,*New Approaches to Produce Ultra-Clean Diesel Fuel by Deep Desulfurization* , Appl. Catal. B, Vol. 41, PP. 207.
- Xiaoliang, Ma., Sun, L., and Song,C., 2003, *Adsorptive Desulfurization of Diesel Fuel Over a Metal Sulfide – Based Adsorbent*, Prep. Pap. Am. Soc. Div. Fuel Chem.,Vol. 48, No. 2, PP. 522.

ABBREVIATIONS

ACN	acetonitrile
DBT	dibenzothiophene
DBTDO , $DBTO_2$	dibenzothiophene dioxide
DBTO	dibenzothiophene oxide
HDS	hydro desulfurization
NMP	N-methyl-2-pyrrolidone
ODS	desulfurization by selective oxidation

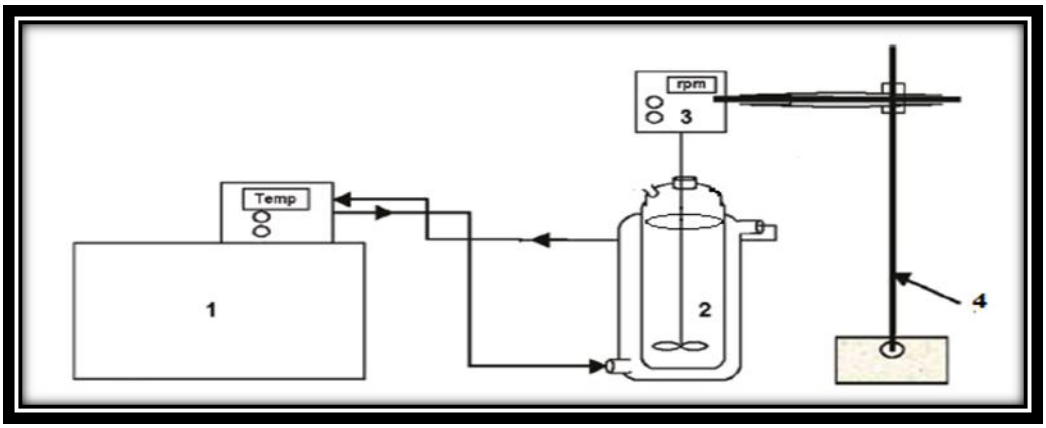

Figure 1. Schematic diagram of the experimental apparatus.

1- water bath; 2- glass beaker; 3- mixer; 4- stand.

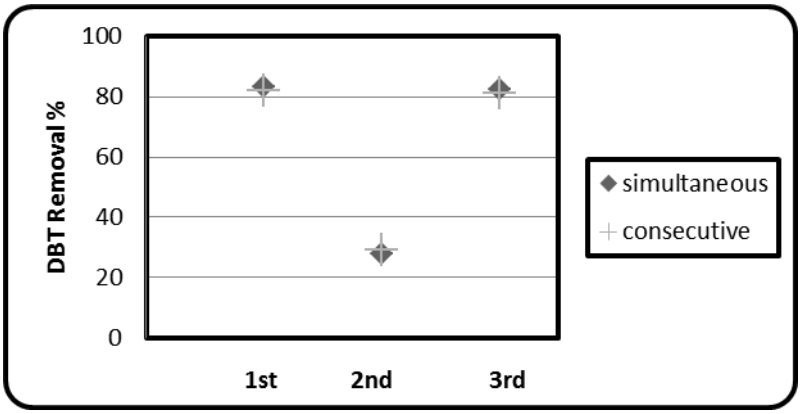

Figure 2. Simultaneous vs. consecutive oxidation/extraction using NMP as extractant.

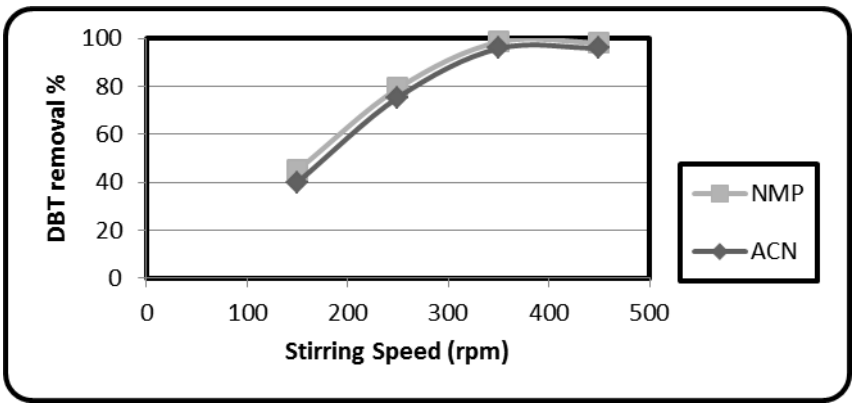

Figure 3. Sulfur removal versus stirring speed.

(Operating conditions: 50 ˚C, 1:1 solvent/simulated diesel fuel ratio, 1:1 H_2O_2/simulated diesel fuel ratio and 0.5:1 acetic acid/H_2O_2 ratio for 2 h reaction time).

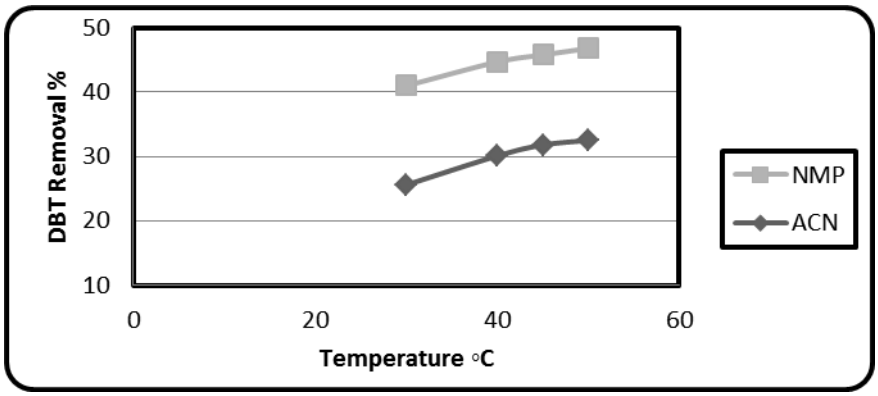

Figure 4. Effect of temperature on DBT removal.

(Operating conditions: 0.5:1 solvent/simulated diesel fuel ratio, 0.5:1 H_2O_2/simulated diesel fuel ratio and 0.125:1 acetic acid/H_2O_2 ratio for 2h reaction time) .

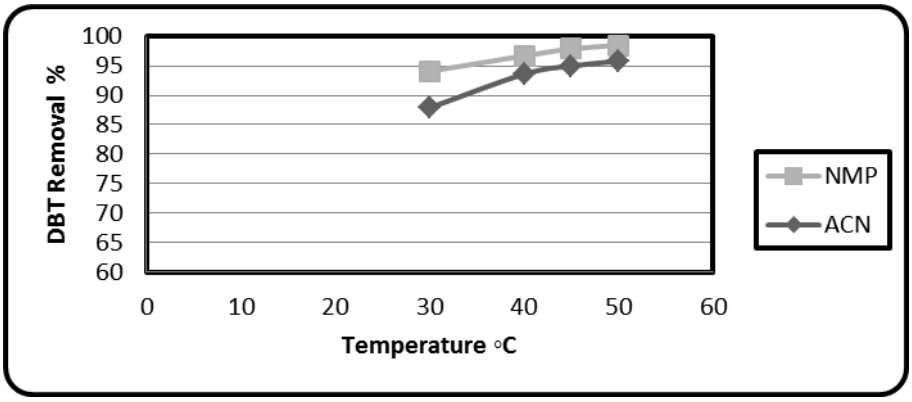

Figure 5. Effect of temperature on DBT removal.

(Operating conditions: 1:1 solvent/simulated diesel fuel ratio, 1:1 H_2O_2/simulated diesel fuel ratio and 0. 5:1 acetic acid/H_2O_2 ratio for 2h reaction time) .

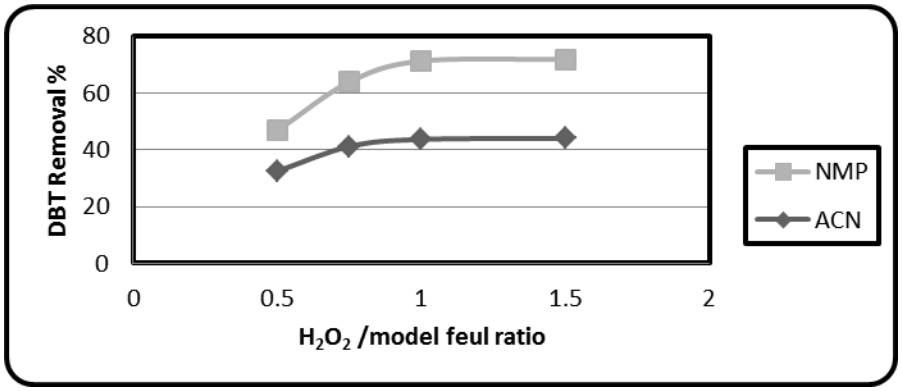

Figure 6. Effect of H_2O_2/simulated diesel fuel ratio on DBT removal.

(Operating conditions: 50 ˚C, 0.5:1 solvent/simulated diesel fuel ratio and 0.125:1 acetic acid/H_2O_2 ratio for 2h reaction time).

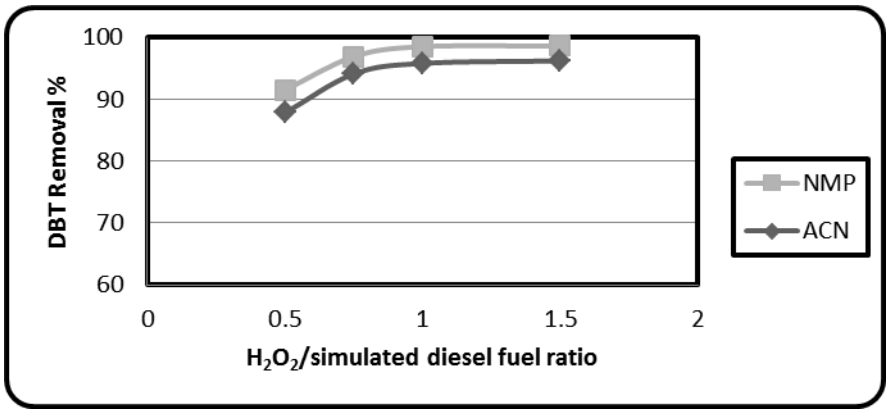

Figure 7. Effect of H_2O_2/simulated fuel ratio on DBT removal.

(Operating conditions: 50 ˚C, 1:1 solvent/simulated diesel fuel and 0.5:1 acetic acid/H_2O_2 ratio for 2h reaction time).

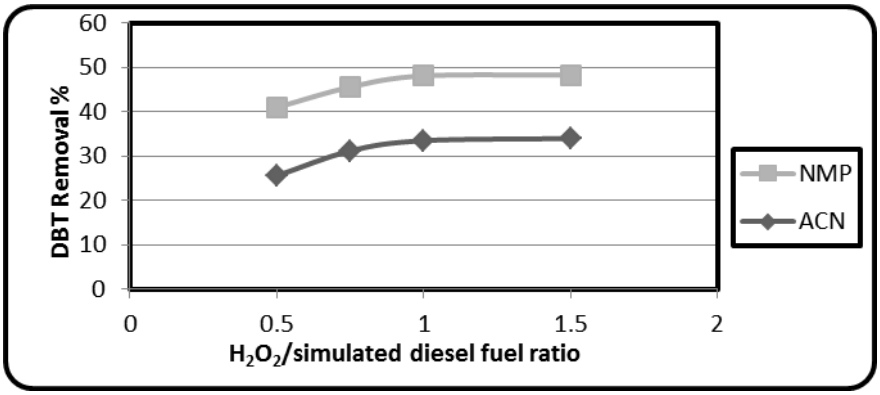

Figure 8. Effect of H_2O_2/simulated diesel fuel ratio on DBT removal .

(Operating conditions: 30 ˚C, 0.5:1 solvent/simulated diesel fuel ratio and 0.125:1 acetic acid/H_2O_2 ratio for 2h reaction time).

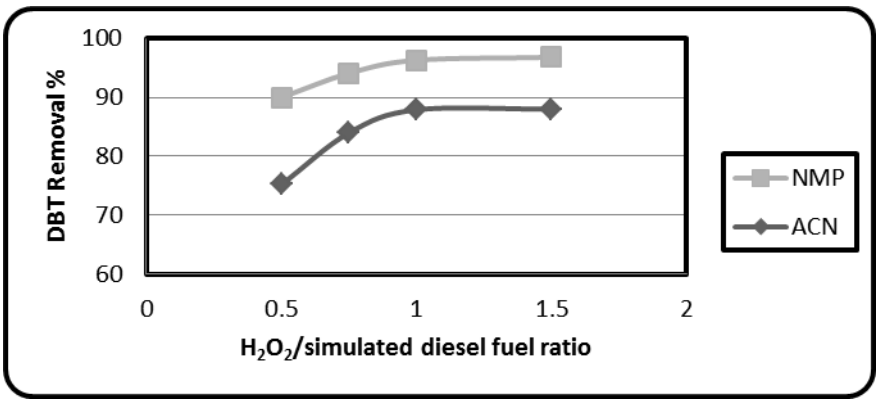

Figure 9. Effect of H_2O_2/simulated diesel fuel ratio on DBT removal.

(Operating conditions: 30 ˚C, 1:1 solvent/simulated diesel fuel ratio and 0.5:1 acetic acid/H_2O_2 ratio for 2h reaction time).

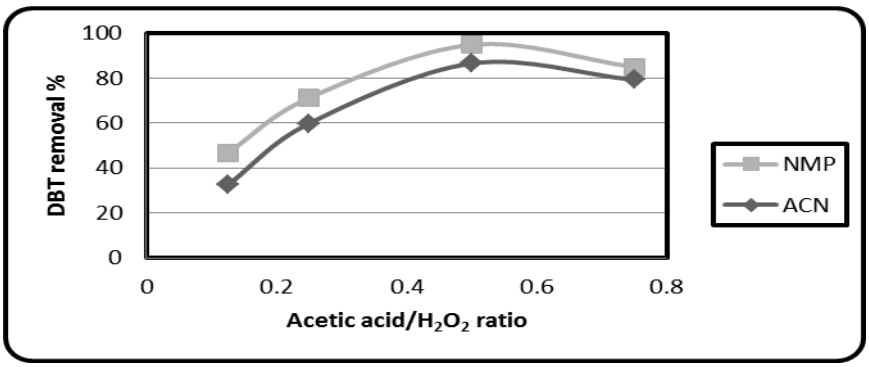

Figure 10. Effect of acetic acid/H_2O_2 ratio on DBT removal.

(Operating conditions: 50 ˚C, 0.5:1 solvent/simulated diesel fuel and 0.5:1 H_2O_2/simulated diesel fuel for 2h reaction time) .

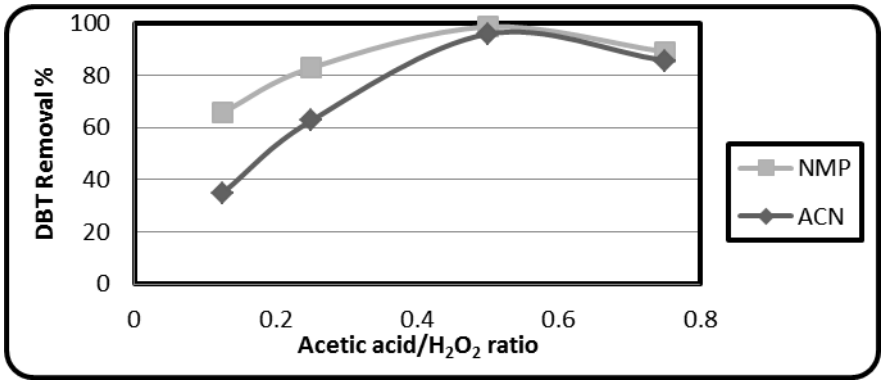

Figure 11. Effect of acetic acid/H_2O_2 ratio on DBT removal.

(Operating conditions: 50 ˚C, 1:1 solvent/simulated diesel fuel and 1:1 H_2O_2/simulated diesel fuel for 2h reaction time).

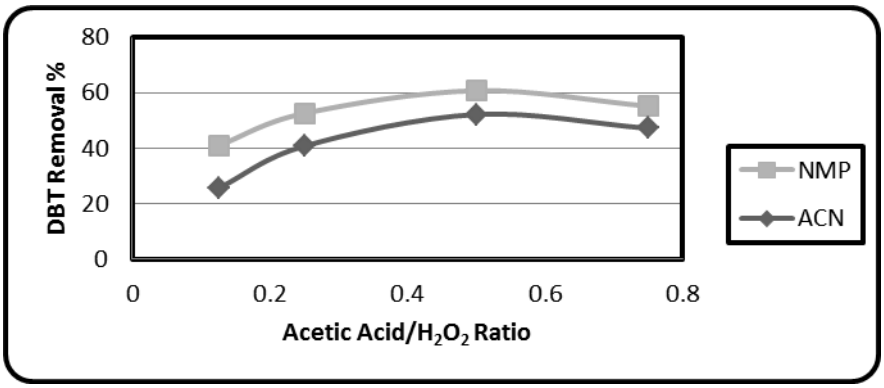

Figure 12. Effect of acetic acid/H_2O_2 ratio on DBT removal .

(Operating conditions: 30 ˚C, 0.5:1 solvent/simulated diesel fuel and 0.5:1 H_2O_2/simulated diesel fuel).

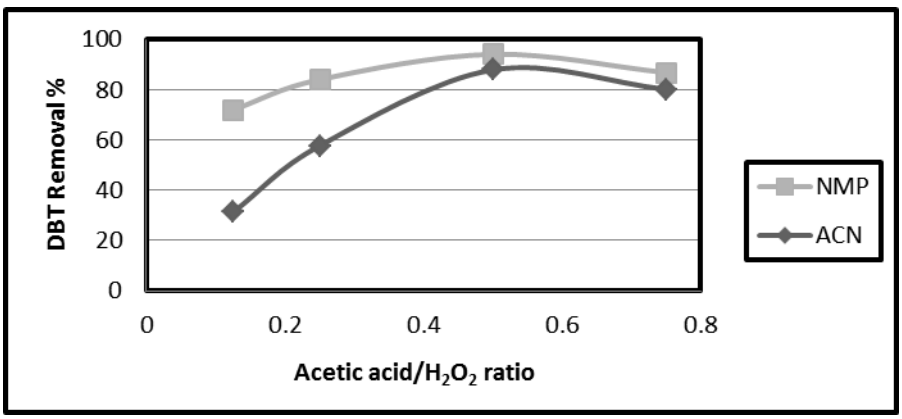

Figure 13. Effect of acetic acid/H_2O_2 ratio on DBT removal .

(Operating conditions: 30˚C, 1:1 solvent/simulated diesel fuel and 1:1 H_2O_2/simulated diesel fuel).

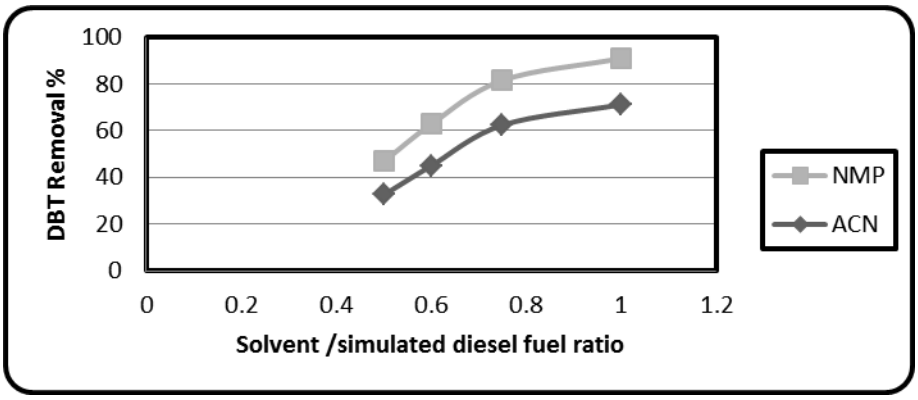

Figure 14. Effect of solvent/simulated diesel fuel ratio on DBT removal.

(Operating conditions: 50˚C, 0.5:1 H_2O_2/simulated diesel fuel ratio 0.125:1 and acetic acid/ H_2O_2) .

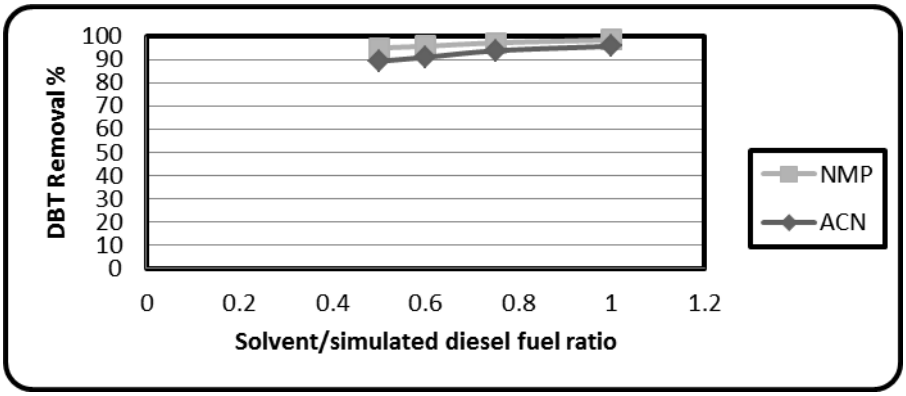

Figure 15. Effect of solvent/simulated diesel fuel ratio on DBT removal.

(Operating conditions: 50˚C, 1:1 H_2O_2/simulated diesel fuel ratio and 0.5:1 acetic acid/ H_2O_2 ratio).

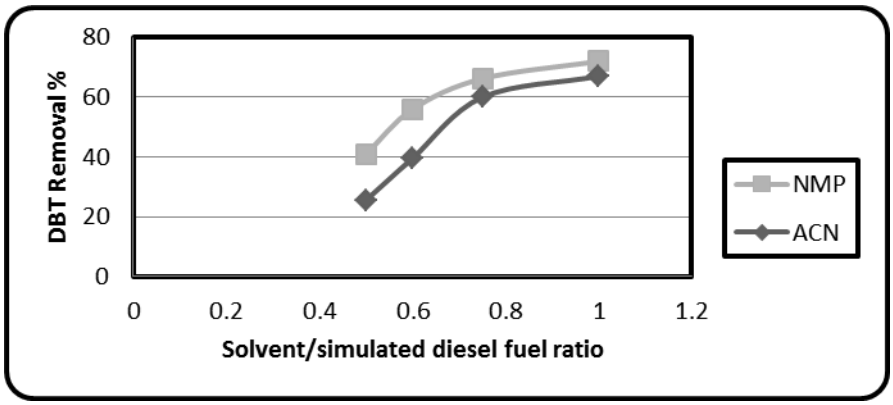

Figure 16. Effect of solvent/simulated diesel fuel ratio on DBT removal.

(Operating conditions: 30°C, 0.5:1 H_2O_2/simulated diesel fuel ratio and 0.125:1 acetic acid/H_2O_2).

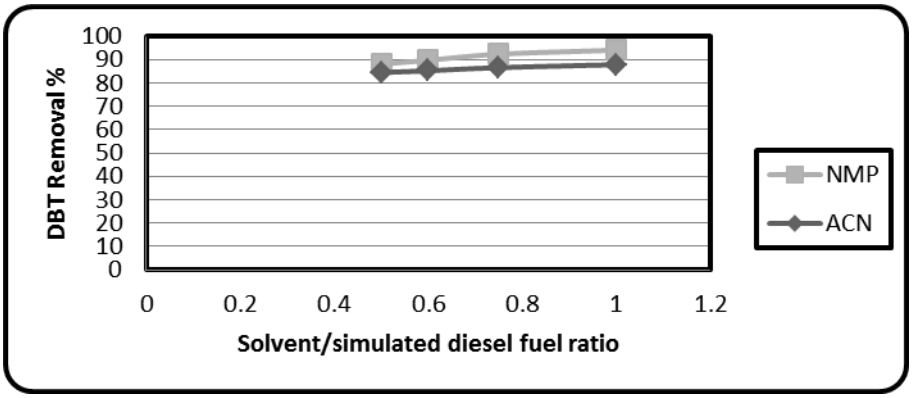

Figure 17. Effect of solvent/simulated diesel fuel ratio on DBT removal.

(Operating conditions: 30 °C, 1:1 H_2O_2/simulated diesel fuel ratio and 0.5:1 acetic acid/ H_2O_2).

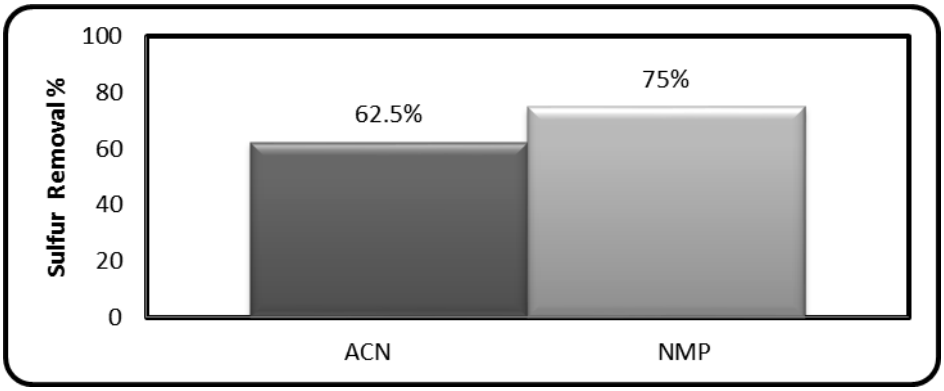

Figure 18. sulfur removal from real diesel fuel.

(Operating conditions: 50 ˚C, stirring speed 350 rpm, 1:1 solvent/real diesel fuel ratio, 1:1 H_2O_2/real diesel fuel ratio and 0.5:1 acetic acid/H_2O_2 ratio for 2h reaction time).

Design a Multi-Choice Fuzzy Control System of the Greenhouse

Prof. Dr. Kais Said Ismail
Department of Computer Engineering
Collage of Engineering
University of Baghdad
Email:Kais_1946@yahoo.com

Qays Jebur Sabr AL-Jewari
Department of Computer Engineering
Collage of Engineering
University of Baghdad
Email:qais_aljuary@yahoo.com

ABSTRACT

Applications of nonlinear, time variant, and variable parameters represent a big challenge in a conventional control systems, the control strategy of the fuzzy systems may be represents a simple, a robust and an intelligent solution for such applications.

This paper presents a design of fuzzy control system that consists of three sub controllers; a fuzzy temperature controller (FC_T), a fuzzy humidity controller (FC_H) and a ventilation control system; to control the complicate environment of the greenhouse (GH) using a proposed multi-choice control system approach. However, to reduce the cost of the crop production in the GH, the first choice is using the ventilation system to control the temperature and humidity of the GH environment according to the external climate if it is possible, if it is not possible then the second choice uses the FC_T to actuate the cooling-heating system to control the temperature and FC_H to actuate the humidifier-dehumidifier to control the humidity of the GH environment. The resultant is a robust, multi choice and multi-mode capability system. The designed system reflects the fuzzy system capability to deal with complicated environments and its flexibility to use the same design in controlling different applications.

Key words: fuzzy controller, multi-choice, ventilation.

تصميم نظام سيطرة ضبابي متعدد الاختيارات للبيت الزجاجي

أ.د. قيس سعيد اسماعيل
قسم هندسة الحاسبات
كلية الهندسة/جامعة بغداد

قيس جبر صبر الجواري
قسم هندسة الحاسبات
كلية الهندسة/جامعة بغداد

الخلاصة

التطبيقات ذات البارامترات المتغيرة, اللاخطية والمتغيرة مع الوقت تمثل تحدي كبير بالنسبة الى انظمة السيطرة التقليدية. ان هذا التحدي ربما يكون اكثر تعقيدا عند استخدامه للسيطرة على الانظمة عبر شبكات الاتصال السلكية او اللاسلكية. من جهة اخرى فان ستراتيجية السيطرة في الانظمة الضبابية ربما تكون حلول بسيطة, متينة وذكية لمثل هذه التطبيقات.

في هذا البحث سيتم تصميم نظام سيطرة ضبابي يتكون من ثلاث مسيطرات: مسيطر ضبابي حراري, مسيطر ضبابي للرطوبة ونظام سيطرة على التهوية, للسيطرة على البيئة المعقدة للبيت الزجاجي باستخدام نظام سيطرة مقترح متعدد الاختيارات. على اية حال, لتقليل كلفة انتاج المحاصيل في البيوت الزجاجية, فان اول اختيار يتمثل في استخدام نظام التهوية للسيطرة على حرارة ورطوبة البيت الزجاجي بالاعتماد على المناخ الخارجي اذا كان ممكن. واذا لم يكن ممكن, فان الاختيار الثاني يستعمل المسيطر الضبابي الحراري لتشغيل نظام التدفئة-التبريد للسيطرة على درجة الحرارة والمسيطر الضبابي للرطوبة لتشغيل نظام الترطيب-التجفيف للسيطرة على الرطوبة.

ان النتيجة التي تم الحصول عليها هي نظام متين, متعدد الاختيارات والانماط في السيطرة. ان هذا النظام في تصميمه يعكس قابلية النظام الضبابي في التعامل مع البيئات المعقدة ومرونته في استخدام نفس التصميم لعدة تطبيقات.

الكلمات الرئيسية: مسيطر ضبابي, متعدد الاختيارات, التهوية.

1. INTRODUCTION

Traditional control design methods are based on some knowledge, or model, of the dynamic system to be controlled. Most of real life dynamic systems are nonlinear, high complex and too difficult to derive an accurate mathematical model which is crucial for optimal and successful implementation of the control algorithm**, Sabri, et al., 2012.**

A new paradigm for nonlinear systems is the fuzzy control approach. It provides a formal methodology for simulating and implementing a human's heuristic knowledge about how to control a system. Fuzzy control approach is unique in its ability to utilize both qualitative and quantitative information. Qualitative information is gathered from the expert operator strategy and from the common knowledge. It has many benefits over traditional controllers in robustness, cost and flexibility**, Sabri, et al., 2012.**

On the other hand, GH environment is one of the nonlinear complicated systems. Its technology depends on providing favorable environment condition to the plants**, Sabri, et al., 2012.**

Different applications have been implemented using the fuzzy logic controller (FC): **Chao, et al., 2000.** A fuzzy logic controller was designed for staged heating and ventilating systems. The controller was implemented in two environments, the greenhouse, and the broiler house. The input variable is represented by six linguistic terms. The output variable represents the heating and cooling stages and it is represented by six linguistic terms, two terms for heating, three terms for cooling, and one term for no change state. The defuzzification method is integer center of gravity (ICOG), where the value of center of gravity is rounded to the nearest integer, to get proper stage value. **Isizoh, et al., 2012.** A fuzzy logic based-microcontroller was designed to control the temperature of an environment by regulating a heater and the speed of a fan. The microcontroller receives the environment temperature from a sensor through analogue to digital converter (ADC), makes the fuzzy control actions, sends control signals to the fan and heater using an output interface device, and displays the controller result temperature using a display unit. It was a combination of software and hardware. **Saudagar, et al., 2012,** a fuzzy PID temperature controller for GH was designed by using Atmel's 89C52 microcontroller and actuating a cooling-heating system. The inputs to the fuzzy controller are the error which is fuzzified to nine triangular membership functions and change in error which is fuzzified to three triangular membership functions. The output is fuzzified to six triangular membership functions. The input to the PID controller is the error signal added with the output of the fuzzy controller, **Hasim, and Aras, 2012,**a room temperature controller was designed using Matlab fuzzy logic toolbox. It was used to control two room parameters, the temperature and the humidity. The input signals are setting value of temperature and temperature difference (have five membership functions), the measured humidity (three membership functions), feeling mode and mode selection. The output signals are the compressor speed (six membership functions), fan speed (five membership functions) and operation mode (humidifier or air conditioner), **Shome, and Ashok, 2012.** Two fuzzy controllers was designed to control the steam temperature and water level in an electric boiler. The input to the fuzzy temperature controller is fuzzified to six parts, while the fuzzy water level controller is fuzzified to four parts. The outputs of the two controllers are fuzzified to three parts. The system with the temperature monitoring was implemented by using a microcontroller programmed with the fuzzy knowledge base rules, **Das, et al., 2013.** A hardware room temperature and humidity controller was designed using fuzzy logic. The controller is a combination of two fuzzy controllers: The first one is the temperature controller to control the speed of a heat-fan and cool-fan, taking the room temperature and its difference with a user set temperature as input variables; and the other is the humidity controller to control the

humidifier and exhaust-fan speed, taking the room temperature and humidity as input variables. The temperature controller input variables each of seven linguistic terms. The defuzzification method is center of average, **Bai, 2013.** An adaptive incremental fuzzy PI controller (AIFPI) was presented for a heating, ventilation, and air conditioning (HVAC) system. A fuzzy controller was used to adapt the gains of a PI controller to overcome different disturbances. It consists of two parts, each one contains a fuzzy and PI controller, the first part is used to control the temperature, and the second part is used to control the humidity. The fuzzy controller receives and delivers two inputs and outputs linguistic variables respectively, each of seven linguistic terms, to determine the change in the PI input gains. The change of calculated PI input gains is added to the previous values to overcome the disturbance effects.

However, most of the systems use the ventilation as a single choice cooling-only control system where the outer climate permits for such applications for most of the seasons. Other applications using a cooling-heating systems without ventilation to control temperature. In Iraq climate, ventilation control systems cannot be applicable only for a few months, also; it may be useful at the night but it is not at the daytime. Therefore, the multi choice control strategy may give a more flexibility with the applications that is designed to operate for all seasons, using the low coast ventilation system if it is possible, otherwise use the other systems which are more expensive without performing any changes in the GH design structure.

2. SYSTEM DESCRIPTION

Three systems will be used to control the temperature and humidity of the GH. They operate in a proposed approach that will be called a multi-choice control system approach. These systems are: cooling-heating system which is controlled by fuzzy temperature controller, humidifier-dehumidifier which is controlled by fuzzy humidity controller and ventilation system which is controlled by fuzzy ventilation system.

However, three modes of operation are suggested to determine the decision making criteria in the ventilation system and organize the cooperation of the ventilation with the other two systems to provide a desired GH climate.

3. GH MODEL AND PARAMETERS

The GH model for the temperature and humidity are derived in Eq. (1) and Eq. (2)**, Nachidi, et al., 2006.** with the internal and external GH environment parameters have been given in **Table 1, Nachidi, et al., 2006.** Some parameters were given in **Rodríguez, et al., 2010** and**, Nachidi, et al., 2008.**

$$T_a(k+1) = \frac{t_s}{C_{cap,q}} \left(\mathrm{E}_q + \tau S_o - C_{cap,q,v}\, V\, (T_a - T_o) - \; h_T\, (T_a - T_o) \right) + \; T_a \tag{1}$$

$$w_a(k+1) = \frac{t_s}{C_{cap,h}} \left(\mathrm{W}_h - V\, (w_a - w_o) - h_w\, (w_a - w_o) \right) + \; w_a \tag{2}$$

4. DESIGN OF FUZZY TEMPERATURE CONTROLLER

4.1. Signals Definition and Parameters Assignment

1. Select the internal GH temperature $T_a(k)$, reference temperature $T_r(k)$.
2. The minimum and maximum reference temperature values are T_{min} = 0 and T_{max} = 100. However, although GH temperature do not reach 100 ◦C but the system will be examined for a higher ranges.
3. The normalized error signal is

$$e(k) = \frac{T_r(k) - T_a(k)}{T_{max} - T_{min}} \tag{3}$$

therefor e(k) ∈ (-1,1).

4. The normalized change in error signal is

$$\Delta e(k) = e(k) - e(k-1) \tag{4}$$

Where Δe(k) ∈ (-1,1).

5. The signals e(k) and Δe(k) are the inputs of the fuzzy controller.
6. Select the controller output signal U(k) ∈ (-1,1).
7. The temperature actuator is represented by three states: off (O), Heating (H), and Cooling (C).
8. Select the inputs and output gains ge, gde and gu respectively. **Fig. 1** shows the Simulink implementation of the closed loop fuzzy temperature controller.

The normalization of input and output signals of the fuzzy controller gives the ability to set and modify the desired operating temperature range with more flexibility and less effort, this will generalize the controller application. For example, the change of the operating range of the controller from (0, 100) to (-13, 87) can be implemented by setting T_{min} = -13 and T_{max} = 87 without modifying the membership functions parameters.

4.1 Input Linguistic Variables

Both e(k) and Δe(k) input linguistic variables are fuzzified into seven linguistic terms, triangular membership functions as follows

1. *Zero (x; -1/3, 0, 1/3):* $ZZ = max(min\left(\frac{x+\frac{1}{3}}{\frac{1}{3}}, \frac{\frac{1}{3}-x}{\frac{1}{3}}\right), 0)$
2. *Positive Small (x; 0, 1/3, 2/3):* $PS = max(min\left(\frac{x-0}{\frac{1}{3}}, \frac{\frac{2}{3}-x}{\frac{1}{3}}\right), 0)$
3. *Positive Medium (x; 1/3, 2/3, 1):* $PM = max(min\left(\frac{x-\frac{1}{3}}{\frac{1}{3}}, \frac{1-x}{\frac{1}{3}}\right), 0)$
4. *Positive Big (x; 2/3 ,1, 1):* $PB = min(max\left(\frac{x-\frac{2}{3}}{\frac{1}{3}}, 0\right), 1)$
5. *Negative Small (x; -2/3, -1/3, 0):* $NS = max(min\left(\frac{x+\frac{2}{3}}{\frac{1}{3}}, \frac{0-x}{\frac{1}{3}}\right), 0)$
6. *Negative Med (x; -1, -2/3, -1/3):* $NM = max(min\left(\frac{x+1}{\frac{1}{3}}, \frac{-\frac{1}{3}-x}{\frac{1}{3}}\right), 0)$
7. *Negative Big (x; -1, -1, -2/3):* $NB = min(max\left(0, \frac{-\frac{2}{3}-x}{\frac{1}{3}}\right), 1)$

where x represents e(k) or Δe(k). **Fig. 2** shows the membership functions for both input signals.

It must be mentioned that PB and NB are open right and open left membership functions.

4.2 Output Linguistic Variable

The output linguistic variable U(k) is fuzzified into three linguistic terms triangular membership function

1. *OFF (U; -0.5, 0, 0.5):* $O = max(min\left(\frac{U+\frac{1}{2}}{\frac{1}{2}}, \frac{\frac{1}{2}-U}{\frac{1}{2}}\right), 0)$

2. *Heating (U; 0, 0.5, 1):* $H = max(min\left(\frac{U}{\frac{1}{2}}, \frac{1-U}{\frac{1}{2}}\right), 0)$
3. *Cooling (U; -1, -0.5, 0):* $C = max(min\left(\frac{U+1}{\frac{1}{2}}, \frac{-U}{\frac{1}{2}}\right), 0)$

Fig. 3 shows the triangle membership functions for the output signal U(k).

For simplicity, the signals e(k), Δe(k), U(k), … will be used as e, Δe, U, … respectively if there is not necessity to use the time sequence (k). Also, for simplicity the unit (◦C) will not be mentioned with temperature values.

4.3 Rule Base

The total number of rules (R) equals the number of linguistic terms of first input linguistic variable times the number of linguistic terms of second input linguistic variable (R=7*7=49). **Table 2** shows the rule base of the fuzzy temperature controller, where the general form of the *i*th rule base is

If e is M_{ei} AND Δe is $M_{\Delta ei}$ THEN U is o_i

where M_{ei} is membership function of the *i*th rule in e domain, $M_{\Delta ei}$ is membership function of the *i*th rule in Δe domain and o_i is membership function of the *i*th rule in U domain.

4.4 Fuzzification

The min operator will be used to implement the AND operation in the premise part. The result of this operation represents the rule certainty. Therefor for the *ith* rule

Rule certainty = min ($\mu^i_j(e)$, $\mu^i_k(\Delta e)$)

Where j and k ∈ (1, 2, …, 7) are the membership functions identifier for e and Δe respectively and μ(.) is the membership functions gradient identified by j or k.

4.5 Defuzzification

The center of gravity (COG) method is used, experimentally it gives more stable response, less oscillation and better performance with wired system. The discrete equation of the COG defuzzification is, **Passino, and Yurkovich, 1998.**

$$z_{COG} = \frac{\sum_{i=1}^{R} b_i a_i}{\sum_{i=1}^{R} a_i} \tag{5}$$

Where b_i and a_i are the output membership functions center and area respectively of the *ith* rule in U domain. The Min operator will be used to implement the AND operation in the premise part, so depending on the defuzzification definition of the Min operator, the output membership function area is a trapezoid area calculated in Eq.(6), **Passino, and Yurkovich, 1998.**

$$a = w(h - \frac{h^2}{2}) \tag{6}$$

Where *w* is the base which is the same for each input membership function, then each rule certainty *h* is used to compute the area *a* using the same equation. The difference of area calculation in each rule will be in the value of *h*.

5. CLOSED LOOP FUZZY TEMPERATURE CONTROLLER

Fig. 1 shows the closed loop fuzzy temperature controller with g_e =1, g_{de} =1 and g_u = 1000000, Fig. 4 shows the response for different T_r values.

6. DESIGN OF FUZZY HUMIDITY CONTROLLER

The same temperature controller properties will be used in constructing a fuzzy humidity controllers. With g_e =1, g_{de} =1 and g_u = 1000; **Fig. 5** shows the system response for different H_r values.

7. DESIGN OF FUZZY VENTILATION CONTROL SYSTEM

The designed fuzzy temperature controller uses a cooling-heating system to track the desired temperature independent of the outer environment temperature. Also, the designed humidity controller uses the humidifier-dehumidifier system to track the desired humidity independent of the outer environment humidity.

On the other hand, the ventilation controller uses the outer environment temperature and humidity to change the internal environment of the greenhouse, but with conditions. The use of ventilation system is proper to reduce the cost of using the cooling-heating system or the humidifier-dehumidifier system.

It is necessary to mention that the ventilation system affects the temperature and humidity at the same time, it tries to make the internal temperature and humidity to converge to the external values. So, the ventilation may be appropriate for the temperature but not for the humidity or vice versa. According to this idea three modes of ventilation operation are suggested.

The ventilation system represents a cheap and a first choice of the fuzzy control system. The other two systems represent an expensive and a second choice. They will be actuated for the following cases:-

1. If it is not possible to reach the desired level by the ventilation system.
2. When the ventilation system was actuated but it cannot perform more modifications to reach the desired level.
3. After actuating the ventilation system, to handle the steady state level. However after the temperature or humidity reaches by ventilation to some percent of the desired value such as 1% or 2% and to avoid out of the desired value changes; the heating-cooling or humidifier-dehumidifier system will be actuated.

Design of ventilation control system is implemented in two stages:

1. Construct of ventilation enable algorithm.
2. Design of fuzzy ventilation rate controller.

7.1 Operation Modes

The ventilation system affects both parameters the temperature and the humidity at the same time. This will affect the control action of these two parameters to set them to the desired values at the same time. However, an operation mode is proposed to handle this case. Three mode of operations are proposed as shown in **Fig. 6**.

1. **Mode 0:** disable the ventilation system, so only the heating-cooling and humidifier-dehumidifier systems will be actuated in a single-choice approach.
2. **Mode 1:** ventilation to change internal temperature to the desired value with negligible effect on the humidity. This mode is used when there is not critical effect of ventilation on the humidity.
3. **Mode 2:** ventilation to change internal humidity to the desired value with negligible effect on the temperature. This mode is used when there is not critical effect of ventilation on the temperature.

7.2 Ventilation Enable Algorithm

Using mode 1, there are two cases that determine the use of ventilation (ON or OFF). **Fig.7.a** shows the first case when the outer temperature T_o is greater than internal greenhouse temperature T_a. In this case the reference temperature may be within one of three levels T_{r1}, T_{r2} and T_{r3}. The following steps represent the algorithm of operating the ventilation:

1. If T_r within T_{r1} level then
   a- Set ventilation V to ON.
   b- Set heating-cooling system energy E to OFF.
   c- When $T_a = T_o$ set V to OFF and E to ON.
2. If T_r within T_{r2} level then
   a- Set ventilation V to ON.
   b- Set heating-cooling system energy E to OFF.
   c- When $T_a = T_r$ set V to OFF and E to ON.
3. If T_r within T_{r3} level then
   a- Set ventilation V to OFF.
   b- Set heating-cooling system energy E to ON.

Fig. 7.b shows the second case when the outer temperature T_o is less than internal greenhouse temperature T_a. In this case the reference temperature may be within one of three levels T_{r1}, T_{r2} and T_{r3}. The following steps represent the algorithm of operating the ventilation:

1. If T_r within T_{r3} level then
   a- Set ventilation V to ON.
   b- Set heating-cooling system energy E to OFF.
   c- When $T_a = T_o$ set V to OFF and E to ON.
2. If T_r within T_{r2} level then
   a- Set ventilation V to ON.
   b- Set heating-cooling system energy E to OFF.
   c- When $T_a = T_r$ set V to OFF and E to ON.
3. If T_r within T_{r1} level then
   a- Set ventilation V to OFF.
   b- Set heating-cooling system energy E to ON.

The same algorithms are used in mode 2 (ventilation to change internal humidity).

7.3 Design of Fuzzy Ventilation-Rate Controller

Starting with mode 1, ventilation may produce large overshot if it is of high rate, or it could not make the internal greenhouse value to converge to the outer value of the temperature if the ventilation rate is below some level. The difference between the outer and

the reference (or setting) temperature (OS) will be used as a criteria to determine the proper rate, and it represents the input signal to the single input fuzzy controller as follow

1. The controller input variable OS=| T_o – T_s |. The absolute value of OS is used to include both cases in figures 7.a and 7.b.
2. OS is normalized, so its range between (0, 1).
3. The controller output variable V-rate.
4. V-rate range is between (1, 10).
5. The input variable is fuzzified into four linguistic terms triangular and trapezoidal membership functions
   a- *Small(OS; -0.01, 0, 0.05, 0.1):* $SM = max(min\left(\frac{OS+0.01}{0.01}, 1, \frac{0.1-OS}{0.05}\right), 0)$
   b- Mid(OS; 0.05, 0.1, 0.2): $MD = max(min\left(\frac{OS-0.05}{0.05}, \frac{0.2-OS}{0.1}\right), 0)$
   c- *Big(OS; 0.1, 0.2, 0.45, 0.5):* $BG = max(min\left(\frac{OS-0.1}{0.1}, 1, \frac{0.5-OS}{0.05}\right), 0)$
   d- *Very Big(OS; 0.45, 0.5, 1, 1.01):* $VB = max(min\left(\frac{OS-0.45}{0.05}, 1, \frac{1.01-OS}{0.01}\right), 0)$

   Fig. 8 shows the input membership functions of the fuzzy ventilation rate controller.
6. The output linguistic variable V-rate is fuzzified into four linguistic terms single tone membership functions V1, V2, V3 and V10 which are at the values 1, 2, 3, and 10, respectively, as shown in **Fig. 9**.
7. The rule base contains the following four rules
   R1: IF OS is VB THEN V-rate is is V1.
   R2: IF OS is BG THEN V-rate is is V2.
   R3: IF OS is MD THEN V-rate is is V3.
   R4: IF OS is SM THEN V-rate is is V10.
8. The defuzzification method that will be used is the center of average
   Sum=VB+BG+MD+SM
   VR1= V1*VB/Sum
   VR2= V2*BG/Sum
   VR3= V3*MD/Sum
   VR4= V10*SM/Sum
   V-rate = VR1+VR2+VR3+VR4

It is necessary to mention that the fuzzy V-rate controller is used when T_r within T_{r2} range in **Figs. 7.a** and **7.b**, otherwise V-rate will take its maximum value which is 10.

The same result is used with mode 2, but V-rate is divided by 10 as determined by experiment.

8. MODE SELECTION IMPLEMENTATION AND PUTTING ALL TOGATHAR

The fuzzy temperature controller FC_T, the fuzzy humidity controller FC_H and the ventilation control system are combined together to construct the heart of the overall control system. The ventilation system represents point of meting, from which the activity of each controller will be decided by implementing the operation mode.

9. SIMULATION RESULTS

Figs. 4 and **5** represent system response for temperature and humidity when M=0, where there is no ventilation effect on the system. **Figs. 10** and **11** show the ventilation effect on system temperature (humidity) for different Tr (Hr) values when M=1 (M=2). In these figures, it is clear that different ventilation rates are obtained for different reference values. It must be noticed that in **Fig. 11**, the ventilation rate is multiplied by 10 for clear simulation show.

10. CONCLUSIONS

1. The important feature of the fuzzy controller, is that its ability to get the appropriate response by tuning the input/output gains. The change of input/output gains produces the change in the membership functions scale, which can assimilate the large scope of signal variation. So during system design steps, the proper response was produced by changing the input/output gains to an appropriate values.
2. Zero steady state error is produced when the fuzzy controller output (U) is treated as (ΔU) and added to the previous value. ($U(k) = U(k-1) + \Delta U(k)$).
3. A large maximum peak overshot is produced when using a product operation instead of minimum operation to implement the AND operator.
4. A long time of oscillation and more settling time produced when using the Gaussian membership function.
5. The multi-choice control approach may be a good introduction with an environments that have different actuation systems based on some application conditions and coast requirements.
6. The multi-choice control strategy with the fuzzy logic controller produces a bit forward step in control system applications, the resultant system is robustness, very low steady state error and there is no peak overshot that affect system performance.

REFERENCES

- Amin, M. S., Mamun, M., Husain, H., and Hashim, F. H., 2011, *A Single Core Hardware Approach of Fuzzy Temperature Controller*, Australian Journal of Basic and Applied Sciences, Vol. 5(12), PP. 675-681, ISSN 1991-8178.

- Bai, J., 2013, *Development an Adaptive Incremental Fuzzy PI Controller for a HVAC System*, Int J Compute Commune, ISSN 1841-9836, Vol. 8(5), PP. 654-661.

- Boeri, C., Silva, F. N., Ferreira, J., and Soares, M. S., 2011, *Optimized Operating Drying Control For Temperature, Relative Humidity And Air Velocity Parameters By Means Of Fuzzy Logic Approach*, European Drying Conference - EuroDrying'2011 Palma, Balearic Island, Spain, 26-28.

- Boobalan, S., Prabhu, K., and Bhaskaran, V. M., 2013, *Fuzzy Based Temperature Controller for Continuous Stirred Tank Reactor*, International Journal of Advanced Research in Electrical, Electronics and Instrumentation Engineering Vol. 2, Issue 12.
- Chao, K., Gates, R. S., and Sigrimis, N., 2000, *Fuzzy Logic Controller Design for Staged Heating and Ventilating Systems*, Transactions of the ASAE, Vol. 43(6), PP. 1885-1894, © American Society of Agricultural Engineers 0001-2351 / 00 / 4306-1885.

- Das, T. K., and Das, Y., 2013, *Design of a Room Temperature and Humidity Controller Using Fuzzy Logic*, AJER, e-ISSN: 2320-0847 p-ISSN: 2320-0936, Vol. 02, Issue-11, PP. 86-97.

- Habbi, H., Kidouche, M., and Bekhadda, N., 2013, *A Fuzzy Supervisory System for Improving Temperature Control in an Industrial Gas Processing Unit*, International Conference on Control, Engineering and Information Technology, Proceedings Engineering and Technology, Vol. 3, PP. 17- 19.

- Hasim, N., and Aras, M. S. M., 2012, *Intelligent Room Temperature Controller System Using MATLAB Fuzzy Logic Toolbox*, International Journal of Science and Research, Vol. 3, Paper ID: 02014549, Issue 6, ISSN (Online): 2319-7064, Impact Factor (2012): 3.358.

- Isizoh, A. N., Okide, S. O., Anazia, A. E., and Ogu, C.D., 2012, *Temperature Control System Using Fuzzy Logic Technique*, IJARAI, Vol. 1, No. 3.

- Mashhadi, S. K. M., Savzevar, M. Z., and Yekan, J. G. D., 2013, *Simulation of Temperature Controller for an Injection Mould Machine using Fuzzy Logic*, Journal of Mathematics and Computer Science, Vol. 7 (2013), PP. 33- 42.

- Mote, T. P., and Lokhande, S. D., 2012, *Temperature Control System Using ANFIS*, International Journal of Soft Computing and Engineering, Vol. 2, Issue 1, ISSN: 2231-2307.

- Nachidi, M., Benzaouia, A., and Tadeo, F., 2006, *Temperature and Humidity Control in Greenhouses using the Takagi-Sugeno Fuzzy Model*, International Conference on Control Applications Munich, Germany.

- Nachidi, M., Rodr´ıguez, F., Tadeo, F., Guzm´an, J. L., and S´anchez, R. G., 2008, *Modeling and Control of Nocturnal Temperature Inside a Greenhouse Using Takagi-Sugeno Fuzzy Models*, Control 2008, 8th Portuguese Conference on Automatic Control, University of Trás-os-Montes and Alto Douro, Vila Real, Portugal.

- Passino, K. M., and Yurkovich, S., 1998 *Fuzzy Control*, Addison Wesley Longman, Inc.

- Rodríguez, E. F., Kubota, C., Giacomelli, G. A., Tignor, M. E., Wilson, S. B., and McMahon, M., 2010, *Dynamic Modeling and Simulation of Greenhouse Environments under Several Scenarios: A Web-Based Application*, Computers and Electronics in Agriculture Vol. 70, PP.105–116.

- Sabri, N., S. A. Aljunid, Ahmad, R. B., Malek, M. F., Yahya, A., Kamaruddin, R., and Salim, M. S., 2012, *Smart Prolong Fuzzy Wireless Sensor-Actor Network for Agricultural Application*, Journal of Information Science and Engineering Vol. 28, PP. 295- 316.

- Shome, A., and Ashok, S. D., 2012, *Fuzzy Logic Approach for Boiler Temperature & Water Level Control*, International Journal of Scientific & Engineering Research, Vol. 3, Issue 6, ISSN 2229-5518.

- Verma, O. P., and Gupta, H., 2014, *Fuzzy Logic Based Water Bath Temperature Control System*, International Journal of Advanced Research in Computer Science and Software Engineering, Vol. 2, PP. 333- 336, Issue 4, ISSN: 2277 128X.

- Zeng, S., Hu, H., Xu, L., and Li, G., 2012, *Nonlinear Adaptive PID Control for Greenhouse Environment Based on RBF Network*, Sensors 12, 5328-5348; doi:10.3390/s 120505328.

Table 1. List of symbols, values and units of GH parameters.

Symbol	Description	Nominal value and unit
ρ	specific mass of air, $kg_{dry\ air}\ m^{-3}$.	1.2
C_p	specific heat of moist air, $Jkg^{-1}K^{-1}$.	1010
$C_{cap,q}$	heat capacity of GH air, $Jm^{-2}{\circ}C^{-1}$.	
$C_{cap,q,v}$	heat capacity per volume unit of GH air, $Jm^{-3}{\circ}C^{-1}$.	
$C_{cap,h}$	volumetric capacity of GH air for humidity, m.	
h_T	heat transmission coefficient through the GH cover of single layer glass, $Wm^{-2}{\circ}C^{-1}$**, Rodríguez, *et al.*, 2010.**	6.2
h_w	leakage air exchange through GH cover, $m\ s^{-1}$.	0.75x10−4
τ	heat load coefficient due to solar radiation, dimensionless**, Nachidi, *et al.*, 2008.**	12.0662
t_s	sampling time, second.	0.01
S_o	outside solar radiation, Wm^{-2}.	800
T_a	GH air temperature, ◦C.	
T_o	outside temperature, ◦C.	
w_a	humidity concentration in GH, $kg\ m^{-3}$.	
w_o	outside humidity concentration, $kg\ m^{-3}$.	
V	ventilation rate, $m^3s^{-1}m^{-2}$.	10
V_g	GH volume, m^3.	45
A_g	soil area of the GH, m^2.	15
E_q	energy supply by heating system, Wm^{-2}.	
E_s	heat load by solar radiation, Wm^{-2}.	
E_v	energy exchange by ventilation, Wm^{-2}.	
E_c	energy exchange by transmission through the cover, Wm^{-2}.	
W_h	water vapor exchange using humidifier and dehumidifier system, $kg\ m^{-3}\ s^{-1}$.	
W_c	water vapor exchange through the cover, $kg\ m^{-3}\ s^{-1}$.	
W_v	water vapor exchange with outside air by ventilation, $kg\ m^{-3}\ s^{-1}$.	

Table 2. Rule base of 7x7x3 fuzzy controller.

e(k) \ Δe(k)		PB	PM	PS	ZZ	NS	NM	NB
	PB	O	H	H	H	H	H	H
	PM	C	O	H	H	H	H	H
	PS	C	C	O	H	H	H	H
	ZZ	C	C	C	O	H	H	H
	NS	C	C	C	C	O	H	H
	NM	C	C	C	C	C	O	H
	NB	C	C	C	C	C	C	O

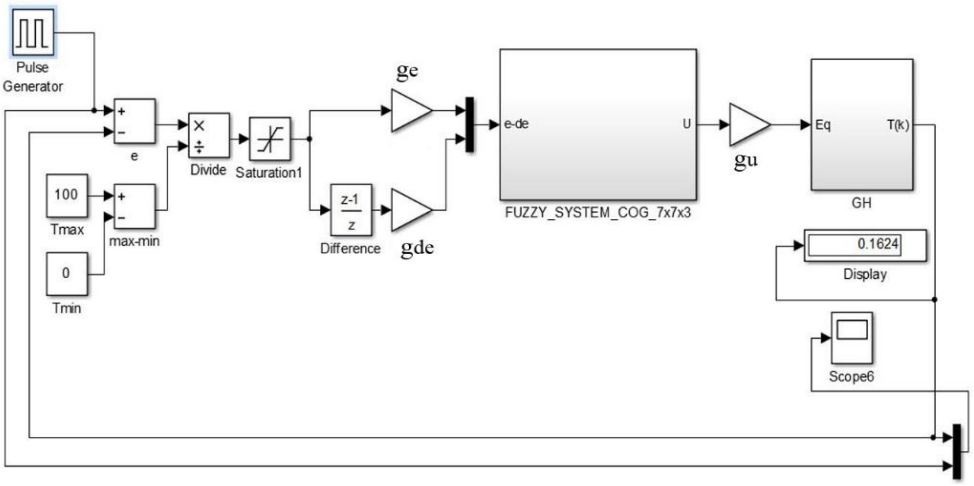

Figure 1. Simulink implementation of connecting the fuzzy controller of the GH system.

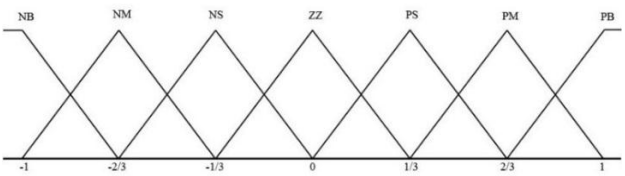

Figure 2. Triangular membership functions for input variables e(k) and Δe(k).

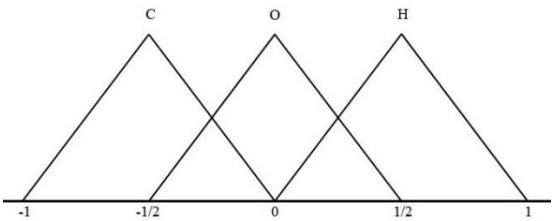

Figure 3. Triangular membership function for the output variable U(k).

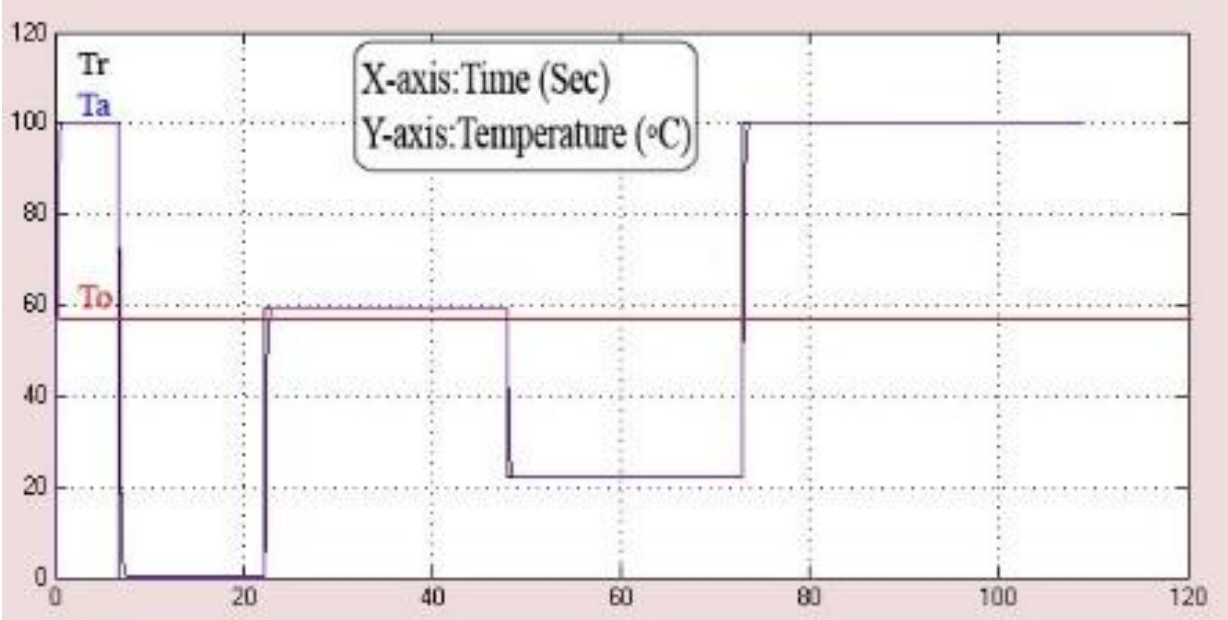

Figure 4. System temperature response where g_e = 1, g_{de} =1 and g_u = 1000000.

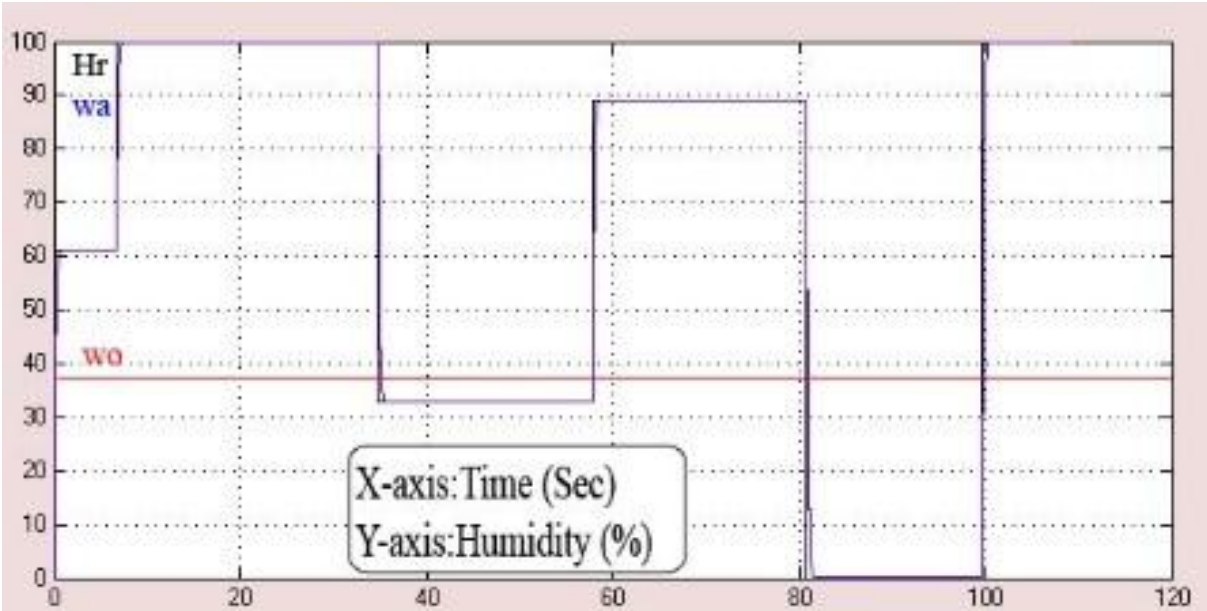

Figure 5. System humidity response where g_e = 1, g_{de} =1 and g_u = 1000.

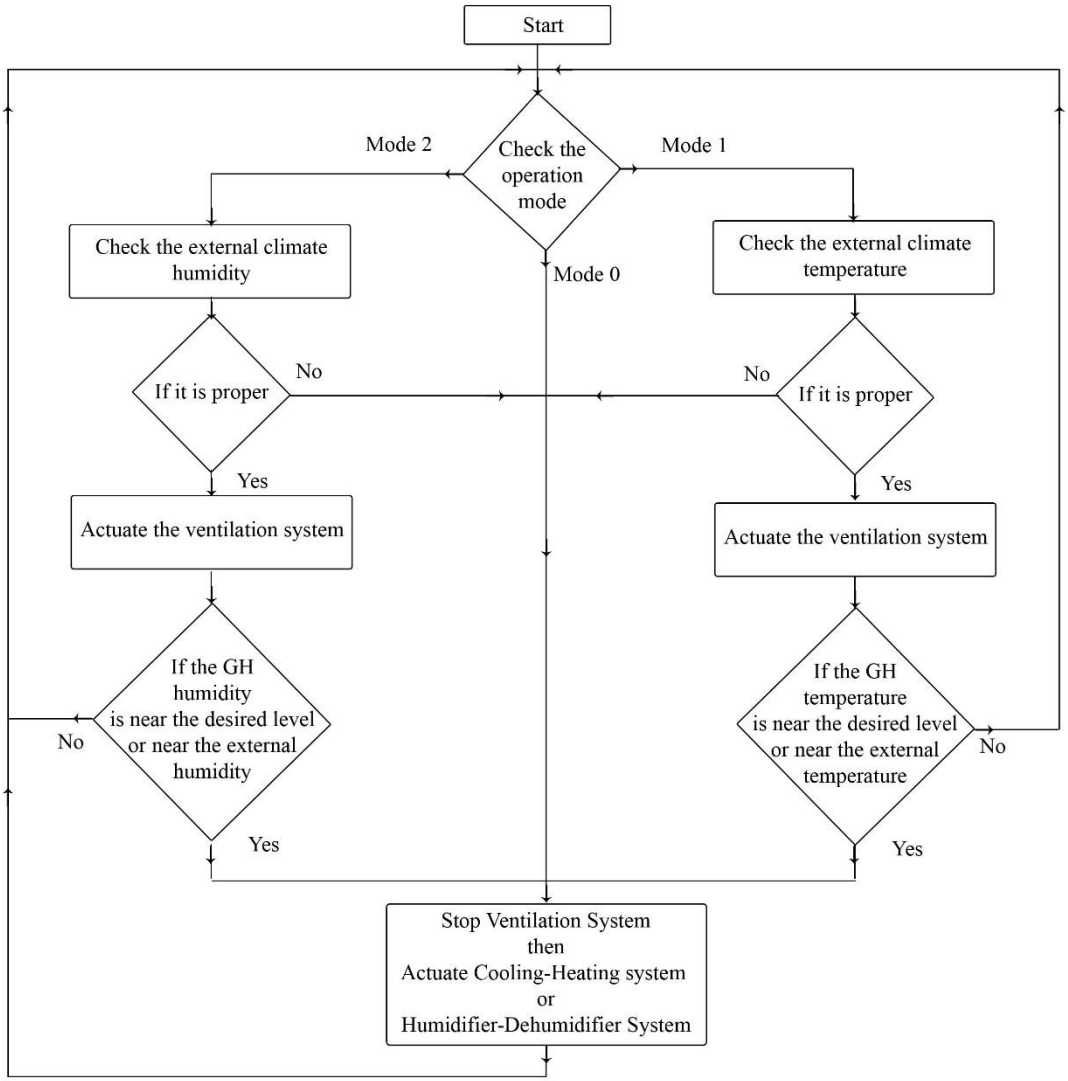

Figure 6. Multi-choice control mechanism.

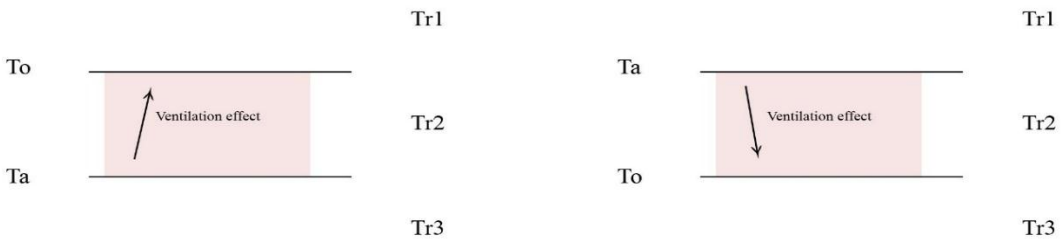

a. $T_o > T_a$ b. $T_o < T_a$

Figure 7. The Outer temperature with respect to the internal GH temperature.

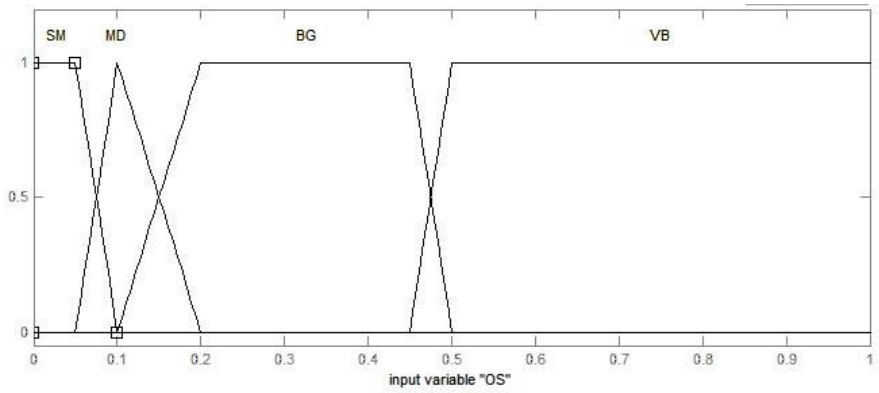

Figure 8. Input membership functions of the fuzzy ventilation rate controller.

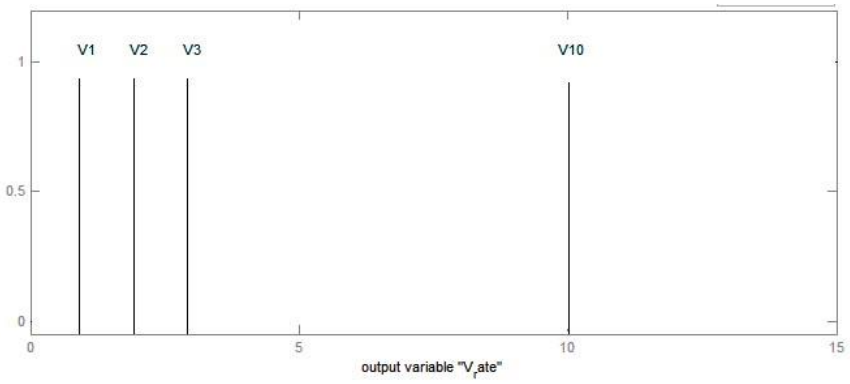

Figure 9. Output membership functions of the fuzzy ventilation rate controller.

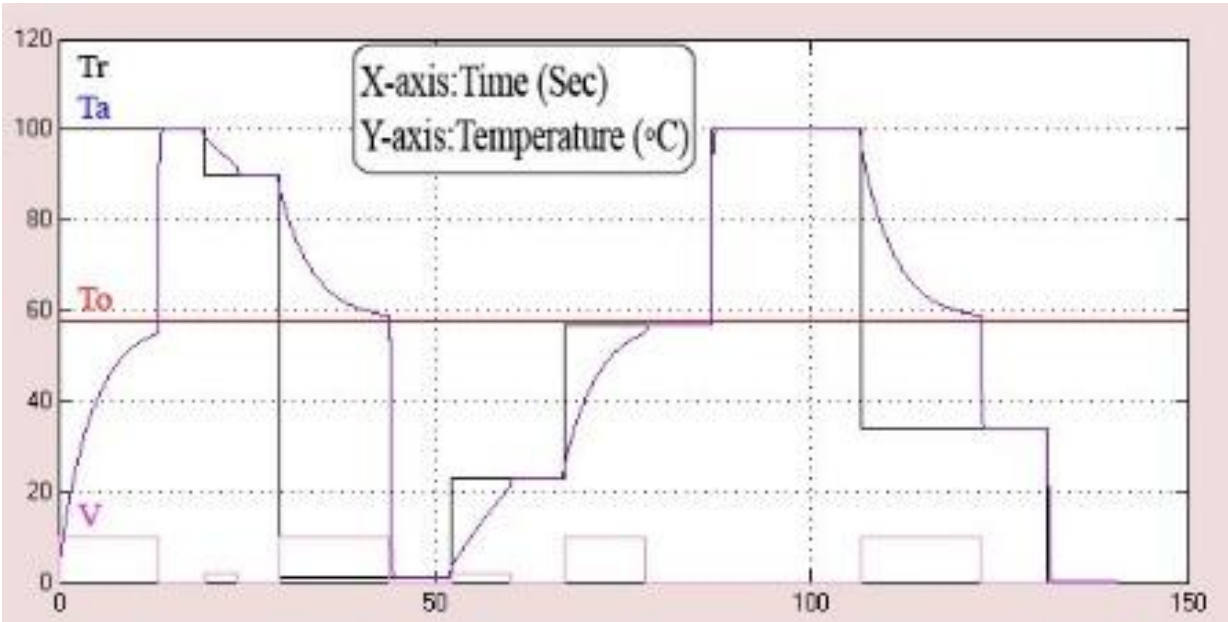

Figure 10. Ventilation effect on system temperature for M=1 and different T_r values.

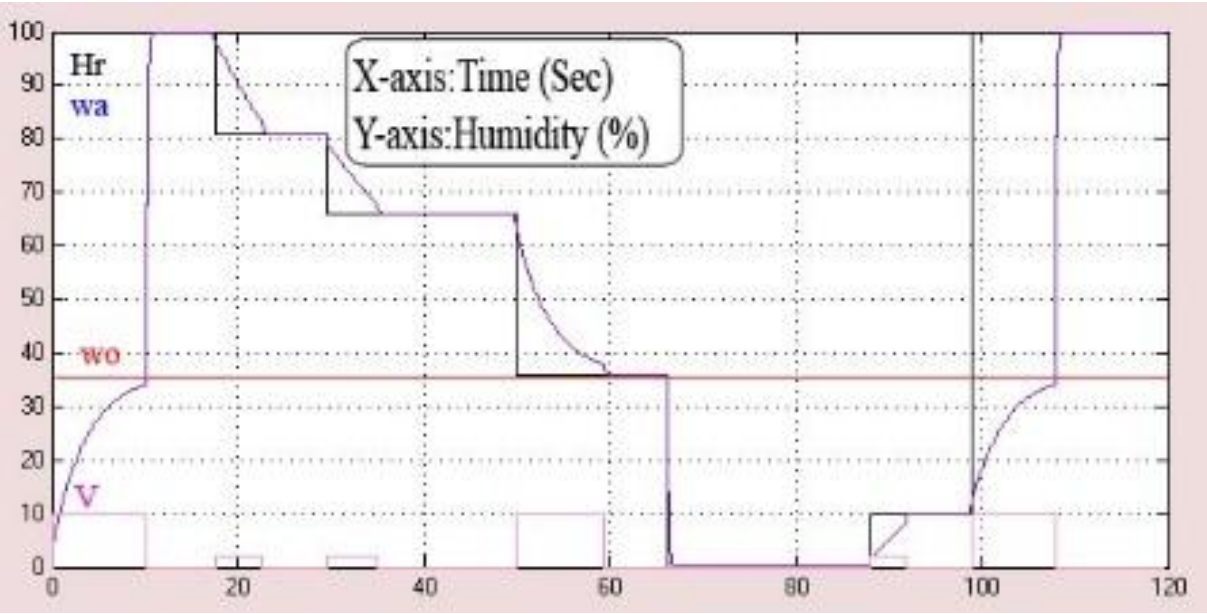

Figure 11. Ventilation effect on system humidity for M=2 and different H_r values.

Non-Linear Analysis of Laminated Composite Plates under General Out-Of-Plane Loading

Dr. Hatem Rahem Wasm
Assistant Professor
College of Engineering -University of Baghdad
email:hatemrwa@yahoo.com

Dr. Ibtehal Abbas Sadiq
Instructor
College of Engineering -University of Baghdad
email:ebtihalabas@yahoo.com

Mohsin Asfoor Lafta
M.Sc
College of Engineering -University of Baghdad
email:asfore2000@yahoo.com

ABTRACT

The theoretical analysis depends on the Classical Laminated Plate Theory (CLPT) that is based on the Von-Kárâman Theory and Kirchhov Hypothesis in the deflection analysis during elastic limit as well as the Hooke's laws of calculation the stresses. New function for boundary condition is used to solve the forth degree of differential equations which depends on variety sources of advanced engineering mathematics. The behavior of composite laminated plates, symmetric and anti-symmetric of cross-ply angle, under out-of-plane loads (uniform distributed loads) with two different boundary conditions are investigated to obtain the central deflection for mid-plane by using the Ritz method. The computer programs is built using Mat lab(R2011a), to solve non-linearity effects on the central deflection values of rectangular cross-ply composite laminated plates, aspect ratio, stresses, orthotropic factor (E/G) and orientations of fiber. The non-linear analysis results of (4.74%) for SSSS of $0^0/90^0/90^o/0^0$cross-ply angle plate, (8.77%) for CCCC of $0^0/90^0$cross-ply angle plate and (10.83%) for CCCC of $0^0/90^0/90^o/0^0$cross-ply angle plate showed a good agreement with **Reddy, 1997** results**.**

Comparing between the analytical linear, non-linear and experimental results gave a big difference between linear and non-linear results, while, non-linear showed close results with experimental results.

Key words: non-linear analysis, large deflection, composite laminated plate, classical laminated plate theory and Ritz method**.**

التحليل اللاخطي في الصفائح المركبه لحمل الانحناءالعام

د. حاتم رحيم وسمي
استاذ مساعد
كلية الهندسه- جامعة بغداد

د. ابتهال عباس صادق
مدرس
كلية الهندسه- جامعة بغداد

محسن عصفور لفته
كلية الهندسه- جامعة بغداد

الخلاصه

التحليل النظري يعتمد على نظرية الصفيحه المركبه الكلاسيكيه التي تستند على نظرية فون كارمن وفرضيات كيرشوف ضمن حدود المرونه وكذلك قوانين هوك في حساب الاجهادات.استخدمت دوال جديده على المحاور المتعامده لحل المعادلات التفاضليه من الدرجه الرابعه حسب الشروط الحديه بالاعتماد على مصادر متنوعه في الرياضيات الهندسيه المتقدمه.التحقق في سلوك الصفائح الطبقيه المركبه,المتناظره وغير المتناظره,تحت حمل الانحناء العام(الموزع بشكل منتظم)لعشرة شروط حديه للحصول على الازاحه المركزيه في المستوي الوسطي باستخدام طريقة ريتز تم استخدام برامج الحاسوب,ماتلاب, لتنفيذ حل الاثار اللاخطيه على قيم الازاحه المركزيه في اللالواح الطبيقيه المركبه المتعامده ,نسبة الطول الى العرض , الاجهادات ,عامل التغاير

المتعامد واتجاهات الالياف.نتائج التحليل اللاخطي الحاليه تختلف عن نتائج البحوث السابقه كما يلي(4.7%) للمثبت بشكل بسيط من الجهات الاربع اللوح ذو الطبقات الاربع المتعامده(صفردرجه/تسعين درجه/تسعين درجه/صفر درجه) , (8.77%) للمثبت بقوه من الجهات الاربع للوح ذو الطبقتين المتعامدتين(صفر درجه/تسعين درجه) و(10.83%) للمثبت بقوه من الجهات الاربع للوح ذو الطبقات الاربع المتعامده (صفردرجه/تسعين درجه/تسعين درجه/صفر درجه).

تم مقارنة نتائج التحليل الخطي واللاخطي والعملي ووجدنا الفارق الكبير بين نتائج التحليل الخطي من جانب وبين نتائج التحليل اللاخطي والعملي من جانب اخر والذي يدعم الاعتماد على نتائج التحليل اللاخطي في التصميم لانها الاقرب الى الواقع.

الكلمات الرئيسيه: التحليل اللاخطي, الازاحه الكبيره, اللالواح الطبقيه المركبه, نظرية اللالواح الطبقيه المركبه وطريقة ريتز.

1. INTRODUCTION

During the last decades, needs for composite materials which contain two or three types of materials mixed together homogenously have appeared.

Composite materials have many advantages such as high strength with low weight compared with traditional engineering materials; furthermore, their properties can be controlled during mixing of their components to meet the suitable design requirements**.** When a flat plate subjected to out-of-plane loads (uniform distributed loads), the real shape of displacement of this plate is nonlinear shape, **Reddy,1997.**

Huai, and Hui, 1990, based on the Von-Káráman theory of plates and they used double Fourier series method to solve the nonlinear bending problems of simply supported symmetric laminated cross-ply rectangular plates under combined action of pressure and in-plane load. The solution which investigated and satisfies the governing equations and boundary conditions is obtained. **Singh, et al., 1991,** investigated the large deflection bending analysis of anti-symmetric rectangular cross-ply plate based on Von-Káráman plate theory is investigated, with one-term approximation for the in-plane and transverse displacement, under sinusoidal loading. The presence of bending-stretching coupling in such plates resulted in an additional square nonlinear term which made the solution load direction dependent, unlike isotropic, orthotropic, symmetric, square anti-symmetric cross-ply and symmetric and anti-symmetric angle-ply plates. **Savithri, and Varadan, 1993,** worked on the non-linear bending analysis of simply supported symmetrically laminated orthotropic plates subjected to uniformly distributed load, using an accurate displacement based higher-order theory is presented. The non-linear governing equations were solved by the Galerkin procedure with the Newton- Raphson method. Numerical given here, based on analytical investigation, will be useful for comparison in future**. Tanriöver, and Senocak, 2004,** discussed a large defection analysis of laminated composite plates. Galerkin method along with Newton-Raphson method was applied to large deflection analysis of laminated composite plates with various edge conditions. The Von-Káráman plate theory was utilized and the governing differential equations were solved by choosing suitable polynomials as trial functions to approximate the plate displacement functions. The solution is compared to that of dynamic relaxation and finite elements. A very close agreement had been observed with these approximating methods. In the solution process, analytical computation has been done wherever it is possible, analytical-numerical type approach has been made for all problems. **Nayyar, 2006,** examined static and vibration analysis of laminated plates were conducted conventional and hierarchical finite element formulation based on First-order Shear Deformation Theory (FSDT). The efficiency and accuracy of the developed formulation is also established in comparison with approximate solutions based on Ritz-method which are also developed for the cases under study. A detailed parametric study has been conducted

on various types of laminated plates, in order to investigate the effects of boundary conditions, laminate configuration, aspect ratio values and elastic modulus to shear modulus (E/G) ratio. **Shfrin, et al, 2008,** studied a semi-analytic approach for the geometrically non-linear analysis of rectangular laminated plates with general boundary conditions and out-of-plane loads had been developed. The solution of non-linear partial differential equations of Von-Káráman plate theory has been reduced to an iterative (sequential) solution of a set of non-linear ordinary differential equations using multi-term extend Kantorovich method. Various combinations of boundary and loading conditions that are beyond the applicability of other semi-analytical methods have been considered the convergence, accuracy, and applicability of the proposed approach have been demonstrated through the quantitative study of various cases of large deflection non-linear response of laminated plates. The semi-analytical method proposed in this paper for the large deflection analysis of laminated plates subjected to out-of-plane loading can be further extended for non-linear analysis of plates with in-homogenous or mixed boundary conditions. **Kim, et al.**, **2008,** performed the non- linear structural analysis of higher- aspect- ratio structures. For the high-aspect-ratio structures, it is important to understand geometric nonlinearity due to large deflections. To consider geometric non- linearity, finite element analysis based on large deflection beam theory were introduced. Comparing experimental data and the present nonlinear analysis results, the current results were proved to be very accurate for the static and dynamic behaviors for both isotropic and anisotropic beams. **Saffari, and Mansouri, 2011,** solved non-linear algebraic equations by an iterative method, the non-linear equations being linearized by evaluating the non-linear terms with the known solution from the preceding iteration. The Newton-Raphson method, which is based on the Taylor series expansion and uses the tangent stiffness matrix, had been extensively used to solve non-linear problems. A new Newton-Raphson algorithm was developed for analyses involving non-linear behavior. **Nishawala, 2011,** studied a thin plate or beam; if the deformation is on the order of the thickness and remain elastic, linear theory may not produce accurate results as it does not predict the in-plane movement of the member. Therefore, a geometrical nonlinearity, large deformation theory is required to account for the inconsistencies. The equation of motion for plates with free and clamped edges was derived using model analysis in conjunction with the expansion theorem. Theoretical results were compared with a finite element simulation for plates.

Concluding Remarks:

In present work the considered cases are as follows:-

(a) Wide coverage to cases of static load (uniform distributed load) which is made of materials E-fiber glass and Polyester, multi-layers of cross-ply angle and thickness (4mm) was observed.

(b) Using a new orthogonal shape functions and Ritz method to cover our boundary conditions which are not used in previous papers.

(c) Making a new device for bending test.

2. ANALYTICAL SOLUTION (CLASSICAL LAMINATED PLATE THEORY)

The classical laminated plate theory is an extension of the classical plate theory to composite laminates. In the classical laminated plate theory (CLPT), it is assumed that the Kirchhoff hypothesis holds:-

1. Straight lines perpendicular to the mid surface (i.e. transverse normally) before deformation remain straight after deformation.
2. The transverse normal do not experience elongation (i.e. they are inextensible)
3. The transverse normal rotates such that they remain perpendicular to the mid surface after deformation.

The first two assumptions imply that the transverse displacement is independent of the transverse (thickness) coordinate and the transverse normal strain ε_{ZZ} is zero. The third assumption results in zero transverse shear strain, $\gamma_{xz}=0$, $\gamma_{yz}=0$. **Reddy, 1997.**

2.1 Displacements: Reddy, 1997

$$u(x,y,z) = u_\circ(x,y) - z\frac{\partial w_\circ}{\partial x} \quad (1.a)$$

$$v(x,y,z) = v_\circ(x,y) - z\frac{\partial w_\circ}{\partial y} \quad (1.b)$$

$$(x,y,z) = w_\circ(x,y) \quad (1.c)$$

2.2 Strains:

The Von-Káráman strains and the associated plate theory is named the Von-Káráman plate theory: **Reddy, 1997.**

$$\varepsilon_{xx} = \frac{\partial u}{\partial x} + \frac{1}{2}\left(\frac{\partial w}{\partial x}\right)^2 \quad (2.a)$$

$$\varepsilon_{yy} = \frac{\partial v}{\partial y} + \frac{1}{2}\left(\frac{\partial w}{\partial x}\right)^2 \quad (2.b)$$

$$\Gamma_{xy} = \frac{1}{2}\left(\frac{\partial u}{\partial y} + \frac{\partial v}{\partial x} + \frac{\partial w}{\partial x} + \frac{\partial w}{\partial y}\right) \quad (2.c)$$

$$\gamma_{xz} = \frac{1}{2}\left(\frac{\partial u}{\partial z} + \frac{\partial w}{\partial x}\right) \quad (2.d)$$

$$\gamma_{yz} = \frac{1}{2}\left(\frac{\partial v}{\partial z} + \frac{\partial w}{\partial y}\right) \quad (2.e)$$

$$\varepsilon_{zz} = \frac{\partial w}{\partial z} \quad (2.f)$$

In view of assumption of the classical laminated plate theory, Eq. (2) becomes:

$$\varepsilon_{xx} = \frac{\partial u_\circ}{\partial x} + \frac{1}{2}\left(\frac{\partial w_\circ}{\partial x}\right)^2 - z\frac{\partial^2 w_\circ}{\partial x^2} \quad (3.a)$$

$$\varepsilon_{yy} = \frac{\partial v_\circ}{\partial y} + \frac{1}{2}\left(\frac{\partial w_\circ}{\partial y}\right)^2 - z\frac{\partial^2 w_\circ}{\partial y^2} \quad (3.b)$$

$$\Gamma_{xy} = \frac{1}{2}\left(\frac{\partial u_\circ}{\partial y} + \frac{\partial v_\circ}{\partial x} + \frac{\partial w_\circ}{\partial x}.\frac{\partial w_\circ}{\partial y}\right) - z\frac{\partial^2 w_\circ}{\partial x\,\partial y} \quad (3.c)$$

$$\gamma_{xz} = \frac{1}{2}\left(-\frac{\partial w_\circ}{\partial x} + \frac{\partial w_\circ}{\partial x}\right) = 0 \quad (3.d)$$

$$\gamma_{yz} = \frac{1}{2}\left(-\frac{\partial w_\circ}{\partial y} + \frac{\partial w_\circ}{\partial y}\right) = 0 \quad (3.e)$$

$$\varepsilon_{zz} = 0 \quad (3.f)$$

$$\begin{bmatrix}\varepsilon_{xx}\\ \varepsilon_{yy}\\ \gamma_{xy}\end{bmatrix} = \begin{bmatrix}\frac{\partial u^\circ}{\partial x} + \frac{1}{2}\left(\frac{\partial w_\circ}{\partial x}\right)^2\\ \frac{\partial v_\circ}{\partial y} + \frac{1}{2}\left(\frac{\partial w_\circ}{\partial y}\right)^2\\ \frac{\partial u_\circ}{\partial y} + \frac{\partial v_\circ}{\partial x} + \frac{\partial w_\circ}{\partial x}\cdot\frac{\partial w_\circ}{\partial y}\end{bmatrix} - z\begin{bmatrix}\frac{\partial^2 w_\circ}{\partial x^2}\\ \frac{\partial^\circ w_\circ}{\partial y^2}\\ 2\frac{\partial^2 w_\circ}{\partial x\,\partial y}\end{bmatrix} \quad (4)$$

2.3 Plane Stress –Reduced Constitutive Relations

A state of generalized plane stress with respect to the XY-plane is defined to be one in which:-

$$\sigma_{xx}=\sigma_{xx}(x,y),\sigma_{yy}=\sigma_{yy}(x,y),\ \sigma_{zz}=0,\varepsilon_{zz}=0 \quad (5)$$

The strain-stress relations of an orthotropic body in plane stress state can be written as:

$$[\sigma_{ij}]=[Q_{ij}][\varepsilon_{ij}] \quad (6)$$

Most laminates are typically thin and experience a plane state of stress. For a lamina in the XY-plane, the transverse stress components are σ_{zz} , τ_{xz} and τ_{yz} . Although these stress components are small in comparison to σ_{xx} , σ_{yy} andτ_{xy}, they can induce failures because fiber-reinforced composite laminates are weak in the transverse direction (because the strength providing fibers are in the XY-plane). For this reason, the transverse shear stress is not neglected in shear deformation theories. However, in most equivalent-single layer theories the transverse normal stress σ_{zz} is neglected. Then the constitutive equations must be modified to this account for this fact. **Reddy, 1997.**

The condition σ_{zz}=zero results in following static constitutive equations for k^{th} layer that is characterized as orthotropic lamina uniform distributed loads **Reddy,1997.**

$$\begin{bmatrix}\sigma_{xx}\\ \sigma_{yy}\\ \tau_{xy}\end{bmatrix}^{(k)} = [Q_{ij}]^{(k)}\begin{bmatrix}\varepsilon_{xx}\\ \varepsilon_{yy}\\ \gamma_{xy}\end{bmatrix}^{(k)} \quad (7)$$

Where i,j=1,2,6 ,k the number of layers and $[Q_{ij}]^{(k)}$ are the plane stress-reduced stiffness founded by **Reddy, 1997.**

$$Q_{11}=\frac{E_1}{1-\nu12\nu21},\ Q_{12}=\frac{\nu12E_2}{1-\nu12\nu21}=\frac{\nu21E_2}{1-\nu12\nu21},$$
$$Q_{22}=\frac{E_2}{1-\nu12\nu21},Q_{66}=G_{12} \quad (8)$$

2.4 Equations of Motion

As noted earlier, the transverse strains (γ_{xz}, γ_{yz}, ε_{zz}) are identically zero in the Classical Plate Theory. Consequently, the transverse shear stresses (τ_{xz} , τ_{yz}) are zero for a laminate made of orthotropic layers if they are computed from the constitutive relations. The transverse normal stress σ_{zz} is not zero by the constitutive relation because of the Poisson effect. However, all three stress components do not enter the formulation because the virtual strain energy of these stresses is zero due to the fact that kinematically consistent virtual strains must be zero [see Eq.(9)]:

$$\delta\varepsilon_{xz} = \delta\varepsilon_{yz} = \delta\varepsilon_{zz} = 0 \qquad (9)$$

Whether the transverse stresses are accounted for or not in a theory, they are present in reality to keep the plane in equilibrium. In addition, these stress components may be specified on the boundary. Thus, the transverse stresses do not enter the virtual strain energy expression, but they must be accounted for in the boundary condition and equilibrium of forces.

Here, the governing equations are derived using the principle of virtual displacement. In the derivations, we account for static effects.

The static version of the energy is:-

$$\delta W = \int_0^{L_x}\int_0^{L_y}(U+V)dxdy = 0 \qquad (10)$$

Where the virtual strain energy δU (volume integral of δU_0), the virtual potential virtual δV and the virtual work done by applied forces are given by:-

$$U = \int_0^{L_x}\int_0^{L_y}\int_{-\frac{h}{2}}^{\frac{h}{2}}[\sigma_{xx}\varepsilon_{xx} + \sigma_{yy}\varepsilon_{yy} + \tau_{xy}\gamma_{xy})dxdydz$$

$$U = \int_0^{L_x}\int_0^{L_y}\{\int_{-\frac{h}{2}}^{\frac{h}{2}}[\sigma_{xx}(\varepsilon_{xx}{}^{(0)} + z\varepsilon_{xx}{}^{(1)}) + \sigma_{yy}\left(\varepsilon_{yy}{}^{(0)} + z\varepsilon_{yy}{}^{(1)}\right) + \tau_{xy}\left(\gamma_{xy}{}^{(0)} + z\gamma_{xy}{}^{(1)}\right))\}dxdydz$$

(11)

$$V = -\int_0^{L_x}\int_0^{L_y}[q_b(x,y)w\left(x,y,\frac{h}{2}\right) + q_t(x,y)w\left(x,y,\frac{h}{2}\right)]dxdy \qquad (12)$$

Where q_b is the distributed force at the bottom ($z=\frac{h}{2}$) of the laminate, q_t is the distributed force at the top ($z=-\frac{h}{2}$).

$$\begin{bmatrix} N_{XX} \\ N_{YY} \\ N_{XY} \end{bmatrix} = \int_{-h/2}^{h/2}\begin{bmatrix} \sigma_{xx} \\ \sigma_{yy} \\ \tau_{xy} \end{bmatrix} dz \;\; ; \;\; \begin{bmatrix} M_{xx} \\ M_{yy} \\ M_{xy} \end{bmatrix} = \int_{-h/2}^{h/2}\begin{bmatrix} \sigma_{xx} \\ \sigma_{yy} \\ \tau_{xy} \end{bmatrix} zdz \qquad (13)$$

The quantities (N_{xx} , N_{yy} , N_{xy}) are called the in-plane force resultants, and (M_{xx} , M_{yy} , M_{xy}) are called transverse force resultants All stress resultants are measured per unit length (e.g., N_i and Q_i in N/m and M_i in N.m/m).

[A], [B] and [D] are the common laminate stiffness matrices of membrane stiffness, bending–membrane coupling stiffness and bending stiffness. For arbitrary laminates, these matrices are defined as **Reddy, 1997.**

$$[A] = \begin{bmatrix} A_{11} & A_{12} & A_{16} \\ A_{12} & A_{22} & A_{26} \\ A_{16} & A_{26} & A_{66} \end{bmatrix};\ [B] = \begin{bmatrix} B_{11} & B_{12} & B_{16} \\ B_{12} & B_{22} & B_{26} \\ B_{16} & B_{26} & B_{66} \end{bmatrix};\ [D] = \begin{bmatrix} D_{11} & D_{12} & D_{16} \\ D_{12} & D_{22} & D_{26} \\ D_{16} & D_{26} & D_{66} \end{bmatrix}$$

$$\left(A_{ij}, B_{ij}, D_{ij}\right) = \int_{-h/2}^{h/2} Q_{ij}(1, z, z^2)dz \qquad (14)$$

$$i, j = 1, 2, 6.$$

2.5 Ritz Method (Energy Method)

Components of the compatible infinitesimal virtual displacements (u, v, w) must be piecewise continuous functions of x, y and z in the interior domain of the body. In addition, they should satisfy the geometrically boundary condition of the elastic system and be capable of representing all possible displacement patterns. If these admissible displacement functions are chosen properly, very good accuracy can be attained.

According to this theorem, as discussed above, of all displacements that satisfy the boundary conditions, those making the total potential energy of the structure a minimum are the sought deflections pertinent to the stable equilibrium conditions.

2.6 Boundary Conditions

In general, the definition of the boundary conditions are procedure to fix edges the elements, plates, as free(F), simply supported(S), clamped(C), built-in or hinged. The boundary conditions that are (clamped-clamped-clamped-clamped, for four edges case, CCCC) or mixing two or more than of these types (clamped-free-simply supported-free, CFSF). The way of fixing edges depend on the application of a structure, plate, dimensions of a structure, the load type and the load amount**. Robbert M. Jones, 1999.**

(a)Free-edges (F):

$M_{x|x=a}=M_{y|y=b}=0;\ V_{x|x=a}=V_{y|y=b}=0$

(b)Simply supported edges (S):

$w|_{x=a,y=b}=0;\ M_{x|x=a}=M_{y|y=b}=0$

(c)Clamped edges(C):

$w|_{x=a,y=b}=0;\ (\frac{\partial w}{\partial x})|(x=a) =(\frac{\partial w}{\partial x})|(y=b)=0.$

\

2.7 Displacement Function

The behavior of a structure, plate, is different from fixing way to other. In present work, the orthogonal arbitrary displacement functions are used to find the exact solution of these cases as following:-

1. CCCC boundary condition,Szilard, 2004.

$u(x,y)=(1/4)\ A_{mn}\ (1-\cos(\alpha\ x))(1-\cos(\beta))$, $v(x,y)=(1/4)\ B_{mn}\ (1-\cos(\alpha\ x))\ (1-\cos(\beta))$,
$w(x,y)=(1/4)C_{mn}\ (1-\cos(\alpha\ x))\ (1-\cos(\beta))$

2. SSSS boundary condition, Szilard,2004.

$u(x,y)=\ A_{mn}\ \sin(\alpha\ x)\ \sin(\beta\ y)$, $v(x,y)=\ B_{mn}\ \sin(\alpha\ x)\ \sin(\beta\ y)$, $w(x,y)=\ C_{mn}\ \sin(\alpha\ x)\ \sin(\beta\ y)$

3. CCCF boundary condition[Present work]

$u(x,y)=(1/2)\ A_{mn}\ (1-\cos(\alpha\ x))(-1)^{\left(\frac{2n-1}{2}\right)}\left(e^{\beta y}-1\right)$,$v(x,y)=(1/2)\ B_{mn}\ (1-\cos(\alpha\ x))\ (-1)^{\left(\frac{2n-1}{2}\right)}\left(e^{\beta y}-1\right)$

$w(x,y)=(1/2)\ C_{mn}\ (1-\cos(\alpha\ x))(-1)^{\left(\frac{2n-1}{2}\right)}\left(e^{\beta y}-1\right)$

4. SSSF boundary condition (Present work):

$u(x,y)=\ A_{mn}\ \sin(\alpha\ x)(-1)^{\left(\frac{2n-1}{2}\right)}e^{\beta y}$, $v(x,y)=\ B_{mn}\ \sin(\alpha\ x)(-1)^{\left(\frac{2n-1}{2}\right)}e^{\beta y}$, $w(x,y)=\ C_{mn}\ \sin(\alpha\ x)(-1)^{\left(\frac{2n-1}{2}\right)}e^{\beta y}$

2.8 Analytical Solution

The solution of SSSS for E-fiber, Polyester (volume fraction 0.3) for cross-ply angle plate(0^0, $0^0/90^0$, $0^0/90^0/0^0$, $0^0/90^0/90^0/0^0$, $0^0/90^0/0^0/90^0$)and dimensions(0.2*0.2*.004m,0.2*0.1,.004m and 0.2*0.05*.004m).It depends on the last sections as follows:

The load q(x,y) can be expanded as Fourier series as:

$$p(x,y)=\sum_{i,j=1}^{m,n}\frac{16p_0}{\pi^2(2m-1)(2n-1)}\ \sin\left(\frac{(2i-1)\pi x}{a}\right)\sin\left(\frac{(2j-1)\pi y}{b}\right) \qquad (15)$$

i, j=1, 2, 3……, and m, n =3(mode shape).

In the case of uniform distributed load over the surface of plate: $q_{mn}=\frac{16q_\circ}{\pi^2 mn}$

The potential energy related with the uniformly distributed load q(x,y) is:

$$V = \frac{16q}{\pi^2 mn} \int_0^a \int_0^b \left\{ \begin{array}{c} \sum_{m=0}^{\infty} \sum_{n=0}^{\infty} \sin\frac{m\pi_x}{a} \sin\frac{n\pi_y}{b} * \\ \sum_{m=0}^{\infty} \sum_{n=0}^{\infty} C_{mn} \sin\frac{m\pi_x}{a} \sin\frac{n\pi_y}{b} \end{array} \right\} dxdy$$

Strain energy: - $U = \frac{1}{2} \int_0^a \int_0^b \left(\sigma_{xx}\, \varepsilon_{xx} + \sigma_{yy}\varepsilon_{yy} + \tau_{xy}\gamma_{xy}\right) d_x d_y$

For pure bending: -

$$U = \frac{1}{2}\int_0^a \int_0^b \left\{ \left[B_{11}\frac{\partial u}{\partial x} + \left(\frac{1}{2}\frac{\partial w}{\partial x}\right)^2 + B_{12}\frac{\partial u}{\partial y} + \left(\frac{1}{2}\frac{\partial w}{\partial y}\right)^2 - D_{11}\frac{\partial^2 w}{\partial x^2} - D_{12}\frac{\partial^2 w}{\partial y^2} \right] \left[\frac{\partial u}{\partial x} + \left(\frac{1}{2}\frac{\partial w}{\partial x}\right)^2 \right] + \left[B_{12}\frac{\partial u}{\partial x} + \left(\frac{1}{2}\frac{\partial w}{\partial x}\right)^2 + B_{22}\frac{\partial u}{\partial y} + \left(\frac{1}{2}\frac{\partial w}{\partial y}\right)^2 - D_{12}\frac{\partial^2 w}{\partial x^2} - D_{22}\frac{\partial^2 w}{\partial y^2} \right] \left[\frac{\partial u}{\partial y} + \left(\frac{1}{2}\frac{\partial w}{\partial y}\right)^2 \right] + \left[B_{66}\left(\frac{\partial u}{\partial y} + \frac{\partial v}{\partial x} + \frac{\partial^2 w}{\partial x \partial y}\right) - 2D_{66}\frac{\partial^2 w}{\partial x \partial y} \right] \left[\frac{\partial u}{\partial y} + \frac{\partial v}{\partial x} + \frac{\partial^2 w}{\partial x \partial y} \right] \right\} dxdy = \frac{1}{2}\int_0^a \int_0^b \left\{ B_{11}\left(\frac{\partial u}{\partial x}\right)^2 + B_{11}\frac{\partial u}{\partial x}\left(\frac{\partial w}{\partial x}\right)^2 \frac{B_{11}}{4}\left(\frac{\partial w}{\partial x}\right)^4 + B_{12}\frac{\partial u}{\partial x}\frac{\partial v}{\partial y} + \frac{B_{12}}{2}\frac{\partial u}{\partial x}\left(\frac{\partial w}{\partial y}\right)^2 + \frac{B_{12}}{2}\frac{\partial v}{\partial y}\left(\frac{\partial w}{\partial x}\right)^2 + \frac{B_{12}}{4}\left(\frac{\partial w}{\partial x}\right)^2\left(\frac{\partial w}{\partial y}\right)^2 - D_{11}\frac{\partial u}{\partial x}\frac{\partial^2 w}{\partial x^2} - \frac{D_{11}}{2}\frac{\partial^2 w}{\partial x^2}\left(\frac{\partial w}{\partial x}\right)^2 - D_{12}\frac{\partial u}{\partial x}\frac{\partial^2 w}{\partial y^2} - \frac{D_{11}}{2}\frac{\partial^2 w}{\partial y^2}\left(\frac{\partial w}{\partial x}\right)^2 + B_{12}\frac{\partial u}{\partial x}.\frac{\partial v}{\partial y} + \frac{B_{12}}{2}\frac{\partial u}{\partial x}\left(\frac{\partial w}{\partial y}\right)^2 + \frac{B_{12}}{2}\frac{\partial u}{\partial y}\left(\frac{\partial w}{\partial x}\right)^2 + \frac{B_{11}}{4}\left(\frac{\partial w}{\partial x}\right)^2\left(\frac{\partial w}{\partial y}\right)^2 + B_{22}\left(\frac{\partial v}{\partial y}\right)^2 + B_{22}\frac{\partial v}{\partial y}\left(\frac{\partial w}{\partial y}\right)^2 + \frac{B_{22}}{4}\left(\frac{\partial w}{\partial y}\right)^4 - D_{12}\frac{\partial v}{\partial y}\frac{\partial^2 w}{\partial x^2} - \frac{D_{12}}{2}\frac{\partial^2 w}{\partial x^2}\left(\frac{\partial w}{\partial y}\right)^2 - D_{22}\frac{\partial v}{\partial y}\frac{\partial^2 w}{\partial y^2} - \frac{D_{22}}{2}\frac{\partial^2 w}{\partial y^2}\left(\frac{\partial w}{\partial y}\right)^2 + B_{66}\left(\frac{\partial u}{\partial y}\right)^2 + B_{66}\left(\frac{\partial v}{\partial x}\right)^2 + 2B_{66}\frac{\partial u}{\partial y}.\frac{\partial v}{\partial x} + 2(B_{66} - D_{66})\frac{\partial u}{\partial y}\frac{\partial^2 w}{\partial x \partial y} + 2(B_{66} - D_{66})\frac{\partial v}{\partial x}\frac{\partial^2 w}{\partial x \partial y} + (B_{66} - D_{66})\left(\frac{\partial^2 w}{\partial x \partial y}\right)^2 \right\} dxdy$$

The displacement functions of SSSS Boundary condition is:

$$u(x,y) = \sum_{m=1}^{\infty}\sum_{n=1}^{\infty} A_{mn}\sin\frac{m\pi_x}{a}, v(x,y) = \sum_{m=1}^{\infty}\sum_{n=1}^{\infty} B_{mn}\sin\frac{m\pi_x}{a}\sin\frac{n\pi_y}{b}$$
$$w(x,y) = \sum_{m=1}^{\infty}\sum_{n=1}^{\infty} C_{mn}\sin\frac{m\pi_x}{a}\sin\frac{n\pi_y}{b} \quad (16)$$

By using separation of variables technique as:

$$X_m(x) = S_{mn}\sin\alpha x\ , \alpha = \frac{m\pi}{a}, Y_n(y) = Z_{mn}\sin\beta x\ , \beta = \frac{n\pi}{b} \quad (17)$$

Becomes:

$$u(x,y) = \sum_{m=1}^{\infty}\sum_{n=1}^{\infty} A_{mn}X_m(x)Y_n(y)\ , v(x,y) = \sum_{m=1}^{\infty}\sum_{n=1}^{\infty} B_{mn}X_m(x)Y_n(y)$$
$$w(x,y) = \sum_{m=1}^{\infty}\sum_{n=1}^{\infty} C_{mn}X_m(x), Y(y)$$

The function Xm(x) and Yn(y) are chosen so as to satisfy the boundary conditions.

Then the strain energy equation for SSSS becomes:-

$$U = \left\{ \frac{1}{2}\int_0^a \int_0^b \alpha^3 B_{11}(\cos\alpha x \sin\beta y)^2 A^2 m + \alpha^3 B_{11}(\cos\alpha x \sin\beta y)^3 A_m C^2 m + \frac{\alpha^4 B_{11}}{4}(\cos\alpha x \sin\beta y)^4 C^4 mn + \alpha\beta B_{12}(\cos\alpha x \sin\beta y)(\sin\alpha x \cos\beta y) A_m B_m + \frac{\alpha\beta^2 B_{12}}{2}(\cos\alpha x \sin\beta y)(\sin\alpha x \cos\beta y)^2 A_m C^2 m + \right.$$

$\frac{\alpha^2\beta B_{12}}{2}$ $(\sin\alpha x\cos\beta y)(\cos\alpha x\sin\beta y)^2 B_m C^2 m + \frac{\alpha^2\beta^2 B_{12}}{4}(\cos\alpha x\sin\beta y)^2(\sin\alpha x\cos\beta y)^2\ C^4 m +$
$\alpha^3 D_{11}(\sin\alpha x\cos\alpha x\sin^2\beta y)A_m C_m + \frac{\alpha^4 D_{11}}{2}(\sin\alpha x\cos^2\alpha x\sin^3\beta y)\ C^3 m +$
$-\alpha\beta^2 D_{12}(\sin\alpha x\cos\alpha x\sin^2\beta y)A_m C_m + \frac{\alpha^2\beta^2 D_{12}}{2}(\sin\alpha x\cos^2\alpha x\sin^3\beta y)\ C^3 m +$
$\alpha\beta B_{12}\ (\sin\alpha x\cos\alpha x\sin\beta y\cos\beta y)A_m B_m + \frac{\alpha\beta^2 B_{12}}{2}\ (\sin^2\alpha x\cos\alpha x\sin\beta y\cos^2\beta y)A_m C^2 m +$
$\frac{\alpha^2\beta B_{12}}{2}(\sin\alpha x\cos^2\alpha x\sin^2\beta x\cos\beta y)B_m C^2 m + \frac{\alpha^2\beta^2 B_{12}}{4}(\sin^2\alpha x\cos^2\alpha x\sin^2\beta y\cos\beta y)C^4 m +$
$\beta^2 B_{22}(\sin\alpha x\cos\beta y)^2 B^2 m + \beta^3 B_{22}(\sin\alpha x\cos\beta y)^3 B_m C^2 m + \frac{\beta^4 B_{22}}{4}\ (\sin\alpha x\cos\beta y)^4 C^4 m +$
$\alpha^2\beta D_{12}(\sin^2\alpha x\sin\beta y\cos\beta y)B_m C_m + \frac{\alpha^2\beta^2 D_{12}}{2}\ (\sin^3\alpha x\sin\beta y\cos^2\beta y)\ C^3 m +$
$\beta^3 D_{22}\ (\sin^2\alpha x\sin\beta y\cos\beta y)B_m C_m + \frac{\beta^4 D_{22}}{2}(\sin^3\alpha x\sin\beta y\cos^2\beta y)\ C^3 m +\ \beta^2 B_{66}(\sin\alpha x\cos\beta y)^2 A^2 m +$
$\alpha^2 B_{66}(\cos\alpha x\sin\beta y)^2 B^2 m + 2\alpha\beta B_{66}(\sin\alpha x\cos\alpha x\sin\beta y\cos\beta y)A_m B_m +$
$2\alpha\beta^2(B_{66} - D_{66})(\sin\alpha x\cos\alpha x\cos^2\beta y)A_m C_m\ + 2\alpha^2\beta(B_{66} - D_{66})(\cos^2\alpha x\sin\beta y\cos\beta y)B_m C_m +$
$\alpha^2\beta^2(B_{66} - D_{66})(\cos\alpha x\cos\beta y)^2 C^2 m\Big\}\,dxdy$

$$U = \frac{1}{2}\int_0^a\int_0^b\{K_1 A^2 m + K_2 A_m C^2 m + K_3 C^4 m + K_4 A_m B_m + K_5 A_m C^2 m + K_6 B_m C^2 m + K_7 C^4 m + K_8 A_m C_m + K_9 C^3 m + K_{10} A_m C_m + K_{11} C^3 m + K_{12} A_m B_m + K_{13} A_m C^2 m + K_{14} B_m C^2 m + K_{15} C^4 m + K_{16} B^2 m + K_{17} B_m C^2 m + K_{18} C^4 m + K_{19} B_m C_m + K_{20} C^3 m + K_{21} B_m C_m + K_{22} C^3 m + K_{23} A^2 m + K_{24} B^2 m + K_{25} A_m B_m + K_{26} A_m C_m + K_{27} B_m C_m + K_{28} C^2 m\}\,d_x d_y \quad (18)$$

K_i=constant as follow:

$K_1=\alpha^3 B_{11}(\cos\alpha x\sin\beta y)^2$, $K_2=\alpha^3 B_{11}(\cos\alpha x\sin\beta y)^3$, $K_3=\frac{\alpha^4 B_{11}}{4}\ (\cos\alpha x\sin\beta y)^4$,

$K_4=\alpha\beta B_{12}(\cos\alpha x\sin\beta y)(\sin\alpha x\cos\beta y)$, $K_5=\frac{\alpha\beta^2 B_{12}}{2}(\cos\alpha x\sin\beta y)(\sin\alpha x\cos\beta y)^2$,

$K_6=\frac{\alpha^2\beta B_{12}}{2}\ (\sin\alpha x\cos\beta y)(\cos\alpha x\sin\beta y)^2$, $K_7=\frac{\alpha^2\beta^2 B_{12}}{4}(\cos\alpha x\sin\beta y)^2(\sin\alpha x\cos\beta y)^2$,

$K_8=\alpha^3 D_{11}(\sin\alpha x\cos\alpha x\sin^2\beta y)$

By using the Ritz method, the coefficients Amn , Bmn and Cmn are determined boundary conditions can be obtained from :-

From: $\frac{\partial U}{\partial A_{mn}} = \frac{\partial V}{\partial A_{mn}}$

$$\int_0^a\int_0^b\{2K_1 A_m + K_2 C^2 m + K_4 B_m + K_5 C^2 m + K_8 C_m + K_{10} C_m + K_{12} B_m + K_{13} C^2 m + \quad + 2K_{23} A_m + K_{25} B_m + K_{26} C_m\}\,d_x\,d_y = 0$$

$$\int_0^a\int_0^b\{R_{11} A_m + R_{12} B_m + R_{13} C_m + R_{14} C^2 m\}\,d_x d_y = 0 \quad (19)$$

Where:

$R_{11}=2(K_1+K_{14}),R_{12}=K_4+K_{12}+K_{25},R_{13}=K_8+K_{10}+K_{26},R_{14}=K_2+K_5+K_{13}$

from: $\frac{\partial U}{\partial B_{mn}} = \frac{\partial V}{\partial B_{mn}}$

$\int_0^a \int_0^b \{ K_4A_m+K_6C^2m + K_{12}A_m + K_{14}C^2m + 2K_{16} B_m+ K_{17}C^2m +K_{19}C_m + K_{21}C_m +2K_{24}B_m+ K_{25}A_m +K_{27}C_m\}d_x\, d_y=0$

$$\int_0^a \int_0^b \{ R_{21}A_m+R_{22}B_m+R_{23}C_m+R_{24}C^2m \}d_x\, d_y=0 \quad (20)$$

Where:

$R_{21}=K_4+K_{12}+K_{25},R_{22}=2(K_{16}+K_{12}),R_{23}=K_{19}+K_{21}+K_{27},R_{24}=K_6+K_{17}+K_{17}$

And from $\frac{\partial U}{\partial C_{mn}} = \frac{\partial V}{\partial C_{mn}}$

$$\int_0^a \int_0^b \{ 2K_2A_mC_m+4K_3C^3m +2K_5A_m C_m+2K_6B_mC_m +4K_7C^3m + K_8A_m+3K_9C^2m + K_{10}A_m+3K_{11}C^2m +2K_{13}A_m C_m +2 K_{14}B_mC_m +4 K_{15}C^3m +2K_{17}B_mC_m +4K_{18}C^3m +K_{19}B_m +3 K_{20}C^2m + K_{21}B_m +3 K_{22}C^2m +K_{26}A_m + K_{27}B_m +2 K_{28}C_m \}d_xd_y=\int_0^a \int_0^b \{ F_{31}\}d_xd_y \quad (21)$$

Where:

$R_{31}=K_8+K_{10}+K_{26},R_{32}=K_{19}+K_{21}+K_{27},R_{33}=2K_{28},R_{34}=3(K_9+K_{11}+K_{20}+K_{22}),R_{35}=4(K_3+K_7+K_{15}+K_{18}),R_{36}=2(K_2+K_5+K_{13}),R_{37}=3(K_9+K_{11}+K_{20}+K_{22}),F_{31}=\frac{16q}{\pi^2 mn} C_{mn} \sin^2 \frac{m\pi_x}{a} \sin^2 \frac{n\pi_y}{b}$

The set of equations (19), (20) and (21) are solved by using program Mat lab (R2011a)

2.9 Verification of Case Studies

For verifying the solution of present work, we compare our results with those obtained by other researchers as shown in **Tables (1, 2 and 3)** which give good agreement with non-linear results of, **Reddy, 1997.**

3. EXPERIMENTAL WORK

Experimentally, the steps of manufacturing specimens (plates) from E-fiber and Polyester are as follows:-

1. Taking volume fraction (0.3) from E-fiber glass and Polyester.

2. Connecting fiber coils on the edges of mold.

3. Adding the Polyester on fiber coils and move to release bubbles.

4. Loading weights on the plates to comprise to thickness (4mm).

Finally, the plates are left a while to dry and undergo to three tests: tensile test to find mechanical properties of plates, tensile test to find the Poisson's ratio and the bending test,50 specimens are manu

factored to find the displacement of cross-ply angle plates undergoes to uniform distributed load(0-8750N/m^2) for 10-different boundary conditions.

3.1 Tensile Test

Each laminate was oriented in longitudinal, transverse, (45^0) angle relative to designated (0^0) direction and sample for pure polyester to determine the engineering parametersE_1,E_2, G_{12}. Every samples are divided according to dimensions, as set by ASTM Number (D3039/D03039M) as shown in **Fig. 1**.And the sample shape for present study before and after the tensile test. The specimen tensile test is mounted vertically in a servo-hydraulic testing machine, and pulled hydraulically with stroke control with large steel grips, maximum capacity of tensile machine (50KN) and it occurred in Ministry of scientific search as shown:

3.2 Bending Test

The displacement of composite plate under uniform distributed load which can be measured by bending device. It measures results for any dimension of plates (length, width and thickness) as shown in **Fig. 3**.

4. RESULT AND DISCUSSION

4.1 Analytical Results

The purpose of the study is to find a theoretical analysis of one of the famous engineering applications, as well as to increase precision in the analysis to achieve results closer to reality. By using the Ritz method in the analysis of nonlinear deformation in composite plates with dimensions (0.2*0.2*0.004m), multi cross-ply angle layers, various boundary conditions and variable of uniform distributed load from (0-8750N/m^2) to obtain the central deflection of the plate. The non-linear behavior of plates or laminated plates begins after ($w>0.3h$) and the consequent application of theories mathematically complex need to be solved by engineering software such as Mat lab (R2011a). The results obtained from linear analysis, it can be observed that central deflection increases with increasing load with (10-100% linearly steps) as well as from layer to others. The results obtained from non-linear analytical analysis with different boundary conditions and three values of aspect ratios how that an increasing aspect ratio caused decreasing the central deflection with(18.5-27%) for aspect ratio(a/b)=2, and(40-53%) for aspect ratio(a/b)=4 with relative to aspect ratio(a/b)=1.

4.2 Experimental Results

The results obtained from non-linear experimental analysis of two different boundary conditions and three values of aspect ratio, it can be observed that same aspect ratios equal to one, two and four.

From the results shown in Tables (1,2 and 3), it can observed that the boundary conditions always effect on the central deflections while changing the lamination from symmetric to un-symmetric may increase the central deflection for aspect ratio as shown in following discussion.

4.3 Linear, Non-linear Analytical and Experimental Results

For the linear, non-linear analytical and experimental results the plates have a=b=0.2m, h=4mm,E_1 =22.049Gpa, E_2=4.163Gpa,G_{12}=1.365Gpa, ν_{12}=0.334, ν_{21}=0.063.The results

for various techniques, experimental, linear and non-linear analytical results are shown in **Figs. (4.a, b and c).**

4.4. Influence Orthotropic Factor (E/G) on Deflection:

In the elasticity law's, the deflection related with modulus of elasticity, from the results we proved that analytical and experimental, as shown in **Figs. 5.a, b and c**, the deflection increased when modulus of elasticity decreased, therefore the reinforcement for any composite sections depended on the increased modulus of elasticity etc, Fiber, Steel coils or any stiffened material was in direction of maximum load. Two of types material, from, **Reddy, 1997,** with different mechanical properties to examine its impact on the results of central deflection for same loads and dimensions as shown in **Figs. 5 a, b and c.**

(a) Material-, Reddy, 1997:
a=b=0.2m,h=4mm,E_1=12.605Gpa,E_2=12.628Gpa,G_{12}=2.154Gpa, ν_{12}=0.2395, ν_{21}=0.239.

(b)Material-2 (present material):-a = b = 0.2m, h = 4mm, E_1 = 22.049Gpa, E_2=4.163Gpa ,G12=1.365Gpa, ν_{12}=0.334,ν_{21}=0063.

(c) Material-3, Reddy N.J, 1997:
a=b=0.2m, h=4mm, E_1=275.8Gpa, E_2=6.895Gpa, G_{12}=0.6E_2 ν_{12}=0.25, ν_{21}=6.25E-3.

4.5 Deflection with Boundary Conditions

In this section, the behavior of cross ply angle plate that exposed to bending distributed load of 2-boundary conditions is examined. The maximum value of deflection strongly connected with the boundary condition for the plates a = b = 0. 2 m, h = 4 mm, E_1 = 22.049 Gpa, E_2 = 4.163 Gpa, G_{12}=1.365Gpa, ν_{12}=0.334,ν_{21}=0.063 as shown in Fig.(3.a and b).

4.6 Influence of Aspect Ratio on the Deflection

Based on the experimental and theoretical results the effect of aspect ratio non-linearity limit(w> 0.3h**)** and large deflection limit(w≧ h) for the ten cases of the boundary conditions are discussed and shown in **Figs. 7.a, b, c and d**.When the value of b is b ,b/2 or b/4 sameness the value of R is R ,R/2 or R/4 respectively. The difference of deflection was nonlinearly when changes the value of aspect ratio(R). So, its nonlinearly after changing the boundary conditions. This inquiring in all cases which are using in present work increasing or decreasing for plates, a=b=.2m,h=4mm,E1=22.049Gpa,E2=4.163Gpa,G12=1.365Gpa,ν_{12}=0.33,ν_{21}

4.7 Stress Analysis

To verify present work results, stresses values in X-and Y-axes (respectively σ_{xx} and σ_{yy}) are compared with those obtained by other researchers, **Reddy, 1997** are shown in **Fig. 8.a and b** for $0^o/90^o$ cross-ply angle plate which shows a good agreement.

5. CONCLUSION

The present analytical investigation is carried out to study non-linear analysis of large deflection of rectangular composite plate undergoes to uniform distributed loads for 10-boundary conditions. Using Classical Laminated Plate Theory and Ritz method were used to solve the forth degree of differential equation and used many shape functions which are changing with the change of boundary condition. A new shape function which depends on the behavior of plate subjects' uniform distributed load and boundary condition are used. Additionally, experimental program is developed to makes the composite plates from E-Fiber glass and Polyester of volume fraction (0.3). The following conclusions can be made:-

(a) Mechanical properties for E-Fiber glass and Polyester with volume fraction (0.3) were obtained. In addition, composite plates were manufactured and subjected to uniform distributed load to find the amount of large deflection.

(b) The elasticity modulus of composite plate (Fiber-Polyester) increased with increasing the Fiberglass coils. Conversely, if underestimated the proportion yarns to less than the value of the modulus of elasticity.

(c) The deflection depends on thickness, width, length of plate, number of layers and orientation of plate.

(d) Comparing between the analytical linear, non-linear and experimental results gave a big difference between linear and non-linear results, while, non-linear showed close results with experimental results.

REFERENCES

- Jones R. M., 1999, *Mechanics of Composite Materials*, Taylor & Francis, 2nd edition.
- Reddy J. N., 1997, *Mechanics of Laminated Composite Plates and Shells Theory and Analysis*, CRC PRESS, 2nd ed.
- Szilard R., 2004, *Theories and Applications of Plates Analysis-Classical Numerical and Engineering Methods*, John Wiley& Sons, Inc.
- Ugrural A .C., 1999, Stress *in Plates and Shells*, nbMcGraw-Hill, printed in Singapore.
- Huai L. R. and Hui H. L.,1990, *Non-linear Bending Simply Supported Symmetric Laminated Cross-ply Rectangular plates* ,Applied Mathematics and Mechanics, English 2ed.Vol.11, 9Sep.
- Singh G., Rao Gz.V., and Iyengar N.G.R., 1991, Some O*bservations on the Large Deflection Bending of Rectangular Anti-symmetric Cross-Ply Plates*, Composite Structures 18p.p.77-91.

- Savithri S., Varadan T. K., 1993, *Large Deflection Analysis of Laminated Composite Plates*, International Journal of Non-Linear Mechanics, Vol. 28, No.1 p.p.(1-12), Printed in Great Britain.

- Tanriöver H., and Senocak E., 2004, *Large Deflection Analysis of Un-symmetrically Laminated Composite Plates: Analytical-Numerical Type Approach*, International Journal of Non-Linear Mechanics 39 p.p.1385-1392.

- Nayyar K., 2006, *Static and Model Analysis of Laminated Composite Plates Using Heretical Finite Method*, Concordia University, Canada.

- Shfrin I., Rabinovitch O. and Eisenberger M., 2008, *A Semi-analytical Approach for Non-linear Large Deflection Analysis of Laminated Rectangular Plates Under General Out-Of-Plane Loading*, International Journal of Non-Linear Mechanics 43 p.p. 328-340.

- Kim K. S., Yoo S. J., Lim I. G. and Lee I., 2008, *Nonlinear Structural Analysis of High-Aspect-Ratio Structures Using Large Deflection Beam Theory*, KASA International journal,Vol.2, p.p. 41-47.

- Saffari H., and Mansouri I., 2011, *Non-linear Analysis of Structures Using Two-Point Method*, International Journal of Non-Linear Mechanics 46, p.p.834-840.

- Nishawala V. V., 2011, A *Study of Large Deflection of Beam and Plates*, New Brunswick, New Jersey.

NOMENCLATURE

a =length of plate, X-axis, meter.

A_{ij}=coefficients of stretching stiffness matrix of composite plate.

b=width of plate, Y-axis meter.

B_{ij}=coefficients of bending- stretching coupling matrix of composite plate.

C =clamped edge.

d =derivative of x, y or z, dimensionless.

D_{ij} =coefficients of bending stiffness matrix of composite plate.

$\hat{e}_x$, $\hat{e}_y$, $\hat{e}_z$=unit vectors in X-,Y- and Z-axes, dimmensionless.

E_1 (E_x or E_0) =modulus of Elasticity in X- xis, GPa.

E_2 (E_y or E_{90})=modulus of Elasticity in Y- Axis, GPa.

E_{12} (E_{xy} or E_{45})=modulus of Elasticity in XY-axis, GPa.

F=free edge.

G_{12}=shear modulus in XY-axis, GPa.

H=thicknesses of plate, meter.

$h_1, h_2, \ldots, h_n, h_k, h_{k+1}$=thicknesses of layers, meter.

Lx, Ly=length of plate in X-, Y- axes, meter.

m, n=the number of modes in X-, Y-axes, dimensionless.

M_{xx}, M_{yy}, M_{xy}=moment in X-,Y-,XY-axis per length, N.m/m.

N_{xx}, N_{yy}, N_{xy}=force in X-,Y-,XY-axis per length, N/m.

q(x, y)=function of uniform distributed load, pressure, N/m^2.

Q_{xx}, Q_{yy}, Q_{xy}=shear force in X-,Y-,XY- axis per length, N/m.

R =aspect ratio (a/b), dimensionless.

$u_\circ$,$v_\circ$,$w_\circ$=mid-plane displacement in X-,Y-,Z- axis, meter.

u(x, y),v(x, y),w(x, y)=function of displacement in X-, Y-,Z-axis.

U=strain energy ,Joule.

V=potential energy, Joule.

W=work done, Joule.

$\propto$= m*π/a , m^{-1}.

β= n*π/b, m^{-1}.

π= constant Ratio (22/7), dimensionless. $\nu = \text{poisson's ratio, dim. less.}$

σ_{xx}, σ_{yy}, τ_{xy}=stress in X-,Y-, XY- axis , MPa.

ε_{xx}= strain in X- axis , dimensionless.

ε_{yy}= strain in Y- axis, dimensionless.

γ_{xy} =shear strain in XY- axis, dimensionless.

ε_x^{NL}=non-linear strain in X-axis (dim.less).

ε_{2l}= transverse strain when the lamination angle0^0, dimensionless

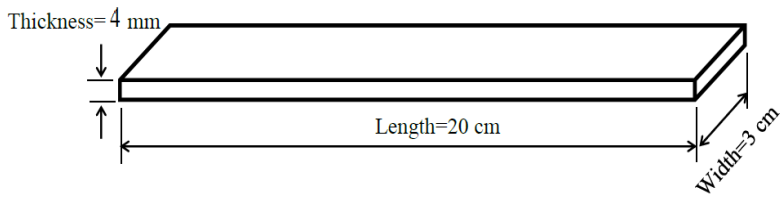

Figure 1. Shape and dimension of tensile test samples.

Figure 2. Tensile test machine.

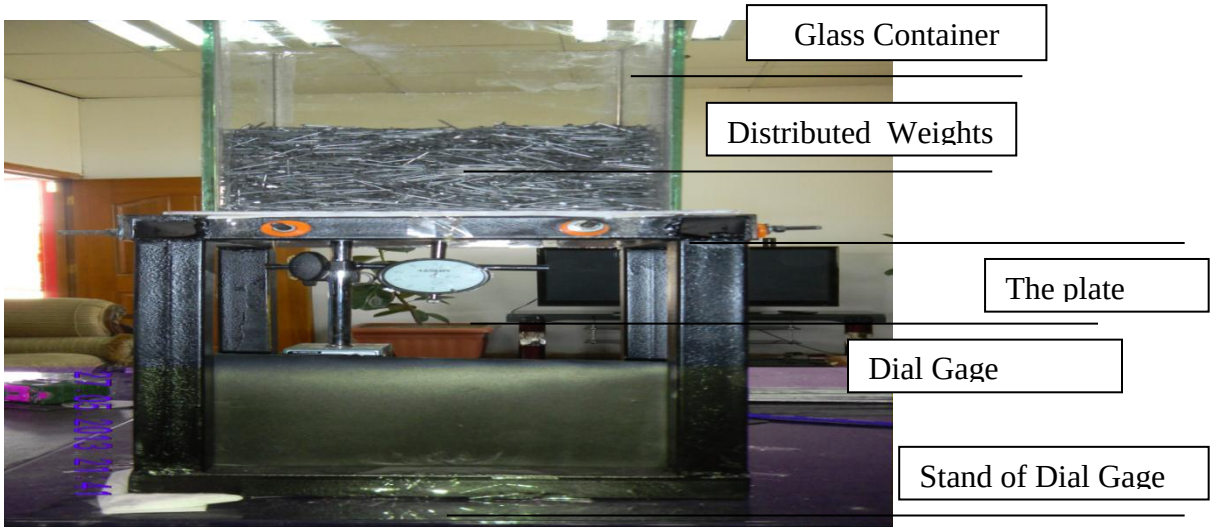

Figure 3. The mechanism of bending test**.**

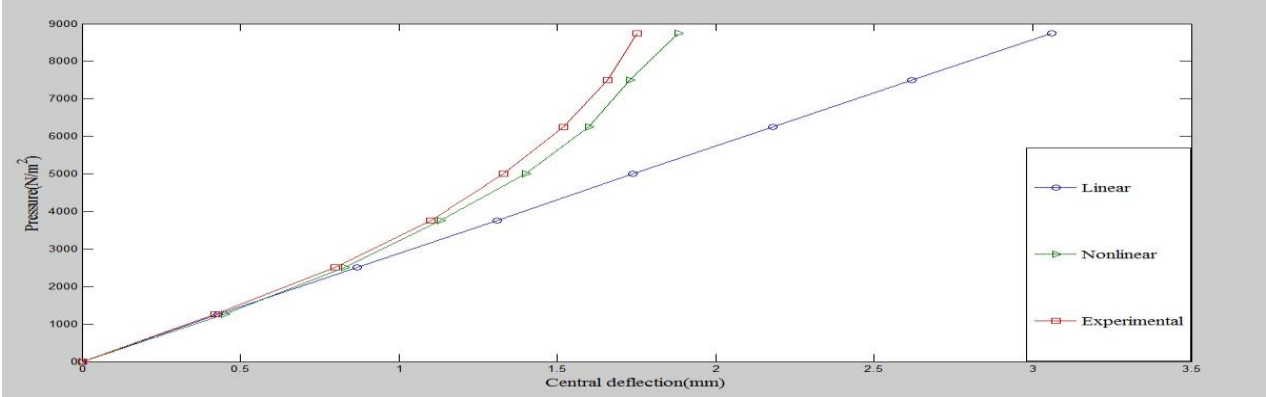

Figure 4.a. Comparison of central deflection for $0^0/90^0$ angle of CCCC B.Cs.

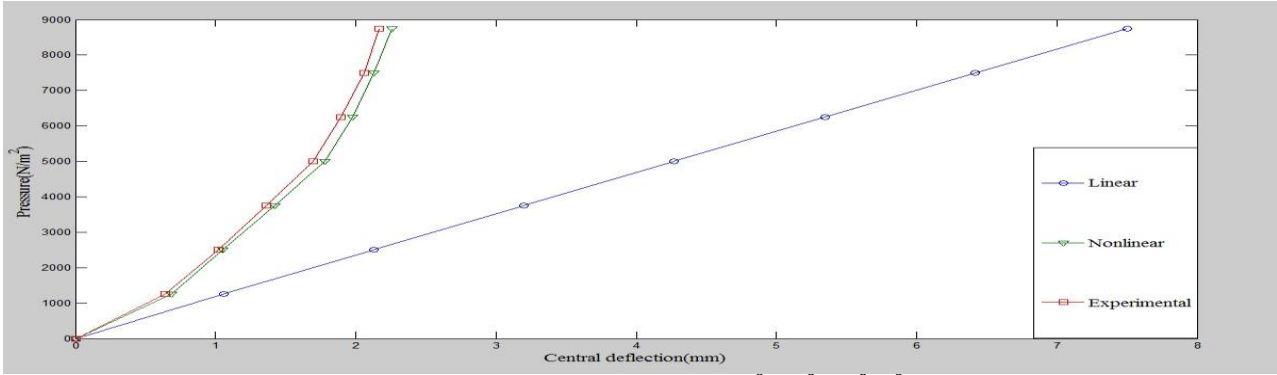

Figure 4.b. Comparison of central deflection for $0^0/90^0/90^0/0^0$ angle of CCCC B.C.

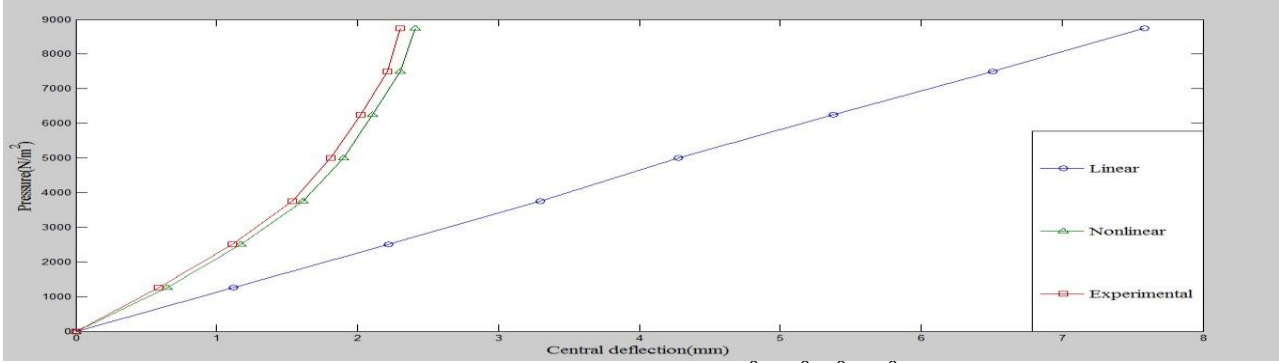

Figure 4.c. Comparison of central deflection for $0^0/90^0/0^0/90^0$ angle of CCCC B.Cs.

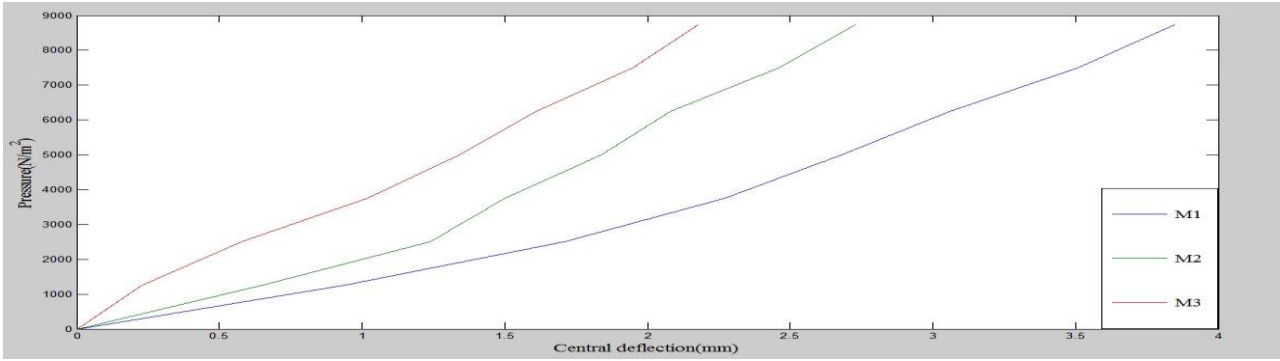

Figure 5.a. Comparison of central deflections of three different materials for $0^0/90^0/90^0/0^0$cross-ply angle plates of SSSS B.Cs.

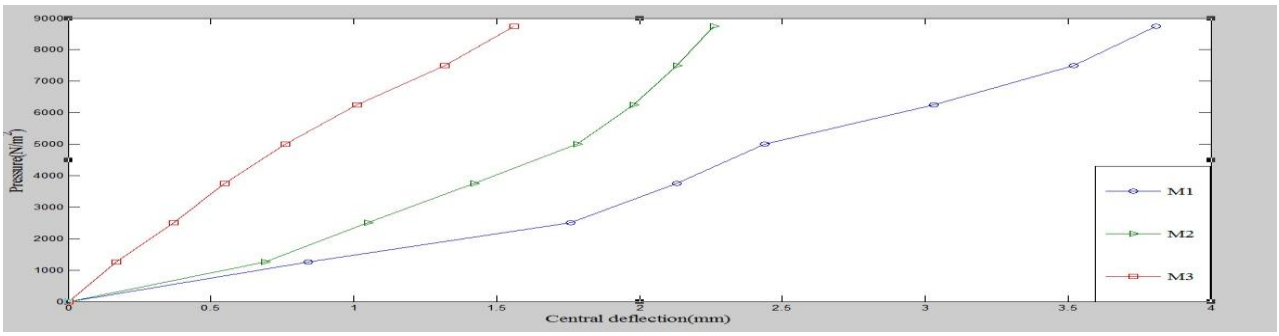

Figure 5.b. Comparison of central deflections of three different materials for $0^0/90^0/90^0/0^0$cross-ply angle plates of CCCC BCs.

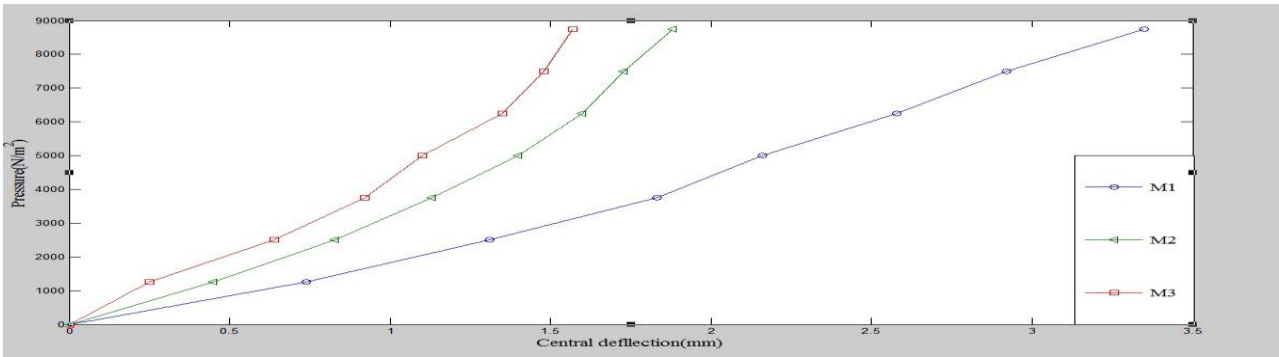

Figure 5.c. Comparison of central deflections of three different materials for $0^0/90^0$cross-ply angle plates of CCCC B.Cs.

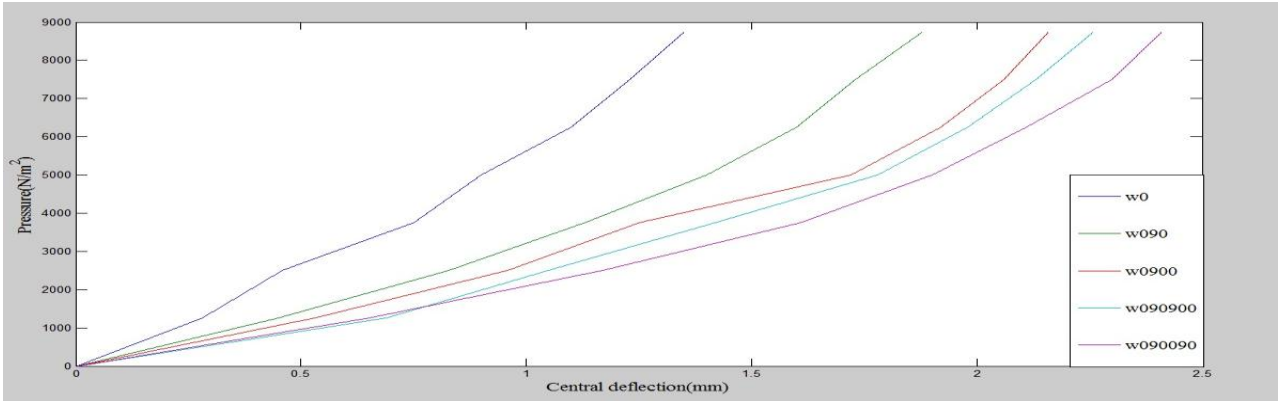

Figure 6.a. Analytical central deflection of 5-cross-ply angle plates of CCCC B.Cs.

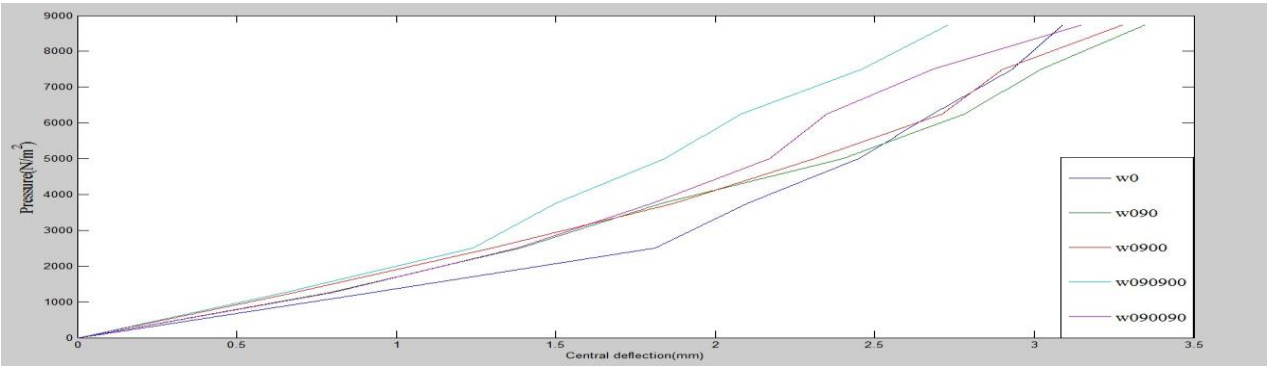

Figure 6.b. Analytical central deflection of 5-cross-ply angle plates SSSS B.Cs.

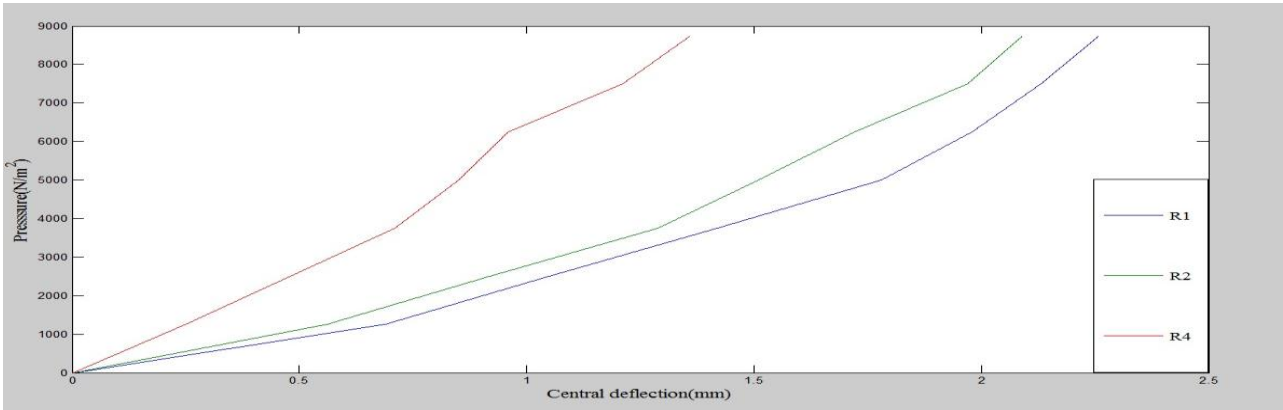

Figure 7.a Comparison the effect of aspect ratio on the central deflection of $0^0/90^0/90^0/0^0$ for CCCC B.Cs.

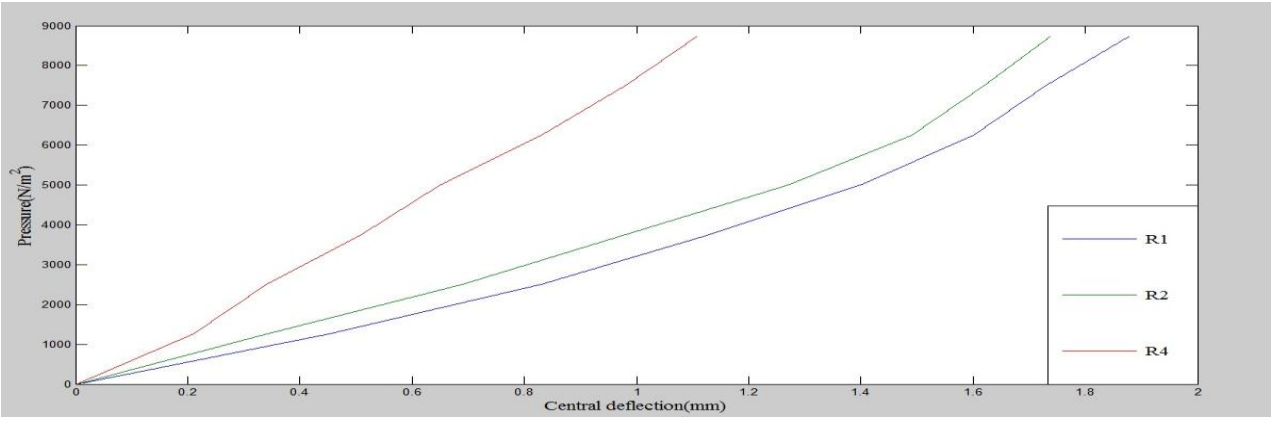

Figure 7.b. Comparison the effect of aspect ratio on the central deflection of $0^0/90^0$ for CCCC B.Cs.

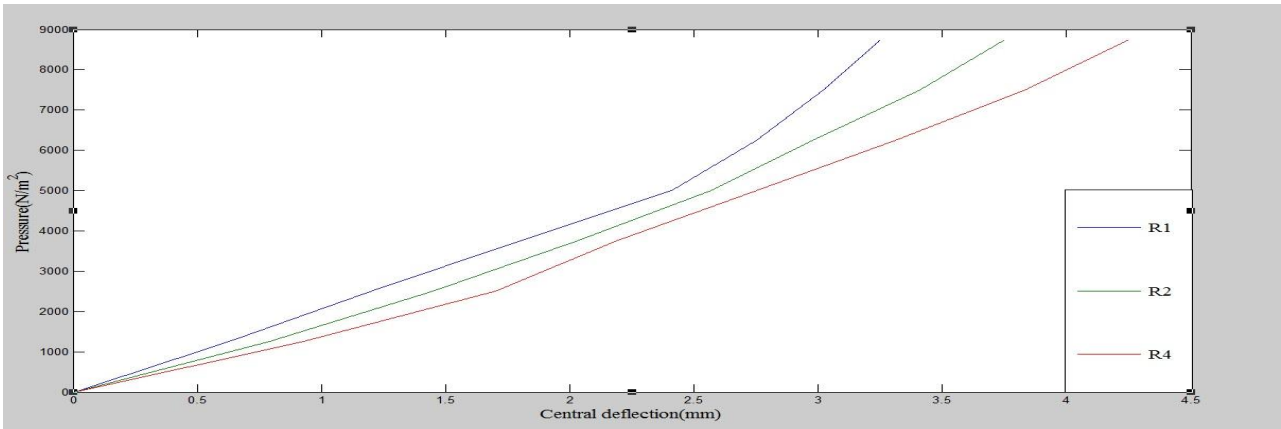

Figure 7.c. Comparison the effect of aspect ratio on the central deflection of $0^0/90^0/90^0/0^0$ for SSSS B.C.s

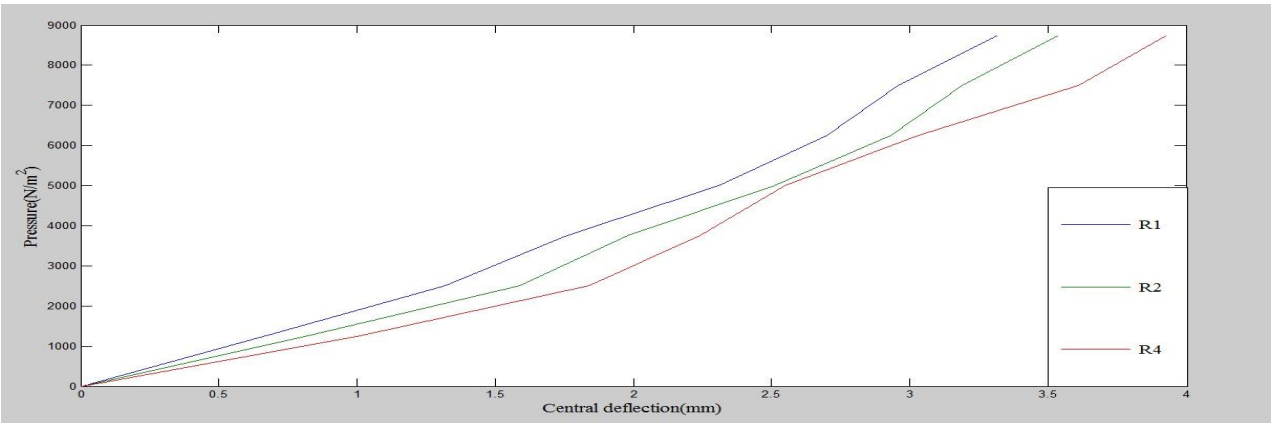

Figure 7.d. Comparison the effect of aspect ratio on the central deflection of $0^0/90^0$ for SSSS B.Cs.

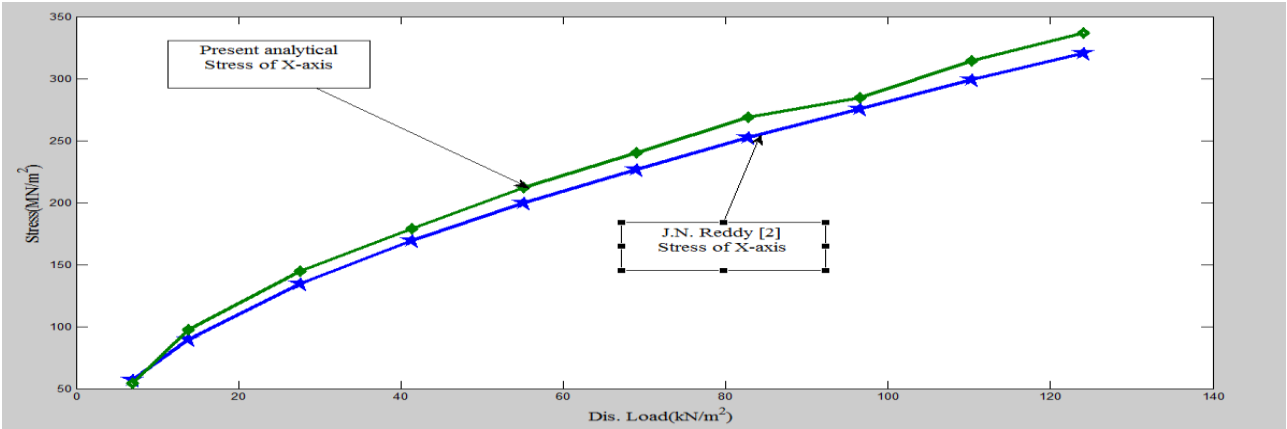

Figure 8.a. Stress analysis of X-axis between Reddy, 1977, and present analytical results for $0^o/90^o$of CCCC B.Cs.

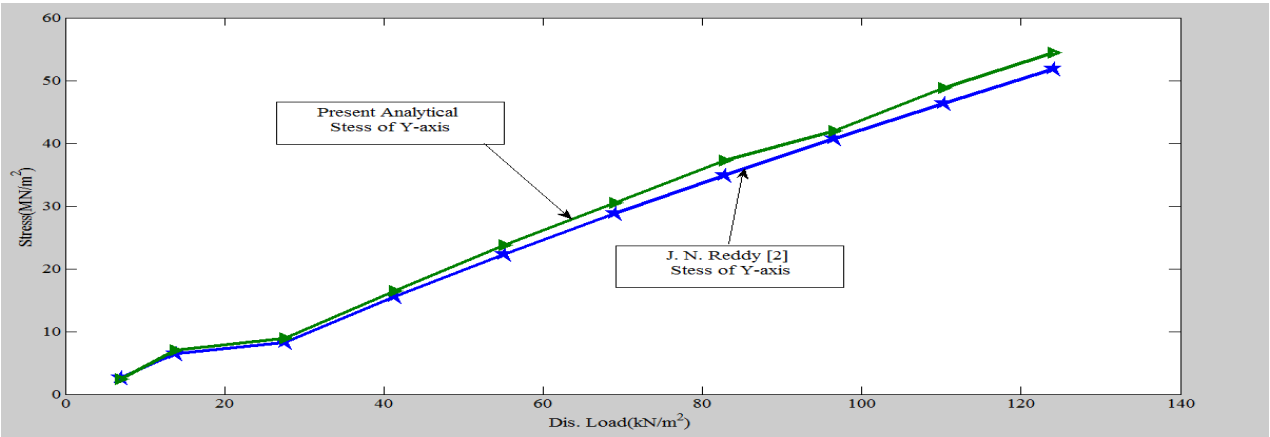

Figure 8.b. Stress analysis of Y-axis between Reddy, 1977, and present analytical results for $0^o/90^o$of CCCC B.Cs.

Table 1. First verification of central deflection between Reddy, 1977, results and present analytical results of CCCC, $0^0/90^0/90^o/\ 0^0$cross-ply angle plate.

a=b=0.3048m, h=2.4384mm, E1=12.605Gpa, E2=12.628Gpa, G12=2.154Gpa, ν_{12}=0.2395, ν_{21}=0.239.			
Pressure (N/m^2)	Reddy, 1997 results (mm)	Present analytical results (mm)	% Difference
1379	0.96	1.00	4
2758	1.65	1.8	8.33
4137	2.16	2.4	10.83
5516	2.55	2.8	8.93
6895	2.87	3	4.33
8274	3.15	3.4	7.35
9653	3.38	3.7	8.65
11032	3.61	4	9.75
12411	3.81	4.2	9.28
13790	4.00	4.40	9.09

Table 2. Second verification of central deflection between Reddy, 1997, results and present analytical results of SSSS, $0^0/90^0/90^o/\ 0^0$cross-ply angle plate.

a=b=0.3048m, h=7.62mm, E1=275.8Gpa, E2=6.895Gpa, G12=0.6E2, ν_{12}=0.25, ν_{21}=6.25E-3.			
Pressure (N/m^2)	Reddy, 1997 results (mm)	Present analytical results (mm)	% Difference
6895	3.91	3.70	5.37
13790	5.70	6.20	8.77
27580	7.80	8.40	7.69
41370	9.17	9.70	5.78
55160	10.24	10.90	6.44
68950	11.14	11.80	5.92
82740	11.91	12.70	6.63
96530	12.6	13.00	3.17
110320	13.21	13.90	5.22
124110	13.80	14.50	5.07

Table 3. Third verification central deflection between Reddy, 1997,results and present analytical results CCCC,$0^o/90^o$cross-ply angle.

a=b=0.3048m, h=2.4384mm, E1=12.605Gpa, E2=12.628Gpa, G12=2.154Gpa, ν_{12}=0.2395, ν_{21}=0.239.			
Pressure (N/m^2)	Reddy, 1997, results (mm)	Present analytical results (mm)	% Difference
1379	1.96	1.98	1.02
2758	2.53	2.65	4.74
4137	2.97	3.07	3.36
5516	3.31	3.42	3.32
6895	3.58	3.70	3.35
8274	3.83	3.95	3.13
9653	4.04	4.18	3.46
11032	4.23	4.38	3.55
12411	4.41	4.52	2.50
13790	4.57	4.68	2.00

Vibration Analysis of a Composite Plate with Delamination

Nabil Hassan Hadi
Assistant Professor
College of Engineering-University of Baghdad
email:nabilhha@yahoo.com

Basim Jameel Hamood
M. Sc. Student
College of Engineering-University of Baghdad
email:basimjameel@yahoo.com

ABSTRACT

The use of composite materials has vastly increased in recent years. Great interest is therefore developed in the damage detection of composites using non- destructive test methods. Several approaches have been applied to obtain information about the existence and location of the faults. This paper used the vibration response of a composite plate to detect and localize delamination defect based on the modal analysis. Experiments are conducted to validate the developed model. A two-dimensional finite element model for multi-layered composites with internal delamination is established. FEM program are built for plates under different boundary conditions. Natural frequencies and modal displacements of the intact and damaged multi-layer composite plates are subsequently analyzed for various samples. Also, composite plates are made for vibration testing and analysis and to comparison of the numerical and experimental results, shows good agreement between them.

Key words: composite plate, delamination, frequency response, finite element method, impact hummer.

تحليل الاهتزاز للوحة مركبة مع التبطين

نبيل حسن هادي
استاذ مساعد
كلية الهندسة-جامعة بغداد

باسم جميل حمود
طالب ماجستير
كلية الهندسة –جامعة بغداد

الخلاصة

لقد زاد استخدام المواد المركبة بشكل كبير في السنوات الأخيرة. مما اجتذب اهتماما كبيرا في الكشف عن العيب في المواد المركبة باستخدام طرق الاختبار غير المدمرة . وقد تم تطبيق عدة طرق للحصول على معلومات حول وجود العيب وتحديد موقعه. وتم استخدام استجابة الاهتزاز لوحة المركبة للكشف عن التبطين وتحديد موقعة استنادا إلى التردد الطبيعي. وتجرى التجارب للتحقق من صحة النموذج المطور . وتم انشاء نموذج ثنائي الأبعاد للمركبات متعددة الطبقات تحتوي على تبطين داخلي . ثم تبنى برنامج FEM باستعمل طريقة العناصر المحددة للوحات مختلفة في ظل ظروف حدية مختلفة. ويتم تحليل الترددات الطبيعية وشكل الازاحة للوحات مركب متعدد الطبقات سليمة و التالفة من برنامج FEM للحصول النتائج المطلوبة لعينات مختلفة. أيضا ، يتم إجراء اختبار الاهتزاز وتحليل و مقارنة النتائج العددية والعملية, وبينت النتائج تطابق جيد بينهما.

الكلمات الرئيسية : صفيحه مركبه ,والاستجابه الترددية, طريقه العناصر المحدده, مطرقه الصدم.

1. INTRODUCTION

Laminated composite plate with reinforced fiber has lighter weight and higher ratios of strength and stiffness to weight, therefore it has been widely applied to many aeronautical and astronautically structures as well as architecture and light industry products. With the quality improvement and occurrence of many new kinds of composite materials, their applications have become more and more extensive. However, laminated composite structures are weak in withstanding shock and likely to be aging, and some damage, such as delamination and crack, may often occur during their usage. These disadvantages will lead to a deterioration of the performance and even failure of the composite materials. Any damage in a composite structure always starts from a very tiny extent and gradually cumulates to some degree that can arouse people's attention. However, when such damage in a structure reaches a notable level, a serious accident will be induced. Obviously, the early discovery of incipient damage and the continuously monitoring for the growth and location of damage are the most essential issues in automatic damage inspection of in-service composite structures **Gobin, et al., 2000.,**and **Takeda, 2000.** Delamination can be often pre-existing or generated during service life. For example, delamination often occur at stress free edges due to the mismatch of properties at ply interfaces and it can also be generated by external forces such as out of plane loading or impact during the service life. The existence of delamination not only alters the load carrying capacity of the structure, it can also affect its dynamic response. Thus detection and quantification of delamination is an important technology that must be addressed for the successful implementation and improved reliability of such structures. All types of damages in composite structures result in change in stiffness, strength and fatigue properties. Measurement of strength or fatigue properties during damage development is not feasible because destructive testing is required. However, stiffness reduction due to damage can be measured since damage directly affects structural response, which provides a promising method for identifying the occurrence, location and extent of the damage from measured structural dynamic characteristics. Existence of delamination causes reduction in natural frequencies and increase in vibratory damping. Although experimental investigations are often used to study these effects, damage simulation using an accurate and efficient modeling technique can be helpful in reducing the number of expensive experiments. Modeling and detection of delamination in composite structures has primarily been based on first-order shear deformation theory (FSDT), **Shen, and Grady, 2000.**

2. THEORY

2.1 Finite Element Formulation

A delaminated composite plate of length *a*, width *b* and thickness *h* consisting of *n* arbitrary number of anisotropic layers is considered as shown in **Fig. 1**. The layer details of the plate are shown in **Fig. 2**. The global coordinate system is considered with respect to the mid-plane of the plate with the Z-axis perpendicular to the X-Y plane and θ is the angle of fiber orientation, measured anticlockwise with respect to X-axis. In the present investigation, the delaminated composite plate is discretized in to a mesh of 5×5 with total 25 elements. An nine nodes two dimensional quadratic isoperimetric element having five degrees of freedom (u^0, v^0, w^0, θ_x, θ_y) per node is chosen.

2.1.1 Displacement field and shape functions

The displacement field of any point at a distance z from the mid surface is assumed to be in the form of:

$$u(x,y,z)=u^0(x,y)+z\theta_x(x,y) \tag{1}$$

$$v(x,y,z)=v^0(x,y)+z\theta_y(x,y) \tag{2}$$

$$w(x,y,z)=w^0(x,y) \tag{3}$$

where u, v, w are displacements in the x,y,z directions respectively for any point, u^0,v^0 , w^0 are those at the middle plane of the plate. θ_x, θ_y are the rotations of the cross section normal to the y and x axis respectively. The middle plane of the plate is considered as the reference plane of the plate. The mid plane strains of the laminate are given by:

$$\varepsilon_{xx}^0=u_{,x}^0;\quad \varepsilon_{yy}^0=v_{,y}^0;\quad \gamma_{xy}^0=u_{,y}^0+v_{,x}^0;\quad \gamma_{xz}^0=\theta_x+w_{,x};\quad \gamma_{yz}^0=\theta_y+w_{,y} \tag{4}$$

Assuming small deformations, the generalized linear in-plane strains of the laminate at a distance z from the mid-surface are expressed as:

$$\{\varepsilon_{xx}\quad \varepsilon_{yy}\quad \gamma_{xy}\quad \gamma_{xz}\quad \gamma_{yz}\}^T=\{\varepsilon_{xx}^0\quad \varepsilon_{yy}^0\quad \gamma_{xy}^0\quad \gamma_{xz}^0\quad \gamma_{yz}^0\}^T+z\{k_{xx}\quad k_{yy}\quad k_{xy}\quad k_{xz}\quad k_{yz}\}^T \tag{5}$$

Where $\begin{Bmatrix}\varepsilon_{xx}^0\\ \varepsilon_{yy}^0\\ \gamma_{xy}^0\\ \gamma_{xz}^0\\ \gamma_{yz}^0\end{Bmatrix}=\begin{Bmatrix}\left(\dfrac{\partial u^0}{\partial x}\right)\\ \left(\dfrac{\partial v^0}{\partial y}\right)\\ \left(\dfrac{\partial u^0}{\partial y}+\dfrac{\partial v^0}{\partial x}\right)\\ \theta_x+\dfrac{\partial w^0}{\partial x}\\ \theta_y+\dfrac{\partial w^0}{\partial y}\end{Bmatrix}$ and $\begin{Bmatrix}k_{xx}^0\\ k_{yy}^0\\ k_{xy}^0\\ k_{xz}^0\\ k_{yz}^0\end{Bmatrix}=\begin{Bmatrix}\left(\dfrac{\partial \theta_x}{\partial x}\right)\\ \left(\dfrac{\partial \theta_y}{\partial y}\right)\\ \left(\dfrac{\partial \theta_x}{\partial y}+\dfrac{\partial \theta_y}{\partial x}\right)\\ 0\\ 0\end{Bmatrix}$

where ε^0_{xx}, ε^0_{yy}, γ^0_{xy} are the mid-plane strains and k_{xx} k_{yy} k_{xy} are the curvatures of the laminated plate .

The element has 4 corner nodes, 4 mid side nodes and mid element node. In the displacement model, simple functions are assumed to approximate the displacements for each element. For the present isoperimetric element, the shape functions which are used to represent the geometry as well as the displacements within the element are expressed by the shape functions N_i.

$$x=\sum_{i=1}^{9}N_i x_i \qquad y=\sum_{i=1}^{9}N_i y_i \qquad u=\sum_{i=1}^{9}N_i u_i^0 \qquad v^0=\sum_{i=1}^{9}N_i v_i^0$$

$$w=\sum_{i=1}^{9}N_i w_i \qquad \theta_x=\sum_{i=1}^{9}N_i\theta_{xi} \qquad \theta_y=\sum_{i=1}^{9}N_i\theta_{yi} \tag{6}$$

where x_i, y_i ,are the co-ordinates of the ith node and u_i^0, v_i^0,w_i, θ_{xi}, θ_{yi} are the displacement functions for different nodes.
Ni for different nodes as shown in **Fig. 3** is defined as,
At corner nodes (i.e. for node 1, 3, 5, 7)

$$N_i=\tfrac{1}{4}(1+\xi\xi_i)(1+\eta\eta_i)(\xi\xi_i+\eta\eta_i-1)$$

At middle nodes (i.e. for nodes 2, 6)

$$N_i=\tfrac{1}{2}(1-\xi^2)(1+\eta\eta_i)$$

At middle nodes (i.e. for nodes 4, 8)

$$N_i=\tfrac{1}{2}(1+\xi\xi_i)(1-\eta^2)$$

At middle element (i.e. for node 9)

$$N_9=(1-\xi^2)(1-\eta^2)$$

Where ξ and η are the local isoperimetric co-ordinates of the element and ξ_i and η_i are the respective values at node i. The correctness of the shape function N_i is checked from the relations

$$\sum N_i=1 \qquad \sum N_i,\xi=0 \qquad \sum N_i,\eta=0 \tag{7}$$

The derivatives of the shape functions N_i with respect to x and y are expressed in terms of their partial derivatives with respect to ξ and η by the relationships:

$$\begin{Bmatrix}\dfrac{\partial N_i}{\partial x}\\ \dfrac{\partial N_i}{\partial y}\end{Bmatrix}=\begin{Bmatrix}\dfrac{\partial\xi}{\partial x} & \dfrac{\partial\eta}{\partial x}\\ \dfrac{\partial\xi}{\partial y} & \dfrac{\partial\eta}{\partial y}\end{Bmatrix}\begin{Bmatrix}\dfrac{\partial N_i}{\partial\xi}\\ \dfrac{\partial N_i}{\partial\eta}\end{Bmatrix}$$

$$\begin{bmatrix}N_{i,x}\\ N_{i,y}\end{bmatrix}=[J]^{-1}\begin{bmatrix}N_{i,\xi}\\ N_{i,\eta}\end{bmatrix} \tag{8}$$

Where $[J]=\begin{bmatrix}x,_\xi & y,_\xi\\ x,_\eta & y,_\eta\end{bmatrix}=\begin{bmatrix}\sum N_{i,\xi}x_i & \sum N_{i,\xi}y_i\\ \sum N_{i,\eta}x_i & \sum N_{i,\eta}y_i\end{bmatrix}$ is the Jacobin matrix.

2.1.2 Stress strain relations

A micromechanical analysis is carried out to establish the relationship between the forces and strains of a laminate. The elastic behavior of each lamina is essentially two dimensional and orthotropic in nature. So the elastic constants for the composite lamina.

2.1.3 Strain displacement relations

Strain displacement is used throughout the structural analysis. It is used to derive the elastic stiffness matrix.

The strains are defined as.

$$\begin{Bmatrix} \sigma_1 \\ \sigma_2 \\ \sigma_6 \\ \sigma_5 \\ \sigma_4 \end{Bmatrix}^k = \begin{bmatrix} \overline{Q}_{11} & \overline{Q}_{12} & \overline{Q}_{16} & 0 & 0 \\ \overline{Q}_{12} & \overline{Q}_{22} & \overline{Q}_{26} & 0 & 0 \\ \overline{Q}_{16} & \overline{Q}_{26} & \overline{Q}_{66} & 0 & 0 \\ 0 & 0 & 0 & \overline{Q}_{55} & \overline{Q}_{45} \\ 0 & 0 & 0 & \overline{Q}_{45} & \overline{Q}_{44} \end{bmatrix}^k \left[\begin{Bmatrix} \varepsilon_1 \\ \varepsilon_2 \\ \varepsilon_6 \\ \varepsilon_5 \\ \varepsilon_4 \end{Bmatrix}^k \right] \tag{9}$$

The strain can be described in term of displacements as

$$\{\varepsilon\} = [B]\{de\} \tag{10}$$

Where $\{de\} = [u_1 v_1 w_1 \phi_{11} \phi_{21} \cdots\cdots\cdots\cdots u_9 v_9 w_9 \phi_{19} \phi_{29}]^T$

$$[B] = [[B_1] \ldots\ldots\ldots [B_8][B_9]]$$

$$[B_i] = \begin{bmatrix} \frac{\partial N_i}{\partial \alpha} & 0 & 0 & 0 & 0 \\ 0 & \frac{\partial N_i}{\partial \beta} & 0 & 0 & 0 \\ \frac{\partial N_i}{\partial \beta} & \frac{\partial N_i}{\partial \alpha} & 0 & 0 & 0 \\ 0 & 0 & 0 & \frac{\partial N_i}{\partial \alpha} & 0 \\ 0 & 0 & 0 & 0 & \frac{\partial N_i}{\partial \beta} \\ 0 & 0 & 0 & \frac{\partial N_i}{\partial \beta} & \frac{\partial N_i}{\partial \alpha} \\ 0 & 0 & \frac{\partial N_i}{\partial \alpha} & N_i & 0 \\ 0 & 0 & \frac{\partial N_i}{\partial \beta} & 0 & N_i \end{bmatrix} \tag{11}$$

2.1.4 Derivation of element matrices

2.1.4.1 Elastic stiffness matrix

The potential energy of deformation for the element is given by

$$U_e = \frac{1}{2}\int\int \{\varepsilon\}^T [\sigma] dA \tag{12}$$

$$\{\varepsilon\} = \{\varepsilon_1^0 \varepsilon_2^0 \varepsilon_6^0 k_1^0 k_2^0 k_6^0 \gamma_5^0 \gamma_4^0\}^T \tag{13}$$

Where $\{\varepsilon\} = [B]\{d_e\} = [[B_1].....[B_8][B_9]]\{d_e\}$ (14)

With $\{de\} = [u_1^0 v_1^0 w_1 \phi_1^1 \phi_2^1 \cdots\cdots\cdots\cdots u_9^0 v_9^0 w_9 \phi_1^9 \phi_2^9]^T$ (15)

Then $U_e = \frac{1}{2}\int\int \{d_e\}^T [B]^T [D][B]\{d_e\} dxdy = \frac{1}{2}\{d_e\}^T [K_e]\{d_e\}$ (16)

Where the element stiffness matrix

$$[K_e] = \int_{-1}^{1}\int_{-1}^{1} [B]^T [D][B] |J| d\xi d\eta \tag{17}$$

[B] is called the strain displacement matrix.

In Eq. (17) $[B_i] = \sum_{i=1}^{9} \begin{bmatrix} N_{i,x} & 0 & 0 & 0 & 0 \\ 0 & N_{i,y} & 0 & 0 & 0 \\ N_{i,y} & N_{i,x} & 0 & 0 & 0 \\ 0 & 0 & 0 & N_{i,x} & 0 \\ 0 & 0 & 0 & 0 & N_{i,y} \\ 0 & 0 & 0 & N_{i,y} & N_{i,x} \\ 0 & 0 & N_{i,x} & N_i & 0 \\ 0 & 0 & N_{i,y} & 0 & N_i \end{bmatrix}$

$|J| d\xi d\eta$, is the determinant of the Jacobian matrix. The element stiffness matrix can be expressed in local natural co-ordinates of the element. The integration of Eq. (17) is carried out using the Gauss quadrature method.

2.1.4.2 Consistent mass matrix

The consistent element mass matrix [*Me*] is expressed as:

$$[M_e] = \int_{-1}^{1}\int_{-1}^{1} [N]^T [P][N] |J| d\xi d\eta \tag{18}$$

Where [*N*], the shape function matrix and [*P*], the inertia matrix

$$[N]=\begin{bmatrix} N_i & 0 & 0 & 0 & 0 \\ 0 & N_i & 0 & 0 & 0 \\ 0 & 0 & N_i & 0 & 0 \\ 0 & 0 & 0 & N_i & 0 \\ 0 & 0 & 0 & 0 & N_i \end{bmatrix} \quad \text{i=1 to 9} \quad , \quad [P]=\begin{bmatrix} P_1 & 0 & 0 & P_2 & 0 \\ 0 & P_1 & 0 & 0 & P_2 \\ 0 & 0 & P_1 & 0 & 0 \\ P_2 & 0 & 0 & P_3 & 0 \\ 0 & P_2 & 0 & 0 & P_3 \end{bmatrix} \tag{19}$$

Where $(P_1, P_2, P_3) = \sum_{i=1}^{9} \int_{z_{k-1}}^{k} (\rho)_k (1, z, z^2) dz$

2.2 Delamination Modeling

A simple two dimensional single delamination model proposed by ,**Gim C.K.1994.** was extended by ,**Mohammad F.Aly.2010** for the vibration of delaminated composite panels. In the present analysis, it is further extended for static and dynamic stability analysis under in-plane uniaxial periodic forces by multiple delamination modelling. In order to satisfy the compatibility and equilibrium requirements at the common delamination boundary, it is assumed that the in-plane displacement, transverse displacement and rotation at a common node for all the three sublaminates including the original one are identical applying multiple constraint condition at any arbitrary delamination boundary. It can be applicable to any general case of a laminated composite plate having multiple delamination at any arbitrary location. Here, the delaminated area is assumed as the interface of two separate sub laminates bonded together along the delamination surface.

Typical composite plate of uniform thickness *'h'* with '*n'* number of layers and '*p'* number of arbitrarily located delamination is considered for the analysis as shown in **Fig. 4**. The principal material axes of each layer are arbitrarily oriented with respect to the mid-plane of the plate as shown in **Fig. 5**.

Considering the sub-laminates as a separate plate, the displacement field within it is expressed as:

$$u_s = u_s^0 + (z - z_s^0)\theta_{xs} , \quad v_s = v_s^0 + (z - z_s^0)\theta_{ys} \tag{20}$$

Where u_s^0 and v_s^0 are the mid-plane displacements of the sth sub-laminate along *x* and *y* direction and z_s^0 is distance between mid-plane of sth sub-laminate and the mid-plane of the laminate in *z* direction

The mid-plane strains of the sub-laminate are:

$$\{\varepsilon_{xx}^0 \quad \varepsilon_{yy}^0 \quad \gamma_{xy}^0\}_s^T = \left\{ \frac{\partial u_s^0}{\partial x} \quad \frac{\partial v_s^0}{\partial y} \quad \frac{\partial u_s^0}{\partial y} + \frac{\partial v_s^0}{\partial x} \right\}^T \tag{21}$$

From Eq. (21) the strain components within the sub-laminate *s* can be expressed as:

$$\{\varepsilon_{xx}^0 \quad \varepsilon_{yy}^0 \quad \gamma_{xy}^0\}_s^T = \left\{ \frac{\partial u_s}{\partial x} \quad \frac{\partial v_s}{\partial y} \quad \frac{\partial u_s}{\partial y} + \frac{\partial v_s}{\partial x} \right\}^T$$

$$=\left\{\frac{\partial u_s^0}{\partial x} \quad \frac{\partial v_s^0}{\partial y} \quad \frac{\partial u_s^0}{\partial y}+\frac{\partial v_s^0}{\partial x}\right\}^T+\left(z-z_s^0\right)\left\{\frac{\partial \theta_x}{\partial x} \quad \frac{\partial \theta_y}{\partial y} \quad \frac{\partial \theta_x}{\partial y}+\frac{\partial \theta_y}{\partial x}\right\}^T$$

$$=\left\{\varepsilon_{xx}^0 \quad \varepsilon_{yy}^0 \quad \gamma_{xy}^0\right\}_s^T+\left(z-z_s^0\right)\left\{k_{xx} \quad k_{yy} \quad k_{xy}\right\}_s^T \tag{22}$$

In order to satisfy the compatibility and equilibrium requirements at the common delamination boundary, it is assumed that the in-plane displacements, transverse displacement and rotations at a common node for all the three sub-laminates including the original one as shown in **Fig.6**, are identical. Applying multiple constraint condition at any arbitrary delamination boundary *c*, the in-plane displacements at *'c'* at a distance *'z'* from the mid-plane of the laminate can be written as:

$$u_c=u^0+z\theta_x \quad , \quad v_c=v^0+z\theta_y$$

From Eq. (20), the displacement at any point, *c* is given by:

$$u_{sc}=u_s^0+\left(z-z_s^0\right)\theta_x \quad , \quad v_{sc}=v_s^0+\left(z-z_s^0\right)\theta_y$$

Equating u_c with u_{sc} and v_c with v_{sc}, the mid-plane displacements of the sub-laminate can be expressed in the form of the mid-plane displacements(u^0, v^0) of the original un-delaminated laminate as,

$$u_s^0=u^0+z_s^0\theta_x \quad , \quad v_s^0=v^0+z_s^0\theta_y \tag{23}$$

From Eq. (23), the mid-plane strain components of the sth sub-laminate can be derived as:

$$\left\{\varepsilon_{xx}^0 \quad \varepsilon_{yy}^0 \quad \gamma_{xy}^0\right\}_s^T=\left\{\varepsilon_{xx}^0 \quad \varepsilon_{yy}^0 \quad \gamma_{xy}^0\right\}^T+z_s^0\left\{k_{xx} \quad k_{yy} \quad k_{xy}\right\}^T \tag{24}$$

The strain components within the sub-laminate can be written as:

$$\left\{\varepsilon_{xx} \quad \varepsilon_{yy} \quad \gamma_{xy}\right\}_s^T=\left\{\varepsilon_{xx}^0 \quad \varepsilon_{yy}^0 \quad \gamma_{xy}^0\right\}_s^T+\left(z-z_s^0\right)\left\{k_{xx} \quad k_{yy} \quad k_{xy}\right\}^T$$

$$=\left\{\varepsilon_{xx}^0 \quad \varepsilon_{yy}^0 \quad \gamma_{xy}^0\right\}^T+z_s^0\left\{k_{xx} \quad k_{yy} \quad k_{xy}\right\}^T+\left(z-z_s^0\right)\left\{k_{xx} \quad k_{yy} \quad k_{xy}\right\}^T \tag{25}$$

For any lamina of sth sub-laminate, the in-plane and shear stresses are found from the following relations

$$\begin{Bmatrix}\sigma_{xx}\\ \sigma_{yy}\\ \tau_{xy}\end{Bmatrix}=\begin{bmatrix}\overline{Q}_{11} & \overline{Q}_{12} & \overline{Q}_{16}\\ \overline{Q}_{12} & \overline{Q}_{22} & \overline{Q}_{26}\\ \overline{Q}_{16} & \overline{Q}_{26} & \overline{Q}_{66}\end{bmatrix}\begin{Bmatrix}\varepsilon_{xx}\\ \varepsilon_{yy}\\ \gamma_{xy}\end{Bmatrix}_s \tag{26}$$

$$\begin{Bmatrix} \tau_{xz} \\ \tau_{yz} \end{Bmatrix} = \begin{bmatrix} \overline{Q}_{44} & \overline{Q}_{45} \\ \overline{Q}_{45} & \overline{Q}_{55} \end{bmatrix} \begin{bmatrix} \gamma_{xz} \\ \gamma_{yz} \end{bmatrix}_s \tag{27}$$

Where σ_{xx} and σ_{yy} are the normal stresses along x and y directions respectively and τ_{xz} and τ_{yz} are the shear stresses in xz, yz planes respectively.

Integrating these stresses over the thickness of the sub-laminate, the stress and moment resultants of the sub-laminate are derived which lead to the elasticity matrix of the sth sub-laminate $[D]_s$ in the form

$$[D]_s = \begin{bmatrix} A_{ij} & z_s^0 A_{ij} + B_{ij} & 0 \\ B_{ij} & z_s^0 B_{ij} + D_{ij} & 0 \\ 0 & 0 & S_{ij} \end{bmatrix} \tag{28}$$

$[D]_s$ is the elasticity matrix of the sth sub-laminate

Where, $[A_{ij}]_s = \int_{-\frac{h_s}{2}+z_s^0}^{\frac{h_s}{2}+z_s^0} [\overline{Q}_{ij}]_s dz$ and $[B_{ij}]_s = \int_{-\frac{h_s}{2}+z_s^0}^{\frac{h_s}{2}+z_s^0} [\overline{Q}_{ij}]_s (z - z_s^0) dz = \int_{-\frac{h_s}{2}+z_s^0}^{\frac{h_s}{2}+z_s^0} [\overline{Q}_{ij}]_s z dz - z_s^0 [A_{ij}]_s$

$$[D_{ij}]_s = \int_{-\frac{h_s}{2}+z_s^0}^{\frac{h_s}{2}+z_s^0} [\overline{Q}_{ij}]_s (z - z_s^0)^2 dz = \int_{-\frac{h_s}{2}+z_s^0}^{\frac{h_s}{2}+z_s^0} [\overline{Q}_{ij}]_s \left[z^2 + (z_s^0)^2 - 2zz_s^0\right] dz = \int_{-\frac{h_s}{2}+z_s^0}^{\frac{h_s}{2}+z_s^0} [\overline{Q}_{ij}]_s z^2 dz$$

$$- 2z_s^0 \int_{-\frac{h_s}{2}+z_s^0}^{\frac{h_s}{2}+z_s^0} [\overline{Q}_{ij}]_s z dz + (z_s^0)^2 [A_{ij}]_s \qquad \text{for i, j = 1, 2, 6}$$

$$[S_{ij}]_s = \int_{-\frac{h_s}{2}+z_s^0}^{\frac{h_s}{2}+z_s^0} [\overline{Q}_{ij}]_s dz \qquad \text{for i,j =4,5}$$

The in-plane stress and moment resultants for the sth sub-laminate can be expressed in a generalized manner as:

$$\begin{Bmatrix} N_{xx} \\ N_{yy} \\ N_{xy} \\ M_{xx} \\ M_{yy} \\ M_{xy} \end{Bmatrix} = \begin{bmatrix} A_{11} & A_{12} & A_{16} & z_s^0 A_{11} + B_{11} & z_s^0 A_{12} + B_{12} & z_s^0 A_{16} + B_{16} \\ A_{12} & A_{22} & A_{26} & z_s^0 A_{12} + B_{12} & z_s^0 A_{22} + B_{22} & z_s^0 A_{26} + B_{26} \\ A_{16} & A_{26} & A_{66} & z_s^0 A_{16} + B_{16} & z_s^0 A_{26} + B_{26} & z_s^0 A_{66} + B_{66} \\ B_{11} & B_{12} & B_{16} & z_s^0 B_{11} + D_{11} & z_s^0 B_{12} + D_{12} & z_s^0 B_{16} + D_{16} \\ B_{12} & B_{22} & B_{26} & z_s^0 B_{12} + D_{12} & z_s^0 B_{22} + D_{22} & z_s^0 B_{26} + D_{26} \\ B_{16} & B_{26} & B_{66} & z_s^0 B_{16} + D_{16} & z_s^0 B_{26} + D_{26} & z_s^0 B_{66} + D_{66} \end{bmatrix} \begin{Bmatrix} \varepsilon_{xx}^0 \\ \varepsilon_{yy}^0 \\ \varepsilon_{xy}^0 \\ k_{xx} \\ k_{yy} \\ k_{xy} \end{Bmatrix}_s \tag{29}$$

Similarly, the transverse shear resultants for the sth sub-laminate are presented as

$$\begin{Bmatrix} Q_{xz} \\ Q_{yz} \end{Bmatrix}_s = \begin{bmatrix} S_{44} & S_{45} \\ S_{45} & S_{55} \end{bmatrix}_s \begin{bmatrix} \gamma_{xz} \\ \gamma_{yz} \end{bmatrix} \tag{30}$$

After finding the elastic stiffness matrices separately for different sub-laminates along the thickness, the sum of all the sub-laminate stiffness's represents the resultant stiffness matrix.

2.3 Characteristics of the Reinforcement-Matrix Mixture

The mechanical properties of constituents of the test specimens, E-glass woven roving fibers and polyester matrix are listed in **Table 1**.

The material elastic properties of the lamina of test specimens are determined experimentally. These properties are Young's moduli (E_1 – in direction 1, E_2 – in direction 2, E_3 – in direction 3), Poisson's ratios ($\upsilon_{12}, \upsilon_{13}$, and υ_{23}), in plane shear modulus (G_{12}) and transverse shear moduli (G_{13} and G_{23}). This figure defines the material principle axes for a typical woven fiber reinforced lamina. Axis 1 is along the fiber length and represents the longitudinal direction of the lamina; axes 2 and 3 represent the transverse in-plane and through the thickness directions respectively.

Some of the elastic constants of the woven fabric composite material are experimentally estimated (E_1, E_2, υ_{12}). The others are estimated by using the relations which are based on elastic constants of the unidirectional specimens. Young's modulus and the Poisson's ratio of the fill and warp directions are calculated by using the three-point bending test, and the interface strain meter is to calculate the Poisson ratio (υ_{12}) from a program using the computer.

2.3.1 Unidirectional ply

The elastic constants of the unidirectional composite are calculated using the simple rule of mixtures by the relations of Eq. (31), **Metin Aydogdu. 2007.** and the results are listed in **Table 2.**

$$E_1 = E_f \nu_f + E_m (1 - \nu_f)$$

$$E_2 = E_m \left[\frac{E_f + E_m + \nu_f (E_f - E_m)}{E_f + E_m - \nu_f (E_f - E_m)} \right]$$

$$\upsilon_{12} = \upsilon_f \nu_f + \upsilon_m (1-\nu_f)$$

$$\upsilon_{23} = \left[\upsilon_f \nu_f + \upsilon_m (1-\nu_f)\right]\left[\frac{1+\upsilon_m - \upsilon_{12}\frac{E_m}{E_1}}{1-\upsilon_m^2 + \upsilon_m \upsilon_{12}\frac{E_m}{E_1}}\right]$$

$$G_{12} = G_m\left[\frac{G_f + G_m + \nu_f (G_f - G_m)}{G_f + G_m - \nu_f (G_f - G_m)}\right]$$

$$G_{23} = \frac{E_2}{2(1+\upsilon_{23})} \tag{31}$$

Where indices *m* and *f* denote matrix and fiber, respectively.

2.3.2 Woven fabrics

The elastic constants of the woven fabric composite material are estimated by using the tensile test device and the relation of Eq. (32) **D.Gay etal.2003** and the results are listed in **Table 3.**

- One is called the warp and,
- The other is called the fill (or weft) direction.

The fibers are woven together, which means the fill yarns pass over and under the warp yarns, following a fixed pattern. **Fig. 7** shows a plain weave where each fill goes over a warp yarn then under a warp yarn and so on.

The fabric layer is replaced by one single anisotropic layer, x being along the warp direction and y along the fill direction (see **Fig. 7**). One can therefore obtain **D.Gay etal.2003.**

$$E_{1w} = k.E_1 + (1-k)E_2$$

$$E_{2w} = (1-k)E_1 + k.E_2$$

$$G_{12w} = G_{12}$$

$$\upsilon_{12w} = \frac{\upsilon_{12}}{(k + (1-k)\frac{E_1}{E_2})} \tag{32}$$

Where $k = \frac{n_1}{n_1 + n_2}$, n_1=number of warp yarns per meter, n_2= number of fill yarns per meter. And, E_{1w}, E_{2w} ,G_{12w} , and υ_{12w} are mechanical properties of woven fabrics in 1 and 2-directions; and E_1, E_2, G_{12}, G_{23}, υ_{12} , and ν_{23} as in Eq. (31).

The stiffness obtained with a woven fabric is less than what is observed if one were to superpose two cross plies of unidirectional. This is due to the curvature of the fibers during the weaving operation. This curvature makes the woven fabric more deformable than the two cross

plies when subjected to the same loading. (There exist fabrics that are of "high modulus" where the unidirectional layers are not connected with each other by weaving. The unidirectional plies are held together by stitching fine threads of glass or polymer).

2.4 Modeling Assumptions

In this study, 8-layer Glass fiber Polyester resin laminated rectangular composite plates (325×325 mm^2) with a total thickness of 4 mm are examined.

The ply orientations are (0,90,0,90,0,90,0,90); the material constants are shown in **Table 1**.

Three plates are considered including an intact plate (plate A) and two damaged plates B and C. Plates B & C have delamination at **Fig. 8** in mid-plane with the size 50×50 mm; plate .Coordinates x and y are measured from the corner of the plate as the origin**.**

3. RESULTS

3.1 Delamination Effects on Natural Frequencies

In the present investigation, both the numerical computation and experimental study are carried out for an eight-layered $[0/90]_4$ woven glass fiber/polyester resin composite plate. The geometrical dimensions of the woven composite plates are: length, a =350 mm width, b = 350 mm, thickness, h = 3.25 mm. The material properties of the woven glass fiber/polyester resin composite plates are considered as given in **Table 3**. Square size delamination was introduced at the mid-plane as shown in **Fig. 8**. In this study, the effects of delamination area, boundary conditions, fiber orientations and number of layers on the natural frequencies are investigated.

Tables 4, 5, 6 and 7 give a comparison of the first five frequencies which is between experimental work and numerical work of the four woven laminated plate with different boundary conditions .These tables show good (harmonies) agreements at the first mode obtained between experimental and numerical works. The deviations for the numerical results and the experimental method are due to some possible measurement errors that can be pointed out such factors as: measurement noise, different positions of the accelerometers and their mass, non-uniformity in specimens' properties (voids, variations in thickness, non-uniform surface finishing). Such factors are not taken into account during the numerical analysis, since the model considers the specimen perfect entirely with homogeneous properties, which rarely occurs in the practice. Another aspect has to be considered is that the input properties in the model came from the application of the rule of mixture and it does not take into account the effects of fiber matrix interface as well as the irregular distribution of resin on the fibers. Also, the computational numerical program does not allow for the consideration of fibers interweaving presented in the fabric use.

3.2 Delamination Effects on Mode Shapes

The results of FEM analysis show the delamination regions clearly **Fig. 9**. The conducted analysis demonstrates that the delamination-induced changes of plate parameters mode

3.3 Effect of Number of Layer

Table 8 shows the effect of the number of layer (with the same thickness) on natural frequency with four boundary condition all sides clamped (CCCC), all sides simple supported (SSSS), cantilever plate (CFFF) and all sides free (FFFF), under step uniform dynamic loading. For (CCCC), shows the effect of the number of layer the natural frequency decreases with the increase number of layer from(1 to 2) with a decreasing percentage (0.88 %), increase when

number of layer increases from (2 to 3) with a percentage of (0.85 %), decreases with the increase number of layer from(3 to 4) with a decreasing percentage of (0.54 %), increase when number of layer increase from (4 to 5) with percentage (0.38 %), decreases with the increase number of layer from(5 to 6) with decreasing percentage (0.32 %), increase when number of layer increase from (6to 7) with percentage (0.25 %), decreases with the increase number of layer from(7 to 8) with decreasing percentage (0.23 %), for (SSSS), shows the effect of the number of layer the frequency response increases with the increase number of layer from(1 to 2) with percentage (4.67 %), decreases when number of layer increase from (2 to 3) with decreasing percentage (4.06 %), increases with the increase number of layer from(3 to 4) with percentage (4.91 %), decreases when number of layer increase from (4 to 5) with decreasing percentage (2.83 %), increases with the increase number of layer from(5 to 6) with percentage (3.04 %), decreases when number of layer increase from (6 to 7) with decreasing percentage (2.10 %), increase with the increase number of layer from(7 to 8) with percentage (2.18 %), for (CFFF), show the effect of the number of layer the frequency response decreases with the increase number of layer from(1 to 2) with decreasing percentage (7.25 %), increase when number of layer increase from (2 to 3) with percentage (7.45 %), decreases with the increase number of layer from(3 to 4) with decreasing percentage (5.44 %), increase when number of layer increase from (4 to 5) with percentage (3.97 %), decreases with the increase number of layer from(5 to 6) with decreasing percentage (3.55 %), increase when number of layer increase from (6 to 7) with percentage (2.78 %), decreases with the increase number of layer from(7 to 8) with decreasing percentage (2.61 %), for (FFFF), shows the effect of the number of layer the frequency response increases with the increase number of layer from(1 to 2) with percentage (12.91 %), decreases when number of layer increase from (2 to 3) with decreasing percentage (9.65 %), increases with the increase number of layer from(3 to 4) with percentage (15.87 %), decreases when number of layer increase from (4 to 5) with decreasing percentage (6.77 %), increases with the increase number of layer from(5 to 6) with percentage (8.13 %), decreases when number of layer increase from (6to 7) with decreasing percentage (4.80 %), increase with the increase number of layer from(7 to 8) with percentage (5.33 %).

5. CONCLUSION

The delamination problem for typical multi-layer composite plates has been analyzed using finite element method and modal analysis. The study incorporated both computational and experimental work. Comparing the intact and damaged plates, the natural frequencies of plate with delamination are smaller than intact plate. Also, natural frequencies of the damaged plate decrease with the increase of delamination area. The analyses demonstrate that the delamination-induced changes of the plate parameters are mode-dependent. The natural frequency and mode shape effect by damage and size of damage and location of delamination between layers. Boundary condition effect the amount of difference in nature frequency and mode shape and result shown the max. in (CCCC) Bc's, change the number of layers with a thickness constant does not affect the natural frequency of the plate, Whenever damage location close to the center of plate at increase the variation of natural frequency.

RERERENCES

- D. Gay, S. V. Hoa and S. W. Tsai, 2003, *Composite Materials Design and Applications*, Book, CRC Press LLC.

- Gim, C.K.**,** 1994, *Plate Finite Element Modeling of Laminated Plates*, Composite Structure, Vol. **52**, pp.157-168.

- Gobin PF., Jayet Y., Baboux JC., Salvia M, Chateauminois A, Abry JC, et al., 2003, *New Trends in Non-Destructive Evaluation in Relation to the Smart Materials Concept*, Int J Syst Sci ;31(11):1351–9.

- Kayser Aziz Ameen, 2011, Genetic Algorithms FOR Damage DETECTION Of Composite STRUCTURES, the Department of Mechanical Engineering College of Engineering University of Baghdad.
- Metin Aydogdu, and Taner Timarci, 2007, *Free Vibration of Antisymmetric Angle-Ply Laminated Thin Square Composite Plates*, Turkish J. Eng. Env. Sci 31,243-249.

- Mohammed F. Aly, I. G. M. Goda and Gala A. Hassan, 2010, *Experimental Investigation of the Dynamic Characteristics of Laminated Composite Beams*, International Journal of Mechanical & Mechatronics IJMME-IJENS, Vol.(10), No.(03), pp.(59-68).

- Parhi, P.K., Bhattacharyya, S.K. and Sinha, P.K.**,** 2000, *Finite Element Dynamic Analysis of Laminated Composite Plates with Multiple Delaminations*, Journal of Reinforced Plastics and Composites, Vol. **19**, pp. 863-882.

- Shen MH, and Grady JE., 1992, *Free Vibrations of Delaminated Beams*, AIAA J;30(5):1361–70.

- SUDIP DEY and AMIT KARMAKAR, 2011,*Characterization of Multiple Delaminated Composite by Finite Element*, Mechanical Engineering Department, Jadavpur University Kolkata – 700032, West Bengal, India.

- Takeda N., 2000, *Structural Health Monitoring for Smart Composite Structure Systems*, in Japan, Ann Chim-Sci Mat;25(7):545–9.

NOMENCLATURE

$[D]_{s=}$ the elasticity matrix of the sth sub-laminate.
$E_1, E_2,$ *and* E_3 = Young's moduli in direction 1, 2 and 3 respectively N/m^2.
E_{1w}, E_{2w} ,G_{12w} , and υ_{12w} =the mechanical properties of woven fabrics in 1 and 2-directions.
G_{12} = plane shear modulus N/m^2.
G_{13} and G_{23} = transverse shear moduli N/m^2.
h = thickness mm.
k_{xx} k_{yy} k_{xy} = the curvatures of the laminated plate, m^{-1}.

m and f = denote matrix and fiber, respectively.
n_1=number of warp yarns per meter.
n_2= number of fill yarns per meter.
N= number of layers.
N_i = the shape function.
P= number of arbitrarily located delaminations.
u, v, w = displacements in the x,y,z directions respectively for any point, m.
u^0, v^0, w^0 = those at the middle plane of the plate, m.
u_s^0, v_s^0 = the mid-plane displacements of the sth sub-laminate along x, y.
$u_i^0, v_i^0, w_i, \theta_{xi}, \theta_{yi}$ = the displacement functions for different nodes.
x_i, y_i = are the co-ordinates of the ith node.
z_s^0 = the distance between the mid-plane of the original laminate and the mid-plane of the arbitrary of sth sub-laminate and the mid-plane of the laminate in z direction mm.
θ_x, θ_y = the rotations of the cross section normal to the y and x axis respectively.
$\varepsilon^0_{xx}, \varepsilon^0_{yy}, \gamma^0_{xy}$ = the mid-plane strains
ξ , η = the local isoperimetric co-ordinates of the element.
ξ_i , η_i = the respective values at node i.
σ_{xx}, σ_{yy} = the normal stresses along x and y directions respectively N/m^2.
τ_{xz}, τ_{yz} = the shear stresses in xz, yz planes respectively N/m^2.
$\upsilon_{12}, \upsilon_{13}$, and υ_{23} = Poisson's ratios.

Table 1. Mechanical properties of fiber and resin, **ref [4].**

Material	Properties	Value
E-Glass fiber	Elasticity modulus (GPa)	74
	Shear modulus (GPa)	30
	Density (kg/m^3)	2600
	Poisson ratio	0.25
Polyester resin	Elasticity modulus (GPa)	4.0
	Shear modulus (GPa)	1.4
	Density (kg/m^3)	1200
	Poisson ratio	0.4

Table 2. Mechanical properties of unidirectional composite material.

Properties	Value
Elastic modulus (E_1) (GPa)	24.7466
Elastic modulus (E_2) (GPa)	6.8989
Shear modulus in plane 1-2 (G_{12}) (GPa)	2.435
Shear modulus in plane 2-3 (G_{23}) (GPa)	2.2211
Poisson ratio in plane 1-2 (υ_{12})	0.3555
Poisson ratio in plane 2-3 (υ_{23})	0.5531

Table 3. Mechanical properties of woven composite material.

Properties	Value
number of warp yarns per meter(n_1)	260
number of fill yarns per meter(n_2)	260
$k=n_1/(n_1+n_2)$	0.5
Elastic modulus (E_{1w}=E_{2w}) (GPa)	15.824
Elastic modulus (E_{3w}) (GPa)	8.0181
Shear modulus in plane 1-2 (G_{12w}) (GPa)	2.4355
Shear modulus in plane 1-3 (G_{13w}) (GPa)	2.3232
Shear modulus in plane 2-3 (G_{23w}) (GPa)	2.3232
Poisson ratio in plane 1-2 (υ_{12w})	0.155
Poisson ratio in plane 1-3 (υ_{13w})	0.4937
Poisson ratio in plane 2-3 (υ_{23w})	0.4937

Table 4. Comparison between experimental work and numerical results for four woven layers laminated plate ([0/90]$_4$), with (CCCC) boundary condition.

Case of plate	**Results (Hz)**	**Mode Number**				
		1	**2**	**3**	**4**	**5**
Plate A	Experimental	174.33	378.62	379.83	542.16	811.71
	Numerical	162.88	365.46	365.46	517.77	775.72
	Errors (%)	7.03	3.60	3.93	4.71	4.64
Plate B	Experimental	172.45	347.50	374.42	512.41	792.18
	Numerical	160.75	334.54	358.53	481.31	748.62
	Errors (%)	7.28	3.90	4.43	6.46	5.82
Plate C	Experimental	167.13	341.69	376.63	540.45	747.28
	Numerical	157.25	331.96	364.26	513.85	707.05
	Errors (%)	6.3	2.9	3.4	5.2	5.7

Table 5. Comparison between experimental work and numerical results for four woven layers laminated plate ([0/90]$_4$), with (SSSS) boundary condition.

Case of plate	**Results (Hz)**	**Mode Number**				
		1	**2**	**3**	**4**	**5**
Plate A	Experimental	81.32	225.54	223.79	343.63	508.44
	Numerical	76.165	210.44	210.44	314.31	473.62
	Errors (%)	6.7	7.2	6.3	9.3	7.4
Plate B	Experimental	77.46	203.36	221.82	324.22	499.72
	Numerical	73.081	192.82	206.99	299.14	470.14
	Errors (%)	6.0	5.4	7.1	8.4	6.3
Plate C	Experimental	75.62	209.11	220.06	334.14	481.55
	Numerical	71.85	195.81	209.97	312.88	443.36
	Errors (%)	5.3	6.8	4.8	6.8	8.6

Table 6. Comparison between experimental work and numerical results for four woven layers laminated plate ($[0/90]_4$), with (CFFF) boundary condition.

Case of plate	Results (Hz)	Mode Number				
		1	2	3	4	5
Plate A	Experimental	19.87	32.11	106.96	130.32	146.34
	Numerical	18.447	30.586	100.12	121.11	137.34
	Errors (%)	7.7	4.98	6.83	7.6	6.55
Plate B	Experimental	18.58	30.86	103.23	127.23	144.56
	Numerical	17.814	30.16	99.407	120.11	136.57
	Errors (%)	4.30	2.32	3.85	5.93	5.85
Plate C	Experimental	18.14	30.7	104.19	125.31	140.83
	Numerical	18.26	30.189	98.453	114.64	134.97
	Errors (%)	0.66	1.69	5.83	9.31	4.34

Table 7. Comparison between experimental work and numerical results for four woven layers laminated plate ($[0/90]_4$), with (FFFF) boundary condition.

Case of plate	Results (Hz)	Mode Number				
		6	7	8	9	10
Plate A	Experimental	0	36.45	87.76	99.00	117.09
	Numerical	0	34.889	82.641	92.371	112.39
	Errors (%)	0	4.5	6.2	7.2	4.2
Plate B	Experimental	0	35.40	87.02	97.11	116.69
	Numerical	0	34.295	80.802	88.914	110.08
	Errors (%)	0	3.2	7.7	9.2	6.0
Plate C	Experimental	0	35.02	86.16	95.14	116.21
	Numerical	0	34.26	79.823	87.469	110.41
	Errors (%)	0	2.2	7.9	8.8	5.2

Table 8. Natural frequency **(ω)** of number of layers for cross-ply plates.

Number of layers	stacking sequences	Natural Frequency (ω) (Hz)			
		CCCC	SSSS	CFFF	FFFF
1	0	162.884	76.16456	18.44723	34.88888
2	0/90	161.457	79.72336	17.11052	39.39233
3	0/90/0	162.825	76.49046	18.38476	35.59151
4	0/90/0/90	161.953	80.24534	17.3841	41.23994
5	0/90/0/90/0	162.572	77.9717	18.07511	38.44712
6	0/90/0/90/0/90	162.045	80.34153	17.43333	41.57182
7	0/90/0/90/0/90/0	162.449	78.65752	17.91777	39.57683
8	0/90/0/90/0/90/0/90	162.077	80.37517	17.45046	41.68726

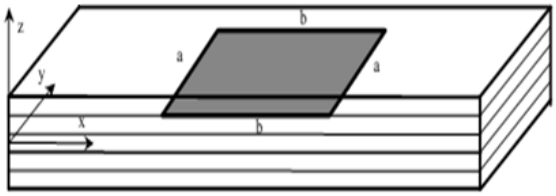

Figure 1. Laminate composite plate with delaminated.

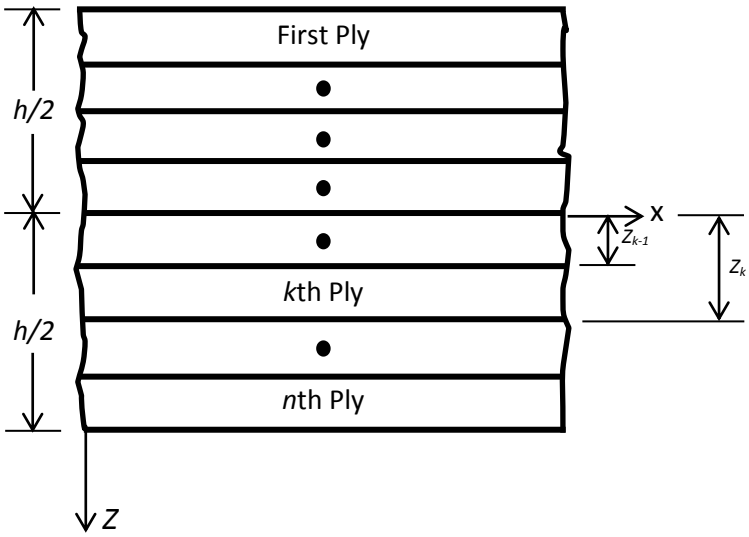

Figure 2. Layer details of the plate.

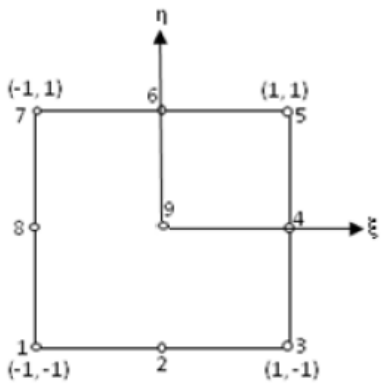

Figure 3. The element in isoperimetric co-ordinates.

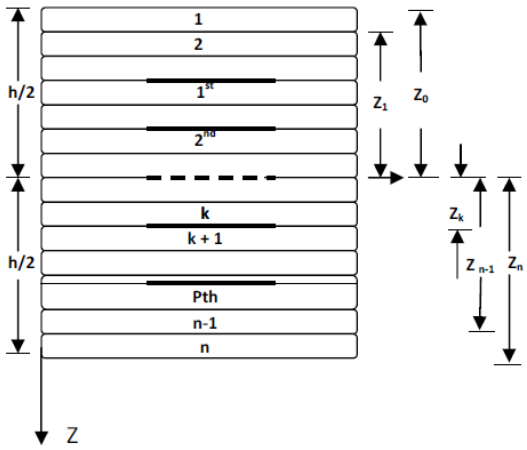

Figure 4. Laminate geometry with multiple delaminations.

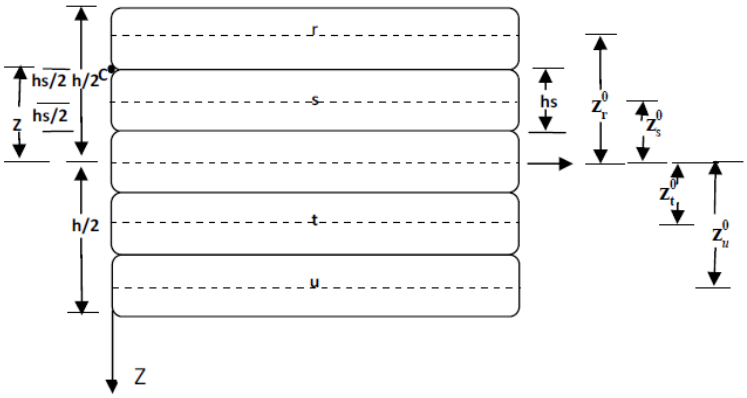

Figure 5. Three arbitrary delaminations leading to four sub-laminates.

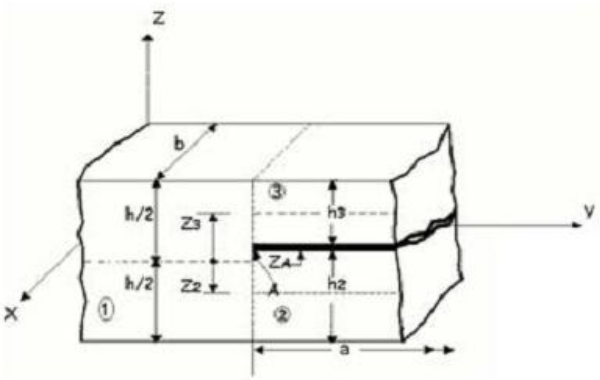

Figure 6. Plate elements at a delamination crack tip **ref.[8].**

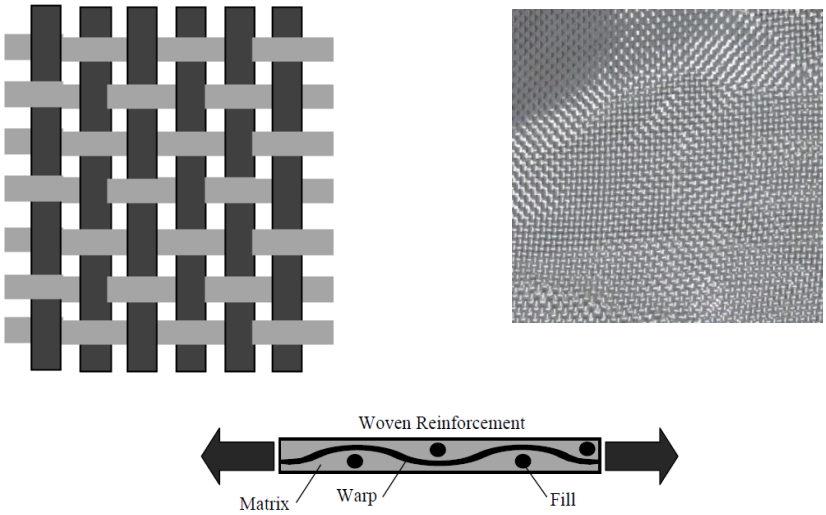

Figure 7. Schematic representation of woven fabric architecture **D. Gay, et al., 2003.**

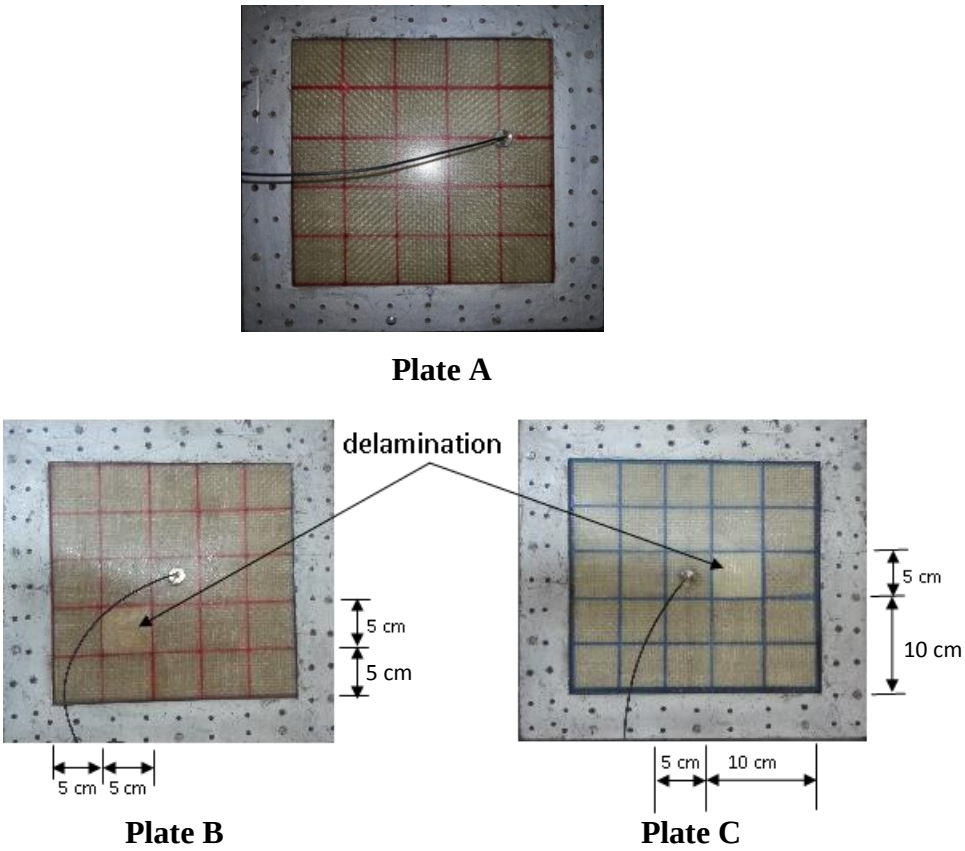

Figure 8. Intact plate and damage plates and clamped all sides.

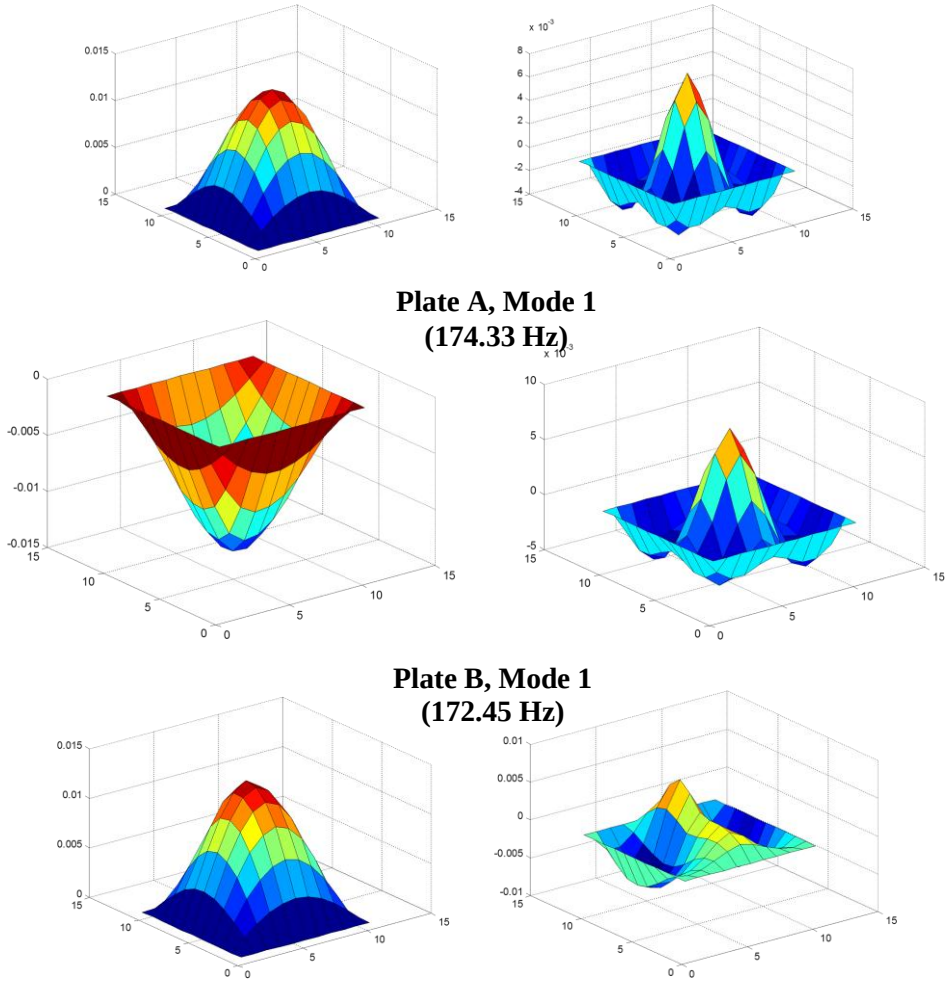

Figure 9. Delamination region in plate A , B and C for some mode shapes of FEM analysis..

Delamination region in plate A , B and C for some mode shapes of FEM analysis

الجماليات الرمزية في أنظمة المنشآت الفولاذية

د. أسامة عبد المنعم خريبط/ مدرس
جامعة بغداد/ كلية الهندسة / قسم الهندسة المعمارية
eng_usama_oat@yahoo.com

الخلاصة

يعد التعبير الجمالي وأنساقه ضروري في صياغة الأنظمة الإنشائية ومنها الفولاذية. فالهياكل الفولاذية هي تجميع لعناصر منشئية وتكون فيها المركبات ذات أبعاد قياسية محددة فهي منشآت مسبقة الصنع. حيث إن أنظمة الإنشاء الفولاذي لا تهدف فقط إلى تحقيق مضامين وظيفية للمستخدم، وإنما لابد لها أيضاً من جماليات رمزية توفر تعبيراً بصريًا وإدراكياً للمشاهد. ومن هذا المنطلق يوّلي البحث اهتمامًا بجماليات التعبير في تلك الأنظمة ويبرز أهميتها بصفتها نصوصًا إنشائية تُصاغ بلهجات تعبيرية متميزة. فالمفردات البصرية المرتبطة مع المنشآت الفولاذية تحتوي بعضاً من أقوى النماذج المميزة للعمارة الحديثة فالهياكل الفولاذية ذات الأكساء الزجاجي والرشاقة ودقة الضبط في صناعة المركبات المنشئية كعناصر بصرية والأعجاب الإنشائي الواضح في أشكال الفضاءات ذات البحور الكبيرة المتفردة أو في المباني ذات الارتفاعات الشاهقة تكون أشكالاً مختلفة في التعبير والتأثير. لذلك يركز البحث في دراسة تلك الأنساق التعبيرية والمرتبطة بخصائص الأنشاء الفولاذي بما في ذلك من مميزات تلك الأنظمة على مستوى القوة والمتانة والمرونة والاقتصاد فضلاً عن الجوانب الجمالية والتعبيرية لها. **وعليه تكمن المشكلة البحثية في القصور المعرفي في جوانب دراسة النظام الإنشائي الفولاذي من نواحي سماته البنائية وأنساقه التعبيرية وسماته الجمالية**، وكيف التعاطي معها على أنها لغة تحمل رموز ومعانّ ولها لهجات إنشائية واضحة. بكونها افضل السبّل لجعل تلك الأنظمة وسيلة اتصال بالمتلقي وذلك انطلاقًا من فرضية أنّ استخدام التعبير الرمزي في الصيغ الإنشاء الفولاذي يزيد من قيمتها الجمالية. **أما الهدف البحثي فيكمن في الوصول إلى ابرز الأنساق التعبيرية وأبجديتها الإنشائية من خلال تحليل آليات التعبير وجماليات الإنشاء الفولاذي.**

الكلمات المفتاحية: المنشأ الفولاذي، المفردات البصرية، الأعجاب الإنشائي، القوة، المرونة، التكتونية، الأنساق التعبيرية.

Symbolic aesthetics in steel structural systems

Dr. Usama Abdul-Mun'em Khuraibet / Instructor
Baghdad University/college of engineering/ Architectural department
eng_usama_oat@yahoo.com

ABSTRACT

The aesthetic expression and its orders are important for steel structures forming. Steel structures are a compilation of structural elements, where its shapes have standard dimensions and pre-fabricated. As the steel construction systems not only aim to achieve the functional requirements for users, but must also have the symbolic aesthetics which provides visually and cognitive expression for viewers. In this sense the research interested in expressional aesthetics in these systems and highlights the importance of attention as structural items. Therefore the visual items which related with steel structures contain some of the most powerful forms of modern architecture, steel structures with a glass cladding, agility and accuracy in manufacture of structural elements as visual items, structural interest in the forms of spaces which have long span systems or in high buildings are different forms of expression and influence. So the research focuses on the study of those expressive patterns related with the steel construction properties, including

the advantages of these systems at the level of strength and firmness, flexibility and economy as well as aesthetic and expression. Accordingly, the research problem concentrated on educational shortage in the study of the structural steel system aspects concerning constructional characteristic, expressive and aesthetic features, and how to deal with them as a language bearing the symbols and meanings which have clear structural style, because it the best ways to make those systems as communication means with users, by premise that the use of expressional symbol in steel construction increases the aesthetic value. Therefore the research aims to reveal the most structural and expressive patterns by analysis the expressional means and steel structural aesthetics.

Key words: steel structure, visual items, structural interest, strength, flexibility, Tectonic, expressional patterns.

المقدمة

تعد علاقة الإنشاء بالعمارة علاقة أساسية منذ بدء التفكير في أول منشأ معماري على الأرض، حيث يمثل الإنشاء الجانب المادي في العمارة، فهو العامل المهم الذى يساعد في نقل الفكر المعماري من حالة الخيال إلى حالة التحقق. ولقد تقدمت تكنولوجيا البناء بدءاً من استخدام المواد والوسائل والنظم وتطوراتها في البناء حتى أن وصلت إلى مفهوم المباني العصرية الذى نعيشه في عالمنا هذا وما يتمتع به من منظر جمالي ونوعية تحمل عالية وسرعة في الأنشاء وتكلفة منخفضة وابتكار. فاليوم أكثر من أي وقت مضى يركز المعماريون (وبدرجات متفاوتة) على أهمية المعرفة الإنشائية في ضوء التطور السريع لتقنيات الإنشاء، ولكن الإلمام بهذه المعرفة يتطلب جهداً كبيراً وقدرة على فهم التطور الحاصل وآلية عمل الجمل الإنشائية ومتطلباتها، ومدى تأثير هذه المتطلبات في الحل المعماري ومحاولة الاستفادة منها وتوظيفها معمارياً بشكل صحيح. وهذا ما برّز أهمية المنشآت الفولاذية كونها إحدى مخرجات تطورات الصناعة البنائية، حيث تساعد التكنولوجيا الحديثة على توسيع مدى الإبداع في تصميم أشكال متنوعة من المباني من خلال توسيع الخيارات المادية والشكلية أمام المصمم.

فالأنظمة الإنشائية عامةً "والفولاذية على وجه الخصوص" لا تهدف فقط إلى تحقيق مضامين وظيفية للمستخدم، وإنما لابد لها أيضاً من جماليات رمزية توفر استمتاعًا بصريًا وإدراكياً للمشاهد الذي يراها، من منطلق أن أنظمة الإنشاء الخفيف لا تُستخدم فقط وإنما تعرض أيضًا، كوُنها تعبير مادي عن أطر ثقافية وتحوّلات تّقنية تجسّد الواقع وتوحي بالمستقبل، وعليه فإن تلك الأنظمة لا تهدف إلى تحقيق مضامين وظيفية للمستخدم فقط، وإّنما لابد لها من رموز تعبيرية توفر الاستمتاع البصري والإدراكي، وتكون وسيلة للتلاقي والتواصل معه. ويتحقق ذلك عند إكساب تلك النظم تأثيرات جمالية ومقاربات رمزية ُتقدم في لغة تصميمية تتضمن صياغات بنائية تعبّر عن القوة والرشاقة، ومعالجات فراغية تؤكد على التواصل والانكشاف، وعلاقات إنشائية دينامية تجمع بين الصرامة والحيوية. ومن هنا يهتم البحث بتلك التأثيرات والمقاربات كأحد أدوات المصمم للارتقاء بالصور التعبيرية للعمارة، كونها عناصر مرنة تتيح له الانتقال من صياغة كتل رتيبة إلى إبداع أشكال إنشائية تحمل قيم ومعاني، وبصفتها وسائل متنوعة لجذب المتلقي والتأثير فيه وتلبية احتياجاته الفكرية والمعنوية. وبالتالي يوّلي البحث اهتمامًا بجماليات التعبير في الصيّغ البنائية للأنظمة الفولاذية، مما يبرز الأهمية في دراسة تلك الأنساق التعبيرية والمرتبطة بخصائص المنشآت الفولاذية بما في ذلك من مميزات القوة والمتانة والمرونة والاقتصاد فضلاً عن الجوانب الجمالية والتعبيرية.

1: المفردات المنشئية:

تعد المفردات المنشئية بشكل عام أحدى الجوانب الرئيسية في التشكيل والتكوين, وتهدف إلى توفير الإطار المادي الذي يحتوي الأنشطة بحيث يحقق الأمان والمرونة ويكون اقتصادياً في تكلفته ولا يعوق تأدية الأنشطة ويتناسب معها.

ويجب أن يتميز المنشأ بالثبات والاتزان المادي, بحيث يتوافق مع مبادئ الطبيعة حيث أن ظاهرة العمارة ما هي إلا جزء من الطبيعة وتخضع لقواعدها وان هذا يتحقق عندما يتبع المنشأ مبادئ الجاذبية والاتزان.

1-1: عناصر المفردات المنشئية:

تتكون المفردات المنشئية في التشكيل من شقين أساسيين هما:

أ. مواد البناء Materials.

ب. الطرق والوسائل Processes and means.

ج. النظم المنشئية Structural systems

1-2: المفردات المنشئية والتشكيل:

لقد أدى التطور التكنولوجي الحاصل في مواد وأنظمة المنشأ إلى أن أصبح المنشأ أداة للتعبير المعماري بدلاً من كونه عائقاً ومحدداً لعناصر الإبداع.

وبالتالي تعاظم الدور المنشئي في العملية الإبداعية والرمزية في العمارة. حيث تتميز المفردات المنشئية في التشكيل بان لها شق رمزي.

وعليه تتكون المفردات المنشئية في التشكيل والتكوين البصري من شقين: [سلام المصري،2006].

– **مادي :** خاص بمواد البناء وأنظمة البناء والتشكيل: و هو يقترن بمجالي العلم والصناعة فيأخذ عنها المواد والتقنيات الحديثة وهو في هذا الشق يخاطب المستوى العقلي للإنسان.

– **رمزي** : خاص بالمعتقدات، فيخاطب المستوى الروحي للإنسان من خلال تعبيره عن المعتقدات والشعائر الخاصة بالمجتمع عبر العملية البنائية.

2: أثر تطورات المواد الإنشائية في العمارة:

تعد مواد البناء من العناصر المهمة التي تؤثر على طابع العمارة في أي عصر من العصور، ولقد لعبت مواد البناء هذا الدور منذ نشأة الإنسان على سطح الأرض، حيث شكلت أفرع النباتات والأخشاب والطين والأحجار، مواد البناء الأساسية التي استطاع بها الإنسان أن يحقق لنفسه المأوى اللازم للحماية من تقلبات البيئة والحيوانات المفترسة وأعدائه من بنى البشر.

ومع تطور إمكانيات مواد البناء التقليدية وزيادة المعرفة بخصائصها وإمكانياتها الإنشائية والمعمارية بجانب العوامل الأخرى المؤثرة (مثل النواحي السياسية والاجتماعية والاقتصادية) تطورت العمارة عبر الحضارات والعصور المختلفة، بل وانتقلت عملية البناء انتقالات واضحة من خلال صيغ معمارية وهيئات جديدة عبرت عن الإمكانيات التي أتيحت في ذلك العصر، فالمتتبع للعمارة في مختلف العصور يستطيع أن يلمس التطور الذي حدث في عملية التصميم المعماري للمباني المختلفة وذلك نتيجة للتطور الذى حدث في المفاهيم التصميمية لتناول المشكلات المعمارية، وبالتالي إيجاد الحلول المعمارية المناسبة لها، والتي مثلت في مجملها تغييراً كبيرًا في طبيعة التصميم المعماري للفضاءات الداخلية، وكذا العلاقة بين هذه الفراغات وبعضها وبينها وبين الفراغ الخارجي، وأيضًا التطور الذى حدث في الهيئات الخارجية للمباني سواء في الارتفاعات أو في التشكيل المعماري لعناصر المبنى أو هيئة المبنى في مجملها.

بالتالي أوجدت مواد البناء الحديثة مفردات جديدة في مجال التصميم والتشكيل المعماري.

وقد تميزت هذه اللغة بمفردات عديدة من أهمها الفراغ الناتئ، والمسطحات الزجاجية الكبيرة (ظاهرة الشفافية)، والتشكيلات الحرة والمتنوعة في الواجهات الخارجية، واستخدام العناصر الإنشائية للمبنى في عملية التشكيل الخارجي بجانب وظيفتها الإنشائية. [Macdonald, 1997, P: 27].

3: المادة البنائية والأثر المنشئي:

تعتمد الكفاءة المنشئية والأداء المنشئي بصورة كبيرة على طبيعة المادة المنشئية المختارة وخصائصها خاصة ما يتعلق بقدرتها عل تحمل الإجهادات وادائيتها المنشئية.

فتلك الطبيعة والخواص الفيزياوية للمواد المنشئية كان لها الدور الكبير في اختيار النظم المنشئية المناسبة، حيث أن اختيار المادة المناسبة لنظام المنشأ تعد من أهم المتطلبات لذلك النظام للوصول للكفاءة المنشئية المطلوبة.

وبالتالي فالمادة بكل ما تحمله من خصائص وإمكانيات من نواحي (الشكل والإسناد والطبيعة الفيزياوية) تؤثر وبدرجة كبيرة على السلوك الإنشائي وعلى الشكل الناتج للمبنى، كما إن للنظام المنشئي الدور الكبير والبارز في اختيار وانتخاب المواد المنشئية التي تتلاءم وتلك المتطلبات أو المحددات وهذا يدل بالنتيجة إلى أن العلاقة بين النظام المنشئي والمادة البنائية متبادلة التأثير، وقد ساهم التطور في إمكانيات وأدائيات المادة في تبني الكثير من الأفكار الجديدة على مستوى المنشأ والتي كان من الصعب تنفيذها بوقت سابق. الشكل(1). [Trebilcock, 2004, P:32].

4: الرموز التعبيرية للعناصر الإنشائية:

يدرك الشكل بالإدراك العقلي عن طريق الحواس، لذلك يضم الشكل معاني عدة: منها حسّية لتمييز مضمون البناء ومعاني بنائية للتعرف على الترابط والتناسب بين أجزائه، وعن ضرورة تضمّن الصيّغ الإنشائية لمعاني، حيث أكد "رأفت" أنه لا يوجد شكل دون معنى يحسّ به، ولا توجد معاني ورموز دون شكل يحملها ويعبّر عنها. وذهب Schiller إلى أنه لا يوجد شكل بغير مادة تمنحه الواقعية، ولا ماده بدون شكل يضفي عليها المعنى ويهبها الهوية والثبات. واعتبر Vischer الإنشاء فن إيحائي يُعنى بالتعبير بواسطة الأشكال عن مضمون أمثل لفكرة محدده عن طريق تجسيدها في ماده ما، بغية تحويل المادي إلى لا مادي[علي رأفت،1997، ص:215]. ورغم ثبات الخواص الهندسية لكل شكل إلا انه لا يمكن تلمس هذا الثبات بالنسبة لما توحي به الأشكال، إذ أن الإيحاء الذي ينبثق من الشكل دائمًا ما يرتبط بالمضمون المحدد له، ويزيد هذا الإيحاء بطريقة معالجة أبعاده ووضعه في الفراغ وترابط عناصره. ويمكن توضيح بعض تلك الرموز، لاحظ مخطط (1).

4-1: الرموز التعبيرية لعناصر الإنشاء الخطية:

لا تكتسب العناصر الخطية أهميتها إلا من خلال صيّغ شكلية تحتويها، فالخط المستقيم أكثر استخدامًا في أنظمة الإنشاء ويوحي بالقوة والتعدد والاستمرارية، والمتجه لأعلى يوحي بالمرح والشموخ، أما المتجه للأسفل فيوحي بالحزن والانكسار، والأفقي يوحي بالخمول والراسي بالاتزان، والمائل حسب طوله واتجاهه يوحي بالحركة والاندفاع والمقاومة، والخط المنكسر حسب زوايا الكسر يتحدد طبيعة الإيحاء سواء بالحدة، الاتجاه، الحركة، القبول، والخط المنحني يعطي إحساساً بالليونة والحيوية وعند اتصاله بخط مستقيم يهدئ من صلابته وحدّته. [أحمد المهندس،2012].

4-2:الرموز التعبيرية لعناصر الإنشاء المستوية:

تختلف التعبيرات الرمزية لعناصر التغطية والاحتواء في المنشأ الفولاذي تبعاً لتحولاتها الشكلية، فالمنتظمة توحي بالإشعاع والانتشار والثبات المادي، وقد توحي بالديناميكية والإنضغاط إذا استطال احد محاورها، والمائلة توحي

بالحركة الصاعدة أو الهابطة تبعًا لمركز الرؤية، أما التغطيات أحادية أو ثنائيه الانحناء فتوحي بالاحتواء التغليف الخفة والاستمرارية، كما تعطي تماثلات السطوح في اللون الموضع والشكل إيحاءاً بالتقدم أو بالتراجع في جهات عده، وتعكس مادة الأسطح ودرجة شفافيتها دلالات معينة كالتواصل، الوضوح، الانغلاق. شكل (2).

4-3: الرموز التعبيرية للتكوينات الإنشائية:

توحي الأنظمة المقببة بالتغليف، أما الأسطوانية فتوحي بالمرونة والثبات، وتوحي الهرمية منها بالاندفاع، الاستقرار والصعود، والأنظمة ذات الأشكال الحلزونية ُتوحي بالحركة، الليونة والاستمرارية، والأنظمة المركبة توحي بدلالات مختلطة: تبدأ بالسكون، الحركة، الثقل والخفة، والأنظمة الانسيابية لها ميزه فسيولوجية حيث تتطلب العين في استيعابها مجهودا أقل عن تلك التي تتسم بالصرامة الهندسية وتحتاج لانتقالات مفاجئة عند أركانها. والأنظمة التي

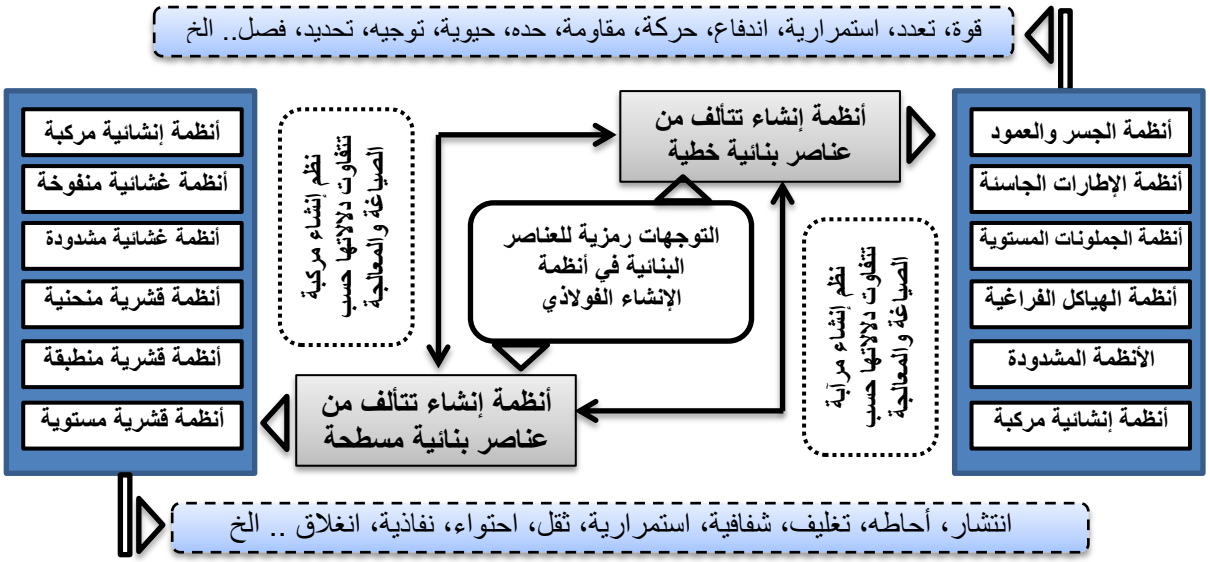

مخطط (1) التوجهات الرمزية للعناصر البنائية [خطية، مسطحة، مركبة] لأنظمة الإنشاء الفولاذي (الباحث)

تنتقل فيها الأحمال راسيًا توحي بالسكون والاستاتيكية، والأنظمة ذات الانتقال المائل للأحمال توحي بالحركة والمرونة، مع ملاحظة أن الاتزان المادي لأي نظام معدني لا يمنع من الإحساس بالديناميكية. وعادة ما يكون للإبهار دلالات رمزية، فالأنظمة الناتئة (Cantilevered) تحقق إبهاراً إنشائياً وشكلياً وتوحي بالاستمرارية، كما تتيح إبهاراً في البحور والعروض والارتفاعات وتوحي بالخفة، وتحقق الأنظمة الفراغية إبهاراً عدديًا في الوحدات البنائية المتشابكة وتوحي بالتداخل والتعقيد. [Allsopp, 1971, P:33].

5: المنشآت الفولاذية:

تعد الهياكل الإنشائية الفولاذية بشكل عام من أكثر الجوانب الإنشائية استخداماً، فقلما نرى في العمارة الحديثة بناء يخلو من استخدام هياكل إنشائية فولاذية رئيسية كانت أو مشتركة مع أنظمة أخرى، استخدمت في إنشاء الواجهات الزجاجية ومظلات الدخول وفي تغطية الأبنية ذات البحور الكبيرة.

حيث تعد المنشآت الفولاذية من المنشآت الخفيفة، والفولاذ هو مادة تمتلك خواصاً منشئية ممتازة كالمتانة وعالية في الشد والانضغاط. لذلك يستطيع مقاومة الإنحناء والقوى المحورية بصورة متساوية. وهو من أقوى المواد المعروفة بصورة عامة لذلك يستخدم لإنشاء المباني ذات الفضاءات والبحور الطويلة ويستخدم بصورة شائعة للمبنى ذي الهيكل المعتدل في البحر في تشكيلات متنوعة. كما إن أنظمة الإنشاء الفولاذي لا تهدف فقط إلى تحقيق مضامين وظيفية

للمستخدم، وإنما لابد لها أيضًا من جماليات رمزية توفر استمتاعًا بصريًا وإدراكيًا للمشاهد الذي يراها. [Trebilcock, 2004, P:34].

1-5: التطور التاريخي في استخدام الفولاذ:

شُيد أول هيكل فولاذي سنة (1903–1906) في بريطانيا بدون جدران خارجية حاملة وهو المبنى الفندقي (Ritz). ويقال بأن السبب في عدم إستخدام الواجهة الحجرية كان في عدم التعرض لأي حمل زائد في المبنى. حيث أعطى المبنى معارضة للتقليد المعماري في إنكلترا في ذلك الوقت, لأنه من الصعب التخيل بان مبنى ذا مظهر غير كلاسيكي يبنى في موقع بارز في لندن [Macdonald, 1997, P: 30]، الارتقاء في إستخدام الفولاذ من شكل الهيكل ذي الأسناد المطلق إلى حالة المساهمة الجدية في الجماليات المتعلقة بالمبنى كان قد تحقق من قبل المحدثين المعماريين في بداية القرن العشرين حيث وجدوا المادة مثيرة في الحقبة بين 1920–1930 وكانوا حريصين على إبتكار مفردات معمارية جديدة للعالم الحديث ذي الصناعة والتكنولوجيا وهذا من وجهة نظرهم. توحدت تكنولوجيا الهياكل الفولاذية مع الجماليات المعمارية في الحقبة بين عام 1920–1930 بطريقتين مفصولتين هما: **الأولى** ترجع إلى تطور المبنى ذي الأكساء الزجاجي **والثانية** الميل نحو الاستخدام الواضح للعناصر المنشئية لتشكل جزءاً من المفردات البصرية الحديثة. [Allsopp, 1971, P:24].

ومن المصادر البصرية لمفردات عمارة الفولاذ والزجاج كانت الهياكل الحديدية للورش والمصانع ومحطات القطار للقرن التاسع عشر تلك المباني التي أهملت بصورة كبيرة في وقتها من قبل المعماريين ولكنها في نفس الوقت كانت تتجه لتحقيق تأثير كبير على المفردات البصرية في حداثة القرن العشرين. [Allsopp, 1971, P:42].

والمثال المعروف كان مخزن القوارب في إنكلترا (1858–66) الذي ظهرت فيه هيئات القرن العشرين الحديث وهو من الأمثلة السباقة، ولكن الأنواع الأخرى للمباني الصناعية وخصوصاً محطة القطار في (Termini) كانت أيضاً مهمة. هذا التقليد بإستخدام الهياكل الفولاذية للمباني وصل إلى ذروته في "القصر البلوري" في لندن والذي بُني لغرض إقامة المعرض الكبير 1851 حيث كان مبنى ضخم من الزجاج والحديد من الناحية البصرية وترك تأثيراً على عمارة القرن العشرين، كانت المباني الفولاذية في الحقيقة تحتوي على عدد من السلبيات التقنية منها العزل الحراري والعزل الصوتي للجدران الخارجية والمتانة القليلة في الربط بين الألواح المفردة للزجاج في القشرات الشفافة والتي كانت تمثل مشكلة كبيرة. أما التحول الكبير فكان نحو كشف الهيكل الفولاذي لأسباب تعبيرية والذي مثّل واحداً من الأساليب المفضلة لما يسمى عمارة التقنيات العالية (Hi-tech) (1970 –1980)، هذه المباني كانت ذات هيكل فولاذي ذو أكساء زجاجي مثيرة بصرياً وتعبر عن خيال متميز لمعمار نهاية القرن العشرين. ومن المشكلات المرتبطة بكشف الهيكل الفولاذي هي تلك المرتبطة بالإدامة والصيانة للمنشأ والحماية من الحريق والذي يبرز جليّاً في المباني المتعددة الطوابق [Macdonald, 1997, P:49]. وهذا سبب كشف المنشآت الفولاذية ذات الطابق المفرد وهناك إستثناء وهو "بومبيدو سنتر" في باريس الذي فيه نظام الحماية من الحريق متوفر لضمان الهيكل الفولاذي المكشوف على الجدران الخارجية للمبنى يحقق الحماية المطلوبة من النار. جميع الهياكل الفولاذية في الداخل مغطاة بمادة عازلة وتكون غير مكشوفة وغير مرئية.

وظهرت في نهاية القرن العشرين أفكار التفكيكية في العمارة التي قادت إلى التوسع في استخدام الزجاج والفولاذ في المباني فالمتانة العالية للفولاذ في مقاومة الشد والانضغاط جعلته قادراً على تحقيق عناصر ذات أشكال حرة قدر الإمكان. [Macdonald, 1997, P:49].

2-5:إيجابيات إستخدام مادة الفولاذ في المنشآت:

هنالك مجموعة من الإيجابيات المستخلصة من استخدام مادة الفولاذ في الهياكل الإنشائية للمباني منها:

- **القوة (Strength):** القوة العالية للفولاذ ونسبة الوزن إلى العمق المنخفضة تجعله مناسباً للاستخدام في هياكل المنشآت ذات الطابق المفرد والمتعدد الطوابق ولحدود كبيرة من المباني ذات البحور المختلفة فضلاً عن الحرية في تحديدات الجدران الحاملة في التخطيط الداخلي والخارجي للمبنى. أما بالنسبة لعلاقة القوة بالوزن (Ratio of strength to weight) فالهياكل الفولاذية تكون أخف من الهياكل الخرسانية ذات المتانة المشابهة خصوصاً أذا أستخدمت أنواع كفوءة من العناصر.
- **السيطرة على النوعية (Quality Control):** يصنع الفولاذ تحت حالات صارمة من السيطرة النوعية وخواصه يمكن أن تكون مع محددات خاصة جداً. وهذا يساعد على إحتساب عوامل أمان قليلة في حسابات التصميم الإنشائي وهذا سبب أضافي لتكون العناصر المنشئية رشيقة وخفيفة. [Macdonald, 1997, P: 52].
- **المظهر الخاص بالفولاذ (Appearance of Steel):** ويعود ذلك للسيطرة النوعية الجيدة التي تحصل خلال عملية تصنيعه والى الطرق المستخدمة في تشكيله النهائي ولعناصره فالمنشأ النهائي يكون ذا مظهر مميز يعبر عن العناصر الرشيقة والسطوح الملساء ذات الحافات الحادة المستقيمة.
- **التصنيع المسبق للفولاذ (Prefabrication):** تمثل المنشآت الفولاذية تجميعاً لمركبات مسبقة الصنع والتي تنتج خارج الموقع وهذا يسمح بأن تكون أبعادها والنوعية العامة تحت سيطرة دقيقة وتساعد بالنتيجة في الأنشاء السريع للمنشأ في الموقع وحتى في المواقع الصعبة. [Macdonald, 1997, P: 53].

ومن الإيجابيات الأخرى للإنشاء الفولاذي:

(جمال الشكل– كفاءة الأداء– قلة التكاليف– فضاءات واسعة دون إسناد– إمكانية زيادة كبيرة في أحمال الأرضية– إمكانية الارتفاع شاقولياً إلى مسافات كبيرة– سهولة التركيب وبالتالي توفير زمن الإنجاز– يمكن أن يكون السقف مؤقتاً وعندئذ يستفاد بفكه ونقله إلى مكان آخر)

3-5: السلبيات المرافقة لإستخدام الفولاذ:

- **صعوبة التشكيل (Intractability):** الفولاذ مادة قوية جداً من الصعب العمل به وتشكيله في أشكال صلبة وهذا له عدد من التبعات أنه يعني أن في أغلب هياكل الفولاذ المصممة, من الضروري تخصيص العناصر من أبعاد قياسية للمركبات التي تنتج من الفولاذ المصنع وتحقيق أقل عدد ممكن من التحويرات لهذه المقاطع القياسية. أنتاج مقاطع فولاذية حسب التصميم المعين أو الهندسيات ذات الخطوط المنحنية تكون صعبة ومكلفة فإستخدام الهيكل الفولاذي في مثل هذه الحالات سوف يفرض تحديدات على الشكل النهائي للمنشآت. [M. Schupack, 1958, P: 52].
- **مقاومة الفولاذ للحريق (Steel Performance in Fire):**

يفقد الفولاذ قابليته لحمل الأثقال في درجة حرارة عالية نسبياً فهذا يعني بأن الفولاذ لا يحترق ولكن سوف يتهاوى في النار أذا لم يحفظ في حدود حرارية معتدلة وهذا عادة يحقق بحماية الهيكل الفولاذي بطبقات مناسبة من عوازل مقاومة النار ولكن عادة تستخدم طرق أكثر تعقيداً مثل أنظمة المياه الباردة. المادة الواقية من النار وبصورة تقليدية هي الخرسانة، فعناصر الهيكل الفولاذي تغطي ببساطة بالخرسانة. [Macdonald, 1997, P: 55].

6: التعامل مع الصيّغ الإنشائية الفولاذية كلغة بنائية:

اللغة نظام من العلامات المنتظمة تقوم بوظيفة اتصالية تؤمّن تبادل المعلومات، والعلامة هي التعبير المادي للظواهر والمفاهيم المستخدمة في عملية التبادل. فضلاً عن كونها نظام تفاعلي للتعبير عن أفكار مستخدميها من خلال رموز وإشارات، حيث تعمل كوسيط للتواصل بين الأفراد ووسيلة لنقل الأفكار بعد اختزالها في رموز، وبالتالي يصبح التعبير بأبجديات الشكل لغة إذا ما تحقق الهدف في نقل الأفكار إلى الآخرين. ووفقًا لنظرية التمثيل اللغوي Linguistic Analogy تشبه العمارة اللغة بشكل عرضي أو رئيسي وذلك لأنها تتشارك في كل أو بعض السمات الجوهرية التي تصنع اللغة خاصة تلك التي لا يستغني عنها. [Scruton, 1979, p:160]. فالوظيفة تقابل المعنى والهيكل يقابل التركيب والجمال يقابل البلاغة وهكذا. مخطط (2).

مخطط (2) توجهات لغة للتواصل بين المصمم والمتلقي (الباحث)

ومن منطلق أن الكلمة هي رمز لمعنى خلفها وأنها تمثل مفرده البناء لأي نصّ، فإن التعاطي مع أنظمة الإنشاء الفولاذي كّلغة بنائية تتيح لمن أدرك أبجديتها قراءتها وفهم معانيها، يصير طالما احتوت على معاني ورموز خلف أشكالها. وبالتالي فإن الاهتمام بعناصر الاتصال في اللغة البنائية غير المنطوقة واستلهام مفاهيمها وتوظيف آلياتها لصياغة أشكال مميزه تحمل رسائل محدده للمتلقي، يتيح للمصمم إقناع المتلقي برسائله، وتيسر على الأخير تفهم وقراءة تلك الرسائل. وعن ضرورة وجود هذا الحوار غير المباشر بين المتلقي وما بصيغة المصمم طالب Rogers بضرورة أن يستطيع المتلقي قراءة المنشأ كما يقرأ كتابًا فيفهم طريقة تركيبة وعناصر إنشائه كما أكدLe doc على أهمية ملاحقة ركب التطور الإنشائي وضرورة الاهتمام بالإنشاء كمصدر للشكل، بغرض إيجاد لغة معمارية مناسبة للخامات الجديدة وبخاصة الفولاذ منها. [علي رأفت،1997، ص:33]. وعادة ما تتكوّن لغة الشكل في مجال الإنشاء الخفيف من رموز ومفردات بنائية يستمر تداولها وإعادة صياغتها بعد إزاحتها باتجاهات معينة لتوحي بدلالات مختلفة تنحصر بالخفة والمرونة والرشاقة، كما تتأثر تركيبات تلك اللغة بالتحولات المستمرة في مرجعيات الشكل [بدءاً بالوظيفة ومرورًا بالتقنية والموقع] التي يشجعها التطور التقني والثقافي في المجتمع، وأن هذا التنوع في المرجعيات وما ينتج عنها من تباين في تطبيقات الإنشاء، هو الذي يميز الخصوصية البنائية لكل عصر ويعطيه تميز اللغة التعبيرية للمنشأ [عضوية، بنائية، تفكيكية ..] وبالتالي فمن المهم للمصمم أن يتفهم التنوع في اللهجات الإنشائية ويلمّ بالمؤثرات التي شكلتها وألا تقتصر مهمته على توليف مفردات بنائية جميله فقط، وإنما لابد من صياغتها معًا في لغة متكاملة. ولان أنظمة الإنشاء الخفيف عادة ما تُقرأ من خلال حواس أخرى غير البصر، وبإدراكات حسية وغير حسية، ووفق قاعدة تستند إلى توافر العين القارئة التي تستطيع أنّ تدرك بوضوح الدلالات التي تولدها عناصر الشكل، فإن استمتاع المتلقي برؤية نظام

فولاذي يتحقق بقدر حضوره المادي ليكون مشتركًا ومشاهدًا في الوقت ذاته. وطالما أن لكل لغة مفرداتها ودلالاتها، فان الإنشاء الفولاذي كلغة لها مفردات ورموز يهدف إلى التأثير على المتلقي عبر خطوط اتصال بصرية مثل: [Trebilcock, 2004, P:42]. (الإحساس بالفراغ، الإيقاع، الحركة واتجاه القوى التوافق بين الكتلة والفراغ)، وان هذا الاتصال عاده ما يُكوّن لدى المتلقي خلفيه من التذوق الجمالي تنمو مع تعدد رؤيته لتلك الأنظمة، فيتولد لديه استيعاب تراكمي لانفعالات جمالية تعطي لكل نظام مدلول مميز يظهر بعد ذلك في ردة فعله اللاشعورية للتنوع في الفراغ والشكل والحجم وعلاقات الكتل وما يرافقها من تمايزات في معالجة المواد وتلاعب الضوء والظل. ومن هنا فإن اللغة الإنشائية، وبسبب مرونة صياغتها وما توفره من وسائل اتصال متعددة، تستطيع أن تتجاوب مع متطلبات المستخدم المادية والمعنوية، ومن ثمّ فإن تعظيم التعاطي مع الإنشاء كلغة بنائية يوفر عالم ثري بلهجات إنشائية متمايزة تتيح للمصمم دعم صياغاته الشكلية بمدي واسع من المعاني والرموز. [Scruton, 1979, p:152].

7: ابرز مفردات الإطار النظري المستخلصة:

يتناول ابرز الجوانب المستخلصة من المحاور المعرفية الأساسية والخاصة بالمفردات التي تم طرحها بغية تشخيص ابرز المؤشرات والقيم الممكنة للرموز التعبيرية والمرتبطة بخصائص الأنشاء الفولاذي ومميزات تلك الأنظمة. والتي إعتمدت بشكل أساسي على جانبين:

إرتبط **الأول** بخصوصية الهيكل الإنشائي المعدني للمبنى، أما **الثاني** فإرتبط بالجوانب التعبيرية وما يرتبط بها من دلالات رمزية تعبيرية لذلك المنشأ، لغرض مناقشة كل مفردة ومن ثم نتائج العلاقة بين تلك المفردات ومن خلال مشاريع منتخبة، للوصول إلى الإستنتاجات النهائية.

8: المفردات الجمالية في أنظمة الإنشاء الفولاذي:

الجمال حالة انسجام تحدث بين الإنسان وما يحيط به، تختلف مقاييسها باختلاف البيئة المادية والثقافية، وهو لا يقوم على آلية إبداعيه واحده وإنما على آليات عدّه يكون لكلّ منها أنساقه التعبيرية ودلالاته الرمزية، ويتضح ذلك من ارتباط التعبير الجمالي في البناء عند المصريين بالحقيقة، وعند اليونانيون بالكمال، وعند الكلاسيكيون بجوهر الواقع، وعند الرومانتيكيون بالإرادة والشعور، وعند المسلمين بالوحدة والتجريد، وعند البنائيون بالحيوية، وعند الوظيفيين بالمنفعة، وعند العضويين بلغة المواد وإيحاءاتها، وعند الحداثيون بالتعبير المتأنق للتقنية، وعند التفكيكيين بالتداخل واللامركزية.

بالتالي يمثل أحد أدوات المصمم لجذب المتلقي والاتصال به وتنمية تجربته البصرية وبيئته العمرانية، ذلك أنه ينبع من شعور الأخير بوحدة النظام، تكامل الأجزاء مع الكل، توافق الشكل مع المضمون وتوافر معالجات فراغيه وبنائية متميزة تعبّر عن تقنيات عصرها. وللجمال في الإنشاء دورًا رمزيًا مزدوجًا الأساس فيه تحقيق التوازن عند المتلقي. [شاكر عبد الحميد،2006، ص:9-8].

وفي الاطار ذاته آمّن Wasser بدور الإنشاء كفن جميل وطالب بتجديد قوالبه عن طريق دمج فناني التصوير والنحت في الصياغة الإبداعية لأنهم أكثر حرية من المصمم المحكوم بمقيدات ماديه كثيرة. لذا يكون من المهم التأكيد على وظيفة المنشأ الجمالية ليس فقط بإنتاج أشكال مبتكرة، وإنما بتحميلها بدلالات ومعاني ملائمة. [A.Macevoy Blanc, 1993,p:49].

المفردات البصرية المرتبطة مع المنشآت الفولاذية تحتوي بعضاً من أقوى النماذج المميزة للعمارة الحديثة فالهياكل الفولاذية ذات الأكساء الزجاجي والرشاقة ودقة الضبط في صناعة المركبات المنشئية كعناصر بصرية والتقبل البصري الإنشائي الواضح في أشكال الفضاءات ذات البحور الكبيرة المبهرة أو في المباني ذات الأرتفاعات الشاهقة تكون أشكالاً مختلفة في التعبير والتأثير. بسبب توفر الفولاذ كمادة للبناء منذ النصف الثاني للقرن التاسع عشر والذي يرجع إلى تطور العمليات الأنتاجية وبصورة أكثر أقتصادية [شاكر عبد الحميد،2006، ص:9].

9: المنشآت الفولاذية وجماليات التعبير:

ترتكز جمالية الفولاذ من جمالية الهيكل الفولاذي الرئيس للمبنى والذي تكون فيه اغلب العناصر رشيقة وبأسلوب ظاهر ومكشوف. حيث تمتلك بصورة واضحة جماليات في تمجيد التكنولوجيا والماكنة فضلا عن كونها ترمز إلى الأشكال ذات الحافات المستقيمة والواضحة والمنتظمة والخطوط الشبكية وبصورة مبالغ فيها للتعبير عن الماكنة.

ويستعمل الفولاذ في أغلب الأحيان في التجارب المرتبطة بالغلاف الخارجي للمبنى حيث يضيف أهمية إلى التأثير البصري العام لذلك المبنى. وهناك خمس علاقات أساسية بين مضمّون البناية والهيكل الأساسي: [Trebilcock, 2004, P:17].

- **الاحتمال الأول:** يوضع الهيكل الفولاذي كليّا داخل غلاف البناية.
- **الاحتمال الثاني:** يوضع الهيكل ضمن مستوى واجهة البناية
- **الاحتمال الثالث:** يكون الهيكل الداخلي مستمر مع واجهة المبنى.
- **الاحتمال الرابع:** يكون الهيكل الخارجي نصف مستقل ويدعم الجدار الخارجي، أو يدعم التغليف الزجاجي.
- **الاحتمال الخامس:** يوضع الهيكل بالكامل خارج واجهة المبنى.

وهذه العلاقات بين الواجهات والهيكل الإنشائي الأساسي تسحب معها قضايا أخرى مهمة لتصميم المبنى، مثل: [Trebilcock, 2004, P:19].

- تعبيرية الإرتباطات.
- الأساسات ونقاط التثبيت.
- الأمن والوصول (للهياكل الخارجية).
- إستراتيجية الوقاية من الحريق.
- حماية تآكل العناصر الخارجية.
- طبيعة الإسناد الثانوي للسقوف والجدران لتكملة الحلّ الإنشائي المقترح. [Trebilcock, 2004, P:19].

إنّ خليط العناصر الإنشائية، بما فيها العناصر المقوسة، الجملونات، المكوّنات المصنّعة، القابلوات، عناصر الفولاذ المقاوم للصدأ، كلها توضح التنوع في التقنيات القابلة للإنجاز. فقد يستخدم استمرار الهيكل الإنشائي الداخلي إلى الخارج في التأثير التعبيري. كما هو الحال في الهيكل المقوّس لمحطة Stratford حيث تم وضعه خارج الواجهة المزجّجة لتأكيد ذلك الحلّ الإنشائي الفولاذي. الشكل (3). [Trebilcock, 2004, P:20].

10: جوانب جماليات التعبير في أنظمة الإنشاء الفولاذي.

بتعدد المنطلقات الفلسفية والإبداعية للباحثين، تعددت الآراء والاتجاهات التي فسّرت جماليات التعبير في أنظمة الإنشاء الفولاذي وأحاطت بمظهرها ورموزها، ومنها:-

أ: اللون في الأنظمة الفولاذية ورموزه التعبيرية:

الألوان أحد العناصر المهمة التي يستعان بها لإبراز القيم الجمالية للمنشأ الفولاذي، لأنها تضيف أبعادًا جديدة لشكله، وتؤثر على علاقاته ومستوياته، وتحدد مدي توافقه مع البيئة المحيطة، وتعمل على تكامل عناصره، وتحقق الاتزان البصري فيما بينها. وحول هذا أكد فاسر على أهمية استخدام الألوان في البناء، ودعا إلى تطبيقها بأساليب مناسبة، معداً أن معالجة العناصر البنائية لونياً له دور هام في وضع المنشأ في محيطه المجاور لكونها علامات أرضية وبصرية له. [Wasser, 2000, p:47]. كما تلعب المعالجات اللونية دورًا مهماً في عملية الإدراك البصري بتوفير إشارات يمكن من خلالها فهم الشكل وتفسير مدلولاته، وهي كذلك وسيلة جيدة وأحياناً لا غنى عنها لتوضيح الفراغ واستيعاب أبعاده ورموزه والتأثير على حجمه الظاهري، كون بعضها أكثر لفتًا للانتباه من غيره. وهي تحمل قيمّ رمزية كالدفء والبرودة، الثقل والخفة، الضوضاء والهدوء، النفور والتقارب، التقدم والتراجع، فضلاً عن أن التباينات اللونية تتيح ميزة إيقاف العين، تقسيم الأسطح، تحقيق الإيقاع. [Wasser, 2000, p:51] شكل رقم (4)

ب: الفراغ في الأنظمة الفولاذية ورموزه التعبيرية:

الفراغ Space بشكل عام هو عنصر جوهري للتشكيل، لأنه يتضمن ويحتوي كل شيء، وهو شرط مسبق لكل ما ومن هو موجود، وهو كما رآه Ching مسافة تتمدد في كل الاتجاهات. [Ching, 1996, p:108]. ويكتسب الفراغ خواصه الهندسية ومعانيه الإيحائية من التوزيع المادي لعناصر بنائية ُتحدده وينشأ على إثرها نظم لها حجم وشكل وحركه نسبيه تتوزع في تشكيلات مغلقه أو مفتوحة، منتظمة أو غير منتظمة، ومن ثمّ يرتبط إدراك المتلقي للفراغ بتحديد وتعريف الأشكال الحاوية له أو المحتوية فيه، وذلك تأكيدًا لقول Govinda باستحالة تخيل هدف أو بناء دون فراغ. [Ching, 1996, p:112]. وحيث أن الفراغ أحد عناصر إدراك وتوصيف الشكل، فإنه يمكن النظر إلي الإنشاء الخفيف على أنه فن صياغة الفراغ وقولبته من خلال ترتيبه وتنظيمه لخدمة غرض استخدامي أو أكثر. شكل رقم (5).

11: تّطبيق آليات التعبير الرمزي على الصّيّغ الإنشائية:

يعد التعبير الرمزي ضرورة لا مفر منها في المعالجات الإنشائية، وعادة لا يبدأ المصمم به وإنما لابد وان ينتهي إلية بعد تحليله لكافة المعطيات واستيفائه لكل المتطلبات والمحددات. بحيث لا يتعمّد الحصول على تعبيرات خاصة بشكل مفتعل، وإنما يراعي في صياغاته التوفيق وفق محورين أساسيين هما (النواحي الوظيفية، النواحي الشكلية التعبيرية) التي تندرج تحتهما عدة آليات منها: لاحظ الجدول رقم (1).

- التأكيد على العلاقة المتزنة بين الحيز والإنشاء.
- استخدام انسب المواد المتوافقة مع الأداء الوظيفي، والتوافق بين المضمون البنائي والوظيفي للنظام.
- الاستفادة من اللهجات الإنشائية لإحداث التنوع التصميمي والتباين الإبداعي.
- التأكيد على مرونة التصميم لإجراء تغييرات مستقبلية باستخدام النظم الإنشائية.
- اللجوء إلى التعبير بالرمز عن المادة، وطريقه الإنشاء.
- استخدام مفردات مناسبة للتعبير عن اللغة الإنشائية المنتقاة (عضوية، بنائية، تفكيكية ..الخ)
- التعبيرات الإنشائية التي تؤكد على مرجعية الشكل.
- صياغة تعبيرات إنشائية تجسد التطورات والتحولات التقنية.
- التعبير عن التوقعات المستقبلية للإنشاء في أشكال قابله للنمو والاندماج

• التأكيد على العلاقة التفاعلية بين المنشأ والمتلقي.

12: المشاريع المنتخبة:

12-1: مبنى الجذع الملتوي لولبياً (Turning Torso)

(السويد- للمصمم Santiago Calatrava 2005).

هو ناطحة سحاب سكنية ارتفاعها 190 متر, 54 طابقاً يقع في مدينة مالمو السويدية. ويعد أعلى مبنى سكني في السويد.

حصل على جائزة (MIPIM) في معرض البناء في فرنسا لأفضل مبنى سكني في العالم، والبرج لم يُعبر فقط عن المفهوم الهندسي المُميز ولكن أيضاً عن التكنولوجيا والتقنية المتقدمة.[أوان الكويتي،2010] شكل (6).

أ- على مستوى الفكرة التصميمة والشكل المعماري:

شيد البرج من الفولاذ والزجاج والخرسانة المسلحة، ويتمحور في تسعة مكعبات دورانية هيكلها الرئيسي هو عنصر أساسي من الخرسانة المسلحة، ومركز البناء فيه يتطابق تماماً مع محور دوران الطوابق، أما الغلاف الخارجي للمبنى فمصنوع من لوحات من الزجاج والألمنيوم. يتميز بشكل ديناميكي. والأسطوانة المركزية الرئيسية التي ترتبط فيها الهياكل الأفقية بشكل ناتئ تحتوي على المصاعد والنظم التكنولوجية والخدمات.

الواجهة لها انحناء مزدوج لكون سطح البناء لولبي، وهذا يجعل بنائها وتشييدها في غاية التعقيد. والواجهات مكونة من 2800 لوحة و2250 نافذة. سطح اللوحات منحني أما الزجاج فهو مسطح. كل مكعب مغطى ب300 لوحة.. [أوان الكويتي،2010]. شكل (6).

وبهدف إعطاء الشكل اللولبي للمبنى، فالنوافذ يجب أن تميل إلى الداخل أو الخارج، وهذا اعتماداً على الجانب الذي تتواجد في من المبنى. ففي الجانب الغربي الميلان هو نحو الداخل، أما في الجانب الشرقي فهو إلى الخارج.

ب- على مستوى الهيكل الفولاذي الخارجي:

يتكون الهيكل الإنشائي الرئيسي من عناصر من الفولاذ والخرسانة المسلحة واللذان مثلا (العمود الفقري للمبنى). فالعناصر الفولاذية للدعم الخارجي ارتبطت ببعضها البعض عن طريق اللحام ومطلية لحمايتها من التآكل. والعنصر الفولاذي للدعم الخارجي يتألف من أنبوب عمودي "A" يصل إلى نهاية طوابق المبنى، وهنالك 20 أنبوب أفقي و18 أنبوب قطري متصلة بالعمود"A". وكل هذه الأنابيب مرتبطة بالجدران الهيكلية وتحتضن طابقين في المنطقة العلوية لكل مكعب. بغية تحويل جهد أنابيب الفولاذ إلى الأسطوانة الخرسانية المركزية. وعلاوة على ذلك، فان العمود الفولاذي مرتبط بعنصرين من عناصر الاستقرار في كل طابق. وتستخدم هذه العناصر لتثبيت ودعم العمود الصلب. [أوان الكويتي،2010].

أما أرضيات الطوابق فتكون مُعززة بقضبان معدنية ترتبط مع الهيكل الفولاذي المركزي. شكل (6).

12-2: مطار ستانستيد (Stansted Airport) (لندن- إنكلترا للمصمم Norman Foster. 1991)

أخذت المطارات ومحطات النقل أهمية تصميمية كبيرة خاصة وان تلك المشاريع بما تمتلكه من متطلبات منشئية وتكوينية ووظيفية وخدمية عالية تتطلب حلولاً فريدة ومبتكرة، حيث قام المعماري نورمان فوستر بتصميم مطار يتسم بأقصى درجة من المرونة لمواجهة التعديلات أو أي توسعات تحدث في المستقبل، فضلاً عن خلق مبنى على

هيئة ضخمة تتكون من خلايا نمطية متكررة لإعطاء أكبر قدر ممكن من المرونة ليواجه الأعداد المتزايدة المستخدمة للمطارات بدون الإخلال بالتصميم.

أ- على مستوى الفكرة التصميمة والشكل المعماري:

جاء المبنى كمظلة ضخمة تتكون من خلايا متكررة بمقياس(36×36) متر وبارتفاع 15 متر ويحمل كل خلية عمود من أنابيب الفولاذ علي شكل شجرة من أربعة أغصان تحمل في نهايتها قبة مفلطحة من ألواح معدنية خفيفة تتوسطها فتحات زجاجية ينساب منها الضوء الطبيعي لإنارة الأجزاء العميقة من المباني، وبهذه الطريقة الإنشائية تم تحرير الواجهات الخارجية الأربعة من أي عوائق وتحولت بذلك إلى ستارة من الزجاج بارتفاع 12م تملأ معظم مساحات المبنى بالضوء الطبيعي الخالي من أي وهج والبعيد عن تساقط أشعة الشمس بفضل البروز الضخم للسقف أمام الواجهتين الشرقية والغربية. [أحمد المهندس،2012]. شكل (7).

ب- على مستوى الهيكل الفولاذي الخارجي:

كانت الفكرة الأساس هي التغطية الفولاذية ثلاثية الأبعاد. حيث إن الرواق المقنطر هو شارع ذو واجهتين من أنواع مختلفة التصميم من المحلات، لها قنطرة أسطوانية منخفضة الارتفاع، وهي تستند وكأنها أجنحة إلى كابلات معدنية موصولة بقمة القنطرة، وأما السقف الخفيف فهو عبارة عن قرص متحرك يتفاعل مع التغييرات البيئية من ضوء وهواء تفصيلة السقف المجنح الذي ينفتح لكي يتم التحكم بالمناخ الداخلي والضوء الداخل ويرمز العنصر الإنشائي الحامل ثلاثي الأبعاد إلى شجرة تتفرع أغصانها للأعلى. شكل (7).

فقد تم تسقيف فضاء بمساحة (32000م^2) لقاعة المسافرين الكبيرة لإعطاء جو من الطمأنينة. حيث يلاحظ عل المطار سقفاً طافياً في الجو (استخدام فكرة الطيران المجازية) فقد استعمل المصمم أقصى تكنولوجيا منشئية متاحة للوصول للمرونة التصميمية.

وشبكة السقف تستند على منشأ فولاذي مكون من الأعمدة وكأنها سيقان أشجار، كما أُظهرت هنا خاصية العمق التنظيمي من خلال الأعمدة وكذلك من خلال قشرة السقف التي أعطت مساحة كبيرة على شكل قباب وشبكة مربعة الشكل ذات مساحة 36م^2، وتتفرع من المساند العمودية المربعة فروع حديدية لحمل قباب السقف وهذه الفروع عبارة عن أنابيب وقابلوات فولاذية مغلفة بنسيج زجاجي مضاد للصدأ والرطوبة، وتتصل تلك الفروع مع بعضها بشكل حلقي مما يجعلها تشبه الأشجار الحاملة لقباب السقف. [أحمد المهندس،2012].

13: استخلاص الجماليات الرمزية لأنظمة المنشآت الفولاذية:

13-1: سبّل التعبير الرمزي عن جماليات الصيّغ الإنشائية الفولاذية.

تقوم أنظمة الإنشاء الفولاذي على سدّ حاجات ومتطلبات إنسانية، بالتالي عملية تصميمها تمثل وسيلة للتلاقي والتواصل مع المستخدم من خلال روابط عده، يعبّر عنها بمواد وطرق وأشكال وتقنيات لها دلالاتها الرمزية والجمالية، بحيث يصبح لتلك الأنظمة وظيفة تعبيريه لنقل المشاعر والأفكار. وحول هذا الإطار رأى Right أن كل ماده تتحدث لغة خاصة كما يتحدث الخط أو اللون، وأن على المصمم أن يكشف هذه الروح ويسمح لها بالانطلاق من خلال عمل يتسم بالحيوية. كما أعتبر Perret أن التعبير عن الإنشاء سواء بكشف الهيكل أو الإشارة إلية هو تعبير عن حقيقة مطلقة تبني على نظام ومنطق سليمين لكونهما أساس الجمال، وأضاف أن من يخفي جزء من هيكل إنشائي يحرم نفسه من أجمل حليه يمكن للإنشاء أن يتحلى بها، وسواء كان الهيكل مكشوف أو مغطى، ففي الحالين يعد الإنشاء المرئي

مخطط (3) تصنيف وتفسير جماليات التعبير في أنظمة الإنشاء المعدني وبعض مصطلحاتها (الباحث)

أو المحسوس من الركائز الجمالية للشكل. [علي رأفت،1970، ص:29]، وكما يتفق مع رأي Scott من أن الجمال النابع من الإنشاء يكون له معنيين هما: تماسك إنشائي يعتمد علية سلامة المنشأ، وحيوية إنشائية constructive vividness تتواجد كمظهر يوحي بالبهجة الناتجة عن تأثير الشكل الإنشائي وتجعل المتلقي يتجاوب معها نفسيًا وعاطفيًا، وهو ما يجعل العمارة إنشاء متسامي sublimated structure يعبر عن الأفكار. وعن أهمية العناصر البنائية في المنشأ الفولاذي أكد Wasser على أن للأعمدة والدعامات دورًا تشكيليًا وجماليًا مهمًا في المنشآت واصفاً إياها أعمدة المنشأ تماثل الوقوف بأمان تحت ظل شجرة، كما أنها مركز للإشعاع والجاذبية لكل ما ومن حولها. [Wasser, 2000, p:47].

13-2: جوانب التعبير الرمزي في أنظمة الإنشاء الفولاذي:

في إطار اهتمامه بجماليات التعبير Expressional Aesthetics فقد صنّفها فيتروفيوس إلى صورتين: شكليهُ تعني بتذوق الكتل والفراغات، وأخرى رمزية symbolic Aesthetics تنبع من ربط عناصر البناء بدلالات ومعاني توحي بفكرة ما. [شاكر عبد الحميد،2006، ص:383]. وقسّمها Perrault إلى نوعين: جماليات تجريدية تُعّني بالشكل والتكوين وعلاقات العناصر، وأخرى وظيفية تنبع من فهم وظائف البناء واستيعاب قدرته على القيام بها. [علي رأفت،1997، ص:6].. لذا تتضح أهمية الاستفادة من جماليات التعبير بالرمز في الإنشاء، مما يدعوا المصمم إلى التعاطي معها على أنها ركنّ هام وحيوي في صياغة المنشأ الفولاذي.

وبالتوازي مع التحولات المستمرة في مرجعيات الشكل، فقد مرّت جماليات الإنشاء الفولاذي بمفاهيم عدة منها: جماليات التأثر بالآلة Mechanical Aesthetics وهو مصطلح لـBerg أكد على ضرورة أن يكون للأشكال تعبيرات جمالية مستمدة من الإمكانيات الجديدة للآلة، ولا يشترط أن تحمل مضمون أو تكون ذات رموز، شكل (8) وأن تصاغ تلك الأشكال من كّتل ومساحات كاملة الزوايا أو كاملة الاستدارة، ملساء، مصقولة وخالية من الزخارف. كما ظهر مصطلح الجماليات الملساء Slick-tech أسّسه هولاين ويعتمد على الاستفادة من دقة التكنولوجيا الحديثة وإمكانياتها في إحداث مبالغات في معالجة أسطح المنشآت وصقلها، والاستفادة من تداخل الأضواء والظلال معًا لإعطاء تأثيرات مميزه. كما بزّغ مع نهاية القرن 20 مصطلح الجماليات الرقمية والذي استفاد من الوسائط التقنية وعوالمها الافتراضية لتقديم أنظمة ذكيه ذات صيّغ وتراكيب بنائية من خارج قاموس الإنشاء التقليدي معقدة فراغياً ومحلله إنشائيًا توحي بالحركة والدينامية وتحمل رؤى ومضامين مستقبلية. [عبد الرحيم سالم ،1991، ص:15].

جدول رقم (1) يوضح مفردات التعبير الرمزي المقترحة في الصيغ الإنشائية

من النواحي الوظيفية والإنشائية	من النواحي الشكلية والتعبيرية
التأكيد على العلاقة المتزنة بين الحيز والإنشاء	الاهتمام بالتفاصيل التي تكون شخصية المنشأ ومظهره العام خارجيًا وداخليًا
التوافق بين المضمون البنائي والوظيفي للنظام	اختيار المديول (Module) الذي يحقق علاقات تناسبية جميله بين عناصر المنشأ وتحقيق التوافق بين الأجزاء والكليات
التأكيد على مبدأ الانسيابية والحيوية الفراغية بين الداخل والخارج	مراعاة العلاقة التناسبية بين مقاييس المستخدم وأبعاد المنشأ
التأكيد على مرونة التصميم لإجراء تغييرات أو امتدادات مستقبلية باستخدام نظم مفتوحة النهايات	تحقيق التوازن في العلاقات الإنشائية والعلاقات اللونية
البحث عن صيغ وقوالب إنشائية مميزه ترتكز إلى معايير إنسانية	الاستفادة من النظم الإنشائية لإحداث التنوع التصميمي والتباين الإبداعي
.الاهتمام بمبدأ الاستمرارية المادية والهندسية	السعي نحو تشكيلات حره وديناميكية
استخدام انسب المواد المتوافقة شكليًا وإنشائيًا واقتصاديًا لتحقيق كفاءة الأداء الوظيفي	الاستفادة من بعض مبادئ التشكيل الجمالي في الطبيعة: كالوحدة، التناسب، الانسجام، التباين، الحيوية، البساطة، القوه.الخ.
استخدام مفردات مناسبة للتعبير عن اللهجة الإنشائية المنتقاة (عضوية، بنائية، تفكيكية.. الخ)	اللجوء إلى التعبير بالرمز عن المادة، اللون، الشكل وطريقه الإنشاء
مراعاة التوافق بين الدلالات الرمزية للعناصر البنائية	لتعاطي مع النظام كأطروحة بنائية نحتية ومعالجة عناصره بطريقة دينامية لإعطائه مدلول حركي
البحث الدائم عن أبعاد جديدة للفراغ وإظهار تنظيماته بطريقة مميزة	مراعاة التعبيرات الإنشائية التي تؤكد على مرجعية الشكل
التعبير عن التوقعات المستقبلية للإنشاء في أشكال قابله للنمو والاندماج	تحقيق الوحدة التعبيرية القائمة على التباين والتنوع
التأكيد على العلاقة التفاعلية بين المنشأ والمتلقي	صياغة تعبيرات إنشائية تجسد التطورات والتحولات التقنية
تجنب استخدام عناصر بنائية غريبة دون سياق واضح	استخدام التعبير الصريح والمجرد في نقل المعاني
عدم الاعتماد على الافتراض المسبق للأشكال الإنشائية	التعبير عن الصياغات الإنشائية بالثنائيات إن أمكن مثل : الكتلة /الفراغ، النمو /التلاشي، الواقع /الخيال، الشفاف / المعتم، البساطة/ التعقيد. الخ.

النتائج العامة وتوصيات البحث:

- تعتمد الكفاءة المنشئية والأداء المنشئي بصورة كبيرة على طبيعة المادة المنشئية المختارة وخصائصها خاصة ما يتعلق بقدرتها عل تحمل الإجهادات وادائيتها المنشئية.
- التحول الكبير في المنشآت كان نحو كشف الهيكل الفولاذي لأسباب جمالية والذي مثّل واحداً من الأساليب المفضلة للعديد من الحركات المعمارية.
- إن أي أفكار تؤدي إلى تطورات في الصيّغ الإنشائية وإثراء للصور العمرانية والبيئية تنبع عادة من رؤية مميزة للعلاقات الفراغية من قبّل المصمم وكيفية تحقيقه للاقتصاد الإنشائي والحيوية الفراغية من خلال مبدأ: الإنشاء بالحدّ الأدنى من الثقل والتواصل بالحدّ الأكبر مع الخارج.
- يختلف الإحساس بجماليات التعبير من نظام فولاذي لآخر باختلاف إيحاءاته الرمزية التي تتأثر بدورها بطريقة انتقال الأحمال [راسية، مائلة] وطبيعة الصيّغ الشكلية [منحنية، مستوية] والتغطيات الخارجية [شفافة ، معتمة] والمعالجات اللونية [منسجمة، متنافرة] والتشكيلات الفراغية [منتظمة، غير منتظمة، مغلقة، مفتوحة] والبيئة المحيطة وحالة المتلقي وثقافته وموقعة من المنشأ.
- المفردات البصرية المرتبطة مع المنشآت الفولاذية تحتوي بعضاً من أقوى النماذج المميزة للعمارة الحديثة.
- يحتاج مصمم الأنظمة الفولاذية في تواصله مع المتلقي لثلاث آليات : **أولها** لغة بنائية لها أبجديات ولهجات للتعبير، يكون المصمم على معرفة ومهارة بها ويستطيع المتلقي قراءتها وفهمها، **وثانيها** رسالة بمحتوى وظيفي–جمالي–رمزي، يحددها ويصيغها المصمم ويستقبلها ويستفيد منها المتلقي، **وثالثها** وسيلة للاتصال تتضمن مفردات ومعالجات بنائية يصيغها المصمم ويتفاعل معها المتلقي.
- تتألف اللغة البنائية في مجال الإنشاء الفولاذي من مفردات يستمر تداولها وإعادة توليفها في صياغات وتركيبات لانهائية لتوحي برموز مختلفة، وأن تلك التحولات المستمرة في الصيغ وما ينتج عنها من تباين في تطبيقات الإنشاء هو الذي يميز الخصوصية البنائية لكل عصر ويعطيه لهجته الإنشائية.
- إن تعظيم التعاطي مع الأنظمة الفولاذية كلغة لها أبجديات واضحة تتضمن رموز ومفردات بنائية، وتصاغ برسائل محدده لنقل أفكار ومعاني، يتيح للمصمم دعم صياغاته الشكلية بمدي واسع من المعاني والدلالات والجماليات وتيسر على المتلقي قراءه رسائل المصمم واستيعابها والتجاوب معها.
- إن التعبير الرمزي ضروري في اللغة البنائية، ولا يشترط أن يبدأ المصمم به وإنما لابد وأن ينتهي إلية بعد تحليله لكافة المعطيات واستيفائه لكل المتطلبات، وكلما كان المصمم متمكنًا من مفردات لغته بارعًا في صياغتها ملمًا بلهجاتها وواعيًا لتأثيراتها كان التواصل مع المتلقي والتأثير في سلوكه ومشاعره أكبر.
- يستعمل الفولاذ في أغلب الأحيان في التجارب المرتبطة بالغلاف الخارجي للمبنى حيث يضيف أهمية إلى التأثير البصري العام لذلك المبنى.

مصادر البحث:

المصادر الأجنبية:

- Allsopp , Bruce. **A general history of architecture**. London: Pitman Publishing, Paperback Edition, 1971.
- Blanc, A Macevoy, and Plank R. **Architecture and construction in Steel**, London, 1993.
- Ching, Francis., ***Architecture* ... Form, Space and Order** , 2ed Edition, Jhon Wiley & sons , Inc, printed in the U.S.A, 1996.
- Dempsey, Paul ,Cross Rail, **The Use of Virtual Reality As Design Tool Passenger Terminal** ,1999.
- Macdonald, Angus, **Structural Design for the Architecture**, Architectural press,London, 1997.
- Nesbitt, Kate, **Theorizing a New Agenda for Architecture**, Anthology of Architectural Theory 1965- 1995, "Tectonic Expression ", New York, 1996.
- Schupack, M., "**Cable –supported Roof cuts cost** "civil Engineering April 1958.
- Scruton, Roger., **The Aesthetics of Architecture** , 1st published, W & J Mackay Limited , Chatman , London, 1979.
- Trebilcock, peter, **Architectural Design in Steel**, Spon Press, London, 2004.
- Wasser, Hundert., **Architecture according to: Art , Nature and Fantasy** , Medina magazine , issue 14 , July-August . Egypt, 2000.

المصادر العربية:

- احمد المهندس ، **المنشآت المعدنية**، مقال منشور في منتديات ستار تايمز، الشبكة الدولية، 2012/09/29.
  - http://www.startimes.com/?t=29224948
- أدور سميث، **الحركات الفنية منذ عام ١٩٤٥** ، الشارقة، مركز الشارقة للإبداع الفكري، 2001.
- أوان الكويتي، تكنولوجيا معمارية بمفهوم عصري، مقال منشور في مجلة بناة، الشبكة الدولية، 2010.
  - http://www.bonah.org/news-extend-article-354.html
- سعد القصاب، **آثر الاتجاهات معاصرة وطليعية ستينيات القرن المنصرم**، مقال منشور، جريدة الزمان، لندن، ٢٠٠٤.
- سلام المصري، **العناصر الإنشائية وعناصر التشكيل**، مقال منشور، الشبكة الدولية، 2006.
  - http://m3mare.com/vb/showthread.php?t=425
- شاكر عبد الحميد، **التفضيل الجمالي ... دراسة في سيكولوجية التذوق الفني**، مقال منشور مجلة عالم المعرفة، عدد267 ، الكويت، 2001.
- عبد الرحيم سالم، **دراسات في الشكل والتطور المعماري**، جامعة العلوم والتكنولوجيا، الأردن، 1991.
- على رأفت، **الإبداع الفني في العمارة، ثلاثية الإبداع المعماري**، الجزء الأول، مركز أبحاث انتركونسالت، القاهرة، 1997.
- على رأفت، **فن العمارة والخرسانة المسلحة** ، مؤسسه فرانكلين للطبع والنشر، القاهرة، 1970.
- فاروق يوسف، **الرسم العربي الآن مفهوم الأصالة الفنية بين خيارين**، مجلة التشكيل العربي، مجلة الألكترونية، 2006.
  - http://tashkeelarab.jeeran.com/archive/2006/10/112329.html
- فخرية بنت خلفان اليحيائية، **إسهامات التكنولوجيا الحديثة في الفنون الجميلة**، جامعة السلطان قابوس - سلطنة عمان 2011

شكل (1) يوضح توفير المواد الجديدة للمرونة التصميمية من خلال بروز قاعة المحاضرات عن مبنى Faculty of Engineering للمعمار Stirling and Gowan 1963

المصدر: http://lebbeuswoods.files.wordpress.com/2010/11/stirling-5.jpg

شكل (2) يوضح التشكيل بخطوط منحنية ومستقيمة وبمعالجات شكلية وتعبيرية مختلفة

المصدر: http://www.steelcaddetailing.co.uk/wp-content/gallery/madeley-academy/new_madeley4.jpg

شكل (3) يوضح الهيكل الإنشائي المعدني المقوّس لمحطة Stratford

المصدر: http://www.flickr.com/photos/55935853@N00/7028902411

شكل (4) يوضح أثر المعالجات اللونية في المنشآت المعدنية وانعكاساتها التعبيرية

المصدر: http://darrellyoungarchive.photoshelter.com/image/I0000uu0b.SyMS4g

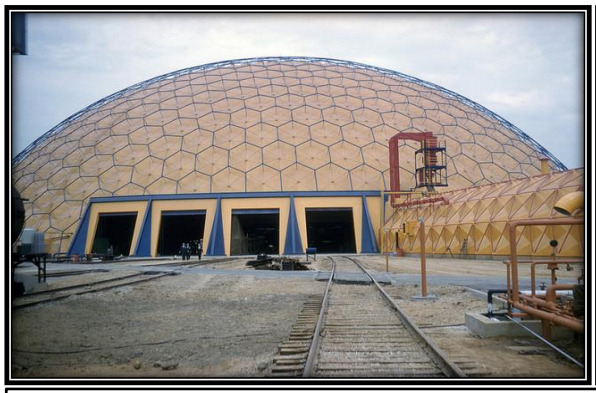


شكل (5) قبة شركة السيارات المتحدة (Union Car Company) في (Boton Rouge) للمعمار (Fuller)

المصدر: http://www.buckminster.info/Index/U/Union_Tank_Car.htm




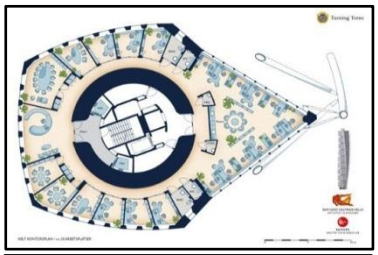

شكل (6) مبنى الجذع المتحول (Turning Torso) للمعمار santiago-calatrava

المصدر: http://sonachavdadotcom.files.wordpress.com/2012/03/turning_torso_santiago-calatrava.jpg


شكل (7) يوضح مطار ستانستيد Stansted Airport لندن للمصمم نورمان فوستر 1991

المصدر: http://www.e-architect.co.uk/images/jpgs/london/stansted_airport_exterior_01.jpg

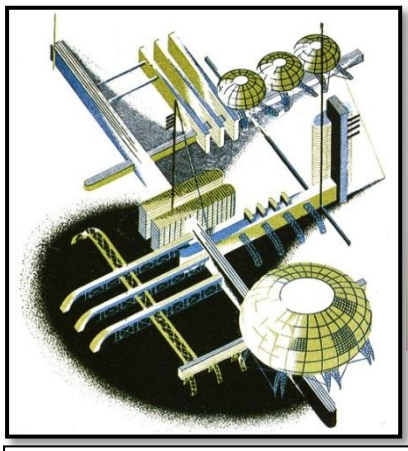

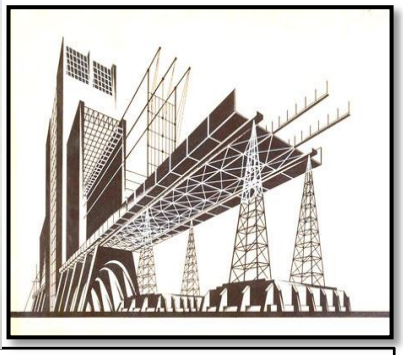

شكل (8) بعض من الأفكار والتصاميم التي مثلّت السعي نحو الاقتران مع أشكال الماكنة

صدر: http://beineckegenmod.wordpress.com/category/constructivism/